# POST-FIRE EXPOSURE BEHAVIOR OF CONCRETE FILLED STEEL TUBE COLUMN UNDER AXIAL LOADING

Thesis submitted in fulfillment of the requirements for the Degree of

DOCTOR OF PHILOSOPHY

By

ADITYA KUMAR TIWARY

Department of Civil Engineering

JAYPEE UNIVERSITY OF INFORMATION TECHNOLOGY
WAKNAGHAT, DISTRICT SOLAN, H.P., INDIA

MARCH, 2021

POST-FIRE EXPOSURE BEHAVIOR OF CONCRETE FILLED STEEL TUBE COLUMN UNDER AXIAL LOADING

Thesis submitted in fulfillment of the requirements for the Degree of

DOCTOR OF PHILOSOPHY

By

ADITYA KUMAR TIWARY

Department of Civil Engineering

JAYPEE UNIVERSITY OF INFORMATION TECHNOLOGY
WAKNAGHAT, DISTRICT SOLAN, H.P., INDIA

MARCH, 2021

……....DEDICATED TO
MY PARENTS………

TABLE OF CONTENTS

DECLARATION BY THE SCHOLAR

I hereby declare that the work reported in the Ph.D. thesis entitled **"Post-Fire Exposure Behavior of Concrete Filled Steel Tube Column Under Axial Loading"** submitted at **Jaypee University of Information Technology, Waknaghat, Himachal Pradesh, India,** is an authentic record of my work carried out under the supervision of **Prof. Ashok Kumar Gupta.** I have not submitted this work elsewhere for any degree or diploma. I am fully responsible for the contents of my Ph.D. Thesis.

Aditya Kumar Tiwary
Enrolment No.: 166610
Department of Civil Engineering
Jaypee University of Information Technology, Waknaghat, India
Date:

SUPERVISOR'S CERTIFICATE

This is to certify that the work reported in the Ph.D. thesis entitled **"Post-Fire Exposure Behavior of Concrete Filled Steel Tube Column Under Axial Loading",** submitted by **Aditya Kumar Tiwary** at **Jaypee University of Information Technology, Waknaghat, Himachal Pradesh, India,** is a bonafide record of his original work carried out under my supervision. This work has not been submitted elsewhere for any other degree or diploma.

Prof. Ashok Kumar Gupta

Head of Department

Department of Civil Engineering

Jaypee University of Information

Technology, Waknaghat

Solan (HP), India Solan (HP), India

Date:

ACKNOWLEDGEMENT

(Aditya Kumar Tiwary)

ABSTRACT

Concrete – filled steel tube (CFST) columns are composite members consisting of concrete in filled steel tubes that are used as load – carrying members. In the construction industry, CFST columns are generally preferred for the development of tall buildings and long – span bridges. With the primary purpose of protecting human life and property during fire hazards, the present study aims at evaluating the behavior of CFST columns for post – fire condition. In order to achieve this, concrete-filled steel tube (CFST) columns under greased and non-greased conditions are treated at elevated temperature of 600 °C and 800 °C and subsequently subjected to axial loading.

The parametric variation for CFST columns with M30 concrete consists of three different diameters of 100 mm, 125 mm and 150 mm with two different steel casing thicknesses of 4 mm and 5 mm respectively. The columns are examined for both before and after – fire exposures. For all the CFST specimens, a constant height of 600 mm is maintained. This study also checks the behavior of CFST columns under two separate cooling regimes (annealing and quenching) after exposure to elevated temperatures of 600 °C and 800 °C.

The test results showed that load carrying capacity of non – greased columns is slightly greater than greased columns it varies from 1% to 2.7% for all specimens. It was also observed that the elastic axial load capacity of non-greased columns was higher as compared to greased columns due to which the initial slope of load-deformation curve of non-greased columns were greater than the greased columns. The secant stiffness and ductility index of non-greased CFST columns was observed to be greater than greased columns. The secant stiffness of greased and non-greased specimens was varying from 18% to 59% and it was observed that the non-greased specimens have more ductility as compared to the greased specimens.

Also, the results obtained by the experimental investigation of CFST columns for post-fire condition were compared with each other on the basis of two cooling regimes. it was observed that the load carrying capacity of heated specimens for post cooling phase got reduced by 9.5% to 2.7% within the case of annealing, whereas for water quenching, the reduction in strength was from 10.6% to 3.4% at an elevated temperature of 600 °C to 800 °C, which is slightly more than compared to of annealing. It was also observed that the reduction in load carrying capacity of CFST columns was varying from 5.2 to 2.9% form ambient to 600 °C elevated

temperature and 14.2 to 6.2% from ambient to 800 °C in case of annealing, whereas, it was 10.2% to 5% from ambient to 600 °C and 17.5% to 8.2% form ambient to 800 °C in case of quenching. Thus, the load carrying capacity of heated specimens as compared with water quenching, annealing is slightly better for post fire cooling of CFST columns.

The value of secant stiffness and ductility index for CFST columns was found to have a lower value for 800 °C as compared to 600 °C. It was found that the reduction in the stiffness of CFST columns in the case of annealing was from 45.5% to 14.4%, whereas it was from 34.6% to 13.2% in the case of water quenching for temperature 600 °C and 800 °C respectively. It was observed that the value of ductility index for water quenching was found to be slightly less than that of annealing. The value of residual strength index was found to be higher for the case of 800 °C for both annealing and water quenching as compared to that of 600 °C.

The comparison of experimental results with design codes was investigated to estimate the axial load capacity of concrete filled steel tube columns. The analytical values predicted by some suggested equations in the design code was good agreement with experimental data. A nonlinear finite element model using the commercial software ABAQUS/CAE 6.14 was also developed in this study. The FE model was verified with tested concrete filled steel tube columns after incorporating the material nonlinearity of both steel tube and concrete infill. A mesh conversion study was also performed by considering different size of mesh on CFST model to get the best size of mesh for the validation to the experimental results. A good agreement between the experimental data and the model's output in terms of the axial capacity and failure mode was observed.

Keywords: CFST, greased, non-greased, elevated temperature, annealing, quenching.

LIST OF ACRONYMS AND ABBREVIATIONS

CFST   Concrete-filled steel tube

C1T4   First column with steel thickness 4 mm and diameter 100 mm

C1T5   First column with steel thickness 5 mm and diameter 100 mm

C2T4   Second column with steel thickness 4 mm and diameter 125 mm

C2T5   Second column with steel thickness 5 mm and diameter 125 mm

C3T4   Third column with steel thickness 4 mm and diameter 150 mm

C3T5   Third column with steel thickness 5 mm and diameter 150 mm

AB   Ambient

AN   Annealing

QN   Quenching

DI   Ductility index

RSI   Residual strength index

ACI   American concrete institute

AS   Australian standard

AISC-LRFD   American institute of steel construction-load and resistance factor design

CECS   China association of engineering and construction Standardization

LIST OF SYMBOLS

D	Steel tube outer diameter
H	Height of the column
A_s	Steel area
A_c	Concrete area
t	Steel tube thickness
f_{cu}	Cube compressive strength
f_y	Steel yield stress
f_{ck}	Characteristic compressive strength of concrete
τ	Shear stress
τ_{crit}	Critical shear stress
ε_t	Strain hardening
ε_u	Ultimate strain
f_{ult}	Ultimate stress
f_{cc}	Confined compressive strength of concrete
f_c	Unconfined compressive strength of concrete
ε_{cc}	Unconfined concrete strain
ε'_c	Unconfined concrete strain
$f_{cp\text{-}max}$	Maximum confining pressure
N_e	Experimental axial load capacity
N_c	Eurocode 4 axial design load capacity

$N_{c,\ ACI,\ AS}$ American Concrete Institute and American Standard axial design load capacity

P_n AISC-LFRD axial design load capacity

N_o CECS 28:90 axial load capacity

LIST OF FIGURES

LIST OF TABLES

CHAPTER 1

INTRODUCTION

1.1   GENERAL

This chapter gives a detail description of the thesis on the topic of performance of concrete-filled steel tube columns before and after exposure to fire, comprising background of the study, concrete filled steel tube columns and their advantages, applications, mechanism under fire, as well as the thesis layout.

1.2   MOTIVATION

The main scope of this study is fire safety for protecting people's lives and property from fire accidents. Fire outbreak has become the third major risk to business continuity and operations, as per recorded by India Risk Survey (IRS) 2018. In the year 2018, 13,099 number of fire accident cases were reported in the India which included fire explosion in cracker factory on July 4, 2018, fire explosion at BPCL plant on August 9, 2018, fire accident in Mumbai hospital on December 17, 2018, etc. In 2016, fire outbreak was placed at eighth rank for being one of biggest threat to businesses in a report of IRS. There was an increase of 300 per cent in the cases of fire accidents in commercial buildings between 2014 (179 cases) and 2015 (716 cases). Also, in government buildings, the fire outbreaks jumped by 218 per cent in the same phase (in 2015(35 cases) and 11 cases in 2014). The ADSI report tells that the residential buildings are most susceptible to fire outbreaks. In 2015, a total of 7,493 fire outbreak cases were reported in residential buildings with an increase of 100 per cent from the previous year, 2014 (3,736 cases). In fact, 42 per cent of the casualties happened due to accidental fire in 2015 in residential buildings. Several steps can be taken to ensure fire protection. First and foremost, step is fire prevention. This can be done by placing fire hazard notices and precautions throughout the building, especially in areas where electricity and fuel are used. If a fire occurs, it should be controlled and the spread of fire across the entire building should be prevented by using fire sprinkler systems, smoke alarms, fire extinguishers and smoking detectors. If spread of the fire becomes difficult to handle using the facilities of the building, the design of the building should be such that it remains stable for a certain period of time during the fire.

This time should be enough to evacuate the occupants of the building and to enable the firemen to extinguish the building fire (The-Concrete-Centre 2004). In the current design guidelines, there is also lack of data on the fire resistance of CFST columns. Further experimental and computational analysis seems to be required to examine the behavior of CFST during fire. National Building Code of India 2016, (NBC) Part IV (Fire and Life Safety) deals with safety from fire. The Code primarily contains administrative regulations, guidelines for development control and general construction standards and requirements for fire safety.

There is a lack of information on fire safety measures with respect to composite construction like CFST. And also, it is a well-known fact that concrete filled steel tube sections provide good fire resistance. All these points provided the motivation to carry out a study on fire behavior of CFSTs before and after fire exposure.

1.3 NEED OF STUDY

As per many incidences of fire cases in India, the temperature during fire was observed up to 800 °C [12]. The high number of deaths and material loss caused by fires is largely due to the poor condition of fire services and negligent application of standards of fire safety in factories and buildings (IRS 2017). The significant loss of high-strength concrete strength when temperature lies among 100°C (on initiation of water removal process) as well as 200°C, while absorbed water and moisture is spread to concrete section's outer layer, therefore, internal forces are affected through entire specimen as well as its strength has been reduced; therefore, when concrete's original strength is high it results in greater strength losses. Hence the steel tube protects the concrete core to come in direct exposure of heat, therefore prevents progressive spalling [70].

The specific heat of concrete remains satisfactory up to a temperature of 400 °C. But when temperature is raised beyond 400 °C concrete undergoes deterioration because of significant reduction in properties like modulus of elasticity, specific heat, mass loss, compressive strength, etc. At temperature more than 600 °C, steel loses most of its stiffness and strength [72, 81]. So, for the present study the worst condition of temperature considered are 600 °C and 800 °C as per the record of fire cases in India. In this investigation the diameter and thickness of steel tubes were varied by considering constant height of CFST columns. This investigation was carried out at increasing temperature (maximum 800 °C) by considering the previous fire cases.

Very little research has been recorded on the performance of CFST columns during fire and related mathematical modelling. Even in the few investigations that have been performed the effects of some variables on the fire behavior of CFST columns have not been studied in them.

1.4   BACKGROUND

High-rise buildings extensively employ the concrete-filled steel tube (CFST) columns because of great resistance offered by CFSTs to axial load even after fire exposure. One of the major concerns in recent time is the accidents that are caused because of fire in buildings that resulted in human life and property loss. Compared to a steel and reinforced concrete component, the CFST structural member has a range of distinct advantages. By virtue of their structural aids such as reduced cross section, high strength, greater apparent stiffness, improved fire resistance and exceptional structural properties related to seismic resistant including energy absorption and higher ductility, the use of CFST beams and columns has become increasingly popular in construction of building structures [65, 99, 152, 220]. Furthermore, the steel tube of CFST member can serve as formwork during infilling of concrete. The inward local buckling usually noticed in bare steel tubes, is efficiently eliminated and obviated in CFST member. Concerning these terms, this study is influential as it examines the behavior of CFST members when exposed to fire.

The CFST member also has different number of applications or functions such as large industrial workshops and tall structures, columns supporting platforms in offshore structures, bridges and open-air overhead traveling cranes, roofs of oil storage tanks and also used as a pile in foundation [24]. For various reasons, the concrete filled tubular as well as other metallic structures concerned infrastructure become structurally inadequate as well as also ageing of metallic structures are often reported [78]. Furthermore, metallic structures deteriorated due to several factors and the main factor is corrosion. As a consequence of deficiencies at the design stage like insufficient factors of safety, poor construction workmanship and usage of inferior materials, the design strength of structures may not be achieved.

For high-rise buildings, fire safety has always been a major issue. In high-rise reinforced concrete buildings, the effect of high temperature is given vital concern since during fire in concrete and steel; there exist a large depletion of strength because of increased temperature in the concrete core. It also results in concrete spalling from reinforced concrete members' exposed surface [3, 80, 163]. With the rising use of CFST in engineering exercise, there is a

thriving demand to investigate the fire resistance as well as CFST members' post fire repairability for the objectives of fire protection [22]. Many researches were performed on the CFST columns' fire resistance in the past [14, 17, 85, 160, 222]. Another point which has drawn the attention of growing research interest in recent times is such composite columns' residual strength [44, 45, 151]. This may be used to evaluate the potential damage which is caused by fire, and assist to set up an approach to calculate the structural fire protection requirements for minimal post fire repair. With a purpose of reinstating their true functionality, suitable repair measures should be practiced for improving the composite columns' ductility and/or strength on account of fire damage. Moreover, such 'repairs' may also be implemented if changes in the use of the structures urge advanced functional requirements than those predicted in the original design.

Composite construction may be regarded as a reliable pick to achieve adequate balance between the cost and the benefits it offers. Nowadays, there is a wide range of beams and composite columns available; however, the CFST sections are the one which are being utilized usually. One of the unique ideas is CFST member; which is a hollow tubular member in-filled with concrete, utilized as columns or beams which are suitable substitute for bridges and tall buildings' reinforced concrete (RC) (or) hot-rolled steel members in structural systems. Concrete's compressive strength is utilized for such composite system as well as steel tube contributes tensile strength and stiffness's large portion which is situated in outer limits. In addition, the steel tube provides the necessary scope for core of concrete that enhances the column member's compressive strength. During compression, CFST short column achieves its maximum potential when both the steel and concrete hits their maximum strength limit [203, 205], that is, concrete crushing as well as steel yielding and stability rules the CFST slender columns as well as failure is caused by either inelastic or elastic column buckling. The CFST member's flexural behavior is working as hollow steel tube. The concrete contributes to moment of resistance by the shifting the neutral axis of the cross section in the direction of compression face of the beam with the addition of concrete.

In addition to corrosion, increasing demand of present-day traffic surpasses the design load capabilities of several bridges; this leads to fatigue cracking in the metallic members. In service, increased safety requirements, a variation in use or modernization resulting in redistribution of stresses, an increase in the magnitude or intensity of the applied loads that need to be supported and improving of design standards may render all or part of a structure

inadequate. When local repair techniques or maintenance cannot bring back an inferior structure to the required specifications, there are two other feasible alternatives such as partial or complete demolition and reconstruct and initiation of strengthening programme. Compared to demolition, improving and strengthening are perpetually more productive and economic than the replacement option. Additionally, time duration and service interruption are also less.

As per the previous studies, the section enlargement was the best approach for rehabilitation and reestablishment of reinforced concrete columns. It was anticipated that this approach of section enlargement will also be efficient in rectifying CFST columns and beams. Despite, it ended in a substantial enhancement in the column cross-section as well as relatively long construction duration and also decreased floor space area. Conventionally, most commonly used method for strengthening or/and rehabilitating a steel structure is providing an external steel plates bonding to the structure by any of these connections like bolting, riveting, welding, clamping and adhesive bonding [11, 230]. Even though these approaches have been shown to be well-to-do in practice, these techniques revealed serious difficulties such as they needed heavy lifting equipment to locate the plates in place, challenge of working in complicated bonding/welding procedures and difficulty in fitting in complex profiles. The additional steel plates are also susceptible to corrosion, which results in the rise of future maintenance costs. Furthermore, the residual stress will set up in to the material, when welding is the part of joining process.

CFST is considered the main cross-sectional type of composite columns. Historically, encroaching on concrete in the column has been considered a protection against steel corrosion and fire [12, 13, 14]. Nowadays, longitudinal and lateral strengthening as included with the concrete encasement, and the potency caused by contact among the embedded steel tube as well as surrounding concrete was deployed in structural uses. On the other hand, CFST columns are made by releasing concrete in hollow steel tubes. Steel tube helps in situ concrete filling and thus abolishes the requirement of more formwork and results in faster construction [15, 16]. Further, it does not require additional support.

CFST columns have been extensively employed as columns in both high and medium rise buildings and large span buildings and bridge columns or piers [24, 28, 87]. In previous studies, ductility improved by confining concrete and the two methods for providing confinement to concrete active confinement and passive confinement [19, 40]. First, confining stress is not binding unless the transverse reinforcement gap is reduced [21]. Second, the effect

of deformation in concrete is introduced by the bending action in transverse reinforcement. The bending stress decreases as the distance from the bend increases [22].

In previous studies of [17, 23, 24, 223] CFST, it was found that the performance of CFST is better as compared to typical RCC construction. In CFST, steel tube also provides function of constant formwork, as well as neglecting to strengthen the bar reduces construction time and costs. The limited pressure produced by the steel tubes on core of concrete slows down development of micro-cracks and decreases the splitting crack width [25]. Under tensile stresses to the CFST columns steel has the potential to show more stress than concrete, for this reason, research was performed for evaluating the de-bonding effect on CFST, and it is concluded that the local buckling phenomenon is more severe in case of circular steel tube in the debonding model than the sample devoid of debonding [23, 32, 115].

In the CFST, concrete core confinement is specified by steel tubes by reversing the lateral stress. The stresses that arise depend on the lateral stresses and the shear stresses in the specimen. And thus, it becomes difficult to evaluate the amount of lateral and shear stress [19, 26, 27, 28]. In the CFST model with rectangular and square cross-sections, the arching action in the corners is not uniform stress in conventional RCC systems such as buckling between center and edges.

Many experimental and analytical researches have been performed by investigators for evaluating the CFST members' behavior after fire exposure [29, 30, 31]. The effect on the composite connections' performance among CFST columns and steel beam after the fire influence was assessed [32, 76]. The residual strength and fire index impact after standard fire exposure for CFST members was also analyzed [34, 151,173].

Residual strength index is an essential variable for evaluating the CFST members' behavior after fire exposure as structural members undergo three stages during fire, viz. loading at cooling, heating as well as ambient temperatures [34, 44]. In the structures' post-fire rehabilitation, columns' residual load carrying capacity evaluation may provide assistance in repair purpose [7]. The CFST columns' cyclic behavior cause to undergo a constant axial load as well as cyclically rising flexural load after fire exposure was explored according to ISO-834 [37, 48, 189]. The outer tubular steel section of the CFST columns contributes to concrete confinement and improves the strength and ductility of the columns [40,117]. It also results in providing better resistance against failure through local buckling and improved stability [30, 41, 43, 45].

Some investigations have been executed on concrete's mechanical properties which are subjected to standard fire signifies that as temperature increased beyond 400 °C, deterioration of the concrete started [44, 81, 229]. The steel tube of CFST columns reduces the clipping of concrete and enhances the columns potential to counter the fire impact through redistribution of stresses among outer steel tube as well as in-filled concrete [46, 47]. Furthermore, bond strength among concrete's outer surface and steel's inner face after CFST columns' fire exposure was also examined [37, 48, 49]. The elevated temperature effect on the CFST columns' behavior was also evaluated [50, 51] as well as it showed that members' overall performance as well as especially ductility improves as well as energy dissipation's higher levels are also involved.

The stiffness characteristics of CFST columns were also investigated [52] and it indicated that for examining the CFST columns' stiffness the effects of exposure to loading as well as elevated temperature are constraints of great importance in comparison with the residual strength index. The design fundamentals and typical features of CFST columns under fire were also given [53]; the behavior of CFST specimens when exposed to fire also gets influenced by cooling approaches utilized for specimen [144]. Also, for structures' cooling various approaches are utilized, when they are subjected to fire. There may be a great influence of cooling methods on CFST columns' functions [45]. Minimum number of studies is accessible on the CFST columns behavior after fire or under fire, without taking into account cooling phase effect on specimen. The cooling stage plays a significant role to assess the CFST columns performance after and during the fire exposure, in case structures are exposed to fire.

1.5 CONCRETE FILLED STEEL TUBES (CFST)

Among various composite columns one which belong to the category of structural systems, where the most excellent characteristics of both the materials i.e. steel and concrete are utilized to their best possible use are CFST (Concrete filled steel tubular) column. When favorable situations are ensured, the tubular shell's local buckling are restricted by the in-filled concrete and the steel casing creates a confinement for better earthquake resistance by confining the core tri-axially.

Tubular columns provide an additional advantage of homogeneity when compared to spirally reinforced concrete columns where both, the concrete cover as well as the core act as 2 separate layers. In case of spirally reinforced concrete columns, the core is superior to the

cover as well as after the spalling of cover occurs, the spiral reinforcement comes into play [199]. While on the contrary, a continuous homogeneous medium is formed by the CFST columns' core. Additionally, the buckling in slender tubular columns takes place by the time concrete is limited as well as strength is built up by the shell. The tubular columns represent columns which have well dispersed reinforcement when considered as reinforced concrete columns. Ties and spirals could even be skipped and in addition to this, the shuttering is formed by the tubes themselves.

For concrete compressive strength/unit cost value is greater than in comparison to the structural steel as well as hence, it appeared as most appropriate material to be utilized in column. Before 1950s, usually a low strength concrete wet mix was utilized and thus the share of the good quality concrete towards the column strength was overlooked. Experiments revealed that opting composite construction for column design and employing better-quality concrete can help in making good savings [55, 56]. This practical method is not established on composite columns' primary research and was evolved by various phases from steel columns' existing design procedures.
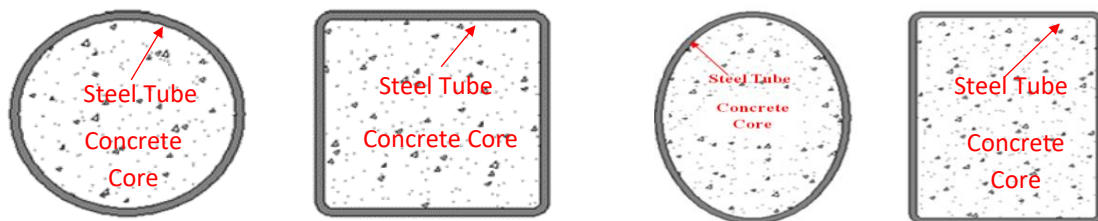
Figure 1.1 Concrete Filled Steel Tube column (CFST) [55]

CFST's can be used in various cross-sectional shapes like square, circular, rectangular and ellipse [124, 161, 200]. The specimens having only one skin of steel tube are single skin CFST columns represented in Figure 1.1.

1.6   CFST COLUMN ADVANTAGES

In both construction system and structural performance's terms, various advantages exist that are associated with structural systems. Also, in its structural performance's terms, materials distribution in the cross section resulted in making very efficient system. The steel is positioned at the outside perimeter where tension and bending work most efficiently. As the substance lies farthest from the centroid, it also has the greatest stiffness. This, together with the much higher

elasticity modulus of the steel, gives moment of inertia the largest contribution. Owing to the presence of the concrete heart, the critical buckling issue connected to thin-walled steel tubes is either avoided or postponed.

CFST structural system's primary advantages as compared with reinforced concrete system or ordinary steel are as follows.

1.6.1 Structural Performance Improvement Due to material properties

The steel tube acts as an external reinforcement. The steel ratio in the CFST cross section is much higher than those in the reinforced concrete sections. Because of concrete in-fill concrete presence, thin-walled steel tubes' characteristic buckling problem is controlled as well as concrete's restraining effect helps in decreasing strength deterioration after the local buckling. Also, steel tube exerted confinement pressure helps in enhancing concrete in-fill's properties improvement. Under bending CFST section's steel is well plasticized as it is situated on section's outside area. The steel tube represented as external reinforcements. In the CFST cross section, the steel ratio is very high in comparison to the RC sections.

1.6.2 Due to Geometrical properties

The steel as the outer part of core concrete performs most effectively both in tension and bending. whereas the concrete core gives the greater contribution to resisting axial compression. While in resisting axial compression, greater contribution is provided by concrete core. As the substance lies farthest from the centroid, it offers the greatest stiffness and thus, gives moment of inertia the largest contribution.

1.6.3 Constructional Performance Improvement During fabrication

Because of easy erection and handling, constructional procedure is fast. Generally, CFST columns' steel tube thickness is less than 40mm as well as available easily. Therefore, can be easily assembled and fabricated. In comparison to the conventional reinforced concrete, they can be easily constructed and fabricated, whereas for reinforcement's complex forms cutting as well as bending, skilled workers are required.

1.6.4 During Construction

There is no need of formwork because the steel tube functions as permanent formwork which then saves time-consuming and costly formwork. Generally, there exists a quick cure for infill concrete. Adverse winds and temperature have less effect on infill concrete. Pumping method is utilized for concrete casting, as it saves constructional time and cost as well as manpower.

1.6.5 During finishing

Slender columns reduce the application time and cost of applied finishes. Mechanical damages do not affect the concrete filling. Decreased construction depth, then, decreases air-conditioning spaces, ventilating spaces, heating, exteriors paneling, foundation costs and storey heights.

1.6.6 Post Constructional Performance Improvement

In comparison to steel columns, better corrosion resistance capabilities are exhibited by them. In comparison to steel columns, CFST column's seismic behaviors are better. Also, fire resistance performance is improved by the concrete, as well as thus it reduces fireproof material amount or its usage can be excluded.

1.6.7 Beams and Columns' Larger spans

Frame beam span 7-8m or more is utilized as for beams, steel beams are utilized. The columns' larger spans can be determined which result in more inside space. In comparison to RC column, The CFST column size is smaller, therefore, visibility and usable floor area is enhanced making it more aesthetically pleasing.

1.6.8 Foundations

In comparison to the RCC columns, CFST columns are light. Thus, reduces the foundation cost, and also reduces resulted earthquake force. In the seismic regions, CFST columns are more dependable and safer since it utilizes high-strength concrete as well as prevents brittle failure. With columns size reduction, foundations are reduced; therefore, results in more economic benefits. Due to columns' large span, there exists increasing vertical loads that acts on columns as well as CFST columns' compressive bearing capacity is effectively brought into play.

1.6.9 Cost reduction

They are low maintenance structures. The columns assembly and transportation cost is decreased as they are developed by hollow steel tube erection first, after that concrete is poured into it. As compared to steel column, half the steel is used in CFST columns. It greatly reduces the cost and makes it judicious and efficient to use. As compared to RC columns, CFST columns utilize less concrete as well as less steel. Therefore, carbon footprint on environment is reduced. Furthermore, as CFST column's core concrete volume is nearly 10% of columns total volume as well as concrete density is $1/3^{rd}$ of steel density. Hence, CFST column weight is less than steel column weight. CFST column's dimension is approximately with the steel

column's outline dimension. Thus, when compared to steel column, CFST column occupies less space and thus makes it similar in terms of space.
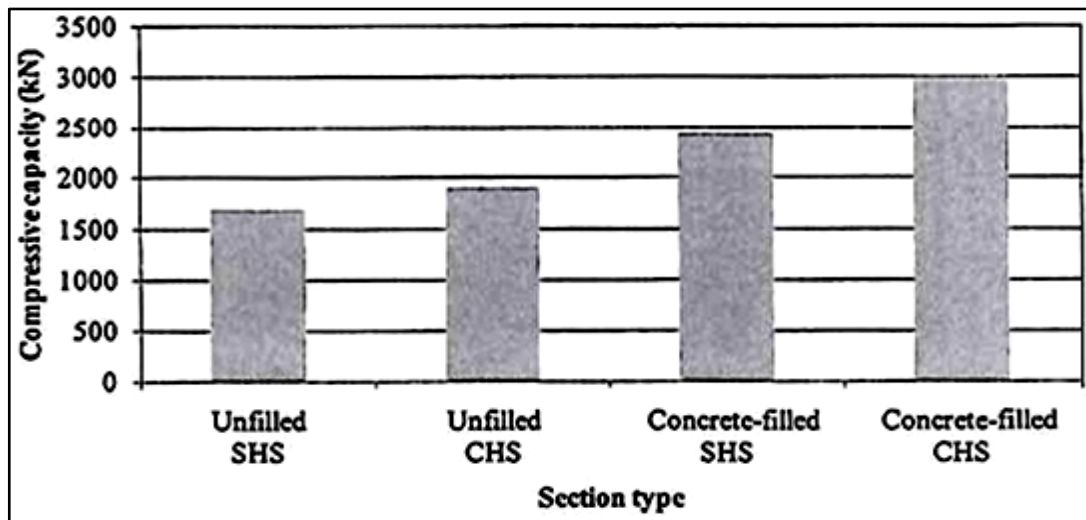
Figure 1.2 Enhancement achieved by filling steel hollow section columns with concrete: compressive capacity [57]

The concrete infill strengthens the tubular columns' fire resistance. CFST columns can withstand fire exposure for a longer duration of time without any need for additional defense, using the required amount of reinforcement. A part from an improvement in the column's load-bearing potential relative to that of empty hollow parts, as can be seen in Figure 1.2, a significant advantage of the column's fire resistance can be obtained by means of concrete filling (Figure 1.3) that can be improved by the required reinforcement form. Due to the containment effect imposed by the steel casing, the efficiency of the concrete in-fill is enhanced. The resisting axial compression is greatly contributed by the concrete core. Comparison of CFST stub column's axial compressive behavior is presented in Figure 1.4 [13].
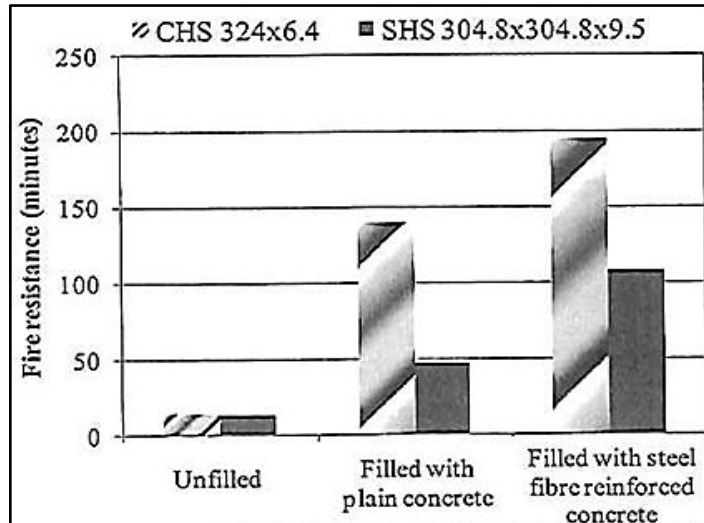
Figure 1.3 Enhancement achieved by filling steel hollow section columns with concrete: fire resistance [57]
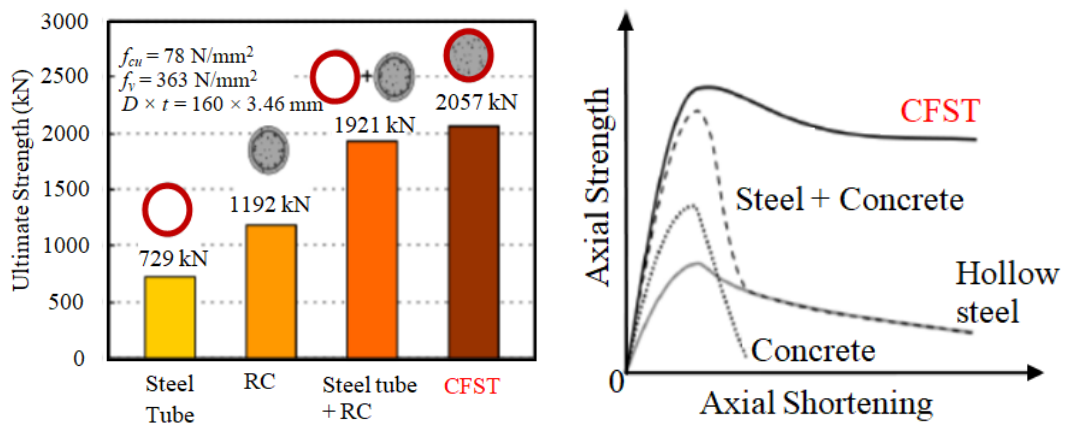
Figure 1.4 Axial compressive behavior of CFST Column [13]

1.7 LIMITATIONS OF CONCRETE-FILLED STEEL TUBES

The inadequate knowledge about CFSTs behavior is the major constrains to implement CFSTs use. Various other factors complicate the design and analysis of CFST's. A CFST member consists of 2 materials having distinctive stress-strain curves as well as peculiar behavior. Due to this difference, it becomes very difficult to predict the combined properties like moment of inertia and modulus of elasticity. The failure process of this composite greatly depends on concrete and steel properties, shape, steel tube thickness, length and diameter. Shrinkage, bond, creep, concrete confinement, type of loading and residual stresses are other parameters also have an effect on CFST's behavior. In recent years some of the above-mentioned parameters have been resolved by studying axially loaded columns and CFST beam-

12

columns and connections worldwide [36, 121]. However, research is still work in progress on topics like local buckling, the effect of bond, scale effect, and confinement on CFST member strength, economical detailing strategies and load transfer mechanisms at beam-CFST column connections at all stages of loading so as to smooth up the development of seismic design provisions. Although with advancement in technology there is increase in experimental research but still the scale of experiment is relatively on small specimens compared to the real-life situations. This is due to economy and load limits of testing apparatus in experiments. Due to these reasons the experimental work done is not easy to implement on full scale and so it remains a debatable question.

1.8 PRACTICAL APPLICATIONS

There exists a long history of CFST column. In 1963, The Beijing Underground Railway Station construction utilized filled steel tubes as columns for the first time in China. Afterward, these columns have been utilized in other projects including bridge and viaduct systems during heavy loads. Large arch bridges have been constructed over rivers with the through span of 140 m and a rise of 22 m. In the refractory materials factory at Semiluka, pipes of diameter 114 x 4 mm filled with concrete were used as stanchions.

Later 1970s, the framing structures that consist of H-shaped beams and CFST columns have, as a result of these thorough investigations, demonstrated considerable benefits in regards to their use in the construction of tall buildings in Japan, so this method has often been used in their construction. In 1985, a steel manufacturer and five general contractors succeeded in winning the "Japan's Ministry of Construction proposal competition" for constructing 21st-century urban apartment houses, which included office towers, high-rise buildings, and industrial and residential buildings. After that, a 5-year experimental research project namely "New Urban Housing Project (NUHP)" was started by these industries as well as Ministry of Construction's Building Research Institute (BRI) that enhanced this system's investigation. In 1993, the U.S.-Japan Cooperative Earthquake Research Initiative's fifth phase, a 5-year research project on hybrid and composite systems, began, and research on the CFST column system was that program's part. Current architecture guidelines for the CFST column framework were generated from results gathered in this project.

The economic, structural, and architectural advantages of composite columns in steel and concrete-filled steel hollow parts are highly appreciated by building engineers as well as modern designers. Structural buildings have been using this material for few decades; however,

their use has significantly increased in recent years. Here are some qualitative features that structural people and architects must remember when making design decisions are as:

1) With the very advanced assembly technique in structural engineering today, there were hardly any issues regarding the joints. Using this modelling technique, it is possible to prepare workshop prefabrication and on site dry and quick assembly is performed.

2) Steel permits a pretentious architectural design along with several colorings. The corrosion protection costs and painting costs, including paints, spray, etc., are small because of columns' smaller external surface area.

3) The concrete filling gives an even greater rigidity and load-bearing strength to the steel hollow sections so as high loads can be bear by the aesthetic columns without changing the exterior dimensions of the components. The reinforcement bars should be added to this.

In comparison to the concrete column, higher ductility is exhibited by composite column as well as by following steel constructions experience, connections might be created. Not only does the concrete filling lead to a bearing capacity that in comparison to steel columns is much high, it also promotes fire resistance [85, 128]. Concrete filled steel columns exhibit best seismic behavior in terms to rotational capacities and ductility in comparison to other composite columns types. The steel profile concrete held the concrete as well as even in case when ultimate concrete strength is attained it cannot break. In world's different parts, a long tradition is followed by the research work in the composite columns with concrete filled hollow sections area. Brick, timber and stone masonry were used for building structures in ancient times [221, 223, 224]. The utilization of pre stressed concrete, modern structural steel, reinforced concrete, and newly established composite (CFST) sections provide various opportunities for long span sections' development and construction. In the seismic architecture of an arch bridge that can involve arch bridges' natural vibration frequencies as well as modal shapes in structural dynamic analysis, arch bridge's natural vibration response has a significant part over the long periods. For longer bridges, the vibration in the lateral direction is more and thus the arch rib must be durable, stronger and stiffer. It is fulfilled by the circular portions of the CFST.

Heavy loading conditions have become the most common columns of CFST, seismic resistant structures which are exposed to bridge piers, extreme flexural loads which make susceptible to traffic impact, columns for supporting railways decks, large sized storage tanks

and high-rise office buildings. Due to the composites between the steel tube and the central concrete, the CFST composite portion provides improved rigidities during an earthquake. In a composite structure, the circular tubular portion of the concrete filled steel is becoming more common in structures. It is because of its excellent resilience to earthquakes including large energy dissipation capacity, high ductility and high strength. Due to the joint influence of the rolled steel tubing and the foundation concrete, the construction of the CFST during an earthquake helps these two components to easily boost compressive strength and structure ductility. In Brazil, Japan [216], and many other countries the CFST structure is commonly used in bridges, viaduct and high-level construction projects.

In recent decades, the CFST use has grown significantly, that is significantly used in bridges and high-rise buildings construction. Various applications involve office blocks, subways, electricity transmitting poles, or industrial buildings [57].

In China there exist various examples that shows CFST columns use in high-rise buildings [24]. Shenzhen's SEG Plaza is China's tallest building, which has used such composite columns, having 361m total height, four-level basement as well as is a 76-storey office block. It has used circular shape CFST columns with 900-1600mm diameters. During this building's construction, nearly 2.5 storey were established/week that represents this technology's efficiency. One more example is WISB (Wuhan International Securities Building) that used rectangular and square CFST columns sections and its height is 249.2m.

Also, in bridge construction, the CFST sections use is very widespread [57]. Until now, in China, more than 100 bridges were built using this type of composite parts. One significant benefit provided in this application by concrete filled steel tubes is that hollow tubes can be used as the coatings to cast concrete when erecting, thereby lowering building costs. Moreover, because of the tubular components' excellent stability, the arch can be constructed without constructing an auxiliary Bridge.

Also, in Japan, there exist various applications, as in present time buildings are being constructed using CFST columns [231,232]. Referred publications list a few design examples being built in Japan from 1993-2004 that uses CFST columns with no external fire protection.

In Japan various buildings are constructed by use of CFTS columns, few of them are: the ENICOM Computer Centre (Tokyo), the Nakanoshima Intes Building (Osaka) and the Mitsui Soko Hakozaki Building (Tokyo) [59]. In 1st example, required external fire protection

thickness was decreased as concrete with fire resistant steel is used for filling the square hollow section columns. The 2nd example is a 22-storeys office building that used 600 and 850mm width or diametric square and circular concrete filled tubular columns. The 3rd example is 19-storeys high-rise residential building comprising 600×600mm square shaped CFST columns and additional external fire protection is used in this.

Canada and United States also represents some construction examples where CFST is used [60]. In "Museum of Flight at King County Airport (Seattle, Washington)" for exhibit hall's roof supporting columns utilizes Bar-reinforced concrete filled hollow sections that allows in achieving essential fire resistance excluding the sprayed fire protection need, therefore, an aesthetic finishing is provided, simultaneously space utilization is minimized as well as natural light's clean entrance is allowed. "St. Thomas Elementary School (Hamilton, Ontario)" is another example wherein different concrete strength concrete filled CHS (circular hollow section) columns were utilized that helps in acquiring slender members with essential 1H fire resistance ratings.

In Europe, the recent advances in the knowledge of these structural solutions and their technology have derived in a growth in the use of concrete filled tubular columns in new buildings. Good examples of practical applications can be found in London [61]. Among these, the below constructions should be necessarily mentioned: Queensberry House, the Peckham Library, the Montevetro apartment block and Fleet Place House. The Queensberry House comprises of 6 storey commercial and office block that used concrete filled CHS columns with a tube-in-tube system (323.9×6.3mm inner tube and 457×10mm outer tube in a typical case). In the Peckham, concrete filled CHS columns supported its front that has 323.9mm diameter, and an irregular façade is formed. In figure1.5 (d) showing the Montevetro apartment block on the facade concrete filled CHS columns were utilized, with 355.6mm external diameter and 244.5mm sections. Lastly, Figure 1.5 (a) representing Fleet Place House is 8-storey office block that utilized 323.9mm external diameter circular CFST columns filled with C40 to C60 grades concrete. On the buildings every longitudinal external face column was arranged such that the inside has clear spans.

In the United Kingdom, the Rochdale Bus Station and Darlington Memorial Hospital are also constructions example with concrete filled members, here RHS columns were used [59].

Square and circular bar-reinforced concrete filled hollow section columns were utilized in the Tecnocent Building (Oulu, Finland). The "Amsterdam Mees Lease Building" is an

example in Netherlands that is 4 storey office building, utilizing CHS columns of 323mm filled with concrete combining with concrete encased HEA beam [59]. In Villebon-sur-Yvette (France) situated Microsoft Head Office, tubular columns variety filled with concrete was utilized.

(a) Fleet Place House (London, UK)　　　　　　(b) City Gate (Dusseldorf, Germany)

(c) Millennium Tower (Wien)　　　　　　　　(d) Montevetro Apartment

Figure 1.5 Some examples of construction with CFT columns (Source: Google image)

DEZ car park in Innsbruck and Figure 1.5 (c) representing Millennium Tower in Wien, a 55 storey high-rise building, both in Austria, are efficient construction examples in which concrete filled tubular columns are utilized combining with another composite element.

Figure 1.5 (b) representing the Dusseldorf (Germany) City Gate which is two 16-storey towers high-rise building wherein a 3-storey attic is utilized for connecting these towers to a

17

portal. 90cm, 55cm and 40cm diameters concrete filled hollow sections columns were utilized combining with concrete partly enclosed beam.

In Australia, in addition to a straining system that resists side forces from wind and earthquake, having a 406mm CHS diagonals diameter, a riverside office building with concrete filled CHS bar-reinforced columns 600mm diameter has been needed for 120 minutes to meet fire-resistance [59].

In certain bridges types, including truss bridges, suspension bridges, cable stayed bridges and arch bridges, CFST members have been used. Members of CFST can be function as arches, bridge towers and piers, as well as in the bridge deck systems. The CFST members' usage in different bridge systems is represented in Figure 1.6.
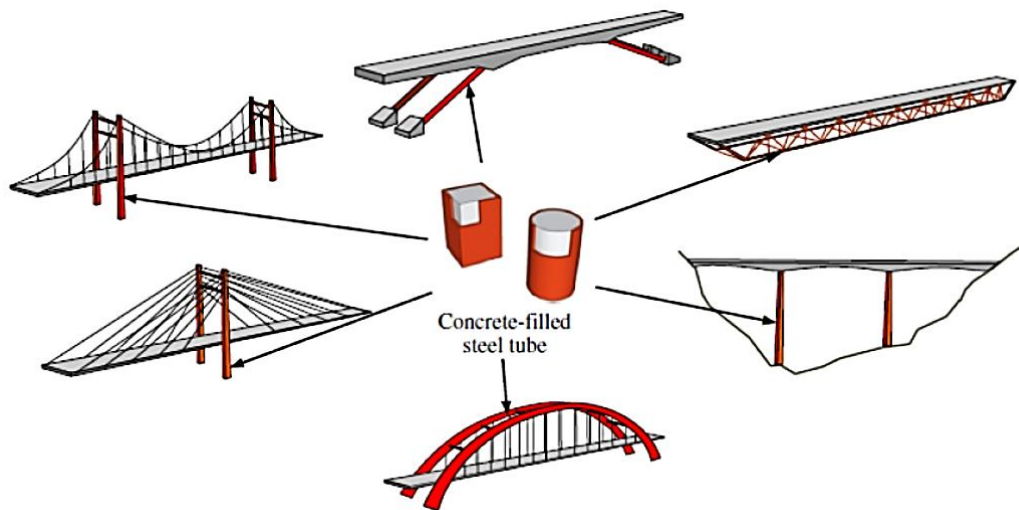
Figure 1.6 CFST utilized in bridges

1.9 CFST COLUMNS MECHANISM UNDER FIRE

The concrete filling of steel hollow parts gives the columns a higher intrinsic strength in the fire without external protection [59]. This is because, on the one hand, to the heat sink effect that concrete produces in the composite section by having a lower thermal conductivity, and on the other hand to the mechanical contribution of the concrete core, which not only helps to sustain the applied load, but also prevents the steel tube from inward local buckling.

During the first stages of the fire exposure, the steel tube expands faster than the concrete core, in such a way that the steel section carries a higher amount of the applied load. The heat flux is gradually transferred from the steel tube wall to the concrete infill, where due to the lower and much favorable thermal properties of concrete (which presents a low thermal

conductivity), the temperature rise is relatively slow. The strength of steel is beginning to weaken rapidly after such fire exposure times (between 20-30 minutes), because of its high temperature, and therefore the load is steadily shifted into the concrete infill. If the temperature progresses through the concrete core, it loses its intensity before the breakdown happens, either because of global compression or buckling. The axial displacement estimated at the top end of the column can be seen in Figure 1.7.
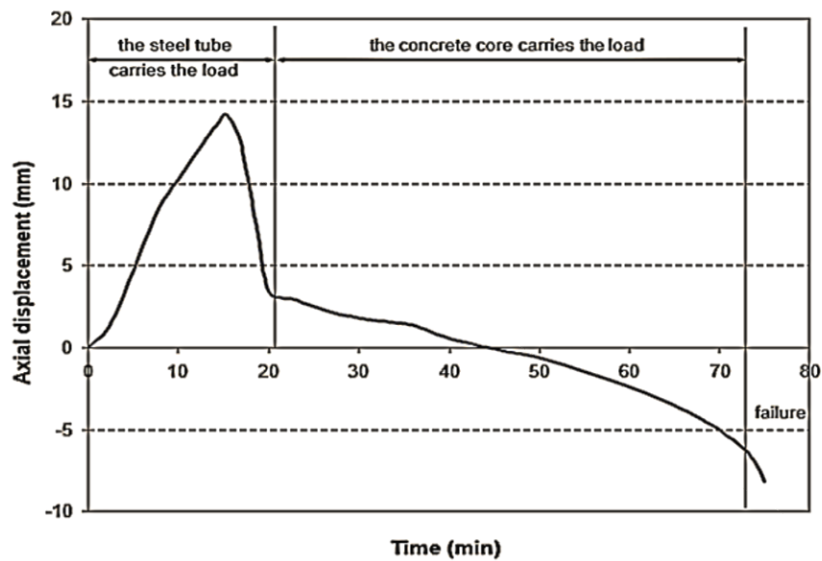
Figure 1.7 Typical behavior of a CFST column subjected to elevated temperatures [59]

In comparison to composite columns' other types, in CFST columns' mechanical properties reduction is slow since this is concrete encased steel sections case, as from direct exposure concrete core is protected by the external steel tube, thus, progressive spalling is prevented [60, 64, 119].

In order to prevent complications resulting from excess inner stresses, it is necessary to remember that at high temperature the moisture found in the concrete core is releasing in the water vapor form, as well as for avoiding various issues resulted due to additional internal pressure, its release must be facilitated [59, 60]. For this purpose, in buildings' each floor, at least 20mm diameter vent holes in columns' bottom and top ends are suggested.

CFST columns have a substantially distinctive heating behavior as compared to empty hollow steel parts (wherein there exists a constant temperature). The material combination with various thermal conductivities – as concrete and steel – contributes to intense transient heating activity in the segment marked by high temperature differentials [59, 123]. CFST columns may

19

be considered having up to 120 minutes or high fire resistance (when sufficient internal strengthening is utilized) with no external protection by using these temperature differentials. Figure 1.8 represents the effect of utilizing various concrete filling types. The concrete core's deterioration was delayed with additional tensile strength by supplying fires resistance up to 3 hours in comparison to the maximum 2 hours for filling with plain concrete (PC) with reinforcing bars (RC) as well as steel fibers [60].
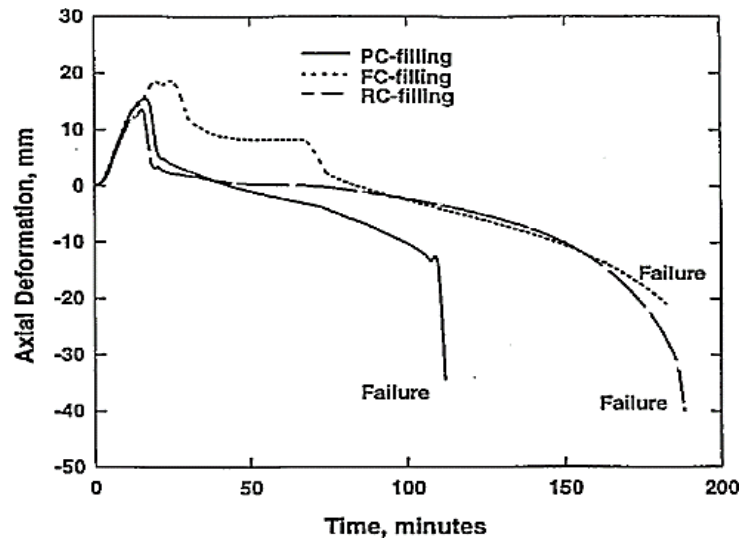
Figure 1.8 Effect of using different types of concrete filling on the fire resistance of CFST columns [60, 61]

Due to the more complex evolution of the temperature field in composite steel-concrete sections, simple calculation models based on the section factor A_m/V cannot be used for the design of CFST columns in the fire situation. Advanced calculation tools which take into account the time dependent thermal properties of the materials and the resulting thermal transients are needed instead.

The CFST column's multiple components have varying strength reduction thresholds during the fire exposure duration based upon their individual place in the cross section [59]. The steel tube, which is immediately exposed to the fuel, heats up quicker and hence greatly decreases its resistance effects after a limited time. The concrete core, in turn, preserves, for a prolonged duration, room temperature strength's greater proportion with low thermal conductivity and high massiveness, particularly in areas near the section's center. When reinforcement bars are utilized, they are generally placed on the exterior wall, although covered by the concrete cover thickness and the outside steel tube. Hence, there exists their strength's slow reduction. It has been represented by the Figure 1.9 that characterization of this behavior is shown by composite section's various components' strength degradation. Therefore, it can

20

be shown that a CFST column's fire behavior is represented as each components' evolution consequence.
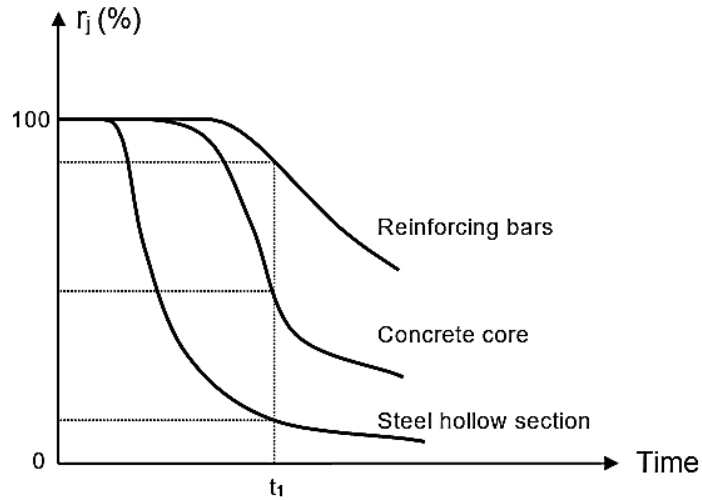
Figure 1.9 Evolution of the strength of the different components of a CFST column [59]

The column cross-section's load-bearing capacity R is stated as its components' r_j capacities sum [59]. The different components' capacities in the fire situation depending on the time of fire exposure t,

$$R(t) = \sum r_j(t) \tag{1.1}$$

At room temperature, the steel tube is likely to be the dominant component of the section, due to the higher strength of steel and its location within the cross- section. Nevertheless, after a certain period of time t_1, only a small percentage of the original capacity of the steel tube remains. This means that, in the fire situation, the amount of load initially sustained by the steel tube will be redistributed to the concrete core, which loses its strength and stiffness at a slower rate.

High resistant capacities with reduced cross-section dimensions can be conveniently accomplished in the room temperature architecture. However, reduced dimensions typically restrict the structural element's fire resistance. Since a minimum column cross-sectional dimension is needed to attain the necessary fire resistance, as the strength decrease in the various sectional components are directly influenced by their relative thermal heating [59].

The material's stiffness and strength decrease as the temperature is elevated, and the structural element's load-bearing capability decreases simultaneously when there is increase in its deformation. The column slenderness must also be considered in the fire configuration.

21

Three different models are required for defining the structural element's fire resistance, these are: a structural model, a heat transfer model and a fire dynamics model. Every model presents a stage where problem is sub-divided: the stress analysis, the heat transfer analysis and the fire dynamics analysis, wherein at elevated temperature the mechanical response can be acquired. Every analysis stage's theoretical background must be overcome in order to predict a CFST column's fire resistance is explained in the following sections.

1.9.1 Fire dynamics analysis

The fire dynamics model allows obtaining the elevation in temperature with time that is developed in compartment wherein structural element is situated that is based on insulation conditions, ventilation and fire load.

An actual fire in a building increases and reduces as per the energy and mass balance in its originated compartment. The energy released is based on the combustible materials' type and quantity as well as compartment's present ventilation conditions.
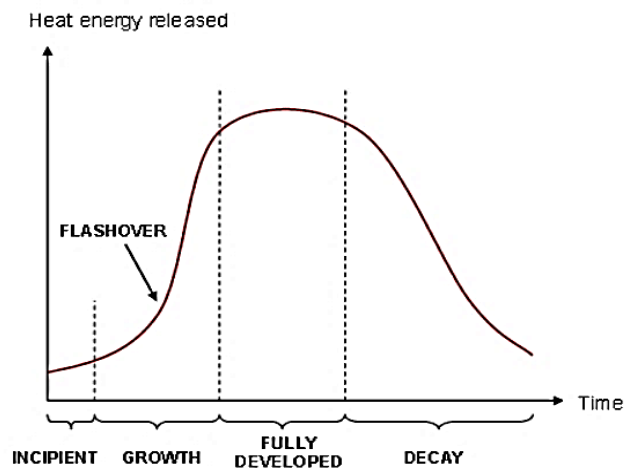
Figure 1.10 Different stages in the fire evolution

There exist four stages in the fire evolution, which are: incipient, growth, fully developed as well as cooling or decay stage (Figure 1.10). Following a rapid generalized ignition point or a flashover, the quickest increase in the temperature happens, where much of the fuel is accidental burning out inside the compartment.

Various natural fire models are included in Section 3.3 of Eurocode-1 Part 1.2 (CEN 2002): simplified models for localized fires or compartment fires as well as advanced fire models that are defined in detail in referred code's Annexes.

Because situations vary in all fires as well to be able to compare and distinguish or validate

the efficacy of the various structural solutions, a standard fire model is widely used that is defined by a temperature curve that increases fire exposure duration, irrespective of compartment situations as well as the fire load degree.

The structural element's fire resistance in several building code is dependent on its efficiency when it is exposed to a fire pattern that follows an accepted international temperature-time curve specified under the ISO 834 (ISO 1980) standard and does not reflect a practical fire. It is distinguished by the steadily rising, but reduced, gas temperature. This curve became a typical pattern for measuring the reliability of structural elements at fire in laboratories. The time obtained during the fire resistance test does not reflect the real-time resistance of the structural feature before its final failure, but rather provides a relative measure and serves as an indication of how serious the fire can be.

EN 1991-1-2 (CEN 2002) Section 3.2 describes nominal fire curves are conventionally agreed curves that are utilized for classifying or verifying the structural element's fire resistance. Among them, the hydrocarbon curve, external fire curve and ISO 834 curve or standard temperature-time curve can be found.

Eurocode-1 Part 1-2 (CEN 2002) Section 3.2.1 describes standard ISO 834 curve as well as its formulation is as:

$$\theta_g = 20 + 345 log_{10}(8t + 1) \tag{1.2}$$

Where, θ_g representing fire compartment gas temperature (℃) and t representing time (min).

Exterior structural elements can be subjected to fire through enclosure building's openings if they are outside the building. There are times where the gas temperature that impacts the member decreases for a brief period of time, at which time a particular temperature distribution known as the "external fire curve" could be utilized.

In such cases, wherein materials' storage having higher calorific values results in serious fires (for example, in petrochemical plants), then they utilize the hydrocarbon fire curve.

The three-nominal temperature-time curves are shown in Figure 1.11 and described in Section 3.2 of Eurocode 1 Part 1-2 (CEN 2002). EC1 Part 1.2 (CEN 2002) presents the parametric temperature-time curves, which are obtained from realistic fire models, with heating and cooling phases and considering specific physical parameters which define the conditions

23

in the fire compartment, as the fire load density, the area of openings and the thermal properties of the compartment itself.
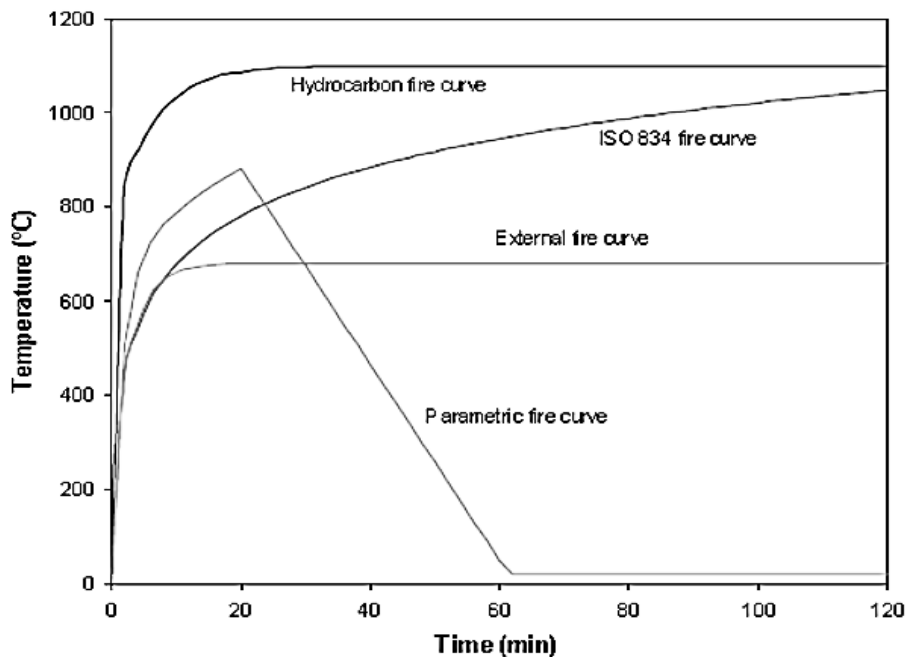
Figure 1.11 Different fire curve types

Also, in Eurocode-1 Part 1.2 (CEN 2002) Section 3.3 natural fire models use is allowed, depending on the problem's certain physical parameters. There exist 2 types of fire models, one is simplified fire model in which ventilation conditions and fire load density are considered, other is advanced fire model which also considers other parameters like the energy exchange, the mass exchange and the gas properties. Further there exist 3 models among second category, which are: 1-zone model, 2-zone model and CFD (computational fluid dynamics) model. In the compartment, a time-dependent, uniform temperature distribution is assumed in one-zone model. Further, lower and upper layers with time dependent uniform temperature and time dependent thickness are considered in two-zone model. Lastly, CFD model provides complete space and time dependent temperature evolution in the compartment.

1.9.2 Heat transfer analysis

The heat transfer model attempts to achieve the distribution of temperature at a time when the member's fire resistance is tested. The material's thermal properties are temperature dependent, as well as thus the issue is incredibly non-linear.

24

Numerical modelling software (depending on either finite elements or finite differentials) is commonly used to estimate the evolution of the temperature field with time of fire exposure otherwise the differential heat transfer equation has to be analytically resolved and this is tedious and difficult to achieve.

The structural member's thermal analysis is categorized in two parts: the heat transfer to the exposed surface from the fire that is radiative and convective heat transfer mechanisms' combination, as well as conductive heat transfer in structural element itself for whose evaluation for heat conduction Fourier differential equation is used.

Conduction can be described as "the transfer of heat from one point to another through a solid or fluid due to the temperature difference". Here, the transfer of heat is observed at molecular levels, and material's net mass movement is not associated. The Fourier's law of conduction equation is used for describing the heat transfer type and is articulated as:

$$q = -\lambda \nabla \theta \tag{1.3}$$

Where, q represents heat flux vector/unit surface, λ represents thermal conductivity tensor as well as θ represents temperature.

The energy conservation equation describes:

$$\rho c \frac{\partial \theta}{\partial t} = -\nabla q + Q \tag{1.4}$$

Where, σ represents density, c represents specific heat, t represents time and Q represents internal heat generation rate/unit of volume.

The material's specific heat may depend on temperature that in this equation presents a non-linearity. Substituting eq. (1.3) in eq. (1.4), result in:

$$\rho c \frac{\partial \theta}{\partial t} = \nabla(\lambda \nabla \theta) + Q \tag{1.5}$$

Eq. (1.5) represents conductive heat transfer equation and for solving this equation, initial conditions as well as corresponding boundary conditions are set up. The initial condition comprises of temperature specification at the initial time. In the fire exposed surface, boundary

conditions are provided by the thermal loads application depicted henceforth, as surface is applied with a net heat flux.

On the exposed surface, boundary conditions are Neumann type that indicates the temperature's normal derivative, i.e.:

$$\lambda \frac{\partial \theta_m}{\partial n} = h_{net} \tag{1.6}$$

Where, n represents normal to the surface as well as h_{net} represents net heat flux/unit surface.

It has been noted that both equation (1.5) and (1.6) exposed surface boundary conditions are nonlinear. Firstly because of specific heat and thermal conductivity variations with the temperature, secondly because of radiation components that indicates temperature's nonlinear term. It clearly elucidates why for solving such heat transfer problem numerical methods are utilized generally.

1.9.3 Thermal boundary conditions

Various thermal loads that are considered while achieving heat transfer analysis are described in the Section 3 of Eurocode-1 Part 1.2 (CEN 2002).

Two distinctive heat transfer modes, which are: radiation (h_{net}, r) and convection (h_{net}, c) are considered for determining the net heat flux (h_{net}), on surfaces that are exposed to fire.

$$h_{net} = h_{net,c} + h_{net,r} \quad (\text{W/m}^2) \tag{1.7}$$

Convective heat transfer, also known as convection, is heat transfer from one place to other through fluids movement, a process which is basically heat transfer through transfer of mass. During natural or free convection, buoyancy forces cause fluid motion which resulted from variations in densities because of fluid temperature variations.

The following expression presents the net convective heat flux component/unit surface:

$$h_{net,c} = \alpha_c(\theta_g - \theta_m) \quad (\text{W/m}^2) \tag{1.8}$$

Where, α_c represents heat transfer coefficient by convection (W/m²K), θ_g represents gas temperature in the fire exposed member vicinity (ºC) and θ_m represents member's surface temperature (ºC).

The heat transfer coefficient through convection has 25W/m² K value if we utilized external or standard temperature-time curve, when parametric fire curve is used it is 35W/m² K as well as in hydrocarbon temperature-time curve it is 50W/m² K.

On separating members' unexposed side, by utilizing $\alpha_c = 4$ W/m²K, the net heat flux is concluded. Through convection, heat transfer coefficient is considered as $\alpha_c = 9$ W/m²K, while it has been assumed that it comprises the heat transfer effects through radiations.

Radiation is defined as "the transfer of energy to or from a body by mean of emission or absorption of electromagnetic radiation". The propagation of thermal radiation takes place through the vacuum of space without any matter presence. The following expression provides net radiative heat flux component/unit surface as:

$$h_{net,r} = \emptyset \mathcal{E}_m \mathcal{E}_f \sigma \lfloor (\theta_r + 273)^4 \rfloor \quad (W/m^2) \qquad (1.9)$$

Where, $\emptyset$ represents configuration factor, $\mathcal{E}_m$ represents member's surface emissivity, $\mathcal{E}_f$ represents fire emissivity, σ represents Stephan-Boltzmann constant, whose value is 5.67×10^{-8} W/m²K⁴, θ_r represents fire environment's effective radiation temperature [ºC] and θ_m represents member's surface temperature (ºC).

As stated by EN 1991-1-2 3.1(7), the configuration factor is considered to be unity. A low value is selected for considering the shadow and position effects. A method is provided in EN 1991-1-2 Annex G for configuration factor's calculation.

In the Eurocode-1 specific materials for fire construction, a $\mathcal{E}_m = 0.8$ value can be utilized, as defined in EN 1991-1-2 Clause 3.1(6). It has been stated by Section 2.2(2) EN 1994-1-2 that for concrete and steel, the emissivity coefficient associated with the member surface must be $\mathcal{E}_m = 0.7$. Generally, the fire emissivity is considered as $\mathcal{E}_f = 1.0$.

According to EN 1991-1-2 3.1(8) (CEN 2002), the radiation temperature surrounding the member is equal to the gas temperature outside the member, in fully fire engulfed members. Alternatively, already described fire models or nominal temperature-time curves can be used for providing gas temperatures.

1.10 CONCRETE FILLED STEEL TUBE BEHAVIOR UNDER LOADING CONDITION

When load is applied over the CFST sample the steel and concrete both take up the load for bearing however each material has its own capacity to bear different loading. The concrete and steel's Poisson's ratio are 0.2 and 0.3 respectively. Initially under compressive stresses in steel tube the lateral strain is greater in comparison to concrete. Because of such separation of concrete from steel tube starts. After a certain level strain, due to micro cracking in the concrete longitudinal strain in concrete starts increases until it reaches the longitudinal strain in steel tube. At this stage the steel expansion remains constant but the dilation of concrete has commenced. Due to which the concrete is now in tri-axial state of compression. Now, it is still under discussion that at what strain value does the confinement of concrete starts. Some scientists [30, 192, 233] believe concrete confinement happen suddenly when it reaches the value of strain of 0.002. On the other hand, some [116, 130] believe confinement steadily increases after occurrence of micro cracking in concrete strain 0.001 till full confinement at strain 0.002. Reference [31] demonstrated the bond behavior among steel and concrete tube in the CFST sample.

It has been observed that the bond strength present between the two materials that are concrete and steel tube get enhanced considerably by welding internal ring onto the inside tube surface followed by the welded shear studs onto the same. The bond between the tube and concrete core becomes less with age and dimensions of CFST specimen. This study also concluded that the bond among concrete as well as steel tube is 32% to 69% is less than that of concrete and carbon steel tube because of steel's smoothness. The average maximum bond stress for the specimens with shear tabs is significantly higher, being more than four times that of the specimens without shear tabs with the same section dimensions and material properties. This is consistent for both square and circular hollow sections and demonstrates favorable effects of the shear tabs in increasing the bond loading capacity as explained previously. In general, the maximum bond stress is higher for columns with smaller dimension-to-thickness ratios (H/t or D/t). This is attributed to the fact that reducing the H/t or D/t ratio improves the confinement effect, hence at the steel-concrete interface contact pressure is increased, and thus results in higher bond stresses.

There are two reasons for lateral pressure in steel tube.

1. Longitudinal stress from loading (Poisson's effect).
2. Lateral stress from concrete dilation.

Due to this biaxial state of stress in steel tube steel usually yields before its normal yield stress which decreases the total yield of the composite. On the contrary, the confinement of concrete infill in steel tube increases the axial capacity. Despite the decrease in axial capacity of steel tube, the increase in capacity of concrete core is far greater which increases the total resultant yield capacity of the composite.

1.11 FAILURE MODE OF CONCRETE FILLED STEEL TUBE COLUMN

For various type of materials used in CFST the specimen failure mode is different as presented in Figure 1.12 and 1.13. The most common failure is the local buckling in steel tube. The local buckling occurs in hollow steel tube by part steel tube going inwards. The concrete infill pushes the steel outwards instead of inwards which interrupt the steel tube's local buckling.
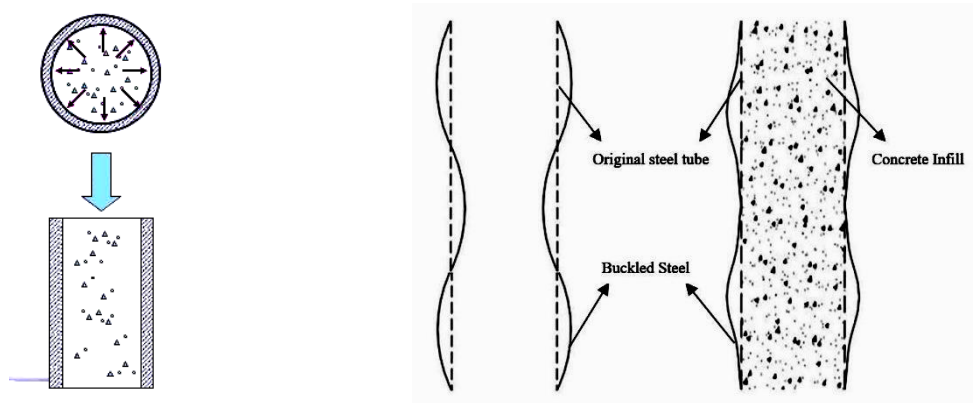
Figure 1.12 Failure comparison of CFST column (Source: Google image)

Due to this delay in buckling the overall axial capacity of CFST sample increases.

1) This type of failure helps in interrupting steel tube buckling which keeps it in the elastic range of stress strain curve.
2) The steel tube's outward buckling allows buckling to spread over a large area hence preventing the strain concentration at one place.
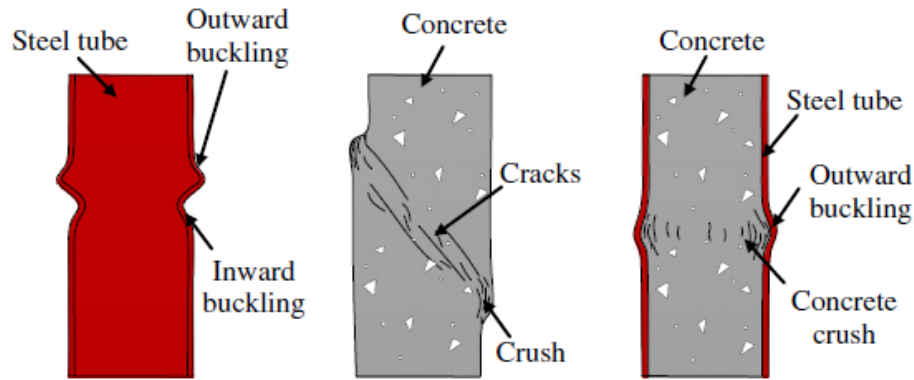
Figure 1.13 CFST column failures [4]

1.12 BOND BEHAVIOR BETWEEN CONCRETE AND STEEL

Concrete being a brittle material is weak in tension and strong in compression whereas steel is a ductile material and strong in tension. When in these two materials' CFST composites tensile stresses is applied, than in comparison to concrete, steel has greater ability showing more lateral strain (Poisson's effect). A study conducted on the debonding effect on circular CFST columns as well as determined that in comparison to specimen without debonding, much more severe local buckling phenomenon is found in debonding specimen of circular steel tube [32,115]. In CFST, bond behavior was also studied by accomplishing a number of push-out tests on CFST specimens [126, 236]. The bond among steel and concrete is due to the three reasons:

1) Chemical adhesion between concrete and steel (Part-A micro locking)
2) Due to the roughness of the surface of steel (Part-B loss of bond)
3) Due to the frictional resistance (Part-C macro locking)

As shown in Fig. 1.14 the first part of the curve is linear and is due to the chemical adhesion between concrete and steel. This chemical adhesion is responsible for resisting the relative displacement or slip. After a certain value of relative displacement (slip), the bond between concrete and steel breaks and the load is transferred through the rough surface of steel and frictional resistance between them [31]. Furthermore, it was concluded that between steel tube and concrete, the bond strength is improved providing the welded steel rings on the steel tube's internal surface [33, 58]. Expansive concrete and welding shear studs have also been proven to be good methods for bond strength improvement after welding internal steel rings.
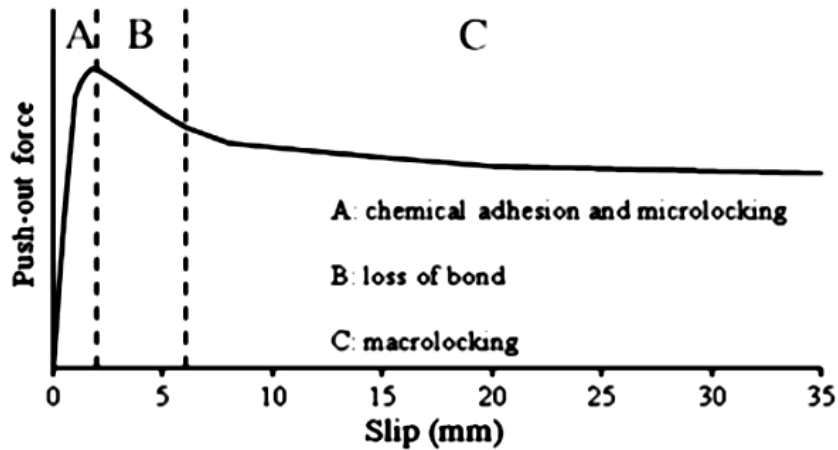
Figure 1.14 Idealized bond behavior between concrete and steel [67]

Bond strength acts essentially on stress transferring among the steel tube and concrete core in the CFST column. It plays important roles on preventing steel tube from local buckling, providing permanent formwork, offering steel-concrete bond strength that make sure the two different component work compositely to resist the external different loadings of tension, torsion, shear, and bending moment. Thus, this bond strength is important to the structural behavior of CFST columns.

Figure 1.15 compares the ultimate bond strengths at different temperatures. It shows that the ultimate bond strength of CCFST columns is larger than those of SCFST at low temperatures. For the prepared ten specimens, the ultimate bond strength of circular CFST is averagely 46% larger than that of SCFST. This difference tends to be larger for the CFST designed with thinner steel tube and low grade NWC, e.g., the ultimate bond strength of specimen C7 with 2.75 mm thick steel tube is 2.14 times of that for specimen S7. This is because the circular shape of steel tube transfers the steel-concrete interfacial bond stress more effectively than the square steel tube. At the working state, the steel tube tends to suffer outward pressure and vertical compression. Outward buckling more likely occurred to the flat side plate in square steel tube than circular steel tube, which results in separation at the interface of steel tube-concrete as well as reduced ultimate bond strength. The bond stress in square CFST columns were thus mainly taken by the corner regions in square CFST columns. This phenomenon tends to be more serious for the square steel tube with lower thickness and suffering larger bond stress. This may explain the large circular-to-square ratios of ultimate bond strength in specimens C3-4, C7, and C8 [19].

31
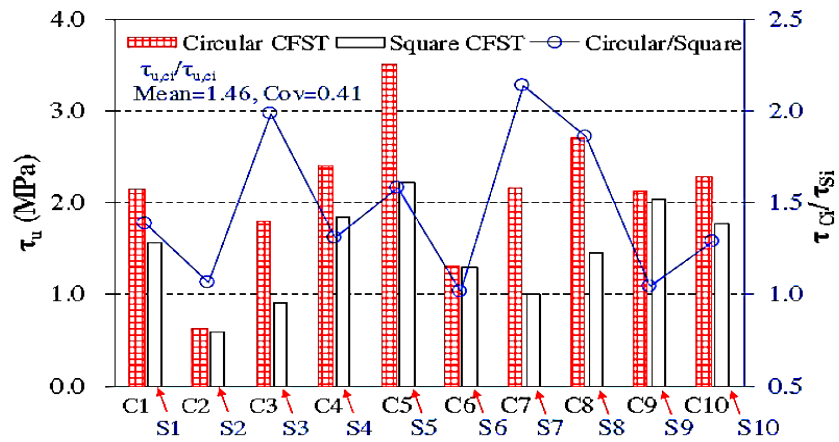
Figure 1.15 Comparisons of ultimate bond strength between circular and square CFST

Columns [19]

1.13 THESIS OUTLINE

There are five chapters in this thesis. Every chapter's summary is provided as below:

Chapter 1 provides introduction to the research topic. The research program's primary objectives as well as motivations are proposed.

Chapter 2 comprises of the review of literature; which determined the material behavior under high temperature condition. The CFST behavior at elevated as well as ambient temperatures is elucidated.

Chapter 3 depicts experimental program in detail as well as FE model built to simulate CFST columns through model comparison results with the experimental program's test results. This chapter also presents the strength aspects of Concrete Filled Steel Tube Columns through design codes. For such aim, a comparison among designs codes such as AISC-LRFD, ACI, AS, Eurocode-4 and CECS 28:90 was implemented in the CFST columns' axial compressive strength evaluation.

Chapter 4 gives the results and discussions drawn from this research. This chapter also provides concrete-filled columns' fire resistance design guidelines.

Chapter 5 provides the conclusion which has been concluded from this research, as well as recommends future work which can be accomplished.

CHAPTER-2

LITERATURE REVIEW

2.1 GENERAL

This chapter gives a detail review of literature of the thesis on the matter of performance of concrete-filled steel tube columns before and after exposure to fire, comprising background of material properties, behavior of CFST column at ambient and elevated temperature, research gap, objective, as well as the scope of this work.

2.2 INTRODUCTION

In construction industry, the selection of a building material depends on various factor including workability, durability, structural strength and availability. But the natural building material does not possess each and every property to required level. It is very important therefore that suitable materials be chosen and combined to form a new element, which would produce a composite element and its desirable properties. The membership of CFST is the revolutionary concept for a steel component to work in conjunction with a concrete part to withstand both axial and bending loads. Because of a range of factors, technical unsatisfactory infrastructure including concrete filled tubular structures and metallic structures is not being met and CFST structures in many cases bear loads well beyond their construction specifications but remain in place due to their conservative design through modern standards. Therefore, the load bearing capability must be restored or strengthened and the systems must last longer. Various innovative applications for concrete structures were discussed, but in steel structures they were constrained.

In this regard, the literature has been studied for understanding the CFST columns behavior under axial loadings in ductility index, secant stiffness, residual strength index, ultimate load capacity and load-deformation pattern terms. Thus, in this chapter relevant study's literature review is presented which gives facts and information related to behavior of CFST column at elevated temperature. Furthermore, CFST's mechanical and characteristics behavior were researched that helps in specifying present study's conceptual and theoretical backgrounds.

2.3 MATERIAL PROPERTIES AT HIGH TEMPERATURES

The main focus of this section is to review the steel and concrete's mechanical and thermal material properties at high temperatures.

2.3.1 Concrete

2.3.1.1 Density

In general, concrete density reduces as the temperature rises [79, 80, 81]. Concrete density (ρ_C) at high temperatures primarily depends on the temperature, curing behavior, moisture content and aggregate materials. The limestone concrete density is approximately constant from the room temperature until, according to heating conditions, the limestone concrete decarbonizes between 600°C-900°C [81]. The concrete density declines substantially after decarbonation due to waste water as well as carbon dioxide depletion by decarbonation. The density is now declining as the temperature increases due to the concrete expansion (increased volume with constant weight). Sintering increases the density then and the melting phase begins to rise at 1200°C [68].

Silicon concrete aggregates (as quartz) have a relatively steep density decline between 20°C-700°C in the temperature range. It is because the silica aggregate has more expansion than the carbonate aggregates [80, 81, 83, 101].
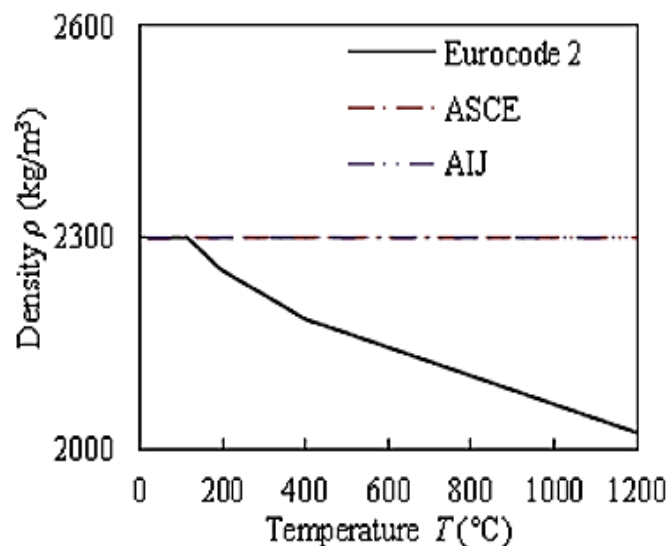
Figure 2.1 Different models for concrete density (Eurocode-2, ASCE, AIJ)

Most analytical models, with the exception of Eurocode-2 (2005), assume that concrete density is temperature-independent. Eurocode-2 (2005) assumes that the concrete density is temperature-dependent, as it is affected by the loss of water from the concrete at elevated temperature. Figure 2.1 shows a comparison between different models of concrete density (Eurocode-2 2005; ASCE 1992; AIJ 1997). As can be seen in Figure 2.1, ASCE (1992) and AIJ (1997) assume that concrete density has a constant value and does not depend on temperature, whereas Eurocode-2 (2005) proposes a temperature-dependent model for concrete density in which the density decreases gradually with increasing temperature.

2.3.1.2 Thermal conductivity

Thermal conductivity is described as the ratio of heat flow rate to temperature gradient, representing uniform heat flow through the concrete of unit thickness over a unit area subjected to a unit temperature difference between the two opposite faces. Concrete contains moisture in different forms; the type and amount of moisture have a significant effect on thermal conductivity [74, 184]. Thermal conductivity does not depend on concrete strength [81].

Important factors influencing the thermal conductivity of concrete are the hardened cement paste, pore volume and distribution, and water content. At low temperatures, moist concrete possesses very high thermal conductivity. At higher temperatures the thermal conductivity increases slightly but decreases as the temperature approaches 100°C, then continues to decrease as more cracking develops [80].
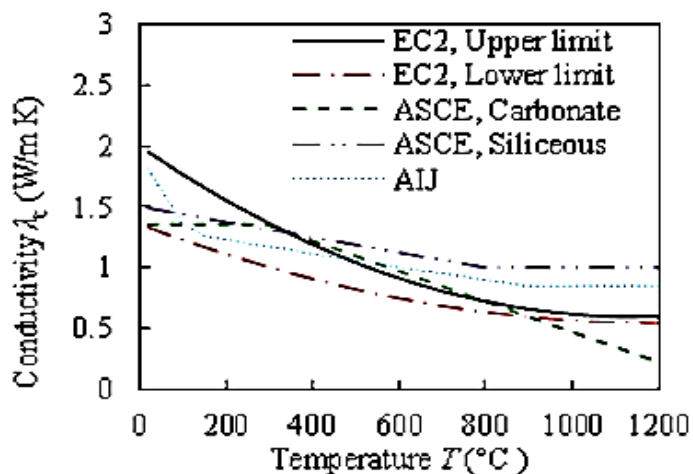
Figure 2.2 Different models for concrete thermal conductivity (Eurocode-2, ASCE, AIJ)

35

In most investigations of thermal conductivity [79, 80, 81, 83, 86, 87, 157], thermal conductivity has been shown to decrease commonly with rising temperature. Figure 2.2 describes multiple models simulating concrete thermal conductivity, in which the ASCE model indicates that there are varying values of concrete thermal conductivity, based on the form of aggregate (siliceous or carbonate). The Eurocode-2 model (2005) (EC2) displays the highest and lowest conductivity limits as well as for CFST columns advises to follow the maximum limits, as they have been reached for composite section test results.

2.3.1.3 Specific heat

It is defined as the amount of heat per unit mass needed to vary the temperature of a material by 1°C, as well as in general, expressed in thermal (heat) capacity that is specific heat and density's product. Concrete's density, aggregate type and moisture content greatly influence the specific heat [80, 81, 86].

The chemically bonded water in the concrete is eventually released at high temperatures as free water that evaporates into a gas mixture. Additional heat is consumed by the concrete during the phase-change step, impacting the temperature in the cement. The basic concrete thermal heat is commonly revised instead of performing complex combined thermo-hydro-mechanical analyses to show this effect when performing analysis for heat transfer.

Figure 2.3 shows multiple models of concrete-specific heat simulation where the ASCE model for concrete specific heat offers different values according to the type of aggregate, while for every aggregates type, EC2 utilizes a single model.

The effects of the content of water in the EC2, shows a specific heat peak value between 100°C-115°C, after that a linear reduction between 115°C-200°C as well as a linear relation among 115°C (Cpeak)-200°C (1000J/kg.K), are taken into consideration. For a water content of 3 percent of weight of concrete, the peak value for 2020J/kg.K is demonstrated, and for 10percent concrete weight, the moisture content is shown at 5600J/kg.K. A linear interpolation is acceptable for other moisture contents. Figure 2.3 shows the peak specific heats.

Also, the release of bond water effect from concrete, evident in Figure 2.3 as for concrete with carbonate aggregate peak value is between 600°C-800°C, as well as for concrete composed of siliceous aggregate it is between 400°C-600°C, are taken into account by the ASCE model.
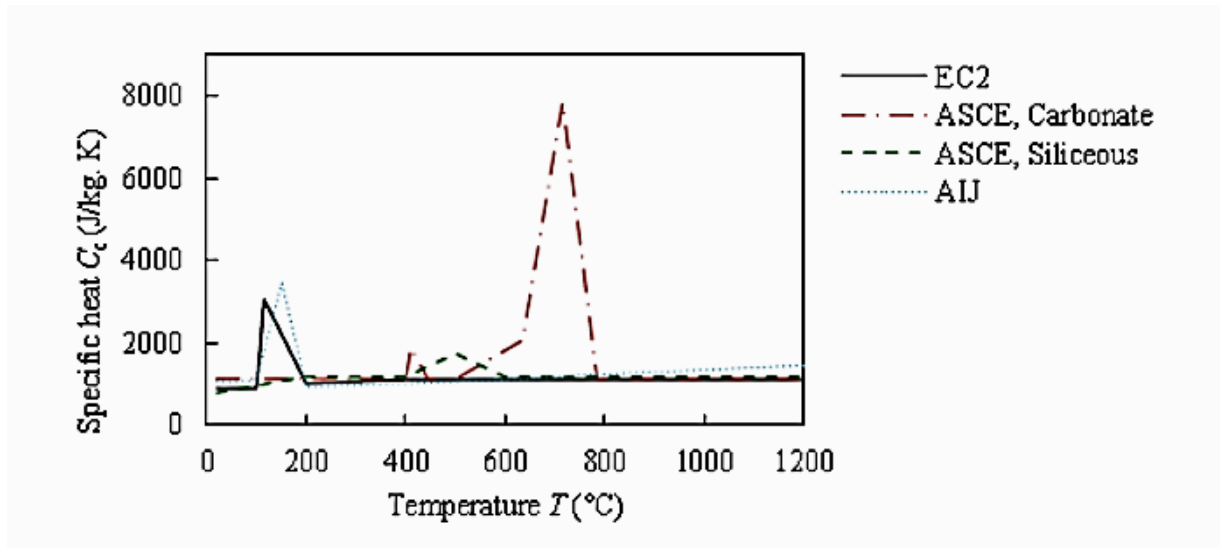
Figure 2.3 Models for concrete specific heat (Eurocode-2, ASCE, AIJ)

2.3.1.4 Thermal expansion

One of the most important factors affecting the performance of concrete in fires is the coefficient of thermal expansion (CTE), which represents the volume change of a material due to temperature change and is expressed as a change in length per degree of temperature change. The importance of the CTE is that it is considered to be a measure of the structural movement and thermal stresses resulting from temperature change that can lead to cracking and spalling.

The thermal expansion of concrete is a complicated phenomenon because of the interaction of its two main components (cement paste and aggregate), each of which has its own coefficient of thermal expansion. A large difference in thermal expansion of the hardened cement paste and aggregate can result in micro-stresses and micro-cracking that disrupt the concrete microstructure. Observations of thermal expansion are complicated by various extraneous effects that accompany the temperature change (e.g., additional volume changes caused by changes in moisture content, chemical reactions leading to dehydration and conversion, creep and micro-cracking resulting from non-uniform thermal stresses) [79,80,83].

For concrete expansion, a constant value is utilized by some investigators [81, 106, 186]. The value of concrete expansion is also assumed by AIJ (1997). Many models like ASCE (1992) and Eurocode-2 (2005) showed that the thermal expansion of concrete is temperature dependent. For concrete expansion ASCE (1992) and Eurocode-2 (2005) demonstrated in Figure 2.4.
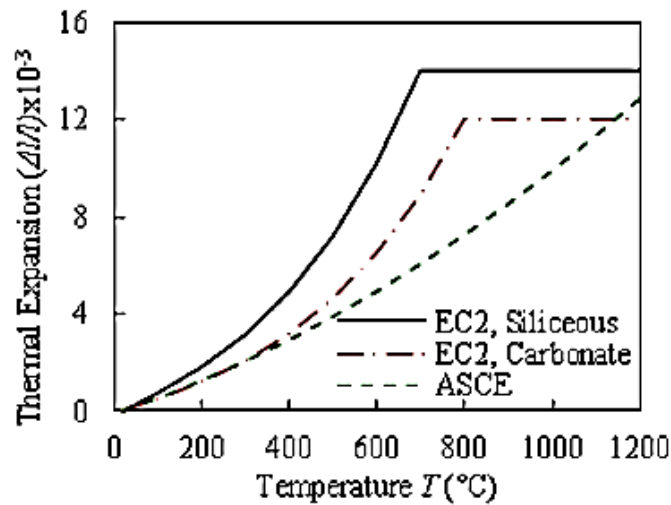
Figure 2.4 Concrete expansion models (Eurocode-2, ASCE)

2.3.1.5 Stress-strain curve

At high temperatures, the stress strain curve of concrete varies from that at room temperature. The elasticity modulus reduces with increasing temperature as well as makes the concrete weaker at times of fire until reaching the peak load [228]. At ambient temperature, the curve's descending branch would be greater. The overall strain is greater than at room temperature [39, 102, 103, 104, 110].

In a fire, concrete behavior is significantly affected by the aggregate. In comparison to the siliceous aggregate concrete, carbonate applied concrete has been reported to be greater resistant of fire [81, 146, 189]. Moisture content is another factor through which concrete behavior is impacted during a fire [69, 74, 79, 83].

Many researchers have concluded that high-strength concrete loses more strength than normal-strength concrete, especially at temperatures below 400°C [83, 84]. This can be explained by the fact that at higher temperatures the tendency of the cement paste is to shrink as the absorption, capillary and hydration water is driven out, but the aggregate expands, resulting in a loss of bond. Thus, in leaner mixes (low cement: aggregate ratio) it is probable that smaller internal stresses develop, therefore resulting in a lower reduction in strength. This temperature-dependent destruction of the cement paste is more significant in high-strength concrete than in normal-strength concrete for two reasons. First, the cement paste matrix of high-strength concrete must carry higher loads than in normal-strength concrete (more homogeneous stress distribution between the aggregate and the cement paste). Because the

cement paste of high-strength concrete is essentially denser than that of normal-strength concrete, it dries relatively slowly at higher temperatures and the so-called 'drying hardening' that is the main cause of the increasing strength in normal-strength concrete between 150° and 350°C does not occur in high-strength concrete.

The second reason concerns the presence of absorbed water at the lower temperatures of 100° to 300°C. When concrete specimens are saturated with water, the water first fills the capillary pores, and the remaining amount is adsorbed between the paste particles; therefore, most of the water present in high-density concrete (with fewer capillary voids than normal concrete) is adsorbed, causing a greater loss of compressive strength. Both of these actions produce larger compressive strength reductions in high-strength concrete than in normal-strength concrete. Concrete spalling is more likely to occur in fires in high-strength concrete due to this loss of water [79, 83, 158, 163]. Figure 2.5 shows the difference between the reduction factors of compressive strength for normal-strength concrete (NSC) and Class 2 high-strength concrete (HSC) as defined in Eurocode-2 (2005). It should be noted that the definitions of NSC and HSC are used as adopted in Eurocode 2. Concrete which has a compressive strength less than 55 MPa is defined as NSC. HSC is divided into three classes (1, 2 and 3). Class 1 is for concrete with a compressive strength between 55 and 60 MPa; Class 2 is for concrete with a compressive strength of 70 and 80 MPa, whilst concrete with a compressive strength of 90 MPa is defined as Class 3.
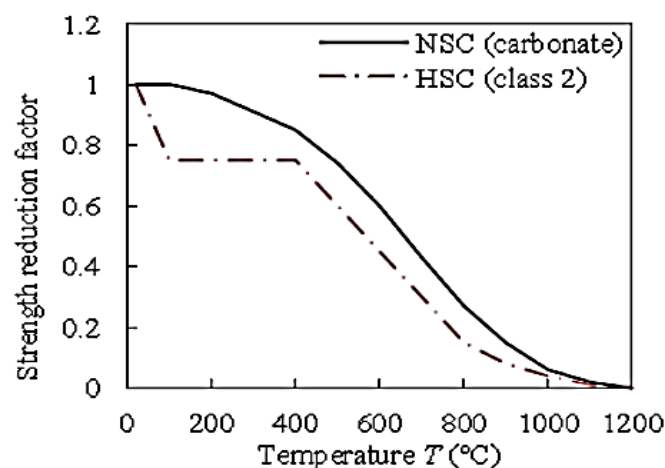
Figure 2.5 Strength reduction factors for different strengths of concrete (Eurocode-2, 2005)

It has been noticed from Figure 2.5 that initially, high-strength concrete loses it strength significantly in the temperature range between 100°C (when the water removal process begins) and 200°C, when the moisture and the absorbed water spread to the outer layer of the concrete section, thus affecting the internal forces throughout the whole specimen and reducing its strength; thus, the higher the original strength of the concrete, the greater its loss of strength. With further increase in temperature the concrete begins to recover and the strength begins to increase due to the general stiffening of the cement gel and the consequent increase in surface forces between the gel particles as the absorbed moisture is removed. The temperature at which the absorbed water is removed and the strength begins to recover depends on the porosity of the concrete.

There is more rapid loss in the strength of high-strength concrete above 400°C. The cement paste dehydration contributes to its slow disintegration at these temperatures. As the paste continues to decrease, and grows with elevated temperatures, the interaction between the paste and the aggregate is decreased and the concrete strength decreases, leading to the different thermal expansion above 100°C temperature [83, 84].

It has also been found that the process of concrete testing affects its residual strength. The compressive strength of hot concrete is higher than its residual compressive strength (tested as the concrete cools) due to the re-absorption of moisture from the atmosphere during cooling, as suggested by the results obtained for different rates of cooling. The hot-strength specimens at the time of testing therefore contained more evaporable water than the specimens tested after cooling [85, 86, 87]. The hot compressive strength tested under an applied load is higher than that tested with no load. A reason for this is that the application of compressive stress during the temperature testing retards the development of cracks in the specimen, which would otherwise be free to propagate in an unstressed specimen [80, 88, 163, 164].

The model of Han et. al., 2007 [43], Eurocode-2 (2005) and ASCE (1992) are the most commonly used models to simulate concrete compressive strength during exposure to fire. Figures 2.6(a)–(c) show concrete strength at different elevated temperatures for these models. The figures are drawn for concrete of 40 MPa cylinder strength.
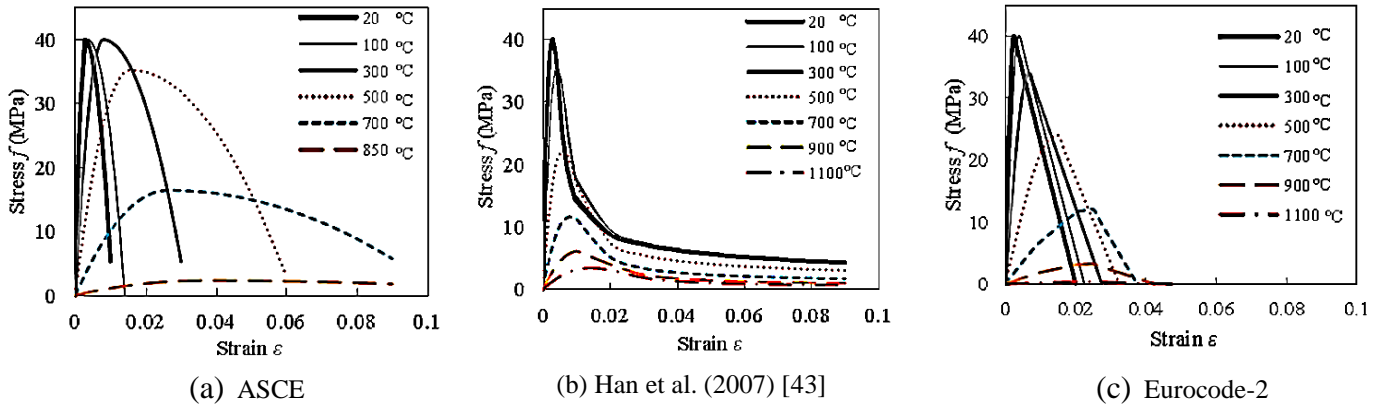
Figure 2.6 Various stress-strain models of concrete at elevated temperatures [ASCE, Eurocode-2, 43]

2.3.2 Steel

The main thermal properties that influence the temperature rise in steel are thermal conductivity and specific heat. There is limited test data available for steel thermal properties, especially for structural steel [70, 81, 204].

2.3.2.1 Density

The density of steel decreases with increasing temperature [81]. This was supported by the test results [4, 5, 91, 165] presented for steel grade SA 533 (Grade B) used in light water reactor. Most of the available numerical models (ASCE 1992; AIJ 1997; Eurocode-3 2005) regard carbon steel density as temperature-independent, and use a constant value of 7850 kg/m3. This assumption is reasonable, because at the steel melting point (1600°C), steel density reduction is only 13% of its ambient temperature density [74, 184].

2.3.2.2 Thermal conductivity

The thermal conductivity of steel is greater than that of concrete. In non-metal materials such as concrete, phonons contribute to thermal conductivity, whereas in metals (steel), both phonons and electrons are responsible for determining the thermal conductivity.

With rising temperature to 800°C, the low alloy steel's thermal conductivity decreases. There is increase in thermal conductivity with rising temperatures in high-alloy steels. This disparity in the low- and high-alloy steel's thermal conductivity is followed by a reduction throughout the crystal lattice with alloy components' increasing proportion, which affect the thermal conductivity' electronic component [81, 83, 204, 232].

For steel thermal conductivity, available models are represented in Figure 2.7 (Eurocode-3 2005; AIJ 1997; ASCE 1992). Similar trends are followed by every model. For a rise in temperature of up to 800°C, steel thermal conductivity reduces and stays steady afterwards.
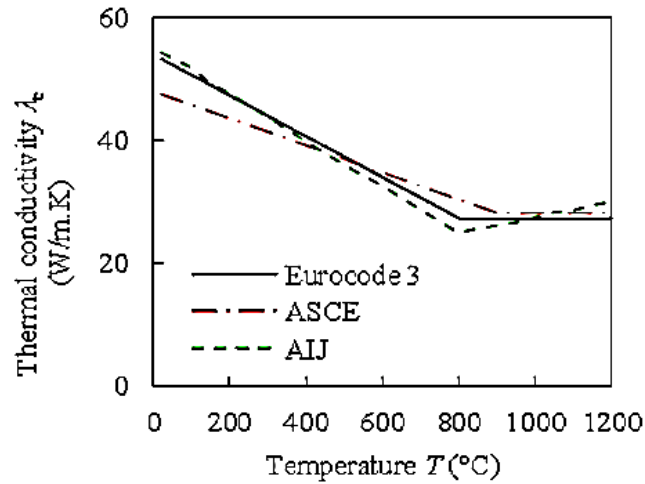
Figure 2.7 Thermal conductivity of different models of carbon steel (ASCE 1992, AIJ 1997, Eurocode-3 2005]

2.3.2.3 Specific heat

Previous test data [79, 166, 184] and models [Eurocode-3 2005, AIJ 1997, ASCE 1992] indicates that with rising temperature the steel's specific heat increases marginally. With temperature, specific heat increase is induced by steel's individual atoms that move apart, therefore high energy states are achieved. The specific heat's high peak value at about 750°C temperature, illustrated in Figure 2.8 is correlated with a phase shift which is caused by the atoms' transition. Great heat amount are absorbed by this process that resulted in peak values [19, 101, 109, 167].
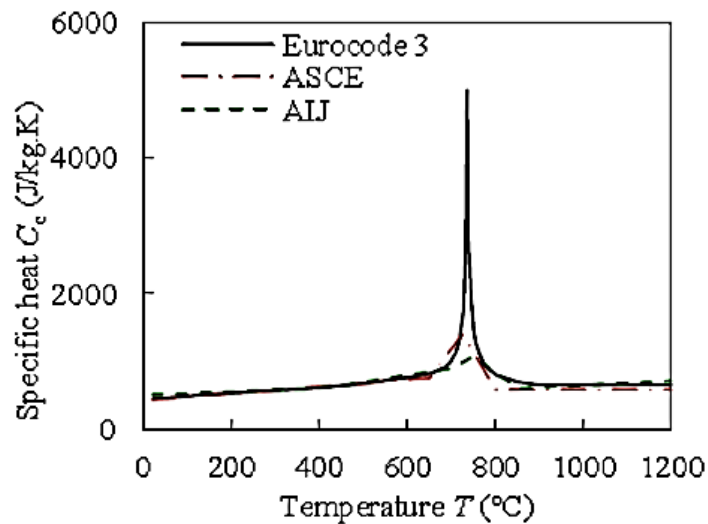
Figure 2.8 Specific heat of different models of steel [ASCE 1992, AIJ 1997, Eurocode-3 2005]

42

2.3.2.4 Thermal expansion

On steel's thermal expansion, there exists several reports. Also, Eurocode-3 (2005) and ASCE (1992) proposed thermal expansion models are represented in Figure 2.9. At 750°C, steel's phase transformation from pearlite to austenite is considered by the Eurocode model. From body-centred to face-centred cubic atomic structure rearrangement is associated with it and between 750°C-860°C a constant expansion value is produced [103, 104, 169].

The thermal expansion is affected by the steel type. [105, 106, 107, 108] showed that the high-strength steel's thermal expansion is low in comparison to both ASCE and Eurocode models prediction which were used for normal-strength steels. It is recognized by high- and normal-strength steel's various chemical compositions.
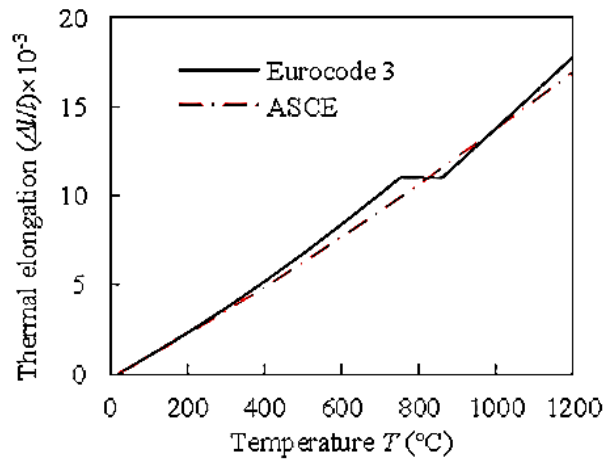
Figure 2.9 Different models for thermal expansion of steel [ASCE 1992, Eurocode-3 2005]

2.3.2.5 Stress-strain curve

At high temperatures, the stress-strain curve of carbon steel is completely dissimilar from the curve at room temperature. With an increase in temperature the modulus of elasticity, the ultimate strength and yield strength decreases. Owing to the atoms' movement and the transition examined above, steel material's fabric degradation can be the product of the increasing temperature and decreased yield strength [109, 170]. At elevated temperature the yield-stress point reduces steadily, rather than the yield point [80, 81] the proof strength is 0.2%. An analysis was carried on the ASTM A992 structural steel's material characteristics at 900°C high-temperature was presented [238]. At up to 900°C temperatures, Steady-state tensile coupon tests were performed. Further at higher temperatures, complete stress-strain curves were acquired. When temperatures as high as 600°C, it was found that yield strength is greatly dependent in a way in which yield strength is described. AISC (2005) and Eurocode-3 (2005) state that yield strength is described as the stress at 2% pressure. When the yield

strength's other description, 0.2% offset, is added, an unacceptable outcome was reached. The results here suggest that in future research additional work needs to be done in this field.

In comparison to normal mild steel, at high temperatures the high-strength steel behavior is different, as determined in the study "the behavior of high-strength steel at elevated temperatures" [79, 81, 198].

It has been observed that modulus of elasticity and 0.2% proof strength reduction factor are same up to 540°C as normal-strength steel. Above 540°C, there exists different situation wherein in comparison to high-strength steel, modulus of elasticity and 0.2% proof strength reduction factor are greater for normal-strength steel.

As shown in Figure 2.10 (a), (b), Eurocode-3 (2005) and ASCE (1992) are two most common adopted models for defining the carbon steel behavior at high temperatures.
It has been observed that between two limits differentiation is provided by Eurocode3, these are: the yield limit and the proportionality limit. In Eurocode3, proportionality limit is described as occurrence at stress-strain curve's linear section's ends, which makes the stress stretching relationship elastic but nonlinear. In Eurocode3, the yield limit is the point after that stress-strain curve turn into both inelastic and nonlinear. In the ASCE model, which takes a sharp point as a limit among the inelastic and linear-elastic material responses, the stress-strain curve of this function does not exist. In the Eurocode3, the idea behind proportionality limit introduction (at higher temperatures) stress-strain curves is to identify viscoelastic activity due in part to the creeping effects. After the proportionality limit, non-linearity suggests that stress after this point produces more strain than the linear elastic ranges. This generalization makes it possible to partially take account of high temperature creep at high temperatures of the Eurocode-3 stress-strain curves.

The disparity between the 2 models comes from the origin of the two models. The Eurocode-3 model depends on a variety of transient test outcomes while the test based on the ASCE model does not have a specific description [110, 208, 175].

ASCE (1992) and Eurocode-3 (2005) are the two most commonly accepted models to describe the carbon steel behavior at elevated temperatures see Figure 2.10(a), (b).

(a) Eurocode 3   (b) ASCE
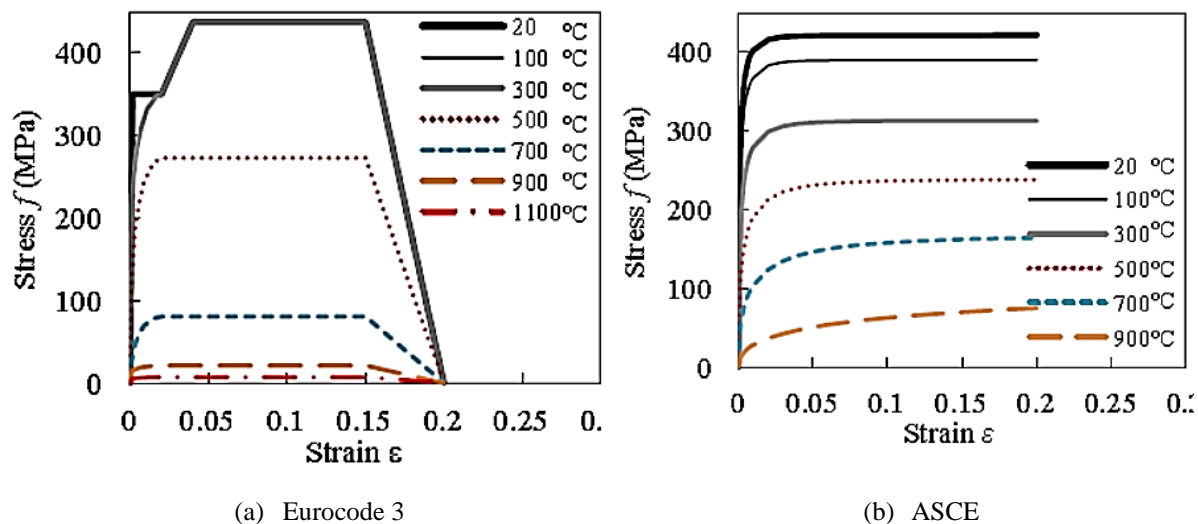
Figure 2.10 Different stress-stain models for steel (350 MPa) at elevated temperatures [Eurocode 3, ASCE]

2.4 BEHAVIOR OF CONCRETE-FILLED STEEL TUBE COLUMNS AT AMBIENT AND ELEVATED TEMPERATURE

Here, an analysis is represented on the CFST columns behavior at high temperatures.

2.4.1 CFST columns at elevated temperature

At ambient temperature, in CFST bond behavior was tested. There have been a total 24 push-out experiments for examining the CFST columns' bond strength with high temperatures, for comparison 16 post-fire specimens and 12 reference specimens at ambient temperature were tested. In this test program various test parameters were investigated, among them primary ones are: applied axial load during heating, hold time heating period (45, 90, 135, and 180 min), temperature levels (20, 200, 400, 600, and 800°C), interface types (interface with an internal ring, interface with shear studs, and normal interface), cross-section type (square and circular sections), concrete type (expansive and normal concretes) and steel types (stainless steels and carbon). Experimental findings reveal that the fire can be completely interrupted in specimens' bonds with standard interfaces. Nevertheless, welding shear studs or internal rings may maintain a bond strength portion in the fire on the steel tube's inner surface [33].
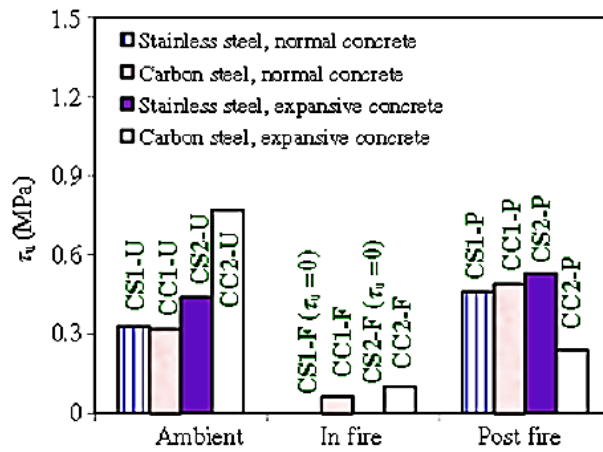
(a) Influence of steel tube type and concrete type for circular specimens
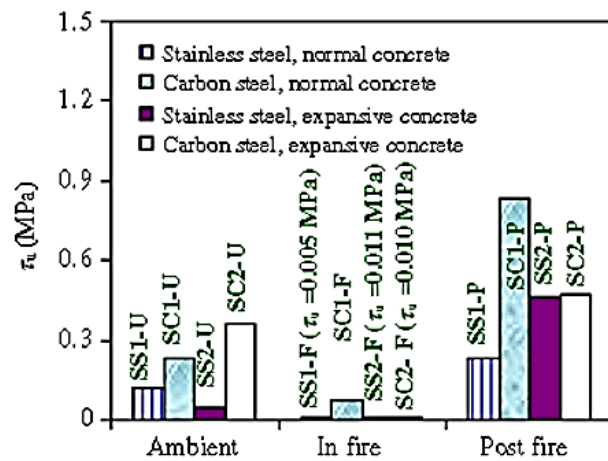
(b) Influence of steel tube type and concrete type for square specimens

Figure 2.11 Influence of steel tube type and concrete type for (a) Circular specimens (b) square

specimens [14]

It has been indicated from experimental results that for each CFST specimen there is negligible bond strength with normal interface while exposed temperature amounted to just 200°C as shown in Figure 2.11. The gap formation between a concrete and steel tube during the exposure to fire is closely related. The stainless-steel specimen's bond strength is typically low at room temperature or after fire than the carbon steel's reference specimen. Nevertheless, the effect of steel form on bond strength was reduced due to the substantial concrete retraction, since the concrete age was comparatively long (over 6months). Expansive concrete has been useful in increasing the bond power of the room temperature in circular columns of CFST [12].

64 CFST columns were utilized for push-out tests that for 90 or 180 min been exposed to ISO 834 standard fire. Simultaneously, for making the comparison preparation as well as testing of 12 unheated specimens was performed. In the bond tests, variables under

46

investigation were: (i) concrete curing condition; (ii) fly ash type; (iii) concrete type; (iv) interface length to diameter (or width) ratio; (v) cross-sectional dimension; (vi) cross-section type; and (vii) fire exposure time. Various parameters' effects on bond behavior were examined. It has been indicated by the test results that bond between its concrete core and a steel tube is significantly affected by the fire exposure as shown in Figure 2.12 (a). In general, after 90 min fire exposure specimens were observed with reduced bond strength; although, on extending the time of fire exposure to 180 min, recovery in bond strength has been seen. Also, to some extent it has been influenced by other factors [14].
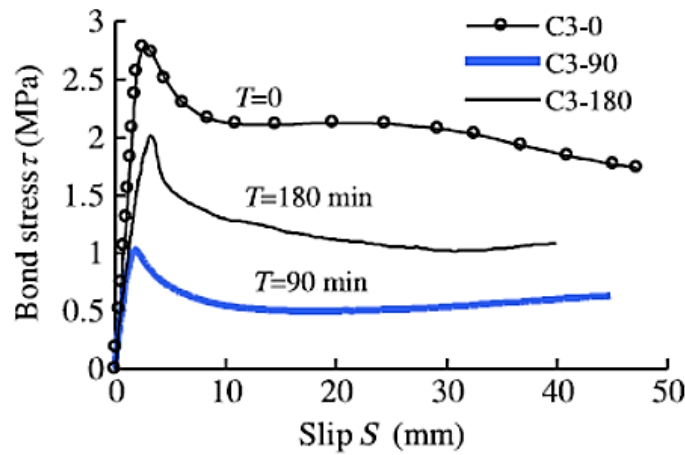
(a) Circular specimens
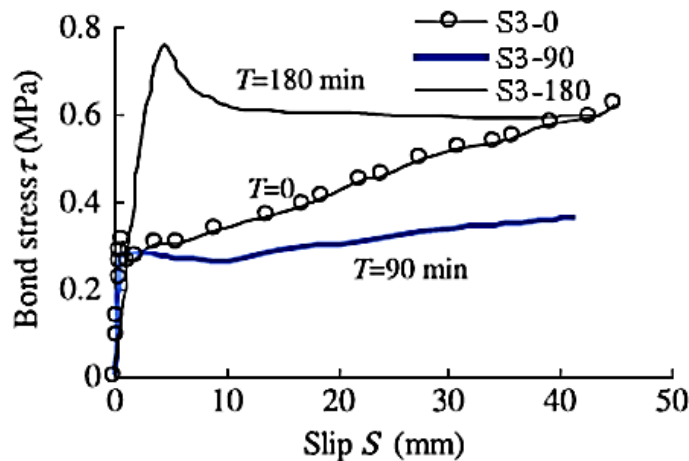
(b) Square specimens

Figure 2.12 Effect of fire exposure time on τ–S curves for (a) Circular specimens (b) Square specimens

For specimens after fire exposure 90 minutes the intensity was usually diminished and the strength was restored when the exposure time was increased to 180 minutes. In general, circular columns were much better as compared to square column as shown in Figure 2.12 (b).

47

In order to be design bond strength for the square and the circular CFST columns, 0.15 and 0.4mpa are required under the current testing constraints. The CFST columns' bond strength was very vulnerable to their sectional dimension because of shrinkage of concrete. For columns with large cross sections further study is required and effective steps might be needed for improving the bond strength [44,126].

The circular steel tubes constraints the slender reinforced concrete columns post-fire behavior that is examined numerically and experimentally. Initially, experiments were implemented for exploring the STCRC (steel tube confined reinforced concrete) slender columns fundamental behavior after ISO 834 standard fire exposure which also includes cooling phases [154]. Failure modes, strains in the steel tube, load versus lateral displacement curves and temperature distributions were acquired as well as examined. The various parameters that were considered were reinforcement ratio, steel tube to concrete area ratio, material strength, slenderness ratio, cross sectional dimension, and heating time. During the examined STCRC slender columns' heating and cooling phases, across the cross-section the max temperature obtained was not uniform, as well as reduced to the concrete center from the outer steel tube as shown in Figure 2.13 (a-d). Due to high thermal ability of concrete and the safety of the surrounding materials, the highest temperatures were not simultaneously reached around the segment [80].
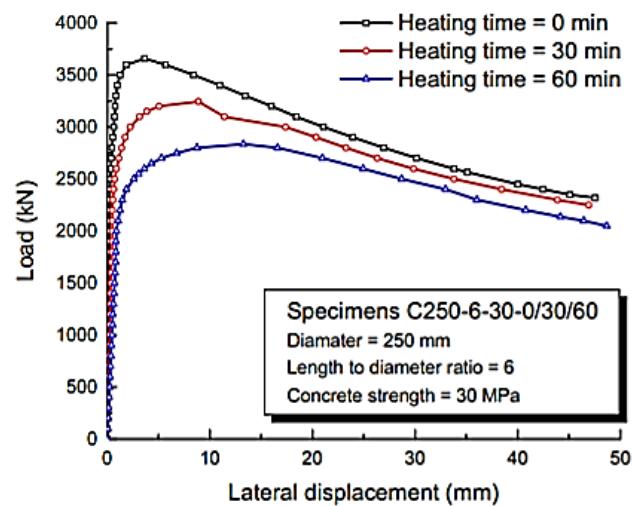
(a) Influence of exposure time on load–lateral displacement curves for C250-6-30-0/30/60
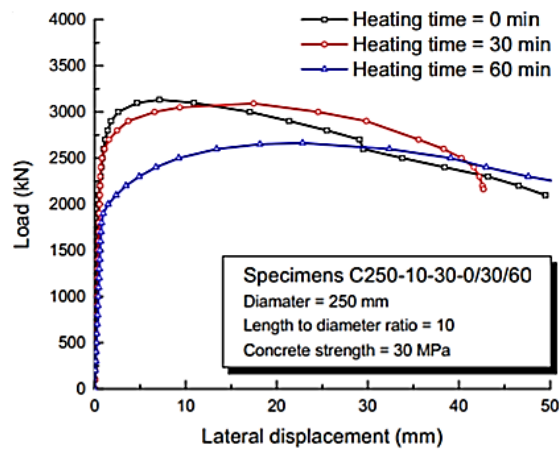
(b) Influence of exposure time on load–lateral displacement curves for C250-10-30-0/30/60
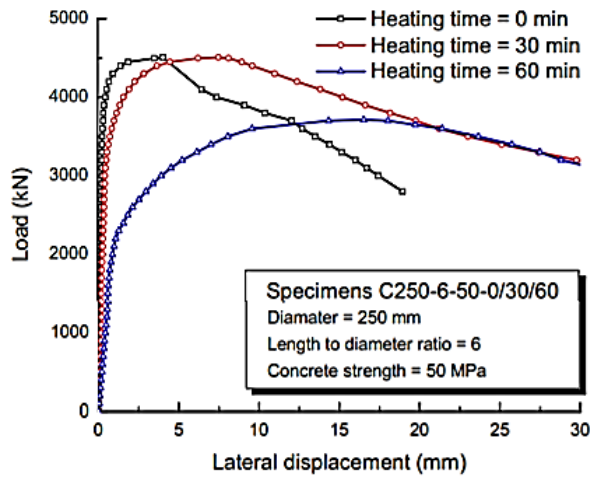
(c) Influence of exposure time on load–lateral displacement curves for C250-6-50-0/30/60
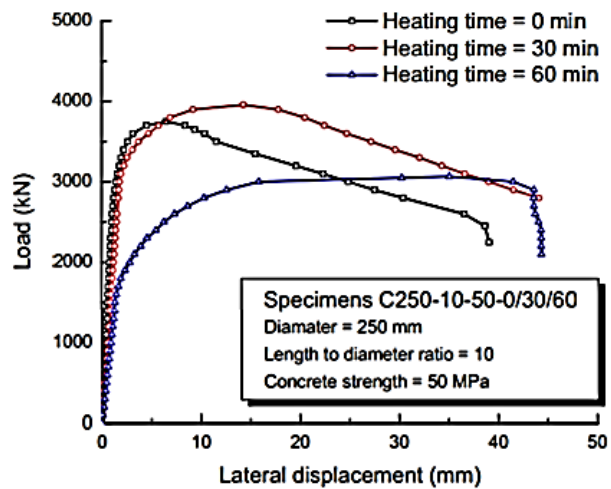
(d) Influence of exposure time on load–lateral displacement curves for C250-10-50-0/30/60

Figure 2.13 Influence of exposure time on load–lateral displacement curves [17]

49

There is development in concrete filled steel tubular (CFST) columns residual strength after fire conditions. The technique is focused on reducing the steel tube and concrete's strength under fire exposure to reach a max temperature. For testing the specimen's residual strength 61 CFST column tests undergoes ISO-834 standard fire or uniform heating. Since it was proven that the after natural fire exposure CFST columns' residual strength is calculated by slenderness ratio, cross-sectional diameter, and fire duration time [153, 175].
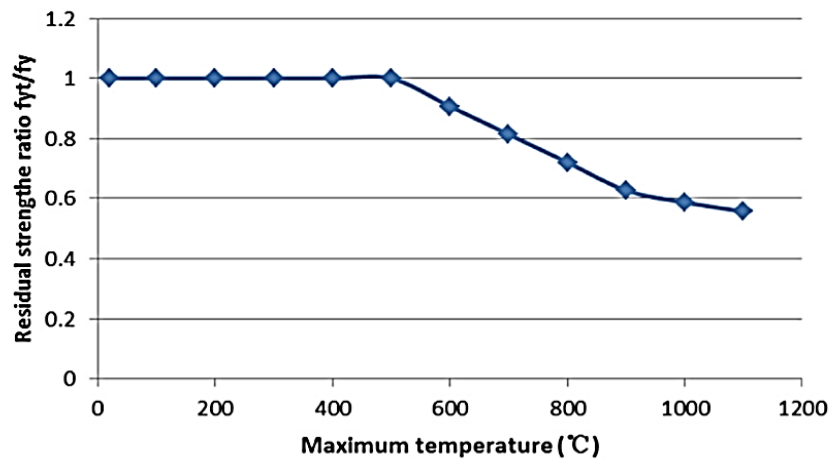
Figure 2.14 The residual strength ratio versus maximum temperature relationships of steel

Steel strength was decreased following exposure to fire, according to the findings of a study performed using the concrete and steel's maximum fire temperature. In general, after the cooling, steel recovers much of its stiffness and strength. But when the maximum temperature in steel is higher, the residual strength in steel is low, primarily when in case steel's maximum temperature is greater than 500°C. The suggested method suggests that the residual strength-maximum temperature of the steel is followed by the steel's strength reduction. Figure 2.14 indicates the residual strength ratio to the highest temperature reference [153, 175].

Various experiments on the impact of various parameters on the CFST fire activity have been carried out. The rise in concrete strength and sectional dimension has shown that fire resistance increases. The CFST column's fire resistance is significantly affected by the column dimensions. Column's increasing load-bearing capacity along with increasing size results in increasing the fire resistance. Another explanation is that the concrete center takes longer than critical column temperature [81, 83, 174, 176]. CFST columns' fire resistance is greatly affected by the concrete strength. Additional parameters including steel ratio, slender ratio and load level are inversely proportional to fire resistance.

Fire resistance and thickness of the tube were inversely proportional to each other and to stocky columns and columns with high fire resistance [58, 120]. Initially, the steel tube bears

the added load during fire exposure because of its higher expansion. If the pressure of the steel tube reduces steadily and the temperature is raised, the load is moved slowly and gently towards concrete. At this time, because of the tube safety and poor heat conductivity, the temperature inside a concrete is also relatively low. The concrete becomes liable until the column struggles for bearing the entire load. A rise in tube thickness ensures that the volume of energy applied to the concrete is higher and that the columns are less resistant to burning.

For slender columns or for low fire resistance columns (lower than 1 hour), fire resistance is increased when there is increase in tube thickness. Such columns' failure started at early stage due to steel tubes' global and local buckling, as well as simultaneously with failure of column, significant contribution of steel tube is observed in load carrying etc., therefore, delay in local buckling occurrence resulted when tube thickness is increased as well as when concrete is replaced with high strength steel material, column strength is also increased.

Myllymaki et. al., 1994[75], Guo et. al., 2007 [182], Park et. al., 2008 [172], specified that in comparison to square columns, the fire resistance of circular columns is high. One explanation is that there is more risk of a local buckling on the steel coat of square columns in comparison to circular column. Local squatting eliminates concrete containment and makes it easier to degrade. Moreover, the square column form produces a different temperature range in the course of a fire and creates more inner tension in the concrete compared with a circular column. These internally created stresses decrease the load carrying capacity square column

It was found that the concrete form affects the fire resistance. Carbonate aggregates may possess 10 to 20% more fire-resistance as compared to concrete's siliceous aggregate, since as compared to siliceous aggregate high heat capacity is exhibited by carbonate aggregates, as a result of an endothermic reaction in carbonate aggregate at around 700°C that hinders a rise in concrete temperatures when exposure to fire [79, 81, 180].

Among the most important ways to increase the fire safety of CFST columns is fire protection coating. Temperature ranges were experimentally explored and the findings were presented inside 12 CFST columns, with and without fire safety, when subjected to the standard ISO 834-fire fire [ISO 834-1 (1999)] [9, 10, 66]. 11 fire experiments with no and with fire safety on rectangular and square concrete filled pillars were presented by [172]. Fire safety has been found to lead to a time delay in the cross-section temperature region. As shown in Figure 2.15 the steel tube's temperature field with various defensive fire thickenings on circular as well as on the square columns increases the delay. Fire protection has greatly improved the

CFST column's fire resistance. For rectangular and square cement-filled columns RHS and SHS the fire protection thickness was decreased by nearly 25-70% from bare steel column [183]. The fire protection thickness effect, as seen in Figure 2.16, enhances the various dimensional rectangular columns' fire resistance [120]. Whilst fire protection has important consequences for increasing the CFST columns' fire resistance, it also exhibits few drawbacks: frequent maintenance is required, care must be taken during the application of fire protection, and fire protection is very expensive. Among its major drawback one is that usable floor area is reduced due to fire protection because column width is being increased.
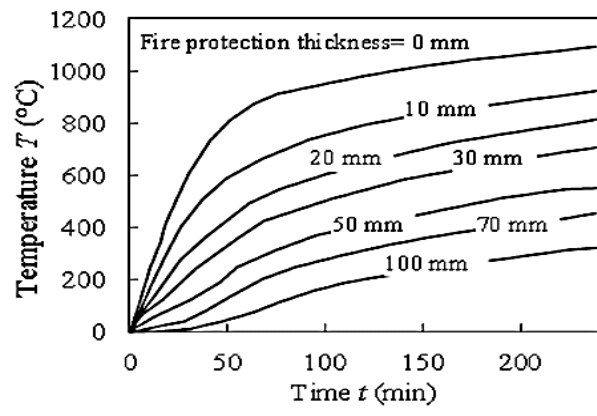
(a) Square
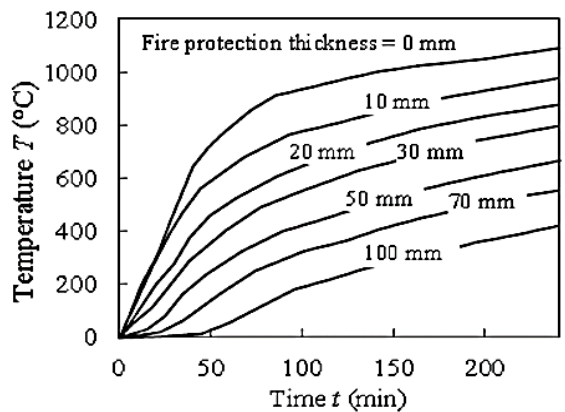
(b) Circular

Figure 2.15 Tubes' surface temperature with fire protection different thicknesses for (a) Square specimens (b) Circular specimens [47]
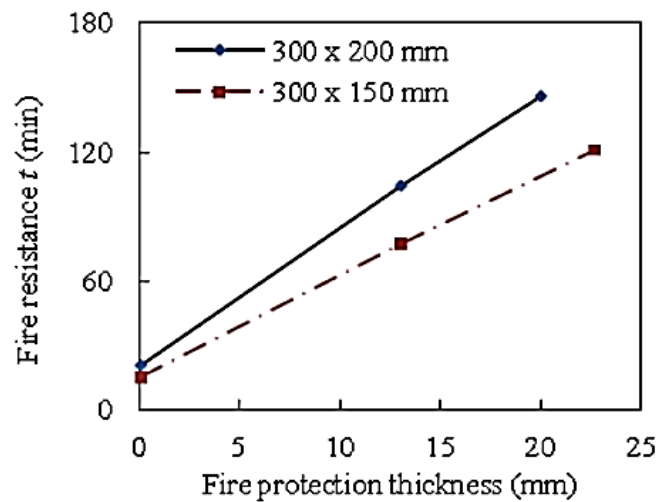
Figure 2.16 Spray thickness influence on fire resistance [47]

Investigators have found ways to enhance the CFST columns' fire safety as well as eliminate fire protection drawbacks, rather than by fire protection. One approach is that instead of PC (plain concrete) for steel tube reinforced concrete (RC) and fibre-reinforced concrete (FC) is utilized as an infill. It has been found that RC significantly improves the CFST columns' fire resistance, particularly in columns loaded with eccentric [129, 141, 143, 211]. It was due to the reinforcement bars' ability for decreasing the cracking which is found in concrete because of concrete core as well as steel tube's different expansions. Moreover, certain loads added to the column may be borne by the reinforcing bars.

Because of its fire endurance and mechanical properties, fibre reinforcement has a major impact in boosting the columns' fire resistance [170]. It has been discovered that steel fibres have been found preventing early cracking as well as also at high temperature lead to concrete's compressive strength. Further, [47] discovered that in increasing fire resistance as compared to fibre-reinforced normal-strength concrete, bar-reinforced normal-strength concrete was more efficient, as seen in Figure 2.17.

The study has found that in comparison to bar-reinforced HSC-filled columns or plain HSC-filled columns, fibre-reinforced high strength concrete-filled columns were highly fire resistant because of fibre-reinforced concrete's fire resistance and mechanical properties [79, 81, 122, 142]. Also, at high temperatures concrete's compressive strength is contributed by fibres. Early cracking is prevented by steel fibres as well as decreases the concrete spalling phenomenon which generally presented in HSC. For such reasons, it has been observed that in comparison to NSC, HSC is exhibiting more effective fibre reinforcement.
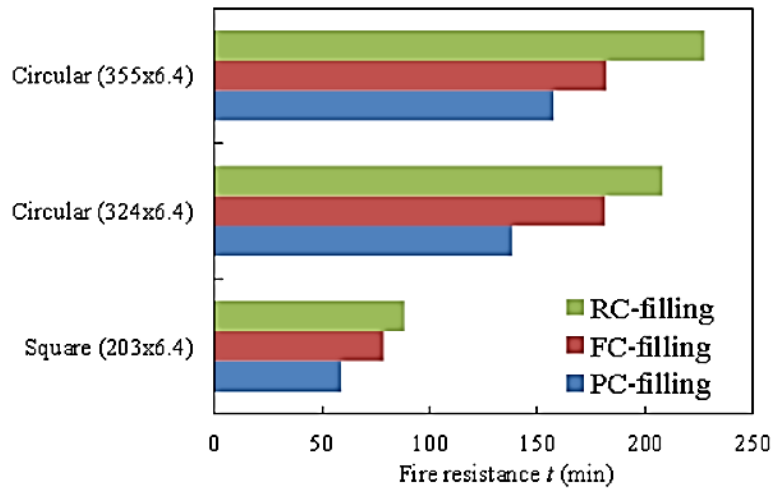
53

Choi et. al., 2012 [171] made the contrary conclusion as that concluded by Tokgoz et. al., 2010 [140]. After performing a total of 16 experiments on slender circular hollow-section columns, filled with either standard- or high-strength concrete, and exposed to concentric axial loads, the researchers discovered that steel fibres applied to slender columns did not provide much of an increase in fire resistance, and this added reinforcement offered no more fire resistance in columns with this configuration. Even though reinforcing bars did not make a big difference, they did help raise fire resistance. This shows that further analysis is needed in this study in order to understand the role of reinforced concrete containing fibres and fibers in CFST column fire resistance.

Several fire tests on CFST column were investigated by [126, 148]. After a standard fire exposure under cyclic or monotonic load, this research group found the results for square and circular shaped concrete filled steel hollow section columns' residual strength. The findings are available on 400mm length stub columns and D/t ratio of 27.7 when duration of fire exposure is 90 minutes. Testing of these columns was performed in Tianjin (China).

Another research was carried out after ISO-834 standard fire exposure on CFST columns for investigating the impact of various significant parameters on the composite sections' flexural stiffness and residual ultimate strength as well as the parametric studies results were utilized for developing formulas for composite section residual ultimate strength calculation under flexural bending or axial compression as well as the residual flexural bending stiffness of composite section [28, 47, 48, 179].

A study conducted on the fire-damaged CFST beam-columns' cyclic performance

restored through carbon fibre reinforced polymer wrap [13, 16, 54]. The research specifically aims to determine the FRP jacketing method's effectiveness and feasibility for CFST beam-column that had been restored after suffering fire damage. Four square and four circular sections of 8 repaired beam-columns were tested using constant axial and cyclic lateral loads. The beam-columns that had been destroyed by the fire were restored by CFRP covering. Axial load level, number of CFRP layers, and cross-section are the test parameters. Depending on the conclusions of the experiments, this was found that all of the test samples performed in a ductile way, whether they were repaired or not. In the case of CFST columns exposed to heat, the flexural stiffness and ultimate lateral strength also decreased. In comparison, load bearing capability and stiffness also improved when the various CFRP layers improved on columns fixed with CFRP. After applying a few extra layers of CFRP, the repaired specimens exhibited slightly greater ductility.

After ISO-834 standard fire exposure, a study was done on cyclically and monotonically loaded beams, column with various cross-sectional types. Due to the restriction of volume, the above tests specimens could not be loaded prior to the fire exposure. Depending on post-fire tests, which were conducted with no pre-load during the cooling phase and fire exposure, the practical formulas for the CFST columns' residual strength calculation after exposure to ISO-834 fire standard were established [47, 148].

The experimentally study carried on the axial compressive CFST columns behavior with pre-loading after high temperature exposure [110, 138]. The findings tested indicate that while sustained preload resulted in CFST columns' substantial residual deformations during the cooling process, residual-deformation fire-damaged columns were compressed axially to fail in a very ductile way. The preload in columns and the cooling process of the fire did not significantly impact the fire-damaged composite column's residual strength. Nevertheless, during evaluation of the fire-damaged CFST columns, the fire cooling phase as well as pre-load effects in columns on the composite column's axial compressive stiffness and residual deformation should be considered.

For analyzing the concrete-filled steel tubular columns' behavior, a FEA program was developed during fire exposure's entire stage which includes post fire loading to failure, cooling to the ambient temperature, heating and loading at ambient temperature. It has been showed by the numerical results that CFST columns' post-fire and cooling behavior is obviously affected by the cooling and heating history and ambient temperature loading. Post-

fire residual strength versus heating time relation is majorly influenced by 3 parameters that are cross-section dimension, slenderness and load ratio. However, experimental results are utilized for verifying the numerical results [153].

The experimental work was carried out on the 8 CFST columns cyclic behaviors under sustained axial load after fire exposure. These specimens were simultaneously heated into the stove through a stackable electric stove and fired liquefied petroleum gas to simulate the real fire attack. The furnace heating can be easily and safely controlled using gas and electricity using such a hybrid heating method that the average furnace temperature has followed the ISO-834 standard fire curve as closely as possible [48, 61, 148]. The axial loading and heating of the CFST columns over a given time period culminated in the fire standards cooling the specimens to room temperature while keeping axial load constant. Lastly, lateral cyclic loading under a constant axial load was carried out on the columns. During the cooling phase, continuous preload resulted in CFST columns increased residual deformations.

It has been found that 3 columns have endured rupture in steel weld and 2 columns have endured steel tube's local buckling. It is therefore advisable that over two vents with a larger-diameter diameter should be used in the CFST column, with the appropriate selection and building of steel sections being a matter of particular attention to engineers. The CFST's energy absorption capacity and post-fire ductility did not deteriorate clearly when compared to fire damaged columns, as well as fire-damaged CFST's residual strength is obviously influenced by the axial load levels in comparison to without pre-load fire-damaged columns as well as at room temperature. Further, for CFST columns' fire-damage assessment, a basis is provided by the experimental results.

The study was conducted on the post-fire bonding among the CFST columns' concrete core and steel tube. The testing of the standard fire of ISO 834 for 90 or 180minutes took place on 64 columns [42, 45]. Also investigation of 12 unheated specimens was conducted. The test results indicate that the relation among the concrete core and the steel tube has a major impact on a fire exposure. They have utilized both square and circular sections, and this was observed that in comparison to square columns, much high bond strength is possessed by circular columns.

Studies were also carried out on concrete-encased CFST structure which is a composite structure type having an outer RC (reinforced concrete) component as well as an inner CFST component [20, 93, 146, 150, 156, 168]. In high-rise buildings and large-scale buildings, they

are becoming more common in China. At ambient temperature, the concrete-encased CFST structures behavior has been studied, however their fire performance, such as the performance during fire and after fire exposure, is rarely discussed. 2 cantilevered RC (reinforced concrete) beams and 1 continuous concrete-encased CFST column comprises the cruciform beam-column joint. Further, such specimens were exposed to full-range and load fire's combined effect. There are 4 phases in test procedure: a loading phase at ambient temperature, a standard fire exposure phase with constant load applied, a sequential cooling phase and a post-fire loading phase. Also, there exist 2 failure types: failure at times of exposure of fire as well as the failure at times of post-fire loadings. On all column specimens, global buckling loss has been observed. Without external fire protection, columns with typical load ratios obtained higher fire ratings. CFST columns contained in concrete have maintained higher residual strength following burning. The beam errors in both situations were found for the joint participants. The deformation during the refractive process was considerably greater for both the joint and column specimens than during the normal phase of fire exposure.

After fire exposure steel reinforced concrete columns' residual bond strength was evaluated [31, 44, 126]. 11 specimens, including 8 specimens that were subjected to standard fire ISO 834 for 90 min or 180 min and 3 unheated specimens, were examined for investigating the following parameters' influence: (i) tie arrangement; (ii) concrete strength; (iii) concrete cover thickness; and (iv) fire exposure time. For fire-exposed specimens a significant decrease was observed in bond strength. The residual bond strength values for specimen with 90min fire exposure were in the range of 10.4-18.1% of the strength of unheated specimens, whilst slight recovery was observed in bond strength while the time of fire exposure was increased from 90 min to180min.

The post fire concrete filled steel tube column's residual strength and cooling behavior was investigated [12, 45, 146], the results showed that after natural fire exposure CFST columns' residual strength is usually affected by slenderness ratio, cross-sectional diameter and fire duration time.

The study conducted on CFST columns. The effect of cooling regimes on the compression action of concrete-filled circular stub columns after exposure to high temperature of 600°C for 3 hours is explored in this study [21, 61, 212]. The experimental program, which comprises of 2 sizes external steel tube, contains 30columns. For the greater column diameter

double skin columns were also considered. Water quenching and annealing cooling regimes were considered in the research. Two potential load transfer modes, namely core load and composite load, were checked for the columns. The columns behavior was examined in stresses, load-deformation pattern and load capacity terms in the materials. In comparison to steel tube alone, high ductility is exhibited by the concrete-filled columns. In composite loaded columns the containment created by external steel pipe was less than in core loaded columns. It was noticed that for columns' post-fire cooling in comparison to water quenching, annealing was a little bit better.

The Concrete-Encased CFST Columns' Experimental Behavior after fire exposure which includes cooling and heating phases was conducted [74, 93, 146, 150]. The results showed that the protective outer reinforced concrete can protect the inner CFST component well. The concrete-encased CFST column having 0.35 load ratio is able to stand the full-range fire with heating time of 137 mins, and retain about 79% of its strength. It is also observed that they exhibit a ductile characteristic in deformation development over the full-range fire.

Due to high load-bearing capability and excellent structural fire comportment [147, 148,177, 195], the analysis of the SFST columns with solid steel core is being used more frequently in high-rise construction practice. The simulation of the structural fire efficiency of these revolutionary, composite columns by sophisticated computational simulations is a promising method for gradually understanding and partially replacing the fundamental thermo-mechanical behavior found in expensive, fully-built fire experiments. In addition, the required data can be compiled using such models from a parametric analysis to build a simpler fire design approach. This research introduces an innovative Finite-Element-Method non-linear model integrating complex experimental calibration results, enabling rigorous simulation of different composite column full-scale fire tests. The model also confirms the revolutionary design principle of such composite column's structural fire behavior by monitoring the load sharing allocation processes among the different components. It has been represented and conditionally validated a condensed model version that allows for partial substitution of complete fire testing or implementation in both a parametric as well as advanced structural studies [218].

The concrete filled hollow steel sections' fire behavior was evaluated [84, 92, 134, 155, 169]. Nearly all of the critical elements that influence their strength were described: contact

problem at the steel-concrete interface, concrete and steel's thermal and mechanical properties, column slenderness, steel tube thickness, reinforcement ratio, concrete filling, and section shape and dimensions. Majority studies have been carried out in standard fire conditions (ISO) and over time, the temperature has risen constantly. It therefore does not necessarily reflect a normal fire that not only covers a heating period, it is also a cooling phase in which the fire's temperature falls down to the atmospheric temperature. The action of columns with natural fire condition axially loaded, filled square hollow concrete has been investigated. The study's primary goals are: firstly, demonstrating such columns' delayed collapse phenomenon after or during fire's cooling phase as well as then examining some determinant parameters' influence which includes column length, concrete cover, reinforcement ratio, tube thickness, and section size. It has been observed from results that low-slenderness ratio, small values of steel tube's thickness and massive sections resulted in delayed failures.

The Residual strength capacity of circular CFST stub columns that are fire-exposed was investigated [26, 59, 61, 110], the results reported that CFST columns after 750°C exposure, for all specimens there is increase in the residual strength capacity, whereas there is slight decrease in stiffness and ductility. It has been also observed from the comparison results that the experimentally obtained residual strength values and predicted ones utilizing EC4 were close.

The CFST column's post heating response was showed [21, 61, 120, 132]. The study presented analysis has 3 stages: heating, cooling and post-fire (under sustained load) conditions. The model finds practical features characteristic of the CFST columns' fire reaction, including the concrete and the steel tube's sliding and separation and the gap conductance existence at the steel-concrete interface. Depending on model, through parametric analysis after heating the CFST columns' response is examined.

The study conducted on the CFST columns' behavior exposed to full range fire reported that in case of failure occurrence in fire conditions, at ambient temperature the internal CFST element held more load a than the time after loading. For post-fire test, the longitudinal reinforcement and steel tube held the high strengths after cooling as well as were therefore bearing much load added after the fire. The load was redistributed to core concrete after the RC portion achieved residue strength and the steel tube yielded [63, 75, 140, 149].

The cooling rate effect on the CFST column' post-fire behavior was investigated [21, 44, 45,

61], the cooling rate influenced the column behavior after fire, so more the temperature of specimen then its behavior is affected more. In comparison to normal cooling, the water cooling was also found to be marginally more. Further, from the parametric study it has been observed that transforming the cross-sectional shape from circular to square, as well as enhancing the concrete and steel's strength, at the cooling phase column's residual strength is lesser as compared to heating phases. Additionally, after the cooling phase, column behavior has not changed with decreasing column height.

The study conducted under standard fire conditions on square CFST columns [172, 182, 202, 206], depending on both eccentric and concentric axial load. In this study, under concentric load, 12square CFST columns were examined, each one is 300×9mm section as well as normal strength concrete is used for filling it. Comparison among the predictions and experimental results indicated that the measurement of the fire resistance could correctly anticipate the column temperatures, column's strength and the deformations during fire exposure. With the column width the fire resistance enhanced and with the column width the sensitivity reduced steadily. Further, with the greater column width the columns' fire resistance grew rapidly and the column width sensitivity increased in line with the rise in the applied load ratio.

2.4.2 Behavior of CFST column at ambient temperature

An experimental study on CFST columns under axial loading was investigated. Concentric load subjected 6 short columns were examined. Rectangular, circular and square cross-section columns with 2 steel tube thicknesses were used. The test results show that the high-strength concrete's ductility enhances as the steel tube is confined, however there is no change in load-carrying capacity. Furthermore, column's capacity is not increased by the confinement effect since high-strength concrete core's axial strain is very low which is equal to the ultimate load point of column. Also, they have proposed a model for predicting the load against strain behavior as well as concrete-filled steel columns' pre-peak and post-peak behavior loaded axially can be measured from the concrete core and steel tube's behavior [1].
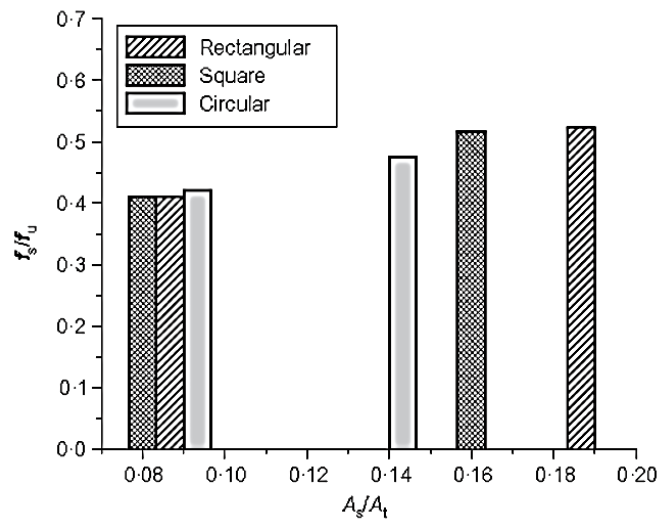
(a) Influence of steel area on CFST columns
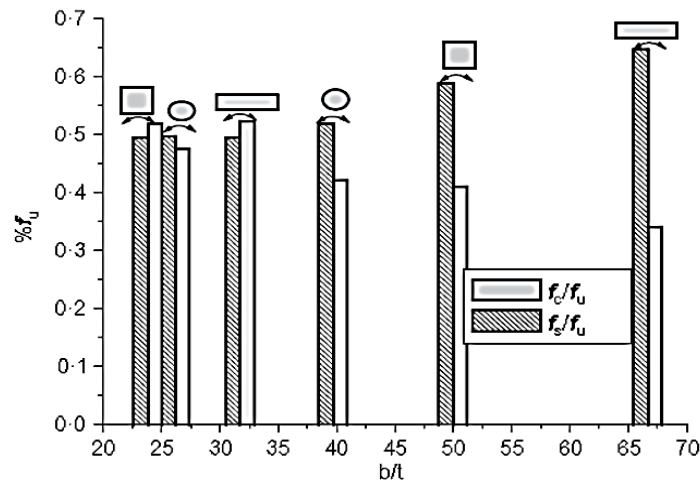
(b) Influence of b/t ratio on CFST columns

Figure 2.18 Steel area and b/t ratio influence

As it is noticed, when the b/t ratio increases, steel tube's contribution to the ultimate load turns out to be more efficient. In terms of the influence of shape, as the b/t ratio rises, it often seems more significant. The best behavior was demonstrated by circular specimens with the same performance in both concrete core and steel tube for applied load resistance. The second-best performance was of square specimens, whereas the rectangular was the least successful [1].

The axially-loaded tubular columns behavior filled with partially replaced concrete and M20 grade concrete was investigated. The varying parameters in the study include concrete debris, partially replaced quarry dust, normal M20 grade concrete and slenderness ratio (13.27, 16.58 & 19.9).
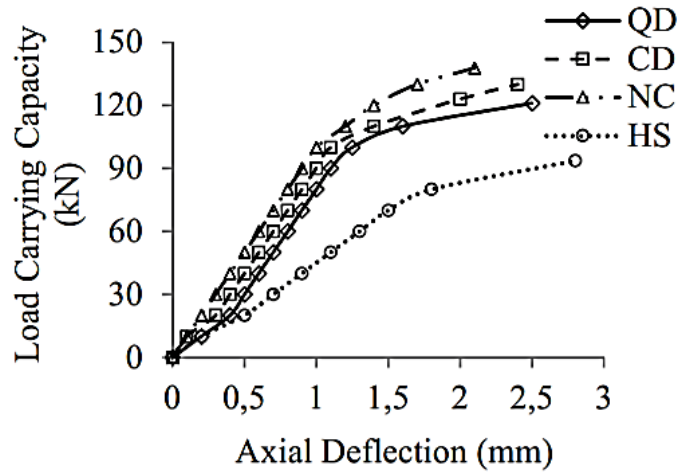
(a) CFST columns load-deflection behavior (L/D = 13.27)
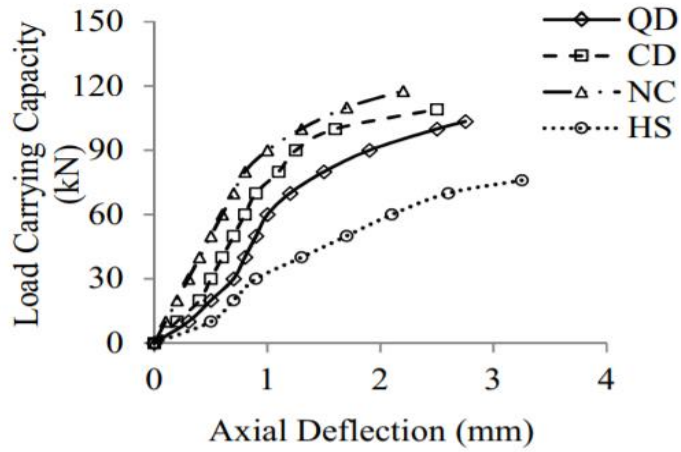
(b) CFST columns Load-Deflection behavior (L/D = 16.58)
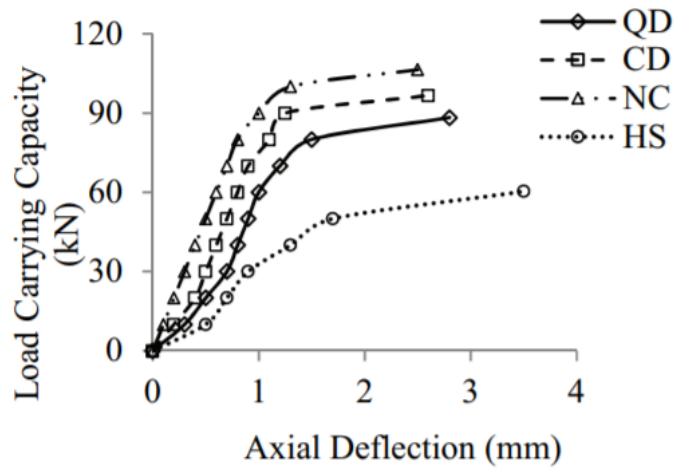
(c) CFST columns Load-Deflection behavior (L/D = 19.90)

Figure 2.19 Load deformation behavior of CFST columns (a) L/D 13.27 (b) L/D = 16.58 (c) L/D = 19.90 [15]

Several concrete mixes' effects as well as composite behavior among concrete core and the steel tube are investigated as well as a graph is plotted that visualizes the axial deflection and the load carrying capacity differences. Various performance indices include strength index (SI), Confinement Index (CI), Concrete Contribution Ratio (CCR) and Ductility Index (DI) were calculated as well as among CFST columns they were compared. The findings show that L/D ratio improvement reduces composite column behavior regardless of filled material. In contrast with hollow steel columns, the composite operation was carried out in the CFST columns filled with concrete debris and partially replaced quarry dust. Compared with hollow tubular columns, CFST column's load capacity is 32% greater [81].
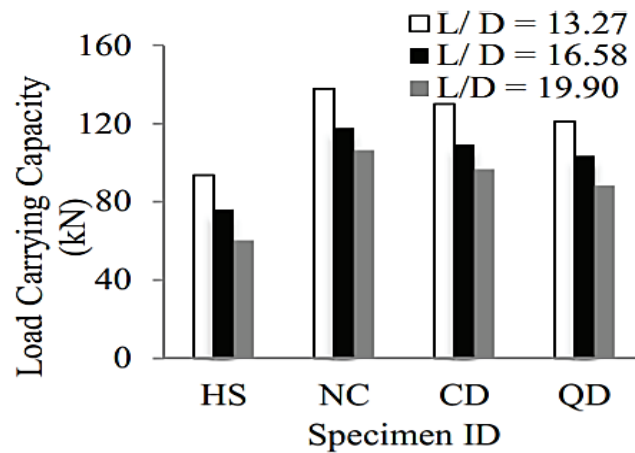
Figure 2.20 Load carrying capacity of different CFST columns [15]

The concrete filled tubular columns behavior with concrete partial replacement (by concrete debris and quarry dust) in the standard M20 grade concrete were investigated. Figures 2.19 (a-c) presents the composite column's L/D behavior for various slenderness ratios. For 3 distinctive slenderness ratio 13.27, 16.58, and 19.90, %age increase in composite columns as well as non- composite column's (hollow column) deflection is 25 to 32%. In comparison to normal M20 grade concrete filled column, for 13.27 slenderness ratio, the column's deflection percentage decrease is noted to be 19% and 14.3% with quarry dust (QD) and concrete debris (CD), respectively. Further, for the 16.58 slenderness ratio, 25% and 13.6% deflection percentage decreases is observed for column changes to quarry dust from normal concrete. For the 19.90 slenderness ratio, in comparison to normal concrete column, column's deflection percentage decrease is 12% and 4% with QD and CD, respectively. For different slenderness ratios the composite columns' load carrying capacity was compared using bar chart diagrams as well as presented in Figure 2.20 [15].

The concrete filled steel columns coupled local and global buckling theoretical and

experimental treatment was investigated [179, 184, 195]. The slender cross-section effect on concrete filled steel column's total buckling capacity was investigated in three experiments. The cross sections plate slenderness was 36.0, 46.4 and 56.8. The experiments were carried out on both concrete filled steel and hollow sections. Each steel section is constructed from a 3mm wall thick steel plate. Per test was carried out in a 5,000 kN capacity loading jack in a self-loading system. Axial load lateral deflection shows that, as the load deflection curves slope show, the concrete presence not only raises the ultimate load, however flexural stiffness is also increased. And also, local buckling effect is dependent of column's component plates slenderness as well as it has a significant role in concrete core provided confinement effect consideration.

A study conducted on the steel tubes confining effect on concrete strength and the concrete fill's restraining effect on steel tube wall's local buckling, as well as evaluated the load–deformation relationships and ultimate load [108, 188, 194]. The main parameters of this tests were tube shapes (circular and square), design concrete strength (20, 40, 80MPa), "tube diameter width-to-thickness (D/t or B/t) ratio and tube tensile strength" (400, 600, 800 MPa). To estimate the CFST short columns' ultimate strength, an analytical model is also developed [100, 201]. In experimental studies on centrally loaded CFST and hollow small columns a total of 114 specimens have been tested. The reduction factor in capacity because of local buckling was empirically extracted from the hollow square steel tube columns' test results with a thin wall and then adjusted for the square CFST columns steel tube" by taking into account the filled concrete's restraining effect on the steel tube wall's local buckling.

CFST subjected to combined axial compression and concentric axial compression used for analytical modeling and an experimental work [18, 22, 56, 71, 102, 106, 188]. The study's main objective was for evaluating the beam-column and CFST short columns members' ductility and strength under various end loading and bond conditions. Each unbonded and bonded specimens were tested. For the unbonded columns, the bond between concrete and steel was prohibited through asphalt layer used on steel tubes inside surface. For ensuring short column behavior, a length-to-diameter ratio of 3 was chosen for CFST's short columns. A Universal Testing Machine with 600 kips was used to measure the small columns. The test results indicate that the CFST short columns' axial strength capacity was 65-75% greater than the composite segment's strength depending on an undivided strength at an axial distance of 0.009 to 0.012. Because of the confinement effect, the unbonded CFST short column's residual and maximum axial load capacities marginally high than bonded specimens.

A study conducted on experimental investigations on rectangular CFST stub columns' behavior's axial load, subjected to concentric loading [59, 73, 82, 110, 125, 214]. Under concentric compression, 26 specimens were tested. Material strength f_c=55 and 106 MPa, f_y=300 and 495 MPa were taken as primary parameters. Cross sectional aspect ratio lied between 1.0 and 2.0. 5000kN capacity Instron Testing Machine used for applying axial load. They compared the experimental data with the design codes (EC4, ACI, AISC), which gave safe estimation by 7 and 8%. During the tests, favorable ductility performance was noticed for each and every specimen. It was observed that EC4 seen not to be safe for predicting the CFST columns' ultimate capacity produced from high strength and mild steel concrete. In contrast, AISC, ACI codes estimated the specimens' failure load by 8, 7and 2% respectively.

A study presented on the confined concrete-filled tubular columns (CFST) in controlling the local buckling of the steel tube and confining the concrete in the potential plastic hinge regions of a CFST column [30, 111, 187, 188]. In order to achieve the objective, severe efficient transverse confinement was proposed and "carbon fibre reinforced polymer (CFRP)" as additional confinement of CFST columns. Experimental studies have tested the specimens. 13 cylinders were tested using a 500T High Stiffness Compression Tester under monotonic axial compression. The number of layers of CFF wraps with or without the distance of the steel tube to the CFRP containment became the test parameters of the CCFT columns. CCFT specimens wrapped directly by CFRP displayed a bilinear behavior close to that of the concrete cylinders contained by the FRP before the CFRP rupture. In contrast with the counterpart CFST specimens, the local buckling and resulting rupture of the tube was essentially retarded.

A study on cyclic performance of concrete filled steel CHS under flexure loading was conducted [139, 196, 197, 215]. The study parameters involve the axial load level (n) and concrete strength (f_{as}). For cyclically increased flexural loading and constant axial load, 8concrete filled steel CHS specimens were tested. Two empty columns were also carried out the same test procedure for comparison purpose. Testing was performed till either lateral load resistance had declined to half the lateral load capacity or because of steel tube fracture. Based on the minimal analysis work, the following findings as well as discoveries were made. The composite c/s ovalization and circumferential deformation have been avoided due to infill concrete, which results in richer ductility, larger bearing capacity and high stiffness.

Another study was conducted on the circular concrete filled thin-walled steel tubes

behavior in flexure [23, 60, 91, 125, 210]. A flexural tests series were performed on full-scale tube specimens both unfilled and filled. Concrete filled tubes utilized the compressive strength whereas steel tube counteracted the tensile strength, when subjected to pure bending and observations made on behavior of section, its ultimate capacities, such as, flexural stiffness, with modes of failures. Larger sections were used that have significant effect on the behavior and the specimens were tested under displacement control. Regarding bare steel sections loading was continued until either a buckle formed or a significant loss in load was observed. Concrete filled specimens were tested to its full capacity. Flexure tests were carried out on 406 mm and 456 mm diameter tubes. This was observed that a circular hollow section's flexural strength and ductility was increased due to the in-filled concrete, which resulted in prevention of local buckling. Ultimate moment of concrete filled tubes were exceeded the nominal moment capacities. The slip was measured at the ends of the sections with minimum slip was observed even at high deformations. The initial stiffness was close to the un-cracked stiffness, at loads less than 5% of ultimate load and the stiffness decreased to a value very close to the stiffness value of bare steel section.

An experimental study was conducted on CFDST beam-columns subjected to cyclic bending [133, 145, 237]. Advantages of CFDST included the better cyclic performance, better damping characteristics, lighter weight, stability enhancement, and section modulus increase. Various test parameters are the section types (square, circular) axial load level (n), and core strength (f_{cu}). 28 CFDST column specimens, out of which 12 specimens with CHS inner and outer and 16 specimens with circular hollow section (CHS) inner and square hollow section (SHS) outer were tested under cyclically increasing flexural loading and constant axial loading. The hollow section ratio varied from 0 to 0.77 and the axial load level (n) selected from 0-0.6. The test lengths of specimens were 1500mm. At the reaction blocks, no displacements were noticed till it reaches its failure load. This was perceived that each composite specimen acted in a ductile way. Based on the experiments conducted and results obtained, it was determined such that very high ductility and energy dissipation levels exhibited by CFDST beam- columns even under high axial loading in case of circular sections then of square sections.

Another experimental study was conducted on concrete filled steel tubular columns [58, 75, 193, 206, 213]. The main parameters included were cross-sections, steel tube thicknesses. The CFST columns' cross-sections were divided in 3 groups, which are: circular section, rectangular section and square section. All the experiments were conducted in a "vertical column testing machine" with 3000kN static capability at 0.005mm/s speed. The standard loss

of the rectangular, circular and square specimens' typical failure subjected to concentric loadings resulted on crushing of concrete core.

Only in the after-peak branch was an external local buckling found in some specimens in the middle long region. There was general instability in circulatory specimens and no local buckling signal was registered at loading stages. The containment effect is more effective for the square section than for the rectangular section, hence the behavior of the post-peak span is more ductile.

A study conducted in various loading stages on the composite steel-concrete element behavior. Their research showed that the development of CFST elements load-bearing capability is mainly due to the steel tube's confining impact on the concrete core [35, 107, 127, 194]. The CFST components' structural behavior considerably impacted the various Poisson ratios of the steel tube and the concrete core. The experimental and theoretical studies demonstrate that the hollow CFST element's action is complicated more than of solid elements, as complex stresses are not uniformly distributed due to the thickness of its transverse parts by all stresses in hollow cement. The study of the results reveals that an association between CFST element components occurs as well as increases the intensity by at least 10 percent during the multi-layer centrifuge process. These results revealed the single-layered composite effect of 12%, with a double-layer effect of 6%. This rise in intensity is demonstrated by the additional contact presence under loading conditions between nearby concrete layers.

The study carried out on the local buckling occurrence in concrete-filled tubes and bare steel as well as how various depth-to-thickness ratio influences the steel component response [15, 43, 182]. Examples were viewed with depth of density values ranging from 50 to 125. The tests were carried out with a compressor capacity of 1000 kN. They noticed that for bare and concrete-filled stainless-steel tubes the initial rigidity is almost identical, and the grease removed the connection and load transition between concrete and steel components. The peak load of the same column size is significantly higher than for the equivalent steel field, which is reached by the concrete filled section. For specimens with high depth-to-thickness ratio, these variations are especially noticeable. The bearing potential found for concrete filled tubes is in reality 23 per cent greater for specimens with 50 depth-to-thickness ratios, than for bare-hollow steel tubes tested. A 75% enhancement was noticed for large depth-to-thickness ratios.

An experimental and theoretical analysis was conducted on beam mid- spans, mass-transverse low velocity beams in the mid-range beams of the concrete filled steel square hollow

section beams and hollow section [67, 135, 162, 178, 185, 219]. The experiments were conducted on three separate, commercially manufactured square hollow section sizes in Australia, slender values ranging from 15-40. The sections were normally 20x20x1.6mm (20SHS), 35x35x1.6mm (35SHS) and 50x50x1.6mm (50SHS) from C350grade steel. The members were technically of 1m long as well as were welded with the 150 mm long gusset plates to rigid end plates for ensuring completely fixed beam end condition. For every section size, both concrete filled square hollow section and hollow sections' one specimen were tested. In general, crack formation initiates a failure at the hollow sections support especially for 50 SHS sections. At the beam mid-span under the load points, for 50SHS substantial local deformations were noticed, and to for 35 SHS a lesser degree, not for all 20SHS and also for concrete filled sections. Comparisons were made between concrete filled sections and hollow sections, observed that concrete filled sections increased for slender sections up to 83% moment capacity. For compact sections, the change in failure deflection as well as strengthening effect became negligible, whereas, the transverse force resistance might be significantly more than that of collapse load because of axial tension actions, provided a substantial reserve of strength. The inclusion of elastic behavior allowed the calculation of absorption energy for applied energy's small magnitudes.

The study conducted on the steel reduced beam section behavior to concrete filled CHS under combined cyclic lateral load and constant axial load [98, 159]. For the purpose of comparison weak-column's 3 specimens with no RBS (reduced beam section) configurations as well as steel beam to concrete filled steel tubular column connection was tested. The involved test parameters are RBS configuration, axial load level and ring width. It has been shown that, compared with weak columns connection, the RBS connection's energy dissipation capacity is increased. The beam failure mode has been recorded for all RBS connections. In addition, relations with the week column were collapsing in a fragile mode. RBS has been shown to have fair seismic efficiency with CFST column relations.

A study presented on the short fibre reinforced polymer's axial bearing capacity confined CFST columns [13]. They have done an experimental investigation with several specimens that were tested under axial compressive loadings. The testing parameters involves the FRP type such as carbon glass fibre reinforced polymer and fibre reinforced polymer, the concrete design strength (C40, C50 and C60), the steel tube thickness (3.0, 4.0, and 5.0mm) and number of FRP wraps layers (1,2, and 3 layers). The thickness of GFRP and CFRP wraps were 0.169 mm and 0.111 mm respectively. The compression tests were carried out in a 5000kN capacity

UTM. All specimens were subjected to plastic stage, Elasto-plastic stage and elastic stage loading. It was observed that in comparison to CFST column, the FRP-CFST column's volume expansion was small as well as the steel tube's local buckling phenomenon was decreased. Also, the column strength was significantly increased due to FRP confinement. Increased number of FRP layers drastically increased the ductility and ultimate bearing capacity.

The failure mechanism of empty and concrete filled carbon fibre reinforced polymer box beams was investigated [90, 170]. In this research, five CFRP laminates types and 20 small scale beams were utilized in experimental study, without and with infill concrete, also subjected to axial load and 4-point bending. Finite element analysis was also employed and the failure mechanism was investigated. Regarding modeling analysis concrete was modeled as an isotropic material which has capabilities of crushing in compression and cracking in tension. CFRP was described as a linear-constitutive orthotropic substance. The beams were interface-slipping and caused CFRP to be extremely deformed at web location. CFRP failure was analyzed using Tsuiwa failure criterion. It describes the relationship between stresses as well as considers various multi-axial stresses, multi-dimensional space, and material axis symmetries. Usually, the empty beams at the loading plate's vicinity on the top flange collapsed. The CFRP beams' damage sequence can be such that, at the loading's early stage, in tension concrete cracking started, which increases slowly in number and extent, majorly happens at 35-55% load where beam's ultimate failure happened. It has been focused such that under 4-point bending all the beams unsuccessful nearby loading plate.

A study showed that in various engineering structures the CFSTs are acquiring enhancing distinction, with basic cross-section shapes being circular, rectangular or square hollow section [42]. The key need is to study CFST columns' characteristics and behavior. The thesis introduces the groundbreaking experimental analysis on CFST columns as well as discusses the columns' characteristics of load deflection response. Several numerical and analytical studies' comprehensive summary on CFST member modeling was presented [191]. The design specification and standards by AIK, ANSI/AISC, Eurocode-4and AIJ are discussed.

Another test carried out on high strength self- consolidating CFST stub columns [11]. 6 columns with 760 mm length and square section with different load level, load case (concentric or eccentric load) and cross-section size were tested. The concrete's cylinder compressive strength at 28 days was 90 MPa. Increasing concrete thickness and outer tube perimeter decreases the temperature of CFDST specimens when the added fiber has little effect on the

temperature spectrum. The addition of steel fiber increases CFDST stub columns' fire resistance particularly at load levels below 0.6. The temperature critical or restricting for CFDST parts is greater than that for unfilled tubes or CFST tubes.

The study was conducted on structural adhesives application in steel–concrete composite and concrete as well as factors that influences the composite connections performance reported that the structural adhesives applications as connecting agents, specifically there is detailed discussion for steel–concrete composites [55]. Interfaces' bond strength is influenced by several factors which includes adherents' surface finishing, fillers' type and amount, environment's temperature and relative humidity during curing and service life, bonded area geometry, adhesive layer thickness, water immersion, adherent's shape and structural adherents and adhesives' chemical, mechanical and physical properties.

Another research was conducted under impact loading on behavior of adhesive bonded and mechanically connected steel-concrete composite reported that the adhesively bonded connection can resist comparatively higher number (twice) of blows for crack initiation but, the number of blows required for final failure were relatively less [112, 217]. The adhesively bonded connection showed a brittle failure in concrete near the adhesive concrete interface whereas the mechanically connected specimen showed ductile failure due to concrete crushing in composite specimen nearby the studs.

Another study conducted on the behavior of CFST column stated that the composite columns' behavior decreases with increasing L/D ratio independent of the substance filled [55, 62, 209]. In the CFST column filled with partially replaced concrete debris and quarry dust, composite action was attained while in comparison with hollow steel column. In comparison to the hollow tubular columns, the CFST column's load carrying capacity improved 32%.

The study conducted on CFST column indicated that the reinforcing bar CFST column has higher bearing capacity, improved plastic conduct, and higher hardness. When the load is around 0.4-0.5 times the last bearing capacity [30, 89, 239], the elastoplastic boundary exists. The change in depth from the rock socks, and the inclusion of the steel tube, would impact the rock sock's overall carrying power. The capacity of the CFST rock-socket columns is less than the capacity of the steel-socketed columns under a vertical load; thus, the higher the rock-socket depth, the higher the rock-socketed piles' carrying capacity.

2.4.3 Parametric study on CFST columns

A detailed parametric study was conducted [17, 91, 125, 133, 207]. An efficient and simple but an accurate analytical system for strength capacity and circular steel filled with concrete of circular geometry, with a standard name CFST, under cyclically changing flexural load and an axial load was presented. Firstly, the ATENA program was used to provide a nonlinear accurate finite element model. Through contrasting the outcomes of the analyses with the experimental evidence reported in the related literature, the validity of this model was also established thoroughly. Further, applying this model, a broad parametric research was carried out for creating a broad and fair databank of the circular CFSTs and the hysteric behavior it shows. It involves a number of CFST columns having different ratios of thickness, strength of the concrete as well as the stress yield of the steel tube.

On the basis of this database, empiric expressions are built to test the phenomenological features of the well-known Ramberg-Osgood hysteric model. In addition, empiric empirical relations giving a precise and efficient description of the final power of the circular columns of the CFST are constructed and validated. Comparisons between analytical and experimental findings reveal that the proposed analytical model can accurately and efficiently characterize the actions of circular CFST columns under the effect of cyclic lateral loading.

A research was performed on efficiency of CFST high strength columns with under the effect of axial loading [94, 162, 227]. This thesis provided a computational analysis to examine the efficiency of high-strength circular CFST under monotonous axial processing. A model is built for the implementation of material non-linearity and constitutive relationships [96]. Calibration contrary to the prior evidence of the experiment indicates a fair deal of consensus. This parametric analysis was performed using the model & is compared to the code provisions. The intensity as well as the ductility of confined concrete is another primary concern to be noted. Variables were also used like the tension yield of the steel tube & the diameter of the column. The efficiency evaluation of the column is focused on axial load capability and improvements in ductility and strength because of containment. Two criteria, namely strength ductility index (μ), and enhancement factor (K_f) are specifically described and developed for evaluation.

Results demonstrate that CFST columns are strengthened both in concrete strength and ductility, albeit at different degrees. The ductile habits are distinctly visible. The growth in steel

tube yield stress has a marginal influence on the concrete strength but a noticeable impact on concrete ductility. The decrease in the ductility, though, is consistent with the usage of Grade 70 high-tensile steel. The overall results suggest that the usage of high-strength tubing in the columns of the CFST was not favorable. In seismic architecture, this result can seriously be regarded.

A finite element analysis program presented on the ultimate strength and behavior of battened columns encased in concrete and ultimate load-carrying capacity of fully encased battened steel columns subjected to axially or eccentrically applied compression [97, 114, 135]. A nonlinear 3-D model was also developed to simulate columns by using ABAQUS program package. Three encased composite columns and their reference battened steel columns have been modeled. The finite element modeling accuracy has been assessed when these results were compared to the corresponding values of the experiment. Parametric studies have been carried out for examining their effects on ultimate and behavior strength of composite columns. Parameters such as relative slenderness (λ), structural steel yield strength (f_y), compressive concrete strength (f_{ck}), load eccentricity, and initial out-of-straightness have been considered. The results were listed in the form of column curves. It is found that composite columns show significantly higher ultimate strength and stiffness compared to their companion steel columns.

A parametric analysis was performed of square concrete filled columns of steel tubes subjected to concentric filling. In contrast with the standard concrete structural member, the CFST member has several advantages [206]. This study through adjusting parameters presents the action of CFST columns under axial load. The criteria are steel tube diameter, concrete grade, and column length. Using ANSYS 13 finite element program, the analysis was performed. Each column was of size 60X60mm. For different variations in the thickness of the tube the values used were, 2, 3, 4, 5 and 6mm. For grade variations the M25, M30, M40, M50, M60 and M70 were used for the infilling of the concrete. 900, 1200, 1500, 1800, 2100 and 2400 mm column lengths were used for the variations. Euro code 4 (1994) was compared with the Buckling load.

A parametric analysis was carried out on the column of the concrete packed steel tube [118]. In recent years, the usage of concrete filled steel tube columns has risen dramatically in medium-rise to high-rise buildings, so in this article, computational finite element research using the software package ANSYS is carried out to objectively consider the load deformation

characteristics of composite columns. This paper focuses on the simulation of the column under axial loading of concrete filled steel tubes (CFST). The key criteria of the FEA are circular and square columns of various concrete classes (30, 50, 70, 90 N/mm^2). It is concluded that 10-15 percent of the deformation of the column decreases with rising concrete grade. This deformation was caused by the CFST section's shape. Due to greater confinement, the circular portion contributes to better conduct than the square section.

2.5 SUMMARY

As per the literature analysis it was found that the concrete filled steel tube column has several benefits. In comparison to the conventionally used system of RCC construction CFST has proven to be a better choice. The steel tube, in CFST, also serves as a permanent formwork and neglecting to strengthen the bar reduces construction time and costs. Today, in the designing and engineering of the buildings, fire prevention has been a very critical issue. Only a limited number of reports on fire testing or the models of finite elements which analyses the actions of CFST are available. The behavior of CFST structures encased with concrete under the conditions of ambient temperature were estimated, however the fire performance was not addressed in the experiment, including the aspects like its performance and conditions under fire exposure. Following the exposure to heat, the output of the CFST specimens is often influenced by cooling methods applied in the process. Different methods for cooling these structures are used after these structures are exposed to flames. CFST columns may be affected by these cooling and heating procedures. Minimal experiments on efficiency of CFST columns, post-fire or during-fire are possible without consideration of the results of specimens after cooling process. A crucial parameter in determining the efficiency of the columns before and after fire exposure is the cooling process of these columns. More analysis in this area needs to be carried out.

The conclusions drawn from the literature also revealed that the index of residual strength is another crucial factor involved in estimating the CFST performance when these columns are exposed to fire as these structures go through 3-stages when they are exposed to fire (a) Heating, (b) Cooling, (c) Ambient Temperature exposure. After natural fire exposure, the residual strength of CFST columns is normally influenced by a time-of-fire, cooling process, slenderness ratio and transverse diameter. In this context, it is concluded from the literature survey that in CFST columns, stiffness characteristics is also noted which indicates that effect

on the loading and high temperature exposure is another crucial aspect in comparison with the residual strength to estimate the stiffness of these columns.

The conclusions drawn from the literature survey also revealed that almost all essential parameters such as dimensions, section shape, mechanical and thermal properties of concrete and steel, column slenderness, thickness of steel tube, reinforcement ratio, concrete filling, and also the problem of contact between the interface of steel and concrete influencing the behavior of CFST. Some investigation was also carried out discovering that higher capacity of load-bearing of the elements of CFST columns is primarily because of the confining impact of the steel tube on the core of the concrete and was discovered that generally the circular columns have higher strength among the bonds as compared to the square columns.

Also, only a limited amount of research has been done on the comparison of the behavior of CFST column with design codes available. Suitable design guidelines need to be developed.

Also, in India the usage of steel building is still at its initial stage. Another main factor behind this is the cost factor. In present day scenario, it was concluded that when green and eco-friendly structure would be the main focus of the designers, CFST columns could be an optimal alternative to the conventional concrete as well as the steel structures because of its number of benefits.

2.6 GAPS IDENTIFIED

The following are the gaps in the reported studies of CFST columns under fire conditions as deduced from study of literature:

1) The parameters such as section shape and dimensions, concrete filling, steel tube thickness, column slenderness, thermal and mechanical properties of steel and concrete, and even the contact problem at the steel-concrete interface influencing the shrinkage effect of concrete filled steel tube columns and hence investigation for such condition becomes necessary.

2) For examining the parametric behavior of CFST columns under axial loading, further experimental and numerical investigations are required to be conducted.

3) Limited work has been conducted on fire exposure behavior of concrete-encased CFST column including the performance in fire and after exposure to fire. And post-fire behavior is an important aspect to consider when assessing a structure. The cooling approach of CFST columns after exposure of fire leaves a gap for further and in depth study to examine the behaviour of concrete filled steel tube columns after exposure to

fire. Therefore, it was regarded to be an important factor of this study to investigate the post-fire behavior of CFST columns. More fire tests are required to obtain a better understanding of the design implications and also to address the majority of the important parameters that affect CFST column efficiency in fires.

4) From the literature review, it is seen that a very limited work has been done on the design guidelines of CFST columns and also lack information on the fire resistance of CFST columns.

2.7 OBJECTIVES OF THE PRESENT WORK

Based on the gaps identified from the literature review, the following objectives have been defined:

1) To investigate the effect of load-deformation behavior, secant stiffness and ductility index of greased and non-greased CFST circular columns under axial loading.

2) To carry out finite element analysis on concrete filled steel tube columns under an axial loading by using ABAQUS/CAE and the FE model is verified against the test results of greased and non-greased columns. The simulations carried out against axial loading to study the parametric response of CFST columns.

3) To investigate the effect of loading, heating temperature and the other parameters such as load-deformation behavior, load carrying capacity, secant stiffness, ductility index and residual strength index of CFST circular columns that may influence by the two cooling regimes, i.e., annealing, and water quenching at elevated temperature of 600 °C to 800 °C.

4) To evaluate the strength aspects of Concrete Filled Steel Tube Columns through design codes such as Eurocode-4, ACI, AS, AISC-LRFD and CECS 28:90.

2.8 SCOPE OF THIS WORK

The study is presented in four sections as follows:

1) The influence of shrinkage of concrete on axial load capacity of CFST columns have been studied in the first part by comparing the test results of greased and non-greased specimens at ambient temperature.

2) In the second part, the response of circular CFST columns have been investigated under axial loading after exposure to elevated temperature of 600 °C to 800 °C.

Two common cooling methods – one involving annealing and another involving water quenching have been studied. Three column sizes were used in this investigation.

3) In the third part, finite element study performed on CFST columns subjected to axial loading using ABAQUS/CAE 6.14 is included along with the verification of FE model against the test results of this experimental program. The simulations carried out against axial loading for studying the response of CFST columns concerning load carrying capacity, displacement and von-mises stresses is also presented in this part. In addition to this, the mesh conversion study for obtaining the accurate mesh size correlating to the experimental load carrying capacity of CFST columns is also carried out.

4) In the fourth part, the analytical equations are put to understand the mechanism of concrete filled steel tube columns under axial loading for both greased and non-greased columns. For this purpose, a comparison between designs codes such as Eurocode-4, ACI, AS, AISC-LRFD and CECS 28:90 has been made in evaluating the axial compressive strength of concrete filled steel tube columns.

CHAPTER 3

METHODOLOGY

3.1 GENERAL

This chapter provides the details of the testing program used for the present study. It also contains the experimental programme of concrete filled steel tube column subjected to axial loading for both greased and non-greased columns. Further, experimental investigation of post – fire exposure behavior under the two cooling regimes of annealing and quenching are also presented in this chapter. The details of material properties, specimen preparation, test setup and procedures are explained in the following subsections.

3.2 DESCRIPTION

To examine the behavior of the CFST column under axial loading, a total of twelve composite (6 greased and 6 non-greased) specimens were cast and for analysing the behavior of CFST columns after exposure to fire when subjected to axial loading, twenty-four CFST specimens were cast which contains twelve specimens to check the annealing behavior and another twelve specimens to check the quenching behavior of concrete filled steel tube columns. The strength aspect of concrete filled steel tube columns through design codes namely AISC-LRFD, Eurocode-4, ACI, AS, and CECS 28:90 is included in this chapter. Further, the finite element study was performed on the CFST columns under axial loading by using ABAQUS/CAE 6.14 and the FE model was validated against the test results of this experimental program of greased and non-greased specimens.

3.3 LIMITATIONS

A lot of factors complicate the design and analysis of concrete filled steel tube column. A concrete filled steel tube column consists of two materials with different stress – strain characteristics. Due to this difference, it becomes very difficult to predict the combined properties like modulus of elasticity and moment of inertia. The failure mechanism of this composite largely depends on concrete and steel properties, shape, steel tube thickness, length and diameter. Shrinkage, bond, creep, concrete confinement, type of loading and residual stresses are other parameters also have an effect on CFST's behavior.

3.4 EXPERIMENTAL PROGRAMME
3.4.1 Material properties

Different properties of steel, which was used for the external tubes, were determined by conducting tensile tests on specimens made up of it. Three different specimens having an outer diameter of 100 mm, 125 mm and 150 mm with thickness of 4 mm and 5 mm were cut out of each steel tube and the sample height was 100mm, 125mm and 150mm respectively. The cutting of CFST specimens is shown in Figure 3.1. The average yield stresses (fy) of the steel specimens were found to be 288 MPa, 380 MPa and 440 MPa respectively as given in the manufacturer's manual and the similar values were observed in the experiment.

Figure 3.1 Cutting of CFST specimens

3.4.1.1 Coarse aggregates

Coarse aggregate is following to IS 383-1970. Local obtainable crushed aggregate utilizes for the present experiment while the maximum particle size should be 20 mm according to code specification as shown in Figure 3.2. Table 3.1 illustrates the physical properties of coarse aggregate employed in the present study.

Table 3.1 Physical properties of coarse aggregate

Sr. No.	Physical Properties	Coarse Aggregate
1.	Fineness modulus (%)	7.88
2.	Water absorption (%)	1.01
3.	Bulk density (kg/litres)	1.42
4.	Rodded Bulk density (kg/litres)	1.54
5.	Percentage voids (%)	45.65
6.	Specific gravity	2.62

Classification of coarse aggregate according to size:

1. Gravel.
2. Crushed stone.
3. Particles having size more than 4.75 mm.

Figure 3.2 Sample of coarse aggregate pass from 20mm sieve

3.4.1.2 Fine aggregates

The present investigation studied fine aggregate confirming to IS 383-1970. Sieve analysis was conducted to determine the gradation of fine aggregate and particle size should be less than 4.75mm according to code as shown in Figure 3.3. Table 3.2 shows the physical characteristics of fine aggregate used in the present study.

Fine aggregate classification according to size:

1. Sand or crushed stone.
2. Particles having size less than 4.75 mm.

3. Fine aggregate content typically 35% to 45% by mass or volume of total aggregate.

Table 3.2 Physical properties of Fine aggregate

Sr. No.	Physical Properties	Fine Aggregate
1	Fineness modulus (%)	2.88
2	Water absorption (%)	2.04
3	Bulk density (kg/liter)	1.48
4	Rodded Bulk density (kg/liter)	1.76
5	Percentage voids (%)	43
6	Specific gravity	2.60

Figure 3.3 Sample of Fine aggregate passed through 4.75mm sieve

3.4.1.3   Cement

The present investigation utilized Portland pozzolana cement (fly ash based) conforming to IS 1489 (Part 1) as shown in Figure 3.4. Pozzolanic materials in conformity with the suitable Indian standards are utilized to carry out this study, provided homogenous mixing with the cement is made sure.

Figure 3.4 Portland Pozzolana cement

3.4.1.4 Water

Freshwater deprived of odor, color, and the taste was used in existing experimental study. The drinking water must be used by concrete for mixing and curing purposes. The concrete has to be cured regularly for 28 days after finishing their final setting time.

3.4.1.5 Design mix

To determine the compressive strength of the concrete, three concrete cube specimens measuring 150 mm × 150 mm ×150 mm were cast. The average compressive strength (f_{cu}) of cubes after 28 days was observed to be 36.7 MPa as shown in Figure 3.5. The grade of concrete used to fill the core of CFST columns was same as utilized for cube specimen casting. The design mix of concrete was prepared as per IS 10262: 2009 to fill the concrete of grade M30 inside of outer steel tube. The detail of mix proportion is listed in Table 3.3.

$$F_{ck} = f_{min} + \text{kS} \tag{3.1}$$

Where, F_{min} is the minimum strength i.e., 30 MPa, k is the Himsworth co-efficient i.e., 1.65 and S is the standard deviation i.e., 5.

The target mean strength, Fck = 38.25 MPa

Figure 3.5 Concrete samples

Table 3.3 Design mix proportion

Weight of cement (kg/m³)	Weight of fine aggregate (kg/m³)	Weight of course aggregate (kg/m³)	Weight of water (kg/m³)
443	584	1158	186
1	1.3	2.6	0.42

3.4.2 Test specimens

A set of 12 composite (6 greased and 6 non-greased) specimens were produced in order to analyze the efficiency of the CFST under axial loading. For the preparation of greased specimens, grease was applied to the inside surface of the outer steel tubes. The different specifications of the specimens are listed in Table 3.4.

The properties of concrete filled steel tube columns with respect to geometry and with varying sizes and thicknesses of steel tubes are presented in Figure 3.6. CFST columns with an external steel tube diameter of 100 mm, 125 mm and 150 mm with a thickness of 4 mm and 5 mm were cast in order to evaluate the performance of concrete filled steel tube columns subjected to axial loading after-fire exposure. For all the specimens, the height remained the same as 600mm.The slenderness ratio of CFST specimens was 6.0, 4.8 and 4.0. The concrete of grade M30 was filled inside steel tube.

Table 3.4 Geometry of circular concrete filled steel tube columns

Specimens	Outer dia. (mm)	Thick - ness of steel (mm)	Height (mm)	D/T	L/D	Yield strength of Steel (MPa)	Compressive strength of Concrete (MPa)	Area (mm²)		
								Steel (As)	Conc. (Ac)	Total
C1T4	100	4	600	25.0	6.0	288	36.7	1206	7235	8441
C1T5	100	5	600	20.0	6.0	288	36.7	1492	7085	8577
C2T4	125	4	600	31.3	4.8	380	36.7	1521	11493	13014
C2T5	125	5	600	25.0	4.8	380	36.7	1885	11304	13189
C3T4	150	4	600	37.5	4.0	440	36.7	1835	16733	18568
C3T5	150	5	600	30.0	4.0	440	36.7	2278	16504	18782
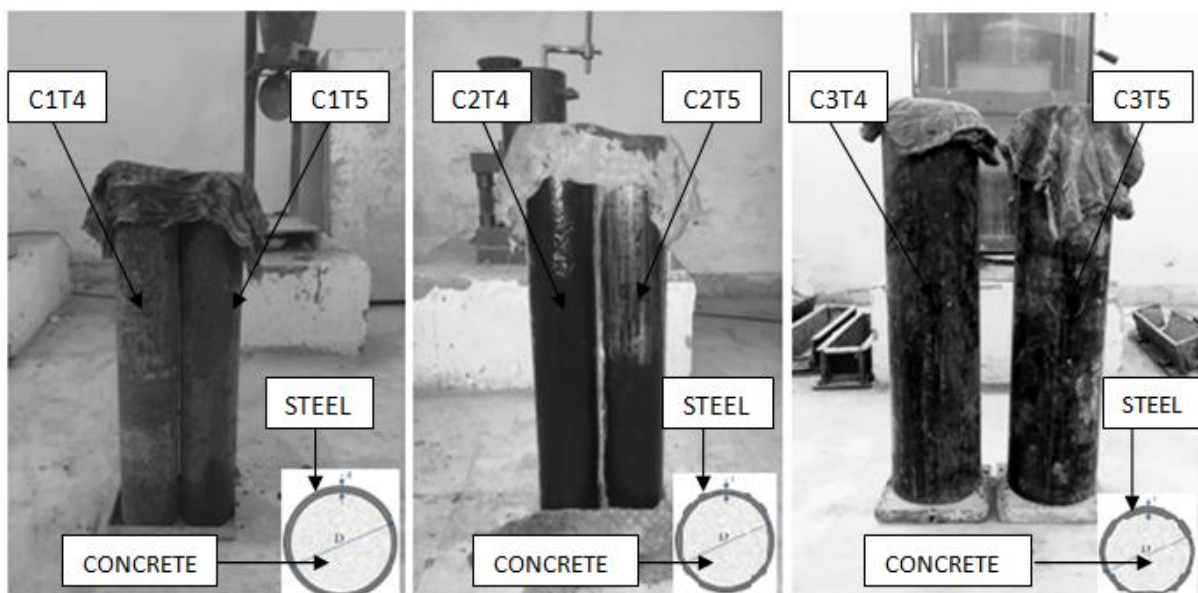
Figure 3.6 CFST composite columns

The specimens were cast in five layers as shown in Figure 3.7(a). Each layer was compacted using vibrator as showed in Figure 3.7(b). After the concrete was poured, the top

faces of all the CFST members were flattened to create a smooth surface for load application. With the help of plastic sheets, the top surfaces of all the specimens were covered for 24 hours as can be seen in Figure 3.7(c) and these sheets were replaced by moist burlap and it was kept on the specimens for 28 days, with water being sprayed on it every day. In Figure 3.8, the concrete filled steel tubular columns post casting are shown.

| (a) Pouring | (b) Compaction of CFST column | (c) CFST specimens closed with a plastic sheet |

Figure 3.7 Casting of CFST specimens (a) Pouring of concrete in steel tube (b) Compaction of CGST column (c) CFST specimens closed with plastic sheet

Figure 3.8 CFST specimens closed with wet burlap

3.4.3 Heating regime

The heating of concrete filled steel tube specimens was done in a furnace available in a steel industry situated in Chandigarh as shown in Figure 3.9. The heating capacity of industrial furnace was 1800 °C. The heating chamber was circular in shape with diameter 2.5 m and height 3 m. The CFST specimens were placed in the furnace in vertical direction with the help of special trolley. After placement of three specimens at a time, the furnace was closed by using furnace cap to heat up at elevated temperature as can be seen in Figure 3.10.

Figure 3.9 Heating furnace   **Figure 3.10** CFST specimens placed in heating furnace

The guidelines provided in the ISO-834 fire curve were followed to heat the specimens as shown in Figure 3.11 and heating was continued up to the temperature of 600 °C & 800 °C. The curves of time-temperature for heated specimens are shown in Figure 3.12 (a, b). To note the temperature reading during the time of exposure, a digital meter was used in the furnace and the readings for all the specimens were noted at an interval of 15 minutes. The furnace was turned off immediately as the required temperature was achieved and for next 24 hours all the specimens were kept in the same furnace.
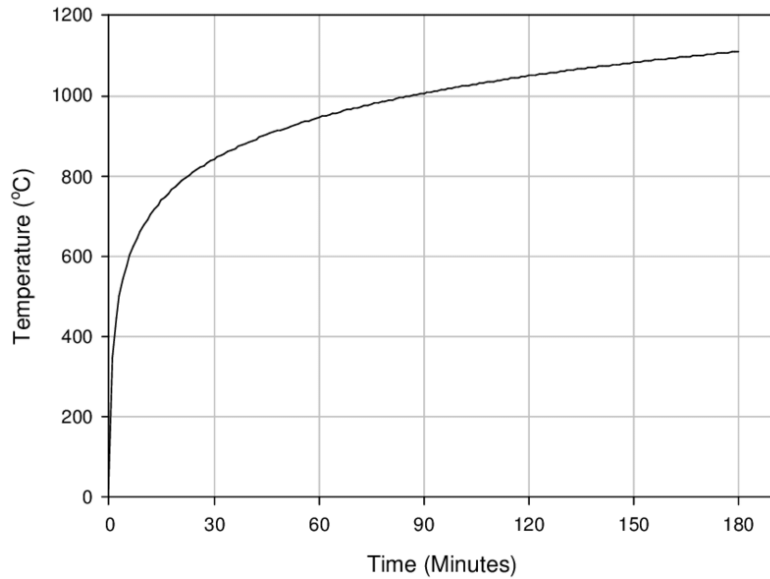
Figure 3.11 Standard time-temperature curve as per ISO 834
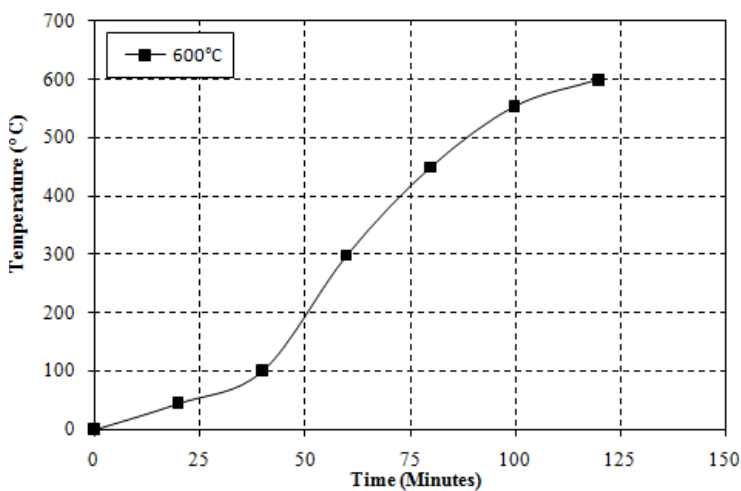
(a) Furnace temperature at 600 °C
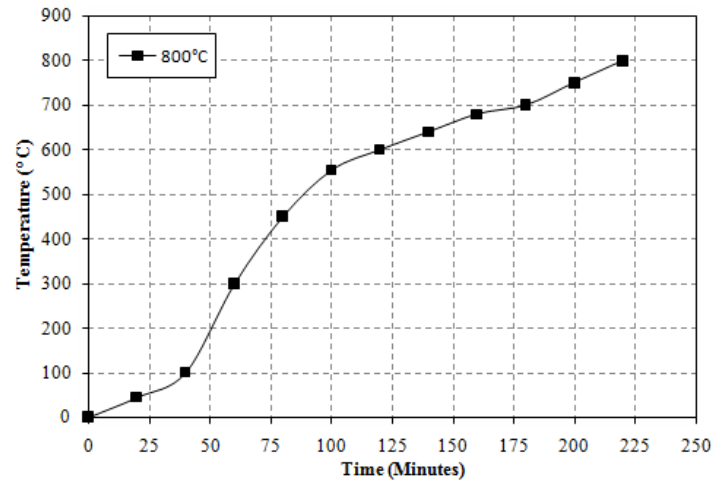
b) Furnace temperature at 800 °C

Figure 3.12 Furnace time-temperature curve at (a) 600 °C (b) 800 °C

3.4.4 Cooling regimes

Two methods were employed to cool down the specimens; water quenching was involved in one technique, while the second method included annealing. The process of annealing was carried out by holding the testing models in the furnace for 24 hours even after turning off the furnace when the target temperature was reached as shown in Figure 3.14. On the contrary, the specimens were heated in the furnace till the target temperature was reached and were then put in a water bath in quenching method. A special trolley was used to lift out the heated specimens from the furnace as shown in Figure 3.13 that also helped in immersing the specimens in the water bath for cooling.

86

Figure 3.13 CFST specimens pulled outside after reached target temperature

Figure 3.14 CFST specimens in heating furnace for annealing

3.4.5 Test setup and measurement

In order to apply axial load on the top of heated specimens, a universal testing machine (UTM) was used with a rate of loading 0.25 of mm/s. For measuring the displacement in the axially loaded specimens, four linear variable displacement transducers (LVDTs) were utilized with 200 mm gauge length. A schematic outline of the heated specimen is represented in Figure 3.15. The test arrangement is shown in Figure 3.16.

Figure 3.15 Specimens after cooling
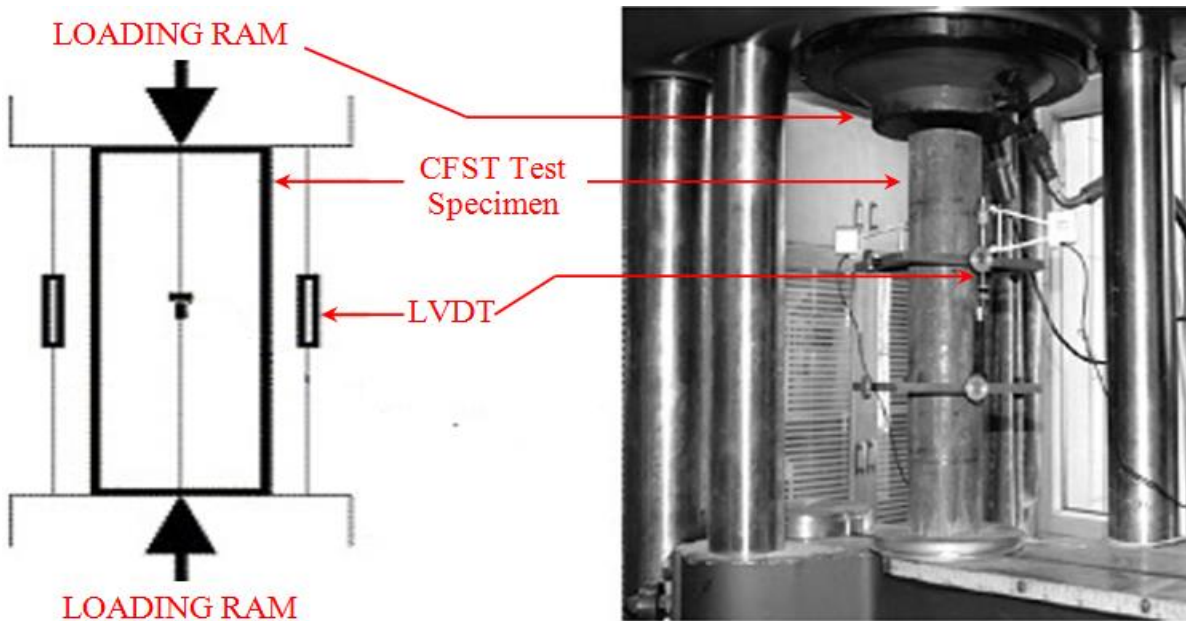
Figure 3.16 Schematic diagram of test arrangement

3.4.5.1   Greased and non-greased CFST columns at ambient temperature

The bond behavior between in-filled concrete and outer steel tube was investigated. For this purpose, twelve CFST specimens (6 greased and 6 non-greased) were cast. For the making of greased specimens, internal surface of the outer steel tubes was coated with grease. To check the behavior of greased and non-greased columns of CFST subjected to axial loading, CFST columns having external steel tube diameter of 100 mm, 125 mm and 150 mm with a thickness of 4 mm and 5 mm were cast as shown in Figure 3.6. The height of all the specimens was maintained at a constant value of 600 mm. Specimens were cast in five layers and compaction of each layer was done using vibrator. After the concrete was poured, the top surfaces of the

specimens were made even in order to provide a smooth surface for load application. The top surface of all the specimens was covered with a sheet of plastic for 24 hours, and then after 24 hours the sheet was replaced with wet burlap. This moist burlap was kept on the specimens for 28 days and water was sprayed over it every day.

3.4.5.2   CFST columns at elevated temperature 600 °C & 800 °C

For checking the post-fire performance of axially loaded CFST columns, the CFST specimens of external steel tube of diameter 100 mm, 125 mm and 150 mm with 4 mm and 5 mm thickness, in-filled with M30 grade of concrete were cast. The height for every CFST specimen was kept same i.e., 600 mm. The CFST specimens were heated in the industrial furnace at raised temperature of 600 °C & 800 °C (as shown in Figure 3.17) as per the guidelines of ISO-834.

Figure 3.17 CFST columns after heated at elevated temperature of 600 °C & 800 °C
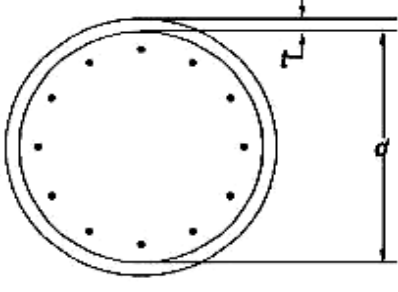
3.5 COMPARISON OF STRENGTH USING DESIGN CODES

3.5.1 Eurocode-4

The most recently developed Eurocode-4 is internationally adopted and provides the guidelines for design of composite columns. The design theory proposed by this code is based on the rigid plastic analysis method which assumes fully yielded steel and fully crushed concrete. The code uses a column curve for determining the slenderness effect in CFST columns. In Eurocode-4 the confinement effect is related to slenderness ratio ($\bar{\lambda}$) and eccentricity (*e*) of the applied loading. Eurocode-4 includes design mechanism for both concrete encased and steel filled tabular columns. Eurocode-4 gives ultimate axial force equations for both square and circular concrete filled steel tube columns. To check local

buckling of CFST columns limiting values of the specimen are governed by the equations given in Table 3.5.

Table 3.5 Limiting value of CFST column

Cross section	Shape	Max(d/t) and Max (b/t)
Circular concrete filled steel tube section		$\dfrac{d}{t} < 90\dfrac{235}{f_y}$

The ultimate axial strength of the CFST column is given by

$$N_c = A_s f_y + A_c f_{ck} \tag{3.2}$$

For circular sections, Euro code- 4 considers confinement effect provided the value of relative slenderness ($\bar{\lambda}$) less than 0.5 and (*e*/d) <0.1. Relative slenderness ($\bar{\lambda}$) is definedas

$$\bar{\lambda} = \sqrt{\frac{N_c}{N_{cr}}} \tag{3.3}$$

N_{cr} is defined as the Euler buckling strength of the composite column, mathematically given by the Eq. (3.4),

$$N_{cr} = \frac{\pi^2 (EI_{eff})}{l^2} \tag{3.4}$$

Further,

$$EI_{eff} = E_s I_s + 0.81 E_{cm} I_c \tag{3.5}$$

Where 0.81 is an empirical multiplier and E_{cm} is the secant modules of concrete. To consider the effect of long term elastic flexural stiffness, the equation is,

$$E_{eff} = \frac{E_{cm}}{y_c}$$ (3.6)

Where, y_c is the safety factor equal to 1.35

$$EI_{eff} = E_s I_s + 0.6 E_{cm} I_c$$ (3.7)

So, the ultimate load carrying capacity of a circular CFST column is calculated by using Eq. (3.8),

$$N_c = \eta_2 A_s f_y + A_c f_{ck} \left(1 + \eta_1 \frac{t f_y}{d f_{ck}} \right)$$ (3.8)

Where, η_1 and η_2 are the factors considering the confinement effect, for members without eccentricity

$$\eta_1 = \eta_{10} \text{ And } \eta_2 = \eta_{20}$$

Confinement effects are determined by relative slenderness as

$$\eta_1 = 4.9 - 18.5\bar{\lambda} + 17\bar{\lambda}^2$$ (3.9)

$$\eta_2 = 0.25(3 + 2\bar{\lambda})$$ (3.10)

χ is termed as column resistance reduction factor and is useful in diminishing the value of compressive resistance of a composite column.

$$\chi = \frac{1}{\phi + \sqrt{\phi^2 - \bar{\lambda}^2}}$$ (3.11)

Where, ϕ is a parameter depending up on the internal reinforcing bars and it is calculated by using Eq. (3.12),

$$\phi = 0.5\left[1 + 0.21(\bar{\lambda} - 0.2)\bar{\lambda}^2\right]$$ (3.12)

3.5.2 ACI– LRDF and Australian Standard

The ACI (1995) and AS (1994) codes make use of a similar formula to evaluate the axial compressive load. None of the above-mentioned codes considers the confinement effect of concrete. To avoid local buckling of the column, the limiting thickness of the steel tube depends on acquiring the yield stress in a hollow steel tube subjected to monotonic axial load which is not an essential condition in case of CFST column. The failure load is calculated as

$$N_c = A_s f_y + 0.85 A_c f_{ck} \qquad (3.13)$$

Also,

$$P_e = \frac{\pi^2 (EI_{eff})}{KL^2} \qquad (3.14)$$

$$EI_{eff} = E_s I_s + C_3 E_c I_c \qquad (3.15)$$

Where,

$$C_3 = 0.6 + 2 \left(\frac{A_s}{A_c + A_s} \right) \geq 0.9 \qquad (3.16)$$

$$\lambda = \left(\frac{KL}{\pi} \right)^2 \times \frac{N_c}{EI_{eff}} \qquad (3.17)$$

$$F_{cr} = (0.658^\lambda) N_c \qquad (3.18)$$

Where, F_{cr} is the flexural buckling stress.

$$P_n = A_s F_{cr} \qquad (3.19)$$

This observation was also made; hence they proposed a modified equation to calculate failure load as,

$$N_c = A_s f_y + 1.3 A_c f_{ck} \qquad (3.20)$$

3.5.3 AISC– LRDF

Code proposes design mechanism for composite structures. According to the LRFD design mechanism it believes that composite materials in a composite structure should act together to resist bending or in other words as one i.e., monolithically. LRFD code takes confinement effect of concrete into consideration in case of circular CFST columns by increasing strength reduction factor from 0.85 in case of rectangular CFST columns to 0.95 in case of circular CFST columns.

The code further suggests the minimum steel required shall be more than 4% in composite elements.

i.e.,$(\rho_{Sr} > 4\%)$

To resist local buckling of steel tubes, the steel tubes thickness is governed by the Eq. (3.21),

$$\frac{D}{t} = 0.15 \frac{E}{f_y} for circular CFST \qquad (3.21)$$

The ultimate load carrying capacity of circular CFST is given by the Eq. (3.22)

$$P_n = A_s f_y + \phi A_c f_{ck} \qquad (3.22)$$

For circular CFST,

$$P_n = A_s f_y + 0.85 A_c f_{ck} \qquad (3.23)$$

Compressive strength reduction factor has been increased from 0.85 to 0.95 in case of circular CFST to incorporate the effect of concrete confinement.

3.5.4 Chinese code (CECS 28:90)

The Chinese code (CECS 28:90) mainly depends upon unified theory in which the CFST column is considered as a composite member instead of discrete elements. The characteristics

of concrete filled steel tube columns are based on the properties and dimensions of both the materials i.e., concrete and steel. To determine the ultimate strength, the composite indices and geometric characteristics are mostly used. The Chinese code varies from both the codes i.e., Euro code 4 and ACI 318. In addition to bending and axial load, the code also includes the shear and torsion. Code CECS (28:90) suggests some basic requirements for CFST members as

a) $D \geq 100$ mm

b) $t \geq 4$ mm

c) $\xi = \dfrac{f_y}{A_s} \bigg/ \dfrac{f_{ck}}{A_c}$

d) $0.3 \geq \xi < 3$

e) D/t should be in the range of $(15 \sim 85)\sqrt{\dfrac{235}{f_y}}$

f) L/D should not exceed permissible limit (20 for CFST columns)

The axial load carrying capacity of CFST column is calculated by

$$N_u = \phi_1 \phi_2 N_o \qquad (3.24)$$

Where, ϕ_1 and ϕ_2 are the reduction factors incorporating the eccentric loading effect and slenderness influence respectively.

For concentric loading,

$\phi_2 = 1$

$$\phi_1 = 1 - 0.115\sqrt{\frac{l_e}{D} - 4}\,\text{for}\,\left(\frac{l_e}{D}\right) > 4 \qquad (3.25)$$

Or

$$\phi_1 = 1\,\text{for}\left(\frac{l_e}{D}\right) \leq 4 \qquad (3.26)$$

N_o is ultimate axial load carrying capacity of the short CFST columns given by

$$N_o = f_{ck}A_c\left(1 + \sqrt{\xi} + \xi\right) \tag{3.27}$$

Where, ξ is the confinement factor explained [139], mathematically given by

$$\xi = \frac{A_s f_y}{A_c f_{ck}} \tag{3.28}$$

Therefore,

(3.29)

$$N_o = f_{ck}A_c + f_y A_s + \sqrt{f_{ck}A_c/f_y A_s}$$

ξ is an important factor which determines the confinement effect on the axial strength of the CFST column. Keeping tensile strength of steel and compressive strength of concrete constant the value of the confinement factor depends up on the area of steel. This implies that when diameter of the steel tube is kept constant and thickness is varied, the more the thickness greater will be the confinement factor. The values of the confinement effect may be higher for the columns of different geometric properties, but neither the corresponding strength nor the axial load capacity will be higher. It should be also noted that confinement factor does not imply to the compressive strength and the ductility of the column.

3.6 METHODOLOGY: NUMERICAL STUDY

A finite element modelling of CFST columns was done using ABAQUS/CAE 6.14 (Computer Aided Engineering). ABAQUS/CAE 6.14 is that software application which is utilized for both modelling and analyzing the mechanical components or parts and assemblies (pre-processing) and anticipating the finite element analysis result. This software provides accurate, stable and high-efficiency of solutions to challenge the nonlinear problems, wide-ranging linear dynamics applications, and regular design simulations. This software helps in creating and importing the geometries from scratch. It allows the users to strategically use the full range of analysis functionality, for instance acoustics, connectors, damage, fracture and also the failure. Familiar concepts of ABAQUS/CAE 6.14 like as steps, interactions, sections, and materials make the interface more user-friendly.

Deng et al., [147] conducted a theoretical and numerical research using ABAQUS/CAE 6.14 software for investigating the behavior of CFSTs and post-tensioned CFSTs subjected to flexural loading. The properties of concrete were simulated using Drucker-Prager plasticity model; whereas the model used to simulate the behavior of steel tube was elastic-perfectly plastic model. The result signified from the theoretical sectional analysis and FE modeling was correlated with the test results.

Starossek et al., [137] presented a study on nonlinear finite element analysis of concrete filled steel tube (CFST) columns. The various aspects were included in the study such as effect of confinement, cracking and crushing models, the behavior of the materials properties post cracking and crushing and many others.

Abbas Y.R. et al., [235] carried out a finite element analysis (FEA) on the circular CFST stub columns using the software ABAQUS/CAE 6.14. A finite element concrete damage plasticity-based model was produced in the study and confinement was controlled by changing parameters. The results obtained from the software analysis were compared to the experimental results and both the results were found to be in good harmony.

In the present study, Johnson Cook model was used to establish the inelastic behavior of the external steel tube whereas the inelastic behavior of concrete was defined by incorporating the concrete damaged plasticity model (CDP) available in ABAQUS/CAE 6.14. The geometry used for creating models of CFST columns is shown in Table 4. The model was built on the idea of isotropic damaged elasticity to reflect the inelastic behavior of concrete. The compressive strength of concrete was observed as 36.7 MPa. The value of Poisson's ratio for concrete was taken to be 0.18 and for steel, it was 0.3. The behavior of external steel tube of CFST columns was consolidated by using Johnson Cook elasto viscoplastic model which has the ability of predicting the fracture behavior of materials which are ductile with less efforts and more efficiency. The effects of strain rate hardening, yielding, isotropic strain hardening, plastic-flow are also introduced using this model. The model utilized for incorporating the behavior of in-filled concrete subjected to composite load was plasticity-based damage model or the concrete damaged plasticity (CDP) model. The plasticity-based damaged model for concrete helps in defining the concrete behavior, when it is going through multi-axial loading conditions.

3.6.1 Element types

In this study, 8-node linear solid element (C3D8R) in ABAQUS/CAE 6.14 with lowered integration and having degree of freedom of three at every node was used for the simulation of in-filled concrete as shown in Figure 3.18. According to the literature, the elements used for the steel tubes of CFST structure were generally simulated using four nodes doubly- curved shell element (S4R) for capturing the deformation due to compression and local buckling [102, 226]. Although, it was noticed that the usage of either shell or solid element can generate results in which local buckling and deformation can be successfully captured. Additionally, utilization of shell element can make the model more receptive to excessive distortion. In addition, since the use of shell elements had no impact in reducing computational time (CPU time) of finite element analysis (FEA), therefore the C3D8R solid element was used for simulating the steel tube. The created model of outer steel tube and concrete core using ABAQUS/CAE 6.14 is shown in Figure 3.19 and 3.20.
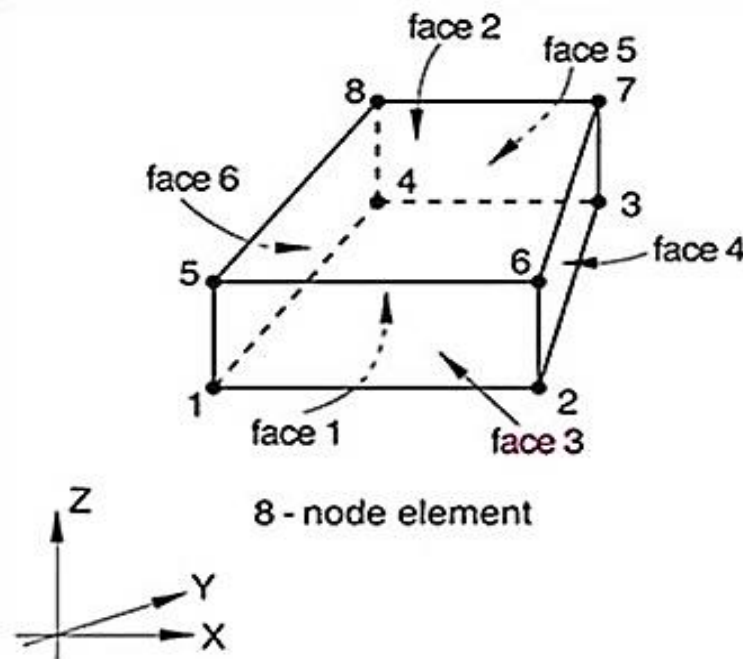
Figure 3.18 C3D8R Element [102]

Mesh convergence study was performed to work out the most appropriate mesh density in order to give precise results within reasonable computational times. The mesh size of the element was taken as 10 mm, 20 mm and 30 mm and the meshing of concrete core and outer steel tube is shown in Figure 3.21.

Figure 3.19 External steel tube

Figure 3.20 In-filled concrete core
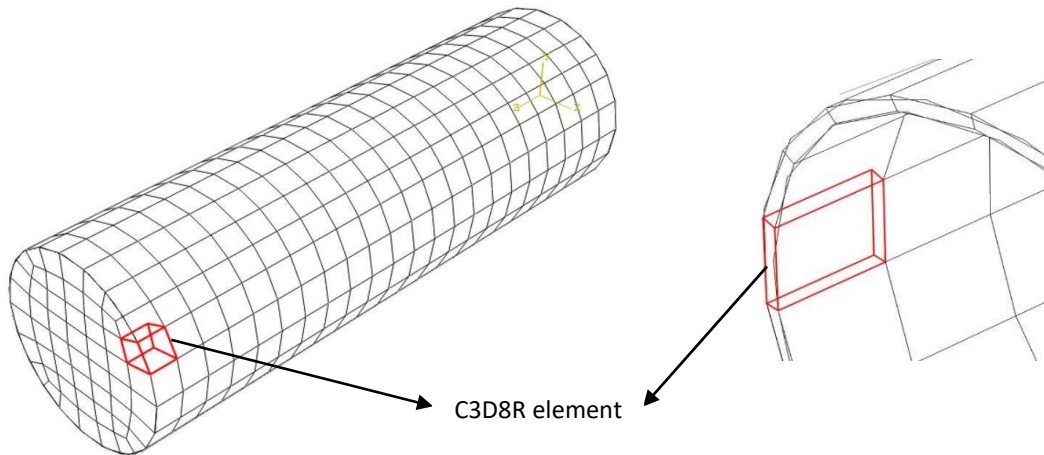
Figure 3.21 Meshing of concrete core and outer steel tube

3.6.2 Boundary conditions

The upper surface of concrete and steel was simultaneously subjected to a vertical compressive axial load using the displacement control option provided in the ABAQUS/CAE 6.14 library. The upper and the lower end of the models were restrained against all degrees of freedom, except the vertical displacement of top end which was loaded.

3.6.3 Interactions between external steel and concrete core

The contact among the inner side of the steel tube and concrete was defined by using the 'surface-to-surface contact' element provided in ABAQUS/CAE 6.14 library. Different friction coefficients (μ) were examined and it was observed that the value of friction coefficient did not have any significant effect on the results, which was expected for simultaneously loaded specimens. Yet, the value of $\mu = 0.6$ was taken [114, 181]. The inner steel surface was assigned as master surfaces and the concrete surface was assigned as the slave. The connection between concrete core and the external steel tube is shown in Figure 3.22.
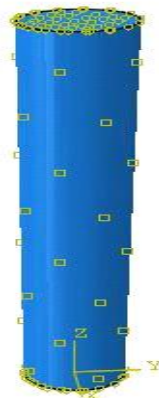
Figure 3.22 Interaction model between outer steel and concrete core

3.6.4 Material modeling

3.6.4.1 Drucker –Prager Model

Drucker-Prager model is addressed for plastic properties in the materials for which compressive stresses are more prevalent than the tensile stresses. Both commercially available software ANSYS and ABAQUS adopts the associated and non-associated plastic flow rule. The plastic flow rule controls the direction of plastic strain vector which should be normal to the Drucker-Prager failure surface that is identical to flow potential surface [147]. The associated flow rule supposes that the failure surface and flow potential surface are perfectly same as shown in Figure 3.23.
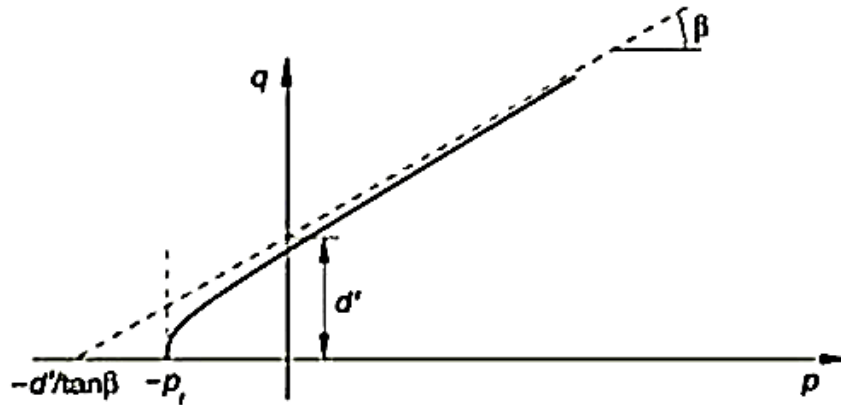
Figure 3.23 Hyperbolic Drucker Prager Rule [147]

The equation of the Drucker-Prager failure surface is as follows

$$F' = \sqrt{J_2} - I_1 \tan \phi_f - c' \tag{3.30}$$

Where, $J2$ = second deviatoric stress invariant, $I1$ = first stress invariant, φf = friction angle, φd = dilation angle and c' = cohesion.

3.6.4.2 Linear Drucker-Prager Rule
The linear Drucker-Prager criterion is as follows:

$$F = t - p tan\beta - d = 0 \tag{3.31}$$

$$t = \frac{1}{2} q \left\{ 1 + \frac{1}{K} - \left(1 - \frac{1}{K} \right) \left(\frac{r}{q} \right)^3 \right\} \tag{3.32}$$

Where, β representing slope linear yield surface in the p-t stress plane, d represents cohesion

of the material and K represents the ratio of yield stress in tri-axial tension to the yield stress in tri-axial compression.

If K = 1 then t = q, which implies that the yield surface is the Von-Mises circle in the deviatoric principal stress plane which further implies that the yield stresses in tri-axial compression and tension are exactly same. To maintain the convexity of the yield surface, the value of K is kept between 0.78 -1.0.
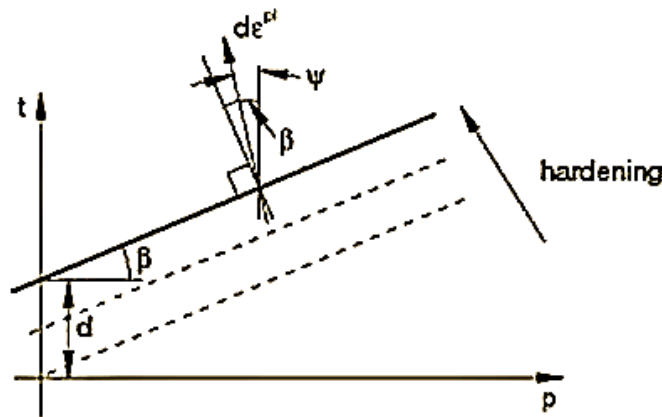
Figure 3.24 Linear Drucker-Prager model: yield surface and flow direction in the *p–t* plane [29]

$$G = t - p tan\phi \tag{3.33}$$

Where, *p* = equivalent stress

G = flow potential

φ = dilation angle

and $t = \frac{1}{2} q \left\{ 1 + \frac{1}{K} - \left(1 - \frac{1}{K}\right) \left(\frac{r}{q}\right)^3 \right\}$

For granular materials the linear model is normally used with non-associated flow, in the sense that the flow is assumed to be normal to the yield surface but with an angle ψ to the t-axis (ψ < β) as shown in Figure 3.24. The original Drucker-Prager model has associated flow with settings ψ = β and K = 1. φ = 0 represents that the inelastic deformation is incompressible. Ψ ≥ 0 means that the material can dilate. Here φ is the dilation angle andβis the friction angle.

3.6.4.3 Bond behavior between concrete and steel

Concrete is a brittle material which is good in compression and weak in tension while steel is strong in tension and has good ductility property. When the CFST, which is made up of these two materials, is subjected to tensile stresses, steel performs better and shows more lateral strain as compared to concrete (Poisson's effect). The effect of debonding on circular concrete

filled steel tube columns reveals that the occurrence of local buckling is much more critical in circular steel tube than in the specimens without debonding [32]. Bond behavior in CFST was also studied by performing a number of push-out tests on CFST specimens [126, 236]. The bond between concrete and steel is due to the three reasons:

- Chemical adhesion between concrete and steel (Part-A micro locking)
- Due to the roughness of the surface of steel (Part-B loss of bond)
- Due to the frictional resistance (Part-C macro locking)
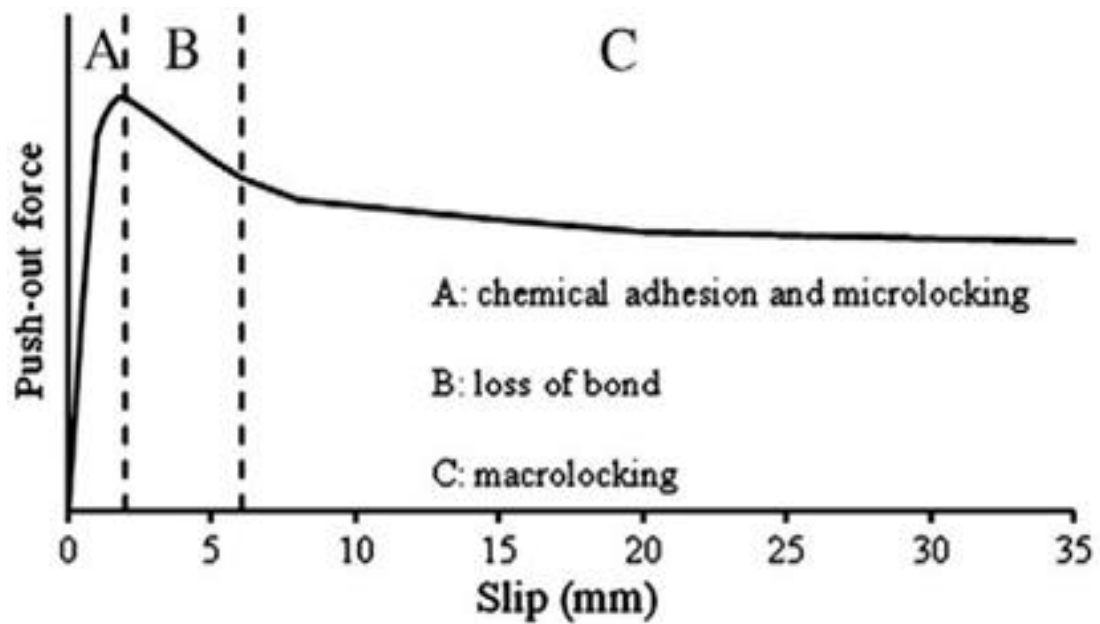
Figure 3.25 Idealized bond behavior between concrete and steel [19]

The curve shown in Figure 3.25 reveals that the first part (A) of the curve is linear and it is due to the chemical adhesion between concrete and steel. Part (B) of the curve shows the loss of bond between steel and concrete. The chemical adhesion is responsible for resisting the relative displacement or slip. After a certain value of relative displacement, the bond between concrete and steel breaks and the load is transferred through the rough surface of steel and frictional resistance between steel and concrete. It was concluded by Tao et al., [14], the bond strength between concrete and steel tube could be improved by providing the welded steel rings on to the internal surface of steel tube. Welding shear studs and expansive concrete have also been proven to be a good method to improve the bond strength after welding internal steel rings.

3.6.4.4 Frictional behavior

Cohesive elements and surface-based cohesive behavior are two methods that can be used for modelling bonded surfaces, adhesives and sticky surfaces in ABAQUS/CAE 6.14, and their modelling capabilities are very similar. They both use traction-separation law. However, the surface based cohesive behavior can be used for a wide range of contacts and it is typically easier to define than using cohesive elements. Furthermore, the surface-based cohesive behavior is intended to define interfaces with negligible thickness. In contrast, the cohesive elements are primarily designed for modelling interfaces and adhesives that have finite thickness and whose macroscopic properties, such as stiffness and strength, are available (ABAQUS, 2012). For this research, since there is not any specific adhesive layer between the steel and the concrete, it is not possible to define a thickness and macroscopic properties for the interface. Therefore, the surface-based cohesive behavior will be employed to simulate the steel-concrete interface.

3.6.4.5 Shear stress versus elastic slip

The surface-based cohesive behavior model expresses the bond between the two contacting surfaces as a linear elastic relationship between the bond stress (traction) and slip (separation). In this model, damage can be defined based on either the maximum allowable displacement or the maximum allowable stress at the interface. Figure 3.26 shows the form elastic-plastic material without hardening where sticking friction is elastic and slipping friction is plastic in nature. A user may specify the physical behavior by fixing the sticking stiffness to a certain value. By default, in ABAQUS/CAE 6.14 using "Penalty" method frictional constraints are enforced with a stiffness having a finite value. In case the sticking stiffness is infinite the elastic slip will be zero.

Where, $\tau_{\text{crit.}}$ = yield stress and k = young's modulus.

$$t = \begin{Bmatrix} t_n \\ t_s \\ t_t \end{Bmatrix} = \begin{bmatrix} k_{nn} & k_{sn} & k_{tn} \\ k_{ns} & k_{ss} & k_{ts} \\ k_{nt} & k_{st} & k_{tt} \end{bmatrix} \begin{Bmatrix} \delta_n \\ \delta_s \\ \delta_t \end{Bmatrix} = k\delta \tag{3.34}$$

Where, t representing traction stress vector, k representing elastic constitutive matrix and δ representing separation vector.

The subscripts in the equation n, s and t stands for normal and tangential behavior ($t_s = t_t$ assumed) [29]. The traction stress vector (t) has three components: the normal traction (t_n), and

the two shear tractions (t_s, t_t). The corresponding separation vector consists of the three respective slip components, in the normal (δ_n) and the two tangential (δ_s, δ_t) directions.
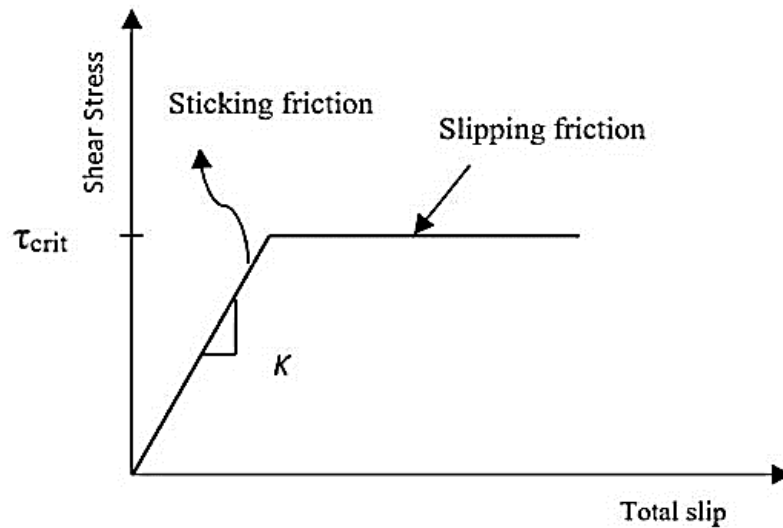
Figure 3.26 Elastic slip versus shear traction relationship for sticking and slipping friction [29].

In concrete filled steel tubular columns, the steel tube only retrains the lateral strain and provides the concrete with passive confinement as shown in Figure 3.27. The stress produced in the specimen due to confinement depends on the lateral strain and this lateral strain itself is dependent on the confining stress and thus it becomes difficult to determine the inter-dependent confining stress and the lateral strain [30].
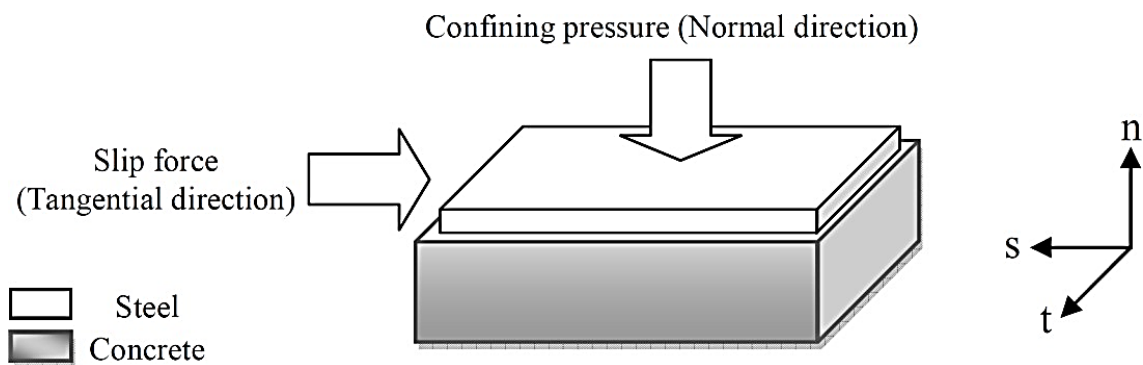
Figure 3.27 Description of directions

To simplify the calculations, it is assumed that the stresses are uniform in the specimens along the two minor principal axes of the cross-section [138,190]. Yet the assumption is theoretical, but has a good hold in the particular instance of a circular steel tube subjected to axial loading without eccentricity [120, 131]. But for the CFST specimens having square and rectangular cross section, the arching action takes place at the corners (such as in case of

104

stirrups in conventional RCC system) and buckling effect at the center of edges, which makes the confining stress non-uniform. Eccentrically loaded CFST specimens also show non-uniformity in confining stresses. Sakino et al. [95] carried out the study on the behavior of centrally loaded CFST with varying shapes and deduced that circular CFST columns have higher ultimate strength as compared to square CFST columns. Nevertheless, in the research by Tailor et. al. [113], it showed that in respect of lateral displacement, the square CFST columns work better than circular CFST columns.

3.6.4.6 Damage Modelling

The bond damage can be modelled in 2 stages: damage initiation and damage evolution as shown in Figure 3.28. Damage initiation can be defined by either the maximum stress or the maximum slip exceeding the corresponding limits. The stress or slip may be treated in isolation or combined. Consequently, there are four possible factors exceeding which damage initiation starts.

- Maximum combined (quadratic) separation (slip).
- Maximum single stress.
- Maximum single separation (slip).
- Maximum combined (quadratic)stress
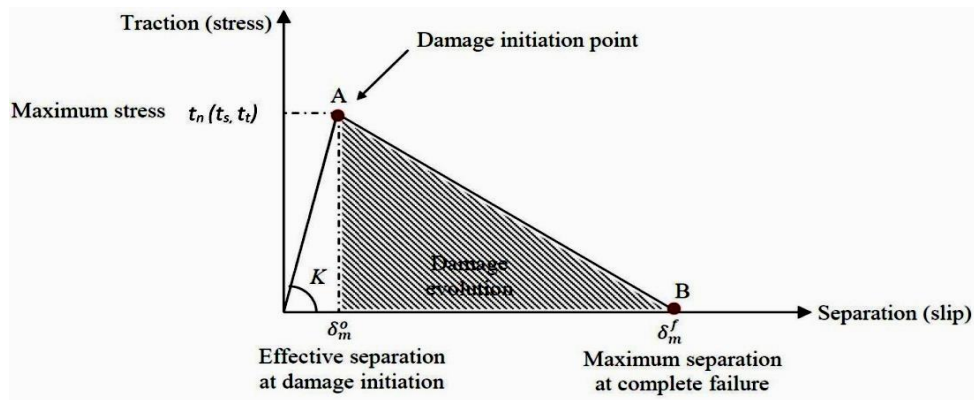
Figure 3.28 Traction-separation response model with linear damage evolution [29]

This research adopts the maximum stress criterion owing to availability of the maximum bond stress, based on existing research. In the maximum stress criterion, damage is assumed to initiate when the ratio of either of the normal or tangential stresses to the maximum allowable stress reaches a value of one. After damage initiation, "displacement type" in conjunction with a linear softening law will be used in this project to describe the evolution of damage.

3.6.4.7 Steel

For simplicity, the ideal tri linear stress-strain curve for steel was used. First, the elasticity of the steel extends along with the modulus to the yield point with a slope. The second part is the nature of plastic, which is stable under yield stress. The ideal tri linear stress-strain curve for steel is given by Figure 3.29. The properties of mild steel are listed in Table 3.6.

Table 3.6 Selection of material parameters of mild steel

Description	Notations	Parameters
Modulus of elasticity	E (N/m^2)	203×10^9
Poisson's ratio	μ	0.3
Density	ρ (kg/m^3)	7850
Yield stress constant	A (N/m^2)	304.330×10^6
Strain hardening constant	B (N/m^2)	422.007×10^6
	n	0.345
Viscous effect	C	0.0156
Thermal softening	m	0.87
Reference strain rate	$\dot{\varepsilon}_0$	0.0001 s^{-1}
Melting temperature	θ_{melt} (K)	1800
Transition temperature	$\theta_{transition}$ (K)	293
Fracture strain constant	D_1	0.1152
	D_2	1.0116
	D_3	-1.7684
	D_4	-0.05279
	D_5	0.5262

$$\varepsilon_t = 10\varepsilon_y \qquad (3.35)$$
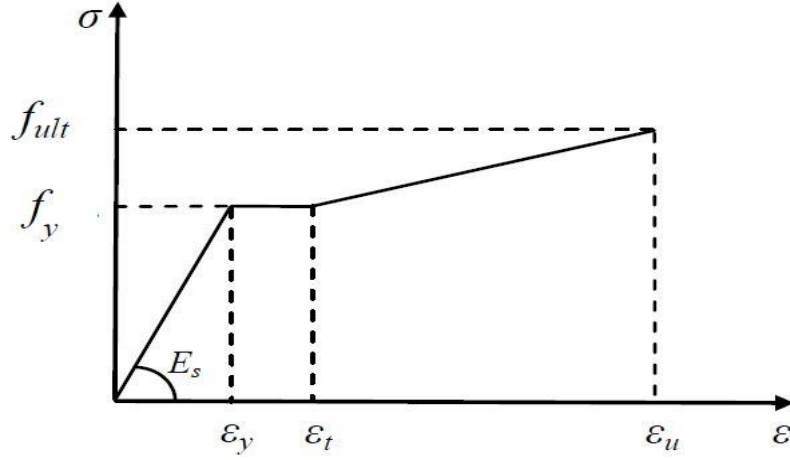
Figure 3.29 Idealized trilinear stress strain curve for steel

For defining the material properties of steel, Johnson Cook model, which is provided in ABAQUS/CAE 6.14, was used to incorporate the ductile behavior of steel tube. The steel tube with thickness of 4 mm and 5 mm was considered. The value of Poisson's ratio for steel was assumed as 0.3. The impact of strain, strain rate and temperature were incorporated using the Johnson cook elasto-viscoplastic model as it is capable to predict the material behavior of the ductile metals like steel.

The equivalent von- Mises stress $\overline{\sigma}$ of the Johnson-Cook model is defined as;

$$\overline{\sigma}(\overline{\varepsilon}^{pl}, \dot{\overline{\varepsilon}}^{pl}, \widehat{T}) = \left[A + B(\overline{\varepsilon}^{pl})^n\right]\left[1 + C\ln\left(\frac{\dot{\overline{\varepsilon}}^{pl}}{\dot{\varepsilon}_0}\right)\right]\left[1 - \widehat{T}^m\right] \qquad (3.36)$$

Where, A, B, n, C and m are material parameters, $\overline{\varepsilon}^{pl}$ is equivalent plastic strain, $\dot{\overline{\varepsilon}}^{pl}$ is equivalent plastic strain rate, $\dot{\varepsilon}_0$ is a reference strain rate and $\widehat{T}$ is non-dimensional temperature defined as;

$$\widehat{T} = (T - T_0)/(T_{melt} - T_0) \; T_0 \leq T \leq T_{melt} \qquad (3.37)$$

Where, T is the current temperature, T_{melt} is the temperature at melting point and T_0 is the room temperature. The fracture model proposed by Johnson-Cook equivalent fracture strain $\bar{\varepsilon}_f^{pl}$ is expressed as;

$$\bar{\varepsilon}_f^{pl}\left(\frac{\sigma_m}{\bar{\sigma}}, \dot{\bar{\varepsilon}}^{pl}, \hat{T}\right) = \left[D_1 + D_2 \exp\left(-D_3 \frac{\sigma_m}{\bar{\sigma}}\right)\right]\left[1 + D_4 \ln\left(\frac{\dot{\bar{\varepsilon}}^{pl}}{\dot{\varepsilon}_0}\right)\right][1 + D_5 \hat{T}] \qquad (3.38)$$

Where, $D_1 - D_5$ is material parameters determined from different mechanical tests, $\frac{\sigma_m}{\bar{\sigma}}$ is the stress triaxiality ratio and σ_m is the mean stress.

3.6.4.8 Concrete

The stress-strain curve of concrete as shown in Figure 3.30 and it is calculated using the formula given by ACI (1999) with Young's modulus E_c.

$$E_c = 4700\sqrt{f_{cc}} \qquad (3.39)$$

Where, f_{cc} is calculated by using equation 3.34. The stress strain curve of confined and unconfined concrete is specified by Figure 3.30.

$$f_{cc} = f_c + k_1 f_1 \qquad (3.40)$$

$$\varepsilon_{cc} = \varepsilon'_c\left(1 + K_2\frac{f_1}{f_2}\right) \qquad (3.41)$$

Where, k_1 and k_2 denotes the constants that could be assumed as 4.1 and 20.5 correspondingly [24, 27].

$$\frac{f_1}{f_y} = 0.043646 - 0.000832\left(\frac{d}{t}\right) \qquad \text{For } 21.7 \leq d/t \leq 47 \qquad (3.42)$$

$$n\frac{f_1}{f_y} = 0.006241 - 0.0000357\left(\frac{d}{t}\right) \text{For } 47 \leq d/t \leq 150 \qquad (3.43)$$
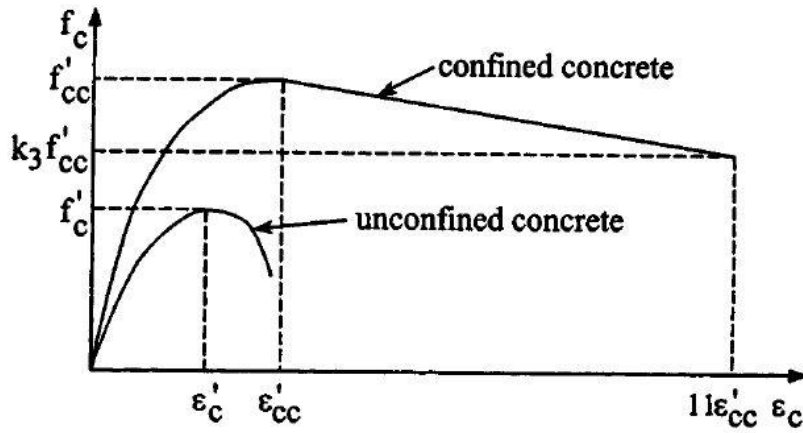
Figure 3.30 Stress strain curve for concrete

The concrete core diameters were taken as 100 mm, 125 mm and 150 mm, while keeping the constant height of 600 mm for all models. The concrete's compressive strength was observed to be 36.7 MPa. The Poisson's ratio value for concrete was assumed to be 0.18. The performance of in-filled concrete subjected to axial loading was incorporated by using the plasticity-based concrete damage model or concrete damage plasticity model. The CDP model is designed to simulate the concrete behavior when subjected to multi-axial loading conditions.

The CDP model considers non-associated plastic flow rule. The Druger-Prager hyperbolic function is used as the plastic potential function for the CDP model,

$$G = \sqrt{(f_c - mf_t \tan\beta)^2 + (\bar{q})^2} - \bar{p}\tan\beta - \sigma \tag{3.44}$$

Where,f_t and f_c are the uniaxial tensile and compressive strengths of concrete, respectively. β is the dilation angle measured in the p-q plane, $\bar{p} = -\frac{1}{3}\bar{\sigma}I$ is the effective hydrostatic stress and $\bar{q} = \sqrt{\frac{3}{2}\bar{S}\cdot\bar{S}}$ is the Mises equivalent effective stress, while $\bar{S}$ is the deviatoric part of the effective stress tensor $\bar{\sigma}$. The eccentricity parameter, m of the flow potential, G with a value of 0.1 has been found out on comparing the experimental data from bi- and tri axial strength results [231].

Lim and Ozbakkaloglu, [240] calibrated the following equations [Eqn. 3.45 and 3.46] for the ratio of the initial equiaxial to uniaxial compressive strength ratio ${f_b'}/{f_c'}$ and the second stress invariant parameter K_c as

$$f_b' / f_c' = 1 \cdot 57 f_c'^{-0.09} \tag{3.45}$$

$$K_c = 0.71 f_c'^{-0.025} \tag{3.46}$$

$$E_c = \left(5000\sqrt{f_c'}\right) \ (MPa) \tag{3.47}$$

Based on the lateral strain and axial strain relation, provided the dilation angle to be:

$$\beta = \tan^- \left[\frac{6(\nu_{c0} - \nu_{ce})}{\frac{3E_c\varepsilon_{cp}}{f_c'} + 2(\nu_{c0} - \nu_{ce}) - 3}\right] \tag{3.48}$$

Where, $\nu_{ce} = 8 \times 10^{-6} f_c'^2 + 0.0002 f_c' + 0.138$, the Poisson's ratio at the elastic condition whereas, $\nu_{c0} = 0.5$ is the Poisson's ratio of concrete at peak engineering stress. The ε_{cp}, strain at the peak compressive stress as follows:

$$\varepsilon_{cp} = \mu_a \frac{f_c'^{0.75}}{E_c} \left(\frac{\rho_C}{2320}\right)^{\varphi} \tag{3.49}$$

Where, $\mu_a = 4.26$ for the crushed aggregates or $\mu_a = 3.78$ for the rounded aggregates and $\varphi = 0.3$.

The compressive and tensile damage parameters, $D_c(\tilde{\varepsilon}_c^{pl})$ and $D_t(\tilde{\varepsilon}_t^{pl})$ can be characterized using the degraded elastic compressive and tensile stiffness as $(1 - D_c)E_c$ and $(1 - D_t)E_c$ respectively, where E_c is modulus of elasticity. The compressive and tensile damage curve for concrete and steel is shown in Figure 3.32.

The damage parameters were defined for the CDP model as:

$$D_c(\tilde{\varepsilon}_c^{in}) = \frac{\tilde{\varepsilon}_c^{in}}{\tilde{\varepsilon}_c^{in} + \frac{2\sigma_c}{E_c}} < 0 \cdot 8 \tag{3.50}$$

Table 3.7 Properties of concrete

Elastic Parameters		
Density, ρ (experiment)	**Elastic Modulus, E (Eqn. 3.39)**	**Poisson's ratio, υ (experiment)**
2240 kg/m^3	27.38 GPa	0.18
CDP Parameters		

$\dfrac{f'_b}{f'_c}$ (Eqn. 3.45)	β (Eqn. 3.48)	Eccentricity, mVan Mier [231]	K$_C$ (Eqn. 3.46)	Viscosity Parameter [240]
1.156	39.023	0.1	0.652	0.0001

The complete stress-strain behavior under uniaxial compression and linear tensile softening was based on the relationship proposed. The stress-strain behavior for concrete and steel is shown in Figure 3.31.
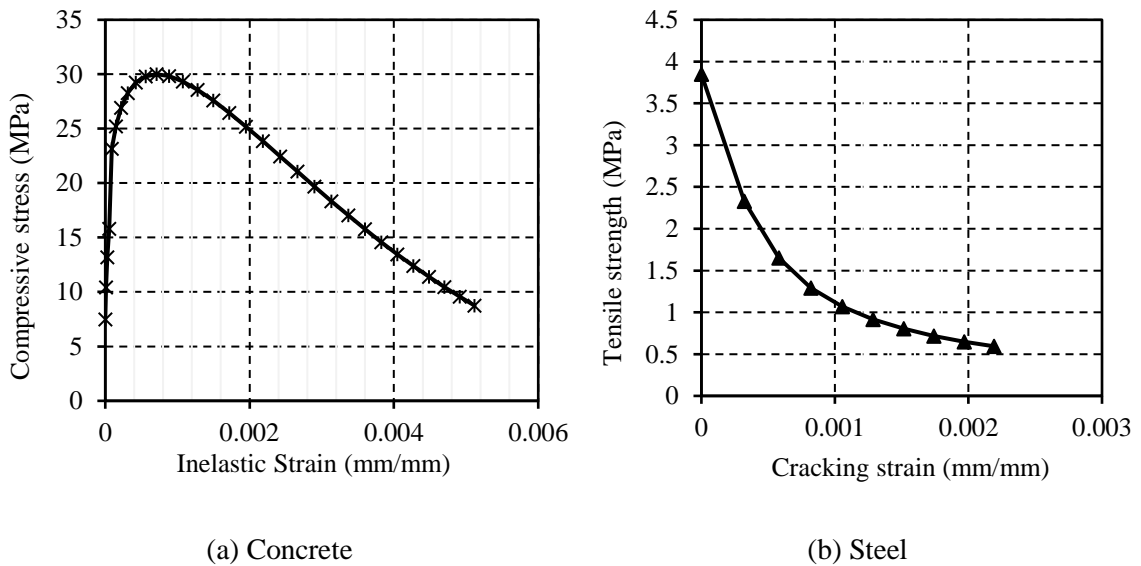
(a) Concrete   (b) Steel

Figure 3.31 Stress-strain behavior of for (a) Concrete (b) Steel

$$D_t(\tilde{\varepsilon}_t^{cr}) = \frac{\tilde{\varepsilon}_t^{cr}}{\tilde{\varepsilon}_t^{in} + \frac{5\sigma_t}{E_c}} < 0 \cdot 8 \tag{3.51}$$

Where, $\tilde{\varepsilon}_c^{in} = \varepsilon_c - \sigma_c / E_c$ is the inelastic compressive strain; $\tilde{\varepsilon}_t^{cr} = \varepsilon_t - \sigma_t/E_c$ the cracking strain.
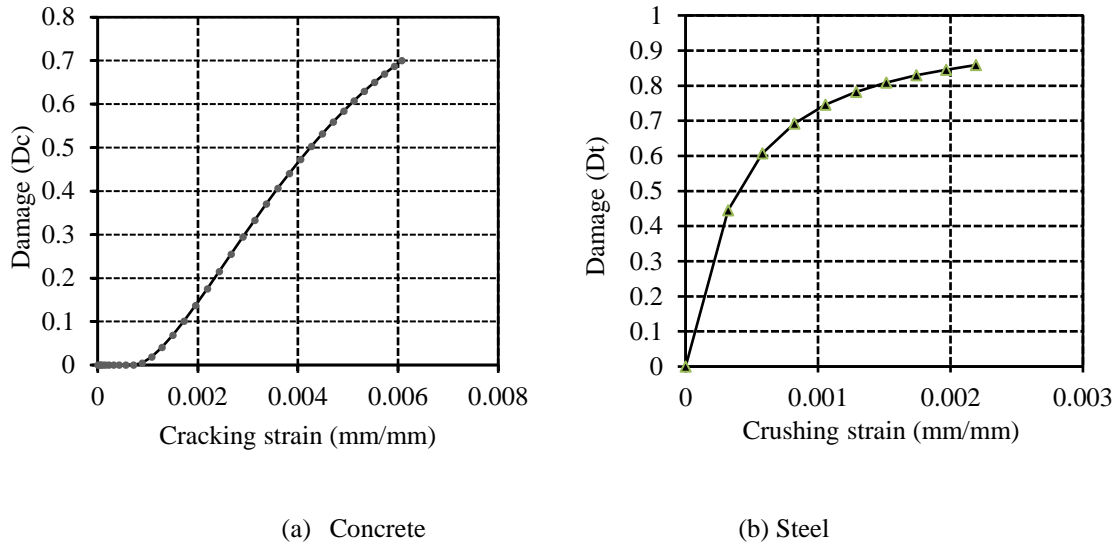
(a) Concrete   (b) Steel

Figure 3.32 Compressive and tensile damage curve for (a) Concrete (b) Steel

3.7 SUMMARY

The experimental work was performed by casting greased and non-greased concrete filled steel tube specimens to examine the bond behavior between concrete and steel. To check the post fire behavior of concrete filled steel tube column, the specimens were heated in furnace at elevated temperature of 600 °C & 800 °Cand two methods were adopted: one was annealing in which the specimens were remained in furnace for 24hours even after reaching the desired temperature and other method was quenching in which the specimens were pulled out of furnace after reaching target temperature and were immersed in water bath immediately. The load carrying capacity of the CFST columns based on different standard codes such as Eurocode-4, ACI-LRDF and Australian Standard, Chinese Code and AISC-LRDF were compared. For analytic modelling, ABAQUS/CAE 6.14 software was used to model the specimens. The various aspects such as failure pattern of specimens, load carrying capacity, load-deformation behavior was analyzed and the results obtained were compared with the experimental outcome.

CHAPTER 4

RESULTS AND DISCUSSIONS

4.1 GENERAL

This chapter encloses the results obtained from the testing programme. The critical observations and its discussions of greased and non-greased CFST tests are included. The performance of axially loaded CFST columns designated as C1T4, C1T5, C2T4, C2T5, C3T4 and C3T5 were investigated for post – fire exposure at temperatures of 600 °C and 800 °C. The results obtained from experiment were compared to the design codes such as Eurocode-4, ACI, AS, AISC-LRFD and CECS 28:90. Comparison between results from model testing with different diameter of CFST columns and thickness of steel tube and its validation by numerical analysis is given in this chapter. A brief discussion on the results obtained and comparison with published results from literature has been done.

4.2 ANALYSIS OF BEHAVIOR OF GREASED AND NON-GREASED CFST SPECIMENS

4.2.1 Axial load-deformation characteristics

The comparison between load-deformation curves of the axial loaded greased and non-greased specimens C1T4, C1T5, C2T4, C2T5, C3T4, and C3T5 are presented in Figures 4.2(a, b), Figures 4.3(a, b) and Figures 4.4(a, b).

Table 4.1 Evaluation on loading capability of greased and non-greased columns

Specimens	Load Carried by Column (kN)			
	Greased Column, P_{GC}	Non-Greased Column, P_{NGC}	% Increase in load	P_{NGC}/P_{GC}
C1T4	823	834	1.3	1.01
C1T5	827	836	1.1	1.01
C2T4	1240	1252	1.0	1.00
C2T5	1248	1263	1.2	1.01
C3T4	1714	1749	2.0	1.02
C3T5	1721	1768	2.7	1.03

The observed experimental results for greased and non-greased specimens depicts that the load-deformation behavior is almost identical to one another. The slope of load-deformation curves of greased and non-greased specimens is almost equal. However, with the increase of axial loading, there is a slightly difference between the load-deformation behavior of both the columns. The elastic axial load bearing capacity of non-greased columns are slightly greater than the greased columns as listed in Table 4.1.

The ratio of P_{NGC} and P_{GC} is found to vary from 1.00 to 1.03 for axial loaded columns. This shows that impact of contraction on the loading capability of CFST columns is relatively irrelevant as shown in Figure 4.1.
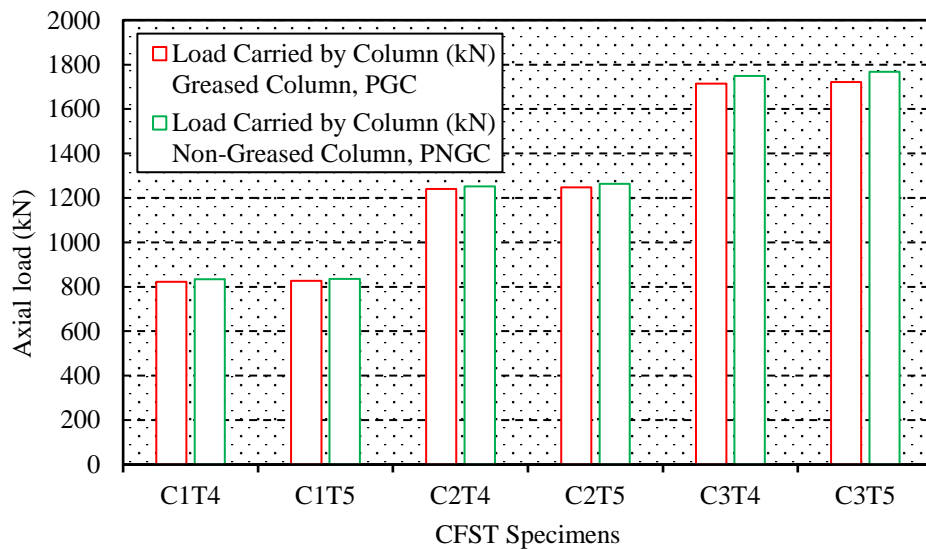
Figure 4.1 Load capacity of greased and non-greased columns
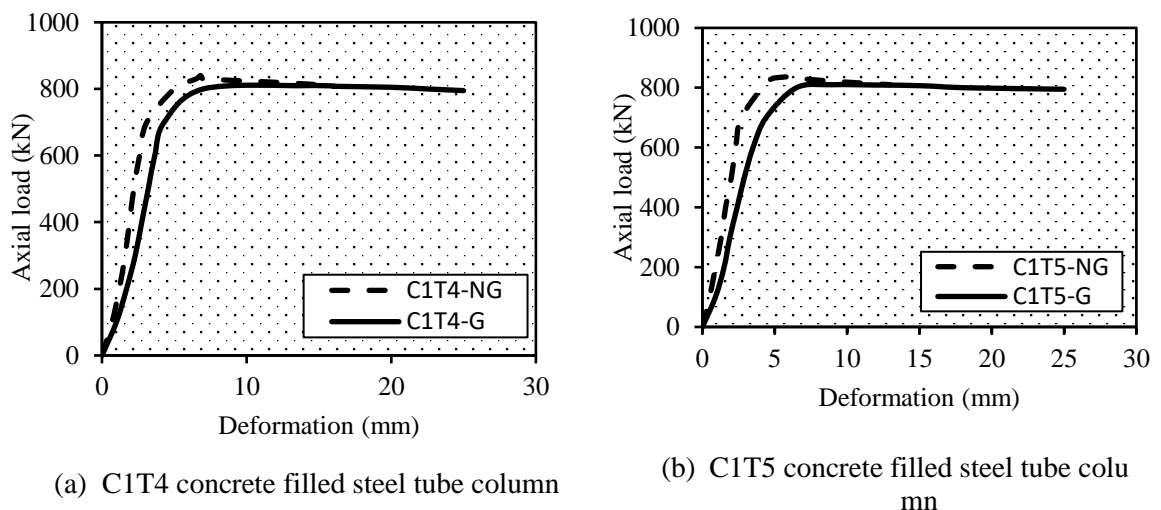
(a) C1T4 concrete filled steel tube column

(b) C1T5 concrete filled steel tube colu mn

Figure 4.2 Load-deformation curves for (a) C1T4 greased and non-greased specimens (b) C1T5greased and non-greased specimens

114

The elastic axial load capacity of non-greased columns (C1T4-NG and C1T5-NG) was higher as compared to greased columns (C1T4-G and C1T5-G). The load carrying capacity of CFST (dia. 100 mm) greased columns is found to be 823 kN and 827 kN for thickness of 4 mm and 5 mm, respectively whereas, for non-greased CFST columns of equivalent thickness, the load carrying capacity is recorded as 834 kN and 836 kN.

The maximum difference in axial load capacity of greased and non-greased CFST columns were 11 kN for 4 mm steel tube thickness, and 9 kN for 5 mm steel tube thickness. The increase in axial load capacity of CFST columns were 4 kN in case of greased columns with the increased steel tube thickness from 4 mm to 5 mm, whereas, it was only 2 kN in case of non-greased columns, which indicated that CFST columns had little influence on axial load capacity of greased and non-greased columns. The ratio of load carried by non-greased column (P_{NGC}) to the greased column (P_{GC}) was found to be 1.01 under axial loading, which indicates that the effect of shrinkage on the load carrying capacity of CFST columns is almost insignificant. The load-deformation behavior of concrete filled steel tube columns (C1T4 and C1T5) for greased and non-greased columns is presented in Figures 4.2 (a, b).
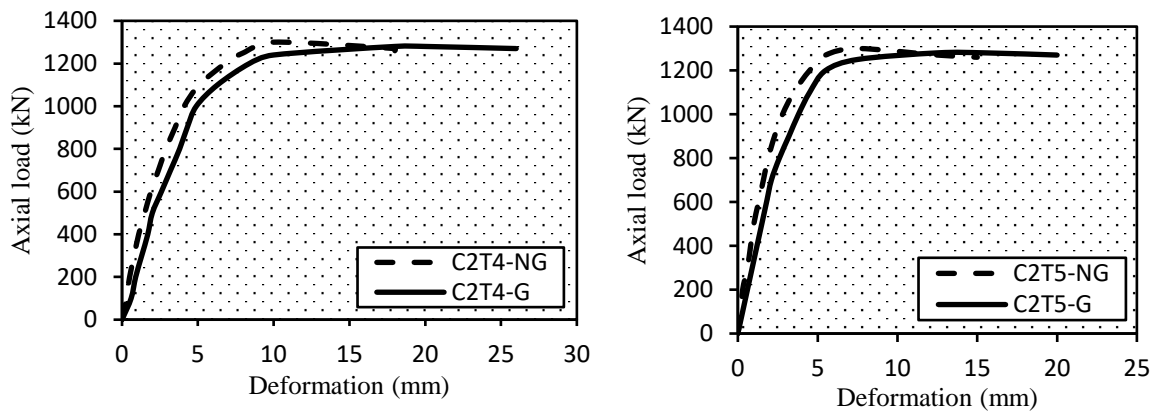
(a) C2T4 concrete filled steel tube column   (b) C2T5 concrete filled steel tube column

Figure 4.3 Load-deformation curves for greased and non-greased specimens (a) C2T4 (b) C2T5

The initial slope of load-deformation curve of C2T4-NG and C2T5-NG columns were slightly greater than C2T4-G and C2T5-G columns. The elastic axial load capacity of non-greased columns (C2T4-NG and C2T5-NG) was higher as compared to greased columns (C2T4-G and C2T5-G). The load carrying capacity of CFST greased columns were 1240 kN and 1252 kN, whereas, for non-greased CFST columns it was 1248 kN and 1263 kN with diameter 125 mm and thickness 4 mm and 5 mm respectively. The maximum difference in

axial load capacity of greased and non-greased CFST columns were 12 kN for 4 mm steel tube thickness, and 15 kN for 5 mm steel tube thickness. The increase in axial load capacity of CFST columns were 8 kN n case of greased columns with the increased steel tube thickness from 4 mm to 5 mm, whereas, it was only 11 kN in case of non-greased columns, which indicated that CFST columns had little influence on axial load capacity of greased and non-greased columns.

The ratio of load carried by non-greased column (P_{NGC}) to the greased column (P_{GC}) was found to be 1.00 and 1.01 under axial loading for 4 mm and 5 mm outer steel tube thickness respectively, which indicates that the effect of shrinkage on the load carrying capacity of CFST columns is almost insignificant. The load-deformation behavior of concrete filled steel tube columns (C2T4 and C2T5) for greased and non-greased columns is presented in Figures 4.3 (a, b).

The load-deformation curves of C1T4 and C1T5 specimens were almost coincident with each other in case of greased and non-greased columns. The initial slope of curves for greased and non-greased columns was almost same. The elastic axial load capacity of non-greased columns (C3T4-NG and C3T5-NG) was higher as compared to greased columns (C3T4-G and C3T5-G). The load carrying capacity of CFST greased columns were 1714 kN and 1721 kN, whereas, for non-greased CFST columns it was 1749 kN and 1768 kN with diameter 150 mm and thickness 4 mm and 5 mm respectively.

The maximum difference in axial load capacity of greased and non-greased CFST columns were observed to be 35 kN for 4 mm steel tube thickness, and 47 kN for 5 mm steel tube thickness. The increase in axial load capacity of CFST columns were 7 kN in case of greased columns with the increased steel tube thickness from 4 mm to 5 mm, whereas, it was 19 kN in case of non-greased columns, which indicated that CFST columns had little influence on axial load capacity of greased and non-greased columns. The ratio of load carried by non-greased column (P_{NGC}) to the greased column (P_{GC}) was found to be 1.02 and 1.03 under axial loading for 4 mm and 5 mm outer steel tube thickness respectively, which indicates that the effect of shrinkage on the load carrying capacity of CFST columns is almost insignificant. The load-deformation behavior of concrete filled steel tube columns (C3T4 and C3T5) for greased and non-greased columns is presented in Figure 4.4 (a, b).
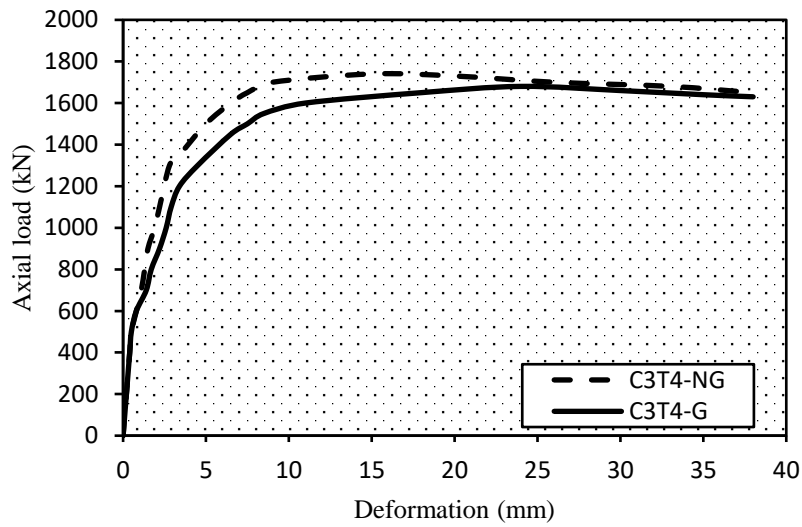
(a) C3T4 concrete filled steel tube column
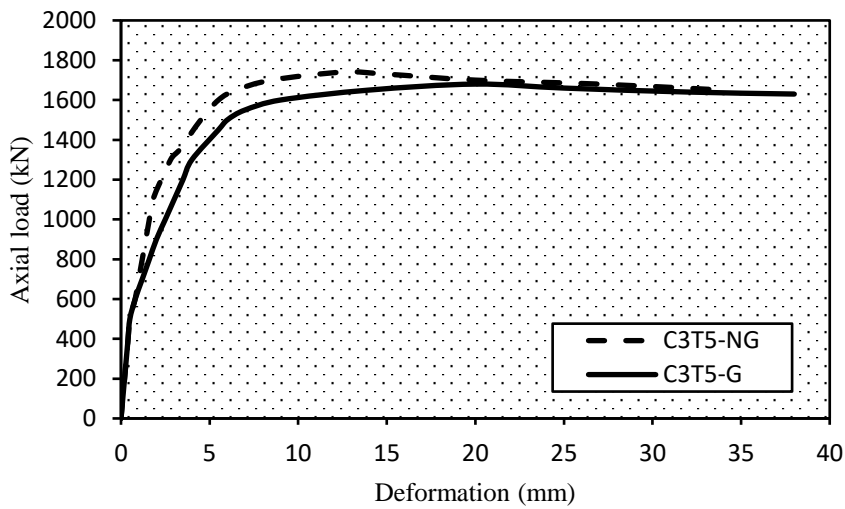
(b) C3T5 concrete filled steel tube column

Figure 4.4 Load-deformation curves for greased and non-greased specimens (a) C3T4 (b) C3T5

4.3 SECANT STIFFNESS

Secant stiffness is obtained by ratio of ultimate compressive load to the displacement at an ultimate compressive load. The obtained outcomes point out that the secant stiffness decreases for the greased specimens as compare to the non-greased specimens as listed in Table 4.2. The greased and non-greased specimen C1T4 and C1T5 loses secant stiffness ranging from 41% to 59%. The greased and non-greased specimen C2T4 and C2T5 loses secant stiffness ranging from 21% to 28%. The greased and non-greased specimen C3T4 and C3T5 loses secant stiffness ranging from 18% to 27% as shown in Figure 4.5.

117

Table 4.2 Secant stiffness of greased and non-greased CFST columns

Specimens	Secant Stiffness, (kN/mm)	
	Greased	**Non-Greased**
C1T4	50.6	123.5
C1T5	90.0	151.8
C2T4	124.0	156.5
C2T5	166.4	229.6
C3T4	71.4	87.5
C3T5	86.1	117.9
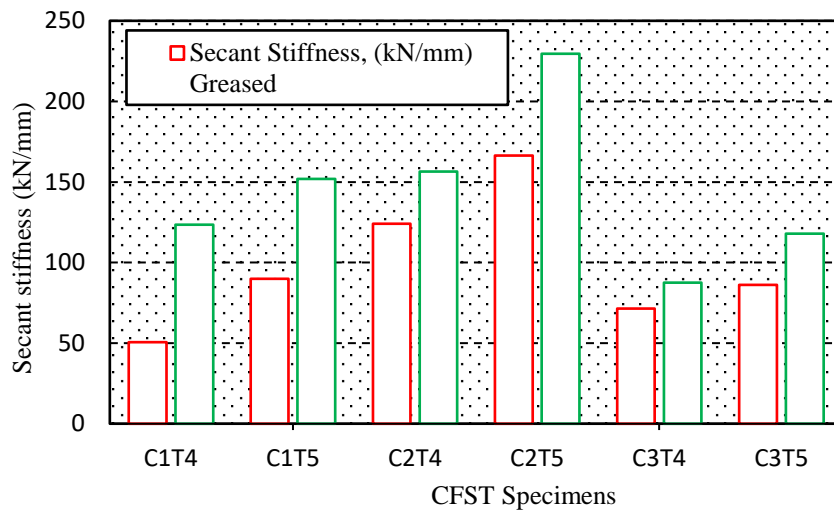
Figure 4.5 Secant stiffness of greased and non-greased CFST columns

4.4 DUCTILITY INDEX FOR GREASED AND NON-GREASED COLUMNS

The Ductility Index was obtained by an equation. DI for greased specimens decreases as compare to non-greased specimens with t = 4 mm and 5 mm as shown in Figure 4.6. This indicates that the non-greased specimens became more ductile under axial composite loading. Chacon et. al., [29] also determines the CFST column's ductility after the rise in fire exposure. The ductility index of greased and non-greased CFST columns is shown by Table 4.3.

Table 4.3 Ductility index of greased and non-greased CFST columns

Specimens	Ductility Index (DI)	
	Greased	Non-greased
C1T4	1.0	1.1
C1T5	1.2	1.2
C2T4	1.6	2.1
C2T5	1.5	1.9
C3T4	1.2	1.5
C3T5	1.4	1.6
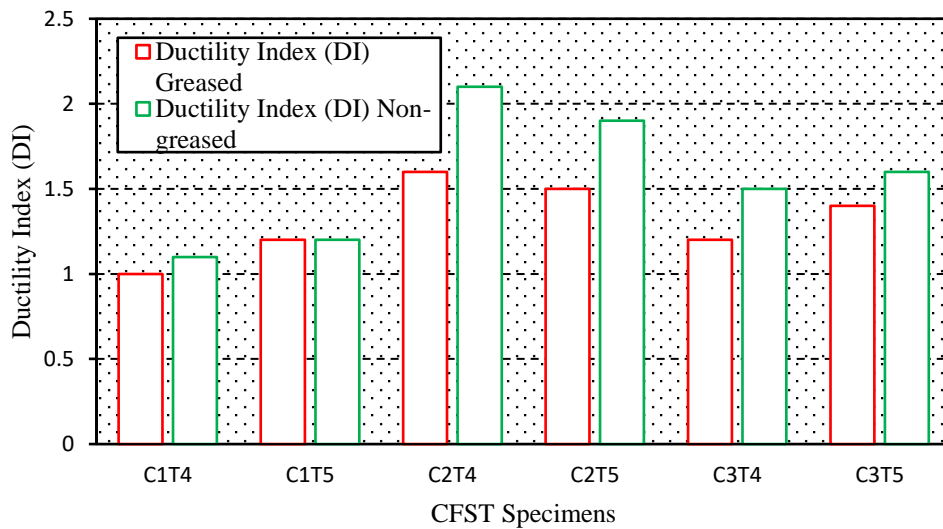
Figure 4.6 Ductility index of greased and non-greased CFST columns

4.5   BEHAVIOR OF CFST COLUMNS AT 600 °C and 800 °C

The load – deformation behavior of CFST columns (C1T4 and C1T5) at three different temperature conditions namely ambient (AB), 600 °C and 800 °C have been shown in Figures 4.7 (a) and 4.7 (b). It can be seen from figure 4.7 (a) that for CFST column with diameter of 100 mm and thickness 4 mm depicts maximum load carrying capacity at ambient temperature.

However, the load capacity for the C1T4 columns is found to reduce as the columns are exposed to increasing temperatures of 600 °C and then 800 °C. The reduction in load capacity ranges from 14.2% to 5.2% to for temperature variation from ambient to 600 °C and then to 800 °. For all the tested specimens that test are ceased at deformation of 20 mm. The decrease in load carrying capacity of the C1T4 CFST column can be attributed to the behavioral variation in thermal properties of steel with the rise in temperature. Similarly, for CFST columns with equivalent diameter of 100 mm and thickness of 5 mm, CFST columns (C1T5) depicts similar nature of load carrying as that of C1T4. However, it can be seen from figure 4.7 (b) that C1T5 columns initially depict a 4.9% higher load carrying capacity at ambient temperature than at 600 °C. However, beyond deformation of 8 mm, it is found that C1T5 columns depict similar load capacity. For C1T5 columns exposed to 800 °C, the load capacity is found to decrease by 13.6 % in comparison with CFST columns at ambient temperature. For CFST columns with same diameter of 100 mm but different steel thickness of 4 and 5mm, the higher load carrying capacity of 5 mm CFST columns can be accounted to the 836 kN.
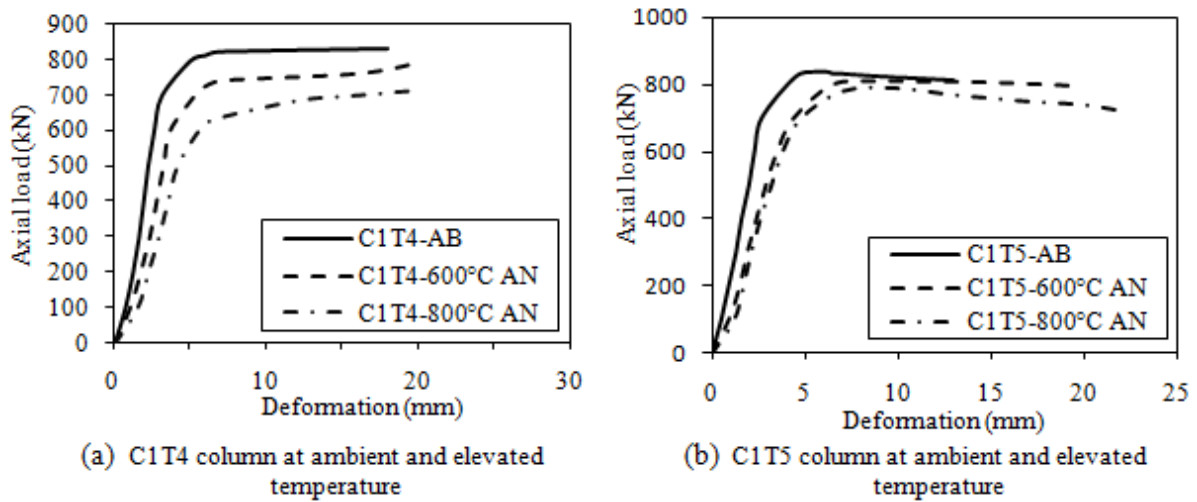
Figure 4.7 Load-deformation curves at ambient and elevated temperature (a) C1T4 (b) C1T5

The load – deformation behavior of concrete filled steel tube columns (C2T4 and C2T5) at three different temperature conditions namely ambient (AB), 600 °C and 800 °C have been shown in Figures 4.8 (a) and 4.8 (b). It can be seen from figure 4.8 (a) that for CFST column with diameter of 125 mm and thickness 4 mm depicts maximum load carrying capacity at ambient temperature. However, the load capacity for the C2T4 columns is found to reduce as the columns are exposed to increasing temperatures of 600 °C and then 800 °C. The reduction in load capacity ranges from 6.2% to 3.5% for temperature variation from ambient to 600 °C and then to 800 °. For all the tested specimens that test are ceased at deformation of 20 mm.

The decrease in load carrying capacity of the C2T4 CFST column can be attributed to the difference in the behavior of thermal properties of steel with the rise in temperature. Consistent with Eurocode, after 400 °C, change in the steel properties was seen, whereas in case of concrete, properties started differing after 200 °C. Similarly, for CFST columns with equivalent diameter of 125 mm and thickness of 5 mm, CFST columns (C2T5) depicts similar nature of load carrying as that of C2T4. However, it can be seen from figure 4.8 (b) that C2T5 columns initially depict a 4.0% higher load carrying capacity at ambient temperature than at 600 °C. However, beyond deformation of 8 mm, it is found that C2T5 columns depict similar load capacity. For C2T5 columns exposed to 800 °C, the load capacity is found to decrease by 6.6 % in contrast to CFST columns at ambient temperature. For CFST columns with same diameter of 125 mm but different steel thickness of 4 and 5mm, the higher load carrying capacity of 5 mm CFST columns can be accounted to the 1263 kN.

(a) C2T4 column at ambient and elevated temperature

(b) C2T5 column at ambient and elevated temperature
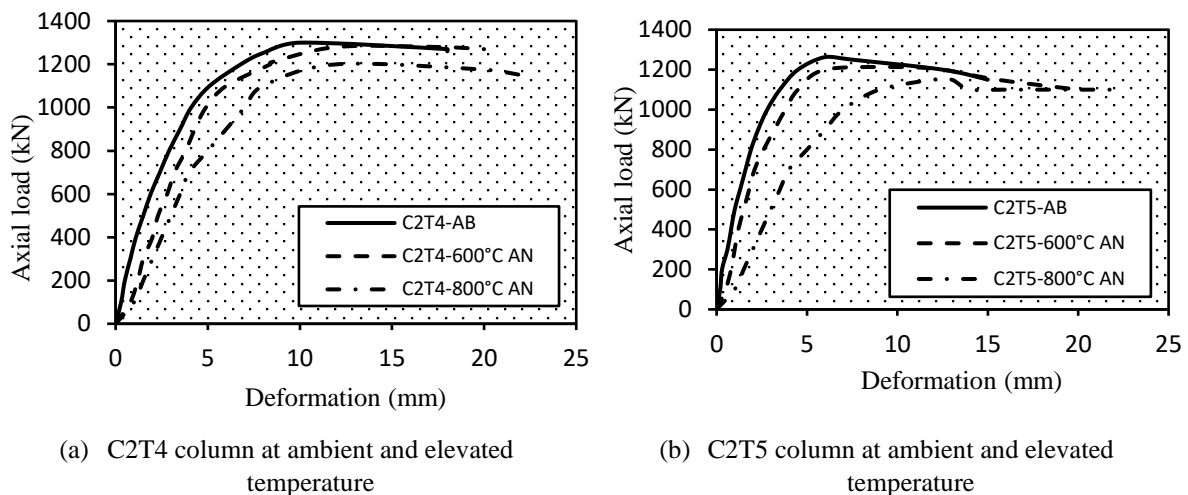
Figure 4.8 Load-deformation curves at ambient and elevated temperature (a) C2T4 (b) C2T5

The load – deformation behavior of concrete filled steel tube columns (C3T4 and C3T5) at three different temperature conditions namely ambient (AB), 600 °C and 800 °C have been shown in Figures 4.9 (a) and 4.9 (b). It can be seen from figure 4.9 (a) that for CFST column with diameter of 150 mm and thickness 4 mm depicts maximum load carrying capacity at ambient temperature. However, the load capacity for the C3T4 columns is found to reduce as the columns are exposed to increasing temperatures of 600 °C and then 800 °C. The reduction in load capacity ranges from 6.9% to 2.9% for temperature variation from ambient to 600 °C and then to 800 °. The decrease in load carrying capacity of the C3T4 CFST column can be attributed to the variation in the performance of thermal properties of steel with the rise in temperature. Similarly, for CFST columns with equivalent diameter of 150 mm and thickness

of 5 mm, CFST columns (C3T5) depicts similar nature of load carrying as that of C3T4. However, it can be seen from figure 4.9 (b) that C3T5 columns initially depict a 3.6% higher load carrying capacity at ambient temperature than at 600 °C. However, beyond deformation of 13 mm, it is found that C3T5 columns depict similar load capacity. For C3T5 columns exposed to 800 °C, the load capacity is found to decrease by 7.5 % in comparison to the CFST columns at ambient temperature. For CFST columns with same diameter of 150 mm but different steel thickness of 4 and 5mm, the higher load carrying capacity of 5 mm CFST columns can be accounted to the 1768 kN.

(a) C3T4 column at ambient and elevated temperature   (b) C3T5 column at ambient and elevated temperature
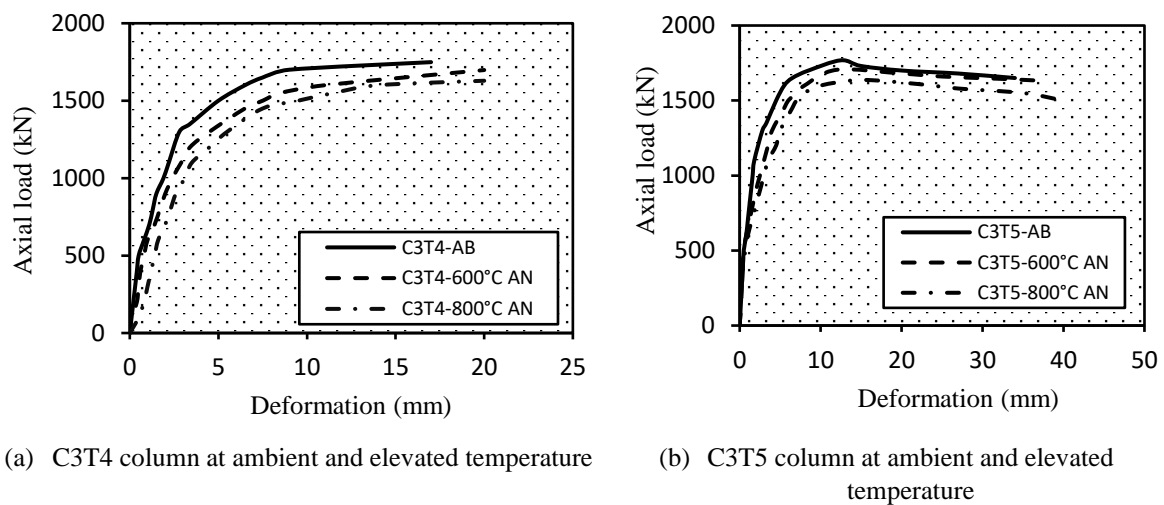
Figure 4.9 Load-deformation curves at ambient and elevated temperature (a) C3T4 (b) C3T5

4.6 EFFECT ON STRENGTH CAPACITY OF CFST COLUMNS AT A MBIENT AND ELEVATED TEMPERATURE

The load carrying capacity of CFST columns at three different temperature conditions namely ambient (AB), 600 °C and 800 °C for two cooling techniques have been shown in Figures 4.10 (a) and 4.10 (b). It can be seen from figure 4.10 (a) that for CFST column depicts maximum load carrying capacity at ambient temperature. However, the load capacity for the CFST columns is found to reduce as the columns are exposed to increasing temperatures of 600 °C and then 800 °C for two cooling processes. The reduction in load capacity ranges from 2.9% to 14.2% for temperature variation from ambient to 600 °C to 800 °. Whereas, it can be seen from figure 4.10 (b) the reduction in load capacity ranges from 17.5% to 5.0% for temperature variation from ambient to 600 °C to 800 °.
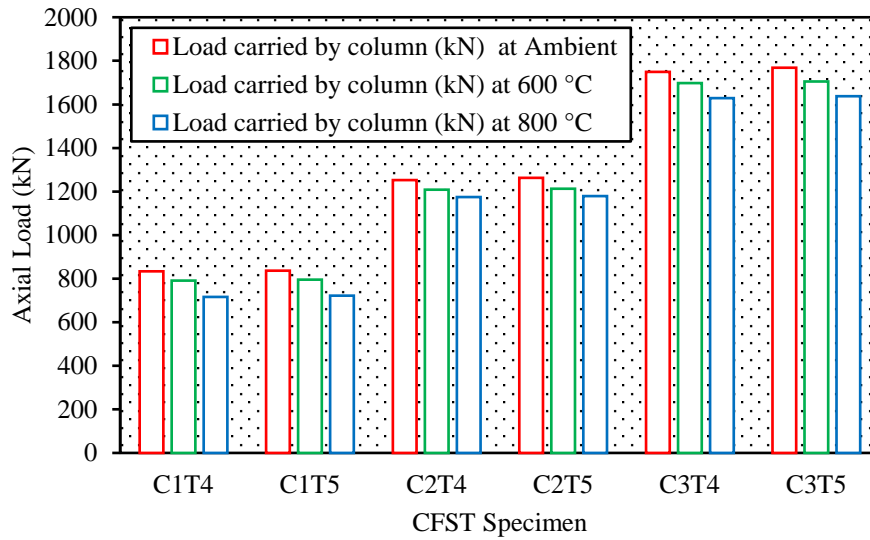
(a) Load carried by specimens for annealing at ambient and elevated temperature
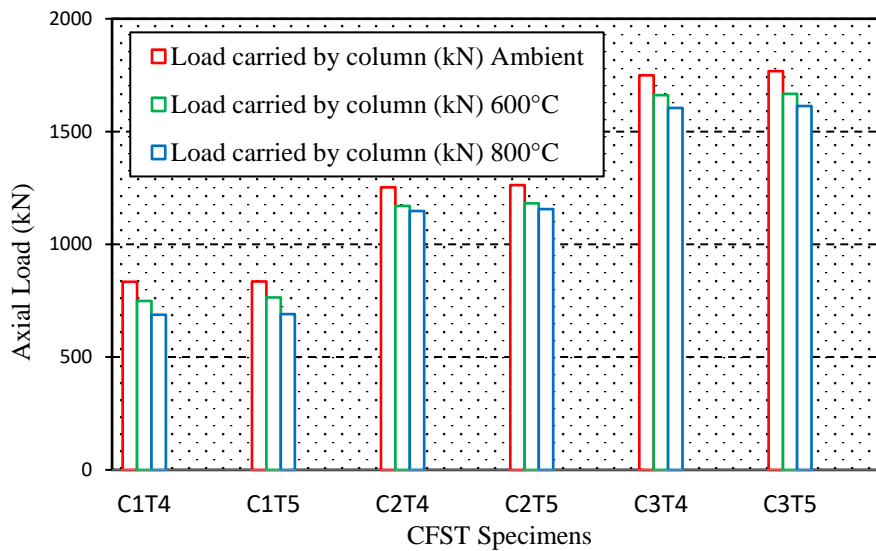
(b) Load carried by specimens for water quenching at ambient and elevated temperature

Figure 4.10 Load carried by CFST specimens at ambient and elevated temperature for (a) annealing (b) water

quenching

4.7 LOAD-DEFORMATION RESPONSE OF CFST COLUMNS AFTER H EATING AND COOLING REGIMES

After being exposed to elevated temperatures, CFST columns were cooled using two methods:

METHOD 1: Annealing

METHOD 2: Water quenching.

The results obtained from the experiment are listed in Table 4.4. The observed results indicate that the load carrying capacity of CFST columns was reduced by 9.5% to 2.7% during the post

cooling process at an elevated temperature of 600 °C to 800 °C in the case of annealing, while the reduction in strength was from 10.6% to 3.4% in the case of water quenching, which is marginally more than the case of annealing.

Table 4.4 Comparison of loading capacity of CFST columns after exposure temperature

Specimens	Size (D × Ts × H) (mm)	Axial load carried by CFST columns (kN)				
		Ambient	Annealing		Quenching	
			600 °C	800 °C	600 °C	800 °C
C1T4	100 × 4 × 600	834	791	716	749	688
C1T5	100 × 5 × 600	836	795	722	764	691
C2T4	125 × 4 × 600	1252	1208	1175	1170	1148
C2T5	125 × 5 × 600	1263	1213	1179	1182	1156
C3T4	150 × 4 × 600	1749	1698	1629	1662	1605
C3T5	150 × 5 × 600	1768	1705	1637	1667	1613

The load – deformation behavior of CFST columns (C1T4 and C1T5) at three different temperature conditions namely ambient (AB), 600 °C and 800 °C for two cooling regimes have been shown in Figures 4.11 (a-d). It can be seen from figure 4.11 (a) and (b) that for CFST column (C1T4) with diameter of 100 mm and thickness 4 mm depicts maximum load carrying capacity at ambient temperature. However, the load capacity for the C1T4 columns is found to reduce as the columns are exposed to increasing temperatures of 600 °C. The reduction in load capacity ranges from 10.2% to 5.15% for temperature variation from ambient to 600 °C in case of annealing and quenching. For all the tested specimens that test are ceased at deformation of 25 mm. Similarly, for CFST columns with equivalent diameter of 100 mm and thickness of 5 mm, CFST columns (C1T5) depicts similar nature of load carrying as that of C1T4 in case of annealing and quenching. However, it can be seen from figure 4.11 (c) and (d) that C1T5 columns initially depict a 4.9% higher load carrying capacity at ambient temperature than at 600 °C. However, beyond deformation of 10 mm, it is found that C1T5 columns depict similar load capacity in case of annealing and quenching. For C1T5 columns exposed to 800 °C, the load capacity is found to decrease by 17.3% to 13.6% in case of annealing and quenching as compared to CFST columns at ambient temperature. The decrease in load carrying capacity of the C1T4 CFST column can be attributed to the sudden escape of gases and extreme hardening in case of water quenching.

(a)   C1T4 at ambient and 600 °C (annealing and quenching)

(b) C1T4 at ambient and 800°C (annealing and quenching)

(c)   C1T5 at ambient and 600°C (annealing and quenching)

(d)   C1T5 at ambient and 800°C (annealing and quenching)
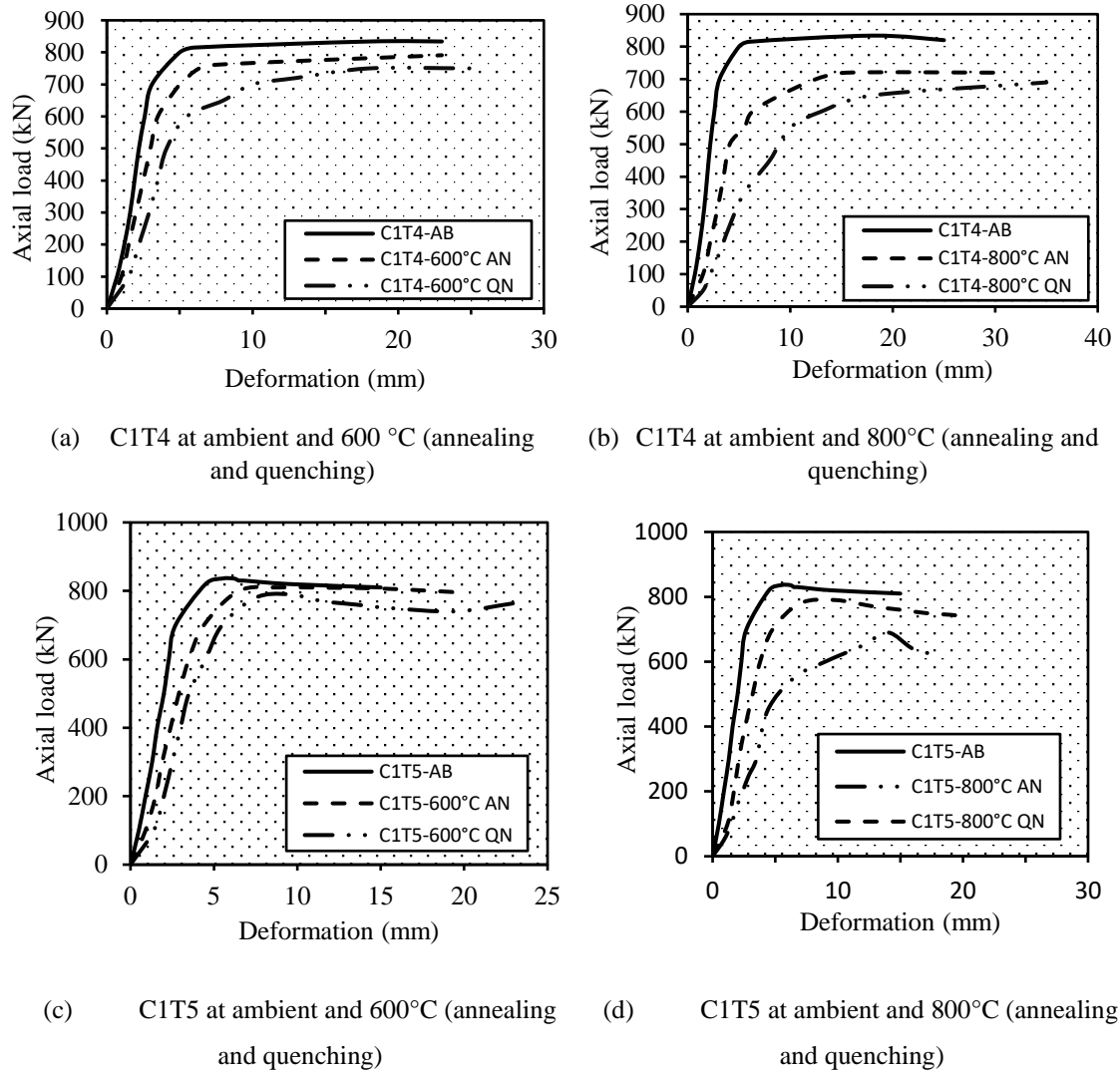
Figure 4.11 Load carried by CFST specimens for annealing and quenching (a) C1T4 at 600 °C (b) C1T4 at 800°C   (c) C1T5 at 600 °C (d) C1T5 at 800°C

The load – deformation behavior of CFST columns (C2T4 and C2T5) at three different temperature conditions namely ambient (AB), 600 °C and 800 °C for two cooling regimes have been shown in Figures 4.12 (a-d). It can be seen from figure 4.12 (a) and (b) that for CFST column (C2T4) with diameter of 125 mm and thickness 4 mm depicts maximum load carrying capacity at ambient temperature. However, the load capacity for the C2T4 columns is found to reduce as the columns are exposed to increasing temperatures of 600 °C. The reduction in load capacity ranges from 6.5% to 3.5% for temperature variation from ambient to 600 °C in case of annealing and quenching. For all the tested specimens that test are ceased at deformation of 20 mm. Similarly, for CFST columns with equivalent diameter of 125 mm and thickness of 5 mm, CFST columns (C2T5) depicts similar nature of load carrying as that of C2T4 in case of annealing and quenching. However, it can be seen from figure 4.12 (c)

and (d) that C2T5 columns initially depict a 3.9% higher load carrying capacity at ambient temperature than at 600 °C. However, beyond deformation of 10 mm, it is found that C2T5 columns depict similar load capacity in case of annealing and quenching. For C2T5 columns exposed to 800 °C, the load capacity is found to decrease by 8.5% to 6.6% in case of annealing and quenching as compared to CFST columns at ambient temperature. The decrease in load carrying capacity of the C2T4 CFST column can be attributed to the sudden escape of gases due to cooling process and extreme hardening which can have exploded a couple of twist or surface flaws that may be introduced due to unbalance heating & cooling phases in case of water quenching.
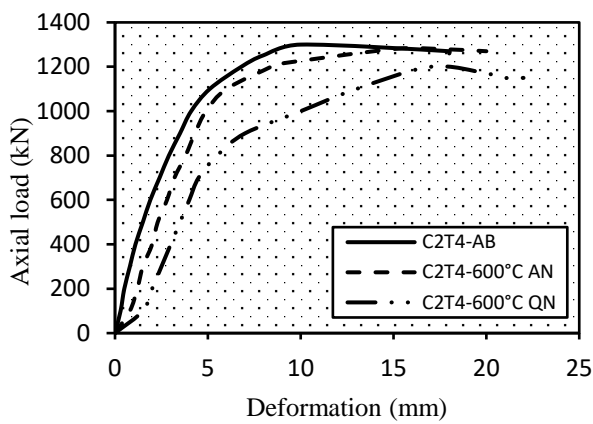
(a) C2T4 at ambient and 600°C (annealing and quenching)
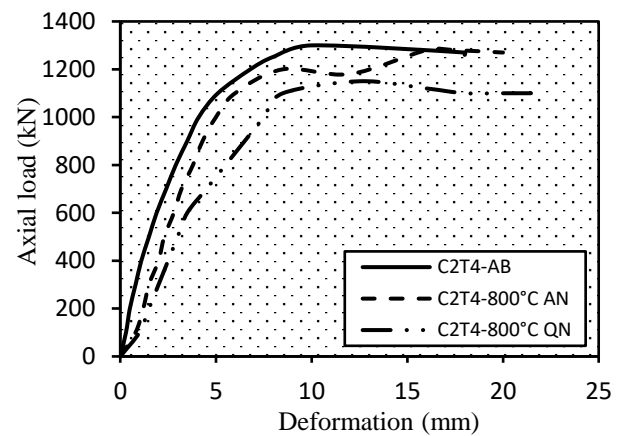
(b) C2T4 at ambient and 800°C (annealing and quenching)
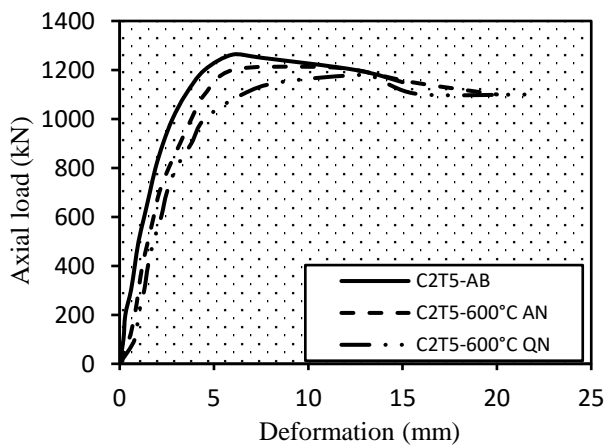
(c) C2T5 at ambient and 600°C (annealing and quenching)
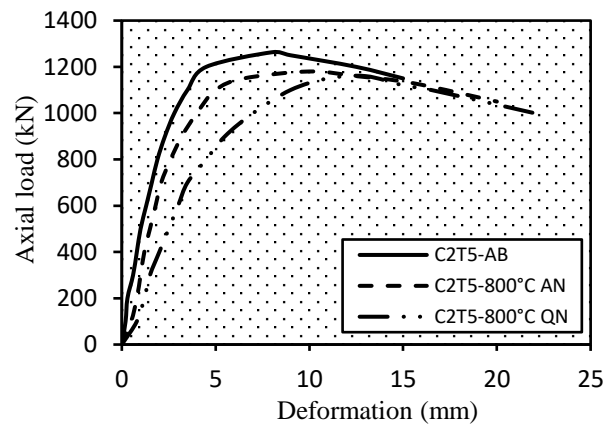
(d) C2T5 at ambient and 800°C (annealing and quenching)

Figure 4.12 Load carried by CFST specimens for annealing and quenching (a) C2T4 at 600 °C (b) C2T4 at 800°C (c) C2T5 at 600 °C (d) C2T5 at 800°C

126

The load – deformation behavior of CFST columns (C3T4 and C3T5) at three different temperature conditions namely ambient (AB), 600 °C and 800 °C for two cooling regimes have been shown in Figures 4.13 (a-d). It can be seen from figure 4.13 (a) and (b) that for CFST column (C2T4) with diameter of 150 mm and thickness 4 mm depicts maximum load carrying capacity at ambient temperature. However, the load capacity for the C3T4 columns is found to reduce as the columns are exposed to increasing temperatures of 600 °C. The reduction in load capacity ranges from 5.7% to 2.9% for temperature variation from ambient to 600 °C in case of annealing and quenching. For all the tested specimens that test is ceased at deformation of 18 mm. Similarly, for CFST columns with equivalent diameter of 150 mm and thickness of 5 mm, CFST columns (C3T5) depicts similar nature of load carrying as that of C2T4 in case of annealing and quenching.
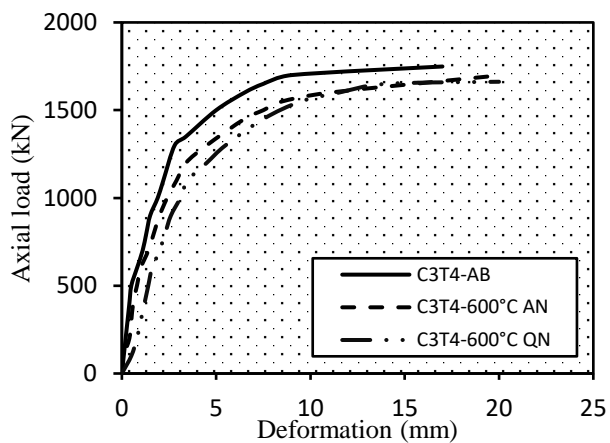
(a) C3T4 at ambient and 600°C (annealing and quenching)
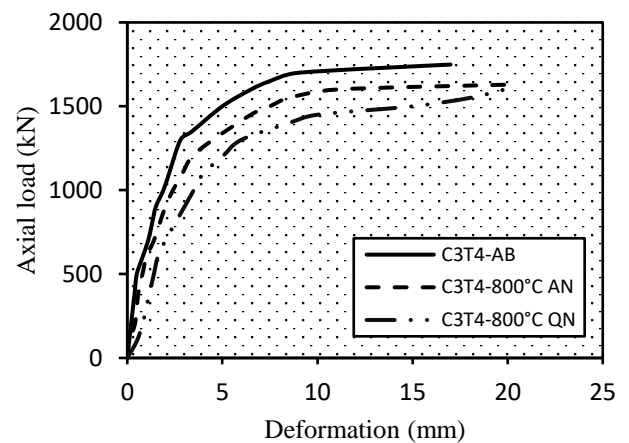
(b) C3T4 at ambient and 800°C (annealing and quenching)
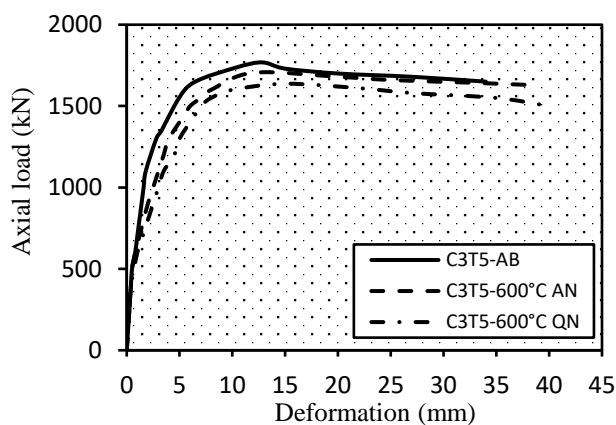
(c) C3T5 at ambient and 600°C (annealing and quenching)
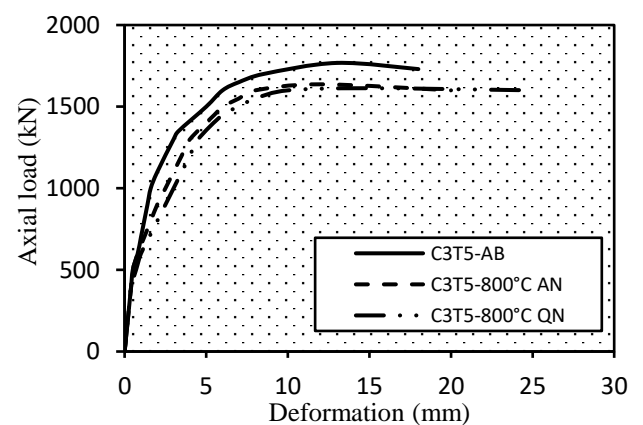
(d) C3T5 at ambient and 800°C (annealing and quenching)

Figure 4.13 Load carried by CFST specimens for annealing and quenching (a) C3T4 at 600 °C (b) C3T4 at 800°C (c) C3T5 at 600 °C (d) C3T5 at 800°C

However, it can be seen from figure 4.13 (c) and (d) that C3T5 columns initially depict a 3.6% higher load carrying capacity at ambient temperature than at 600 °C. However, beyond deformation of 10 mm, it is found that C3T5 columns depict similar load capacity in case of annealing and quenching. For C3T5 columns exposed to 800 °C, the load capacity is found to decrease by 8.8% to 7.5% in case of annealing and quenching as compared to CFST columns at ambient temperature. The decrease in load carrying capacity of the C3T4 CFST column can be attributed to the sudden escape of gases due to cooling process and extreme hardening which can have exploded a couple of twist or surface flaws that may be introduced due to unbalance heating & cooling phases in case of water quenching.

4.8 SECANT STIFFNESS OF CFST COLUMNS AFTER ELEVATED TEMPERATURE

Secant stiffness is the ratio of ultimate compressive load to displacement at ultimate compressive load. Table 4.5 shows that the secant stiffness of CFST columns decreases as temperature increases.

Table 4.5 Secant stiffness of CFST columns after exposure of fire

| Specimens | Secant Stiffness, (kN/mm) | | | | |
| | Ambient | Annealing | | Quenching | |
		600 °C	800 °C	600 °C	800 °C
C1T4	123.5	108.8	93.1	97.3	88.3
C1T5	151.8	123.5	94.1	101.9	93.2
C2T4	156.5	143.8	78.3	117.0	76.5
C2T5	229.6	121.3	88.5	118.2	77.1
C3T4	187.5	145.5	116.4	110.8	89.7
C3T5	217.9	142.1	109.1	111.1	107.5

Figures 4.14 and 4.15 display the secant stiffness of CFST columns at three different temperature conditions: ambient (AB), 600 °C, and 800 °C for two cooling regimes. Figure 4.14 (a) shows that the highest secant stiffness at ambient temperature is for the CFST column. However, when CFST columns are subjected to elevated temperatures of 600 °C and then 800 °C for two cooling regimes, the secant stiffness of the columns is found to decrease. For

temperature increases from ambient to 600 °C and then 800 °C in the case of annealing, the decrease in secant stiffness varies from 45.5% to 14.4%.
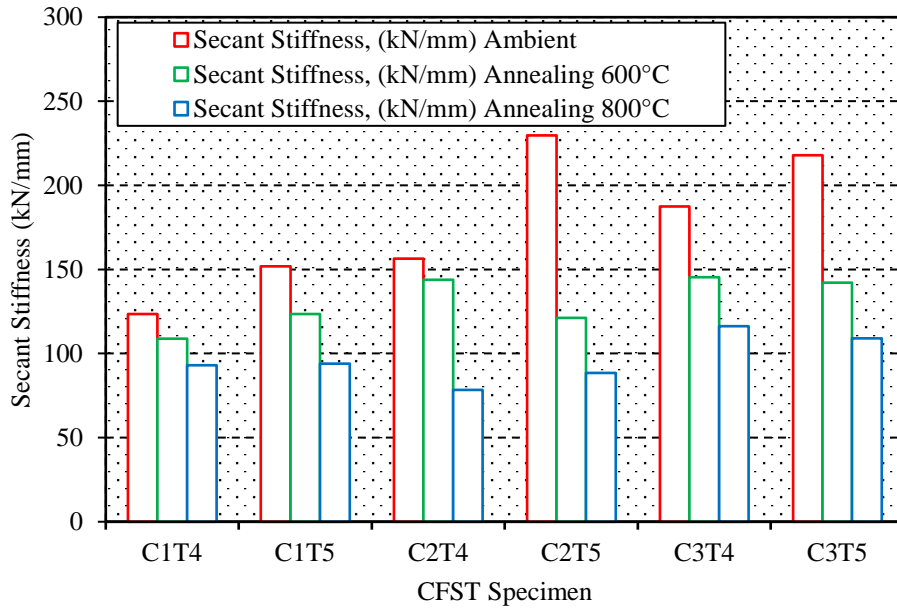
(a) Secant stiffness for annealing at 600 °C and 800 °C
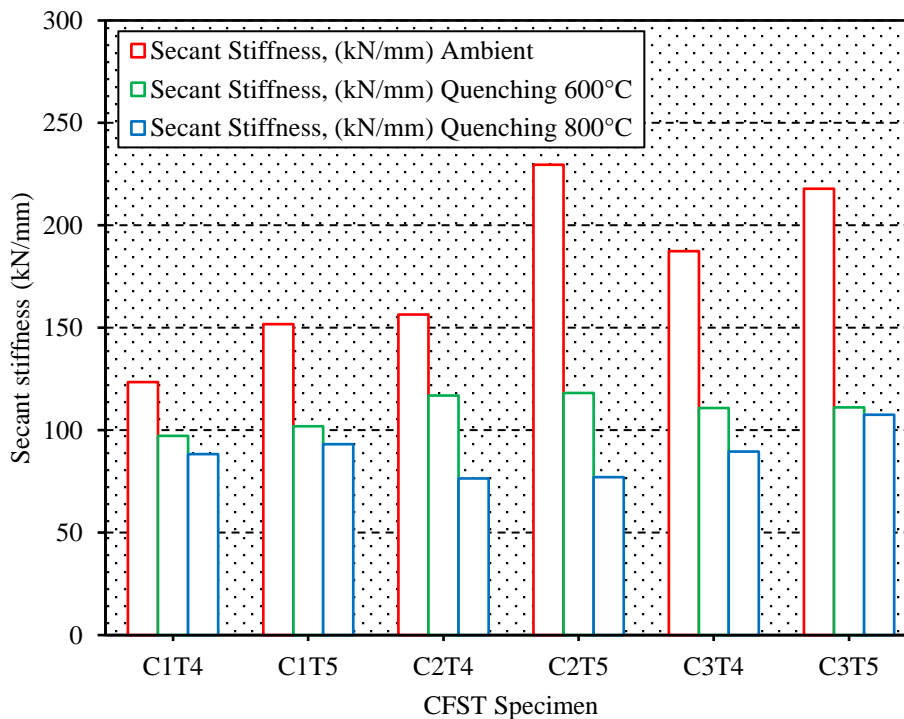
(b) Secant stiffness for water quenching at 600°C and 800 °C

Figure 4.14 Secant stiffness of CFST columns at 600°C and 800 °C for (a) Annealing (b) Water quenching

Whereas, in the case of quenching, the reduction in secant stiffness varies between 34.6% to 13.2% depending on the temperature variation from ambient to 600 °C and then 800 °C, as shown in Figure 4.14 (b). Since there is more heat absorption before the cooling step in the annealing process than in the water quenching process, the loss in secant stiffness of the CFST column is slightly higher.

4.9 DUCTILITY INDEX OF CFST COLUMNS AFTER ELEVATED TEMPERATURE

Figures 4.15 and 4.16 display the ductility index of CFST columns for two cooling regimes at three different temperatures: ambient (AB), 600°C, and 800°C. Figures 4.15 (a) and (b) display the minimum ductility index at elevated temperatures for the CFST column. However, when CFST columns are subjected to elevated temperatures of 600 °C and then 800 °C for two cooling regimes, the ductility index of the columns is found to decrease. This means that after annealing, the CFST columns become more ductile than after water quenching under axial loading. It's often related to changes in concrete and steel properties after being exposed to high temperature as listed in Table 4.6.

Table 4.6 Ductility index of CFST columns after exposure of fire

| Specimens | Ductility Index (DI) | | | | |
| | Ambient | Annealing | | Quenching | |
		600 °C	800 °C	600 °C	800 °C
C1T4	1.1	1.1	1.0	1.0	1.0
C1T5	1.2	1.2	1.1	1.2	1.1
C2T4	2.0	1.9	1.7	1.8	1.6
C2T5	1.9	1.6	1.5	1.4	1.2
C3T4	1.5	1.5	1.4	1.3	1.2
C3T5	1.6	1.5	1.4	1.5	1.3
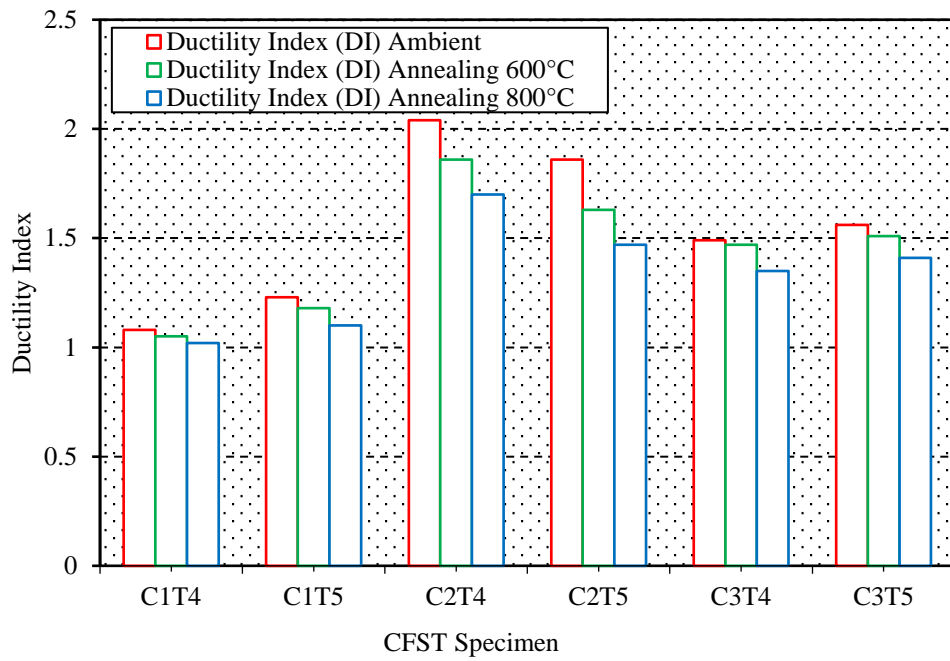
(a) Ductility index for annealing at 600°C and 800 °C
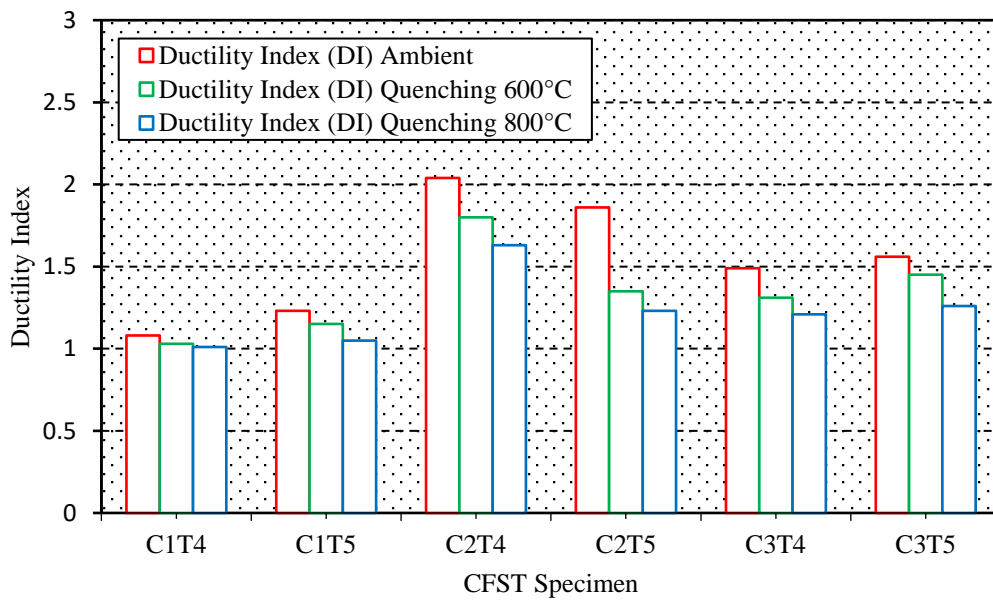
(b) Ductility index for water quenching at 600°C and 800 °C

Figure 4.15 Ductility index of CFST column at 600°C and 800 °C(a) Annealing (b) Water Quenching

4.10 RESIDUAL STRENGTH INDEX OF CFST COLUMNS AFTER EL EVATED TEMPERATURE

The equation [50] was used to measure the residual strength index of CFST columns. The residual strength index (RSI) indicates that if the RSI value is higher than the RSI minimum value, the loss within the strength of CFST columns is greater [34]. Therefore, the value of RSI in the case of the control specimen was zero, suggesting that no failure was observed during the specimen's height. In Table 4.7, the measured RSI values for CFST specimens are listed.

Table 4.7 Residual strength index of CFST columns after exposure of fire

Specimens	Residual Strength Index (%)			
	Annealing		Quenching	
	600 °C	800 °C	600 °C	800 °C
C1T4	83.7	91.4	86.4	95.1
C1T5	81.5	89.8	85.9	94.8
C2T4	93.5	96.5	94.3	97.0
C2T5	91.7	93.6	93.8	96.5
C3T4	92.8	95.0	95.6	98.4
C3T5	91.2	92.3	93.1	97.1

Figures 4.16 display the residual strength index of CFST columns for two cooling regimes at three different temperature conditions: ambient (AB), 600 °C, and 800 °C. Figure 4.16 indicates the overall residual strength index for the CFST column at 800 °C elevated temperature in the case of water quenching. However, as the temperature increases, the residual strength index of CFST columns rises. At 800 °C, the residual strength index was higher than at 600 °C. This may be because a thicker section of steel obstructs heat transfer from steel to concrete. The best temperature obtained by concrete was reduced as a result, reducing the residual strength index value.
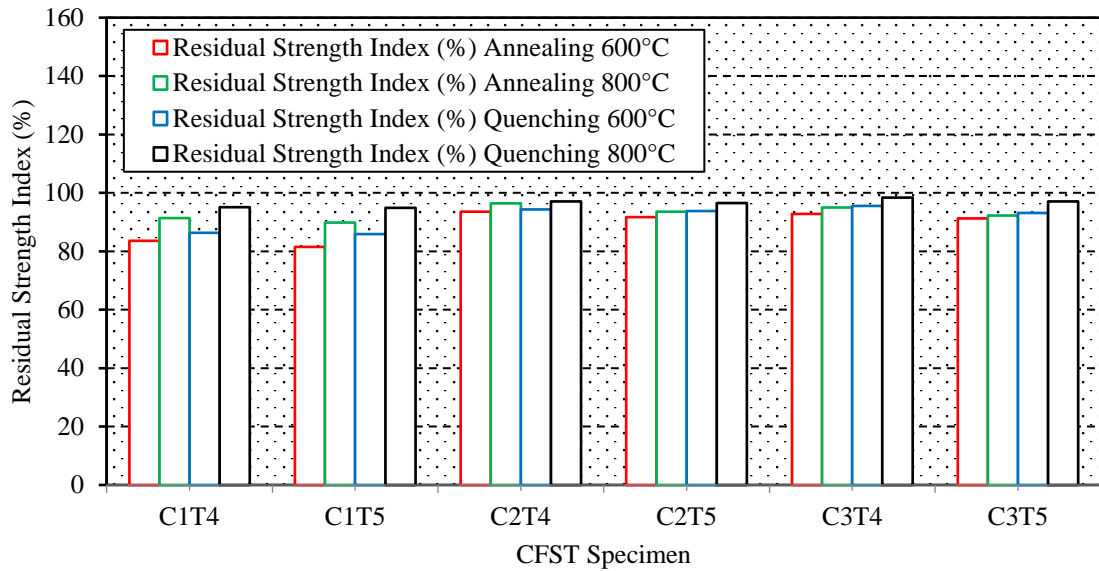
Figure 4.16 Residual strength index of CFST column at 600°C and 800 °C elevated temperature after annealing and water quenching

4.11 COMPARISON OF EXPERIMENTAL RESULTS WITH DESIGN CODES

4.11.1 Eurocode-4

For concrete-filled steel tube columns, the design load was determined using Eq (3.2). The design loads are determined based on the total of the individual ultimate axial capacities of the steel tube and concrete, as specified by Eurocode-4. Tables 4.8 and 4.9 demonstrate the load capacity of CFST columns with Eurocode-4 greased and non-greased surfaces.

Table 4.8 Comparisons of experimental result of greased columns and Eurocodes-4

Specimens	Experimental load capacity, N_e (kN)	Eurocode-4, N_c(kN)	N_e/ N_c	% error
C1T4	823	612.1	1.3	25.6
C1T5	827	688.8	1.2	16.7
C2T4	1240	999.6	1.2	19.4
C2T5	1248	1131.2	1.1	9.4
C3T4	1714	1421.4	1.2	17.1
C3T5	1721	1607.9	1.1	6.6

133

Tables 4.8 and 4.9 display a difference of axial load capacity of experimental results for greased and non-greased columns with Eurocode-4 for CFST columns. The difference in axial load capacity between the exploratory result and Eurocode-4 of greased CFST columns with a steel tube thickness of 4 mm was 25.6%, 17.3%, and 16.3% of the diameter of the outer steel tube 100 mm, 125 mm, and 150 mm, respectively. Whereas, for steel tube diameters of 100 mm, 125 mm, and 150 mm, it was 13.4%, 6.7%, and 5.7% for 5 mm steel tube thickness, respectively.

It was also seen that for steel tube diameters of 100 mm, 125 mm, and 150 mm, the disparity in axial load capacity between experimental results and Eurocode-4 of non-greased CFST columns with steel tube thickness of 4 mm was 26.6%, 20.2%, and 18.7%, respectively. For steel tube diameters of 100 mm, 125 mm, and 150 mm, the percentages were 17.6%, 10.4%, and 9.1%, respectively, for a 5 mm steel tube thickness. As shown in Figures 4.17 and 4.18, the most substantial variations between experimental results and Eurocode-4 for greased and non-greased specimens with a 4 mm steel tube thickness were found to be reduced within the range of 26.6% to 25.6%, respectively, for C1T4 specimens. The average Ne/Nc for greased columns was 1.2, while it was 1.3 for non-greased columns. For greased and non-greased specimens with a 5 mm steel tube diameter, the difference between experimental results and Eurocode-4 was found to be between 6.6% and 9.1% for C3T5 specimens, respectively.
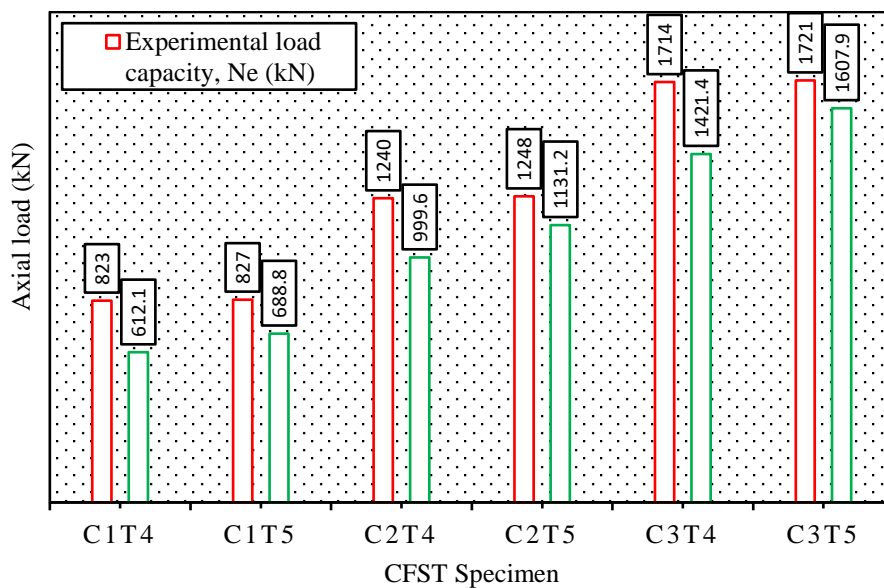
Figure 4.17 Load capacity of greased columns and Eurocodes-4

It was also seen that increasing the external steel tube thickness from 4 to 5 mm, increased the load carrying capacity of CFST columns while decreasing the percentage error.

Table 4.9 Comparisons of experimental result of non-greased columns and Eurocodes-4

Specimens	Experimental load capacity, N_e (kN)	Eurocode-4, N_c(kN)	N_e/N_c	% error
C1T4	834	612.1	1.3	26.6
C1T5	836	688.8	1.2	17.6
C2T4	1252	999.6	1.2	20.2
C2T5	1263	1131.2	1.1	10.5
C3T4	1749	1421.4	1.2	18.7
C3T5	1768	1607.9	1.1	9.1
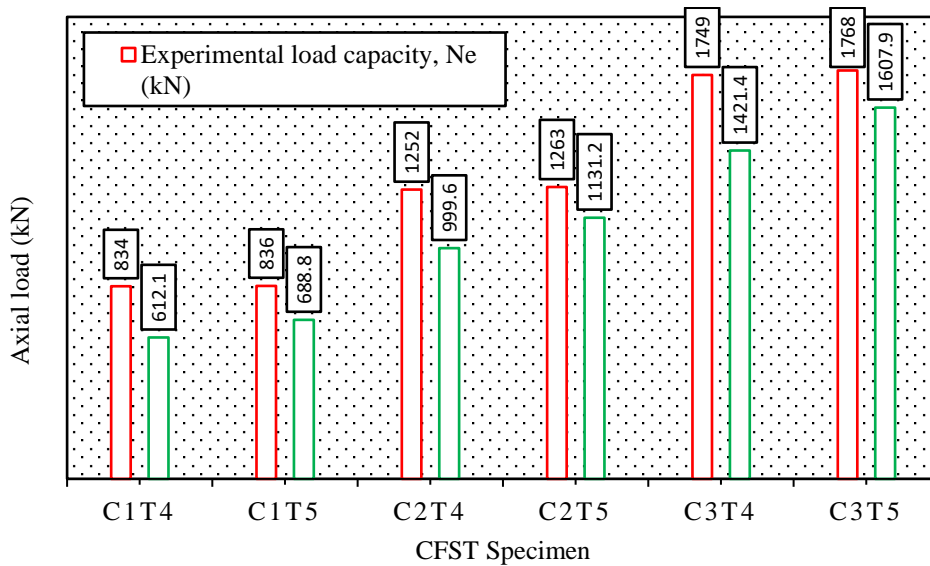
Figure 4.18 Load capacity of non-greased columns and Eurocodes-4

Tables 4.10 and 4.11 demonstrate the axial load potential of experimental results for non-greased CFST columns at 600 °C and 800 °C for annealing with Eurocode-4. The deviations in axial load capability of experimental results and Eurocode-4 of CFST specimens

135

at 600 °C with steel tube thickness of 4 mm were 22.6%, 17.3%, and 16.3%, respectively, for steel tube diameters 100 mm, 125 mm, and 150 mm. Whereas, for steel tube diameters of 100 mm, 125 mm, and 150 mm, it was 13.4%, 6.7%, and 5.7% for 5 mm steel tube thickness, respectively.

Table 4.10 Comparisons of Eurocodes-4 and experimental result of non-greased CFST columns at 600 °C for annealing

Specimens	Experimental load capacity, N_e (kN)	Eurocode-4, N_c (kN)	N_e/N_c	% error
C1T4	791	612.1	1.3	22.6
C1T5	795	688.8	1.2	13.4
C2T4	1208	999.6	1.2	17.3
C2T5	1213	1131.2	1.0	6.7
C3T4	1698	1421.4	1.2	16.3
C3T5	1705	1607.9	1.1	5.7

The difference in axial load capacity between the experimental result and Eurocode-4 of non-greased CFST columns at 800 °C with a steel tube thickness of 4 mm was 14.5%, 14.9%, and 12.7%, respectively. For steel tube diameters of 100 mm, 125 mm, and 150 mm, respectively, the percentages were 4.6%, 4.0%, and 1.8% for 5 mm steel tube thickness. The largest differences between experimental results and Eurocode-4 for the non-greased specimens at 600 °C and 800 °C with 4 mm steel tube thickness was found to be reduce in the range of 14.9% and 22.6% for C2T4 and C1T4 specimens respectively as showed in Figure 4.19 and Figure 4.20. The average N_e/N_c for the non-greased columns was 1.2 at 600 °C and it was 1.1 at 800 °C for annealing. The least difference between experimental results and Eurocode-4 for the non-greased CFST columns at 600 °C and 800 °C with 5 mm steel tube thickness was found to reduce in the range of 5.7% to 1.8% for C3T5 specimen. The percentage error was also reduced as the temperature was increased from 600 °C to 800 °C and the external steel tube thickness was increased from 4 mm to 5 mm.
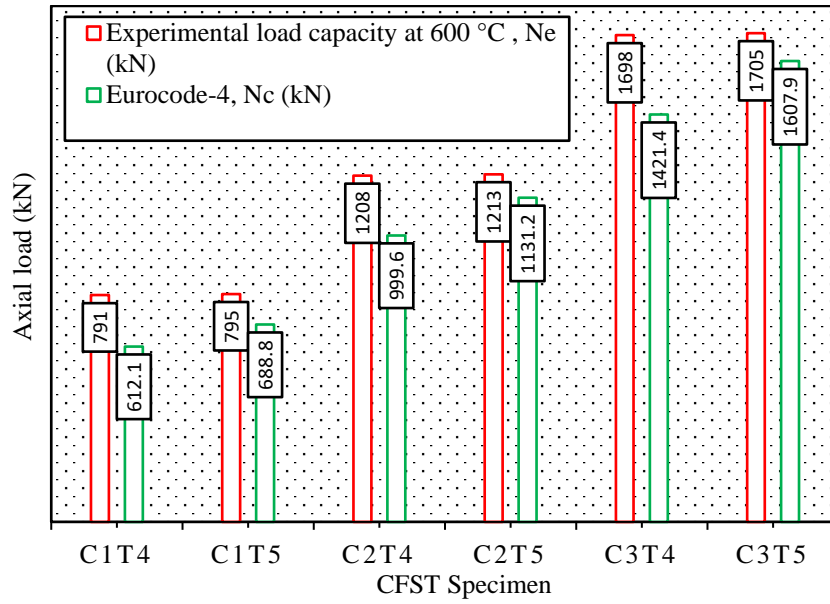
Figure 4.19 Load capacity of non-greased columns at 600 °C for annealing

and Eurocodes-4

Table 4.11 Comparisons of Eurocodes-4 and experimental result of CFST columns at 800 °C for annealing

Specimens	Experimental load capacity, N_e (kN)	Eurocode-4, N_c (kN)	N_e/N_c	% error
C1T4	716	612.1	1.2	14.5
C1T5	722	688.8	1.0	4.6
C2T4	1175	999.6	1.2	14.9
C2T5	1179	1131.2	1.0	4.0
C3T4	1629	1421.4	1.1	12.7
C3T5	1637	1607.9	1.0	1.8
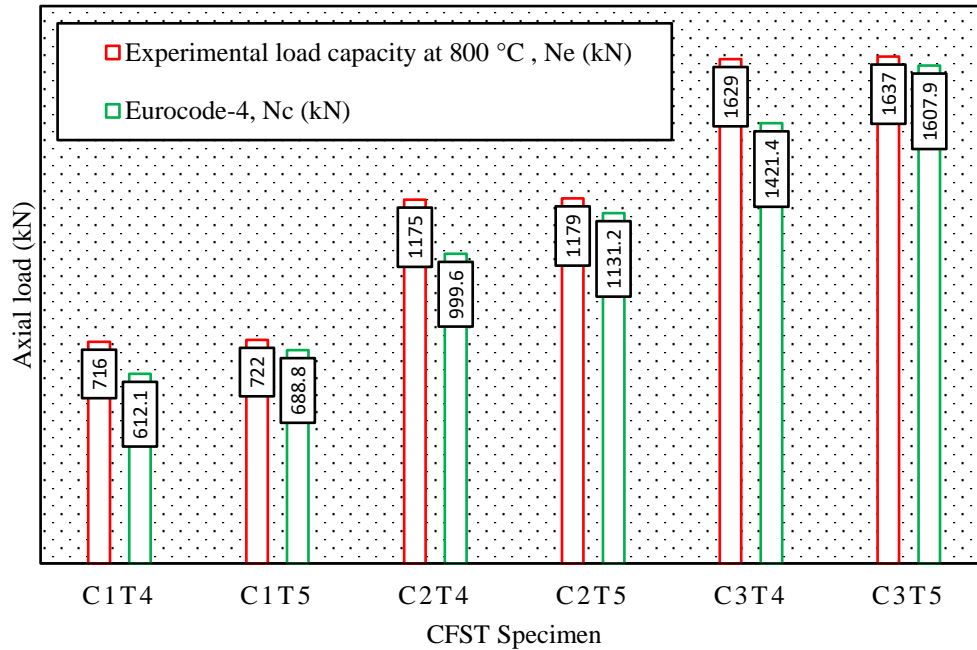
Figure 4.20 Load capacity of non-greased columns at 800 °C for annealing

and Eurocodes-4

The experimental behavior of non-greased CFST specimens at 600 °C and 800 °C for extinguishing with Eurocode-4 are mentioned in Table 4.12 and 4.13. The difference in axial load capacity between the test result and Eurocode-4 of CFST specimens at 600 °C with a steel tube thickness of 4 mm was 18.3%, 14.6%, and 14.5%, respectively. For steel tube diameters of 100 mm, 125 mm, and 150 mm, respectively, it was 9.8%, 4.3%, and 3.5% for 5 mm steel tube thickness. It can also be shown that the disparity in axial load capacity test results and Eurocode-4 of CFST specimens at 800 °C for steel tube thickness of 4 mm was 11.0%, 12.9%, and 11.4%, respectively, and for steel tube thickness of 5 mm, it was 0.3%, 2.1%, and 0.3% for steel tube diameters 100 mm, 125 mm, and 150 mm. As shown in Figures 4.21 and 4.22, the largest discrepancies between experimental results and Eurocode-4 for non-greased specimens at 600 °C and 800 °C with 4 mm steel tube thickness were found to be reduced by 12.9% and 18.3% for C2T4 and C1T4 specimens, respectively.

138

Table 4.12 Comparisons of Eurocodes-4 and experimental result of CFST columns at 600 °C for quenching

Specimens	Experimental load capacity, N_e (kN)	Eurocode-4, N_c(kN)	N_e/N_c	% error
C1T4	749	612.1	1.2	18.3
C1T5	764	688.8	1.1	9.8
C2T4	1170	999.6	1.2	14.6
C2T5	1182	1131.2	1.0	4.3
C3T4	1662	1421.4	1.2	14.5
C3T5	1667	1607.9	1.0	3.5

The average N_e/N_c for the non-greased columns was 1.1 at 600 °C and 800 °C for annealing. The least difference between experimental results and Eurocode-4 for the non-greased CFST columns at 600 °C and 800 °C with 5 mm steel tube thickness was found to reduce in the range of 0.3% and 3.5% individually for C3T5 specimen.
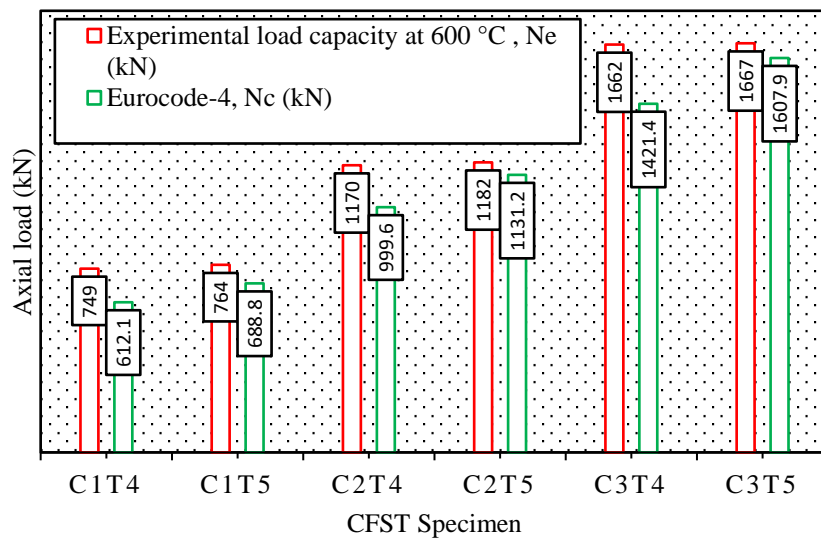
Figure 4.21 Load capacity of non-greased columns at 600 °C for quenching

and Eurocodes-4

It was additionally seen that with the increase of temperature from 600 °C to 800 °C and for external steel tube thickness from 4 mm to 5 mm, the percentage error was decreased.

Table 4.13 Comparisons of Eurocodes-4 and experimental result of CFST columns at 800 °C for quenching

Specimens	Experimental load capacity, N_e (kN)	Eurocode-4, N_c(kN)	N_e/N_c	% error
C1T4	688	612.1	1.1	11.0
C1T5	691	688.8	1.0	0.3
C2T4	1148	999.6	1.1	12.9
C2T5	1156	1131.2	1.0	2.1
C3T4	1605	1421.4	1.1	11.4
C3T5	1613	1607.9	1.0	0.3
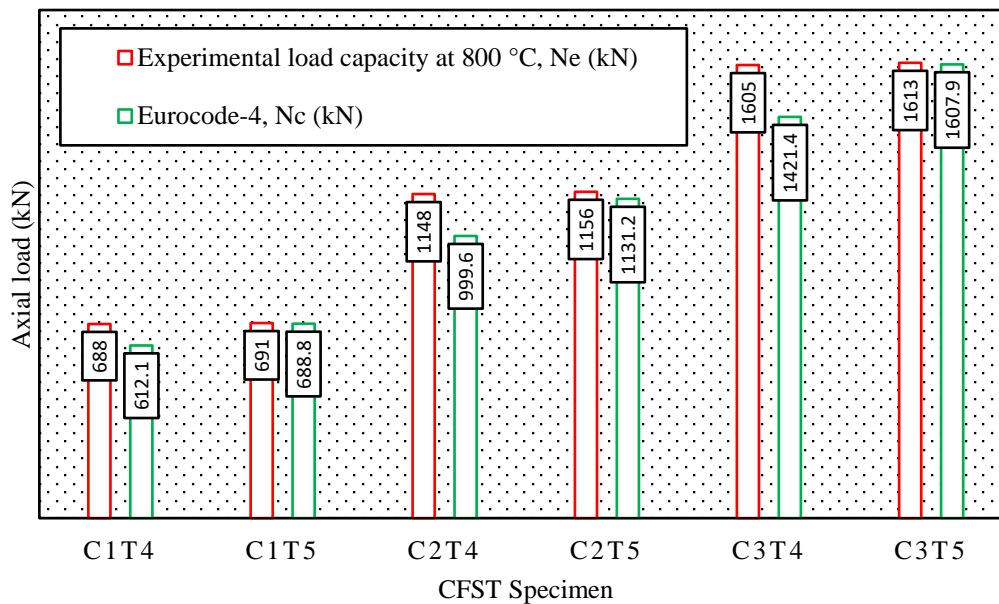
Figure 4.22 Load capacity of non-greased columns at 800 °C for quenching and Eurocodes-4

4.11.2 American Concrete Institute and Australian Standard

The American Concrete Institute (ACI) and Australian Standards (AS) have fair expectations for specimens made of thicker (lower D/t ratio) steel tubes. For determining the design load capacity of CFST columns, the American Concrete Institute (ACI) and the Australian Standard (AS) both use the same equation. The design load capacity of CFST columns predictable with ACI and AS was determined by utilizing Eq. (3.12).

An examination of axial load capacity of experimental test result with ACI and AS, for greased and non-greased CFST columns is mentioned in Table 4.14 and 4.15.

Table 4.14 Comparisons of experimental result of greased columns and ACI, AS

Specimens	Experimental load capacity, N_e (kN)	ACI and AS, $N_{c, ACI, AS}$ (kN)	$N_e/N_{c, ACI, AS}$	% error
C1T4	823	692.5	1.2	15.9
C1T5	827	707.7	1.2	14.4
C2T4	1240	1126.3	1.1	9.2
C2T5	1248	1155.6	1.1	7.4
C3T4	1714	1605.7	1.1	6.3
C3T5	1721	1619.7	1.1	5.8

It can be shown that the experimental test result of axial load capacity was well predicted using ACI and AS of greased CFST columns with a steel tube thickness of 4 mm. The measured results for steel tube diameters of 100 mm, 125 mm, and 150 mm were 15.9%, 9.2%, and 6.3%, respectively. The measured results for 5 mm steel tube thickness were found to be in the range of 14.4%, 7.4%, and 5.8%. The difference in axial load capacity of experimental results, reliable with ACI and AS of non-greased CFST columns with steel tube thickness of 4 mm, was found to be 16.9%, 10.0%, and 8.2%, respectively. For steel tube diameters of 100 mm,

125 mm, and 150 mm, it was 15.3%, 8.5%, and 7.4% for 5 mm steel tube thickness, respectively. Between experimental results and ACI and AS shown in Figures 4.23 and 4.24, the main difference in the axial load of concrete filled steel tube columns (C1T4) for greased and non-greased specimens was found to be 15.9% and 16.9% for 4 mm steel tube thickness.
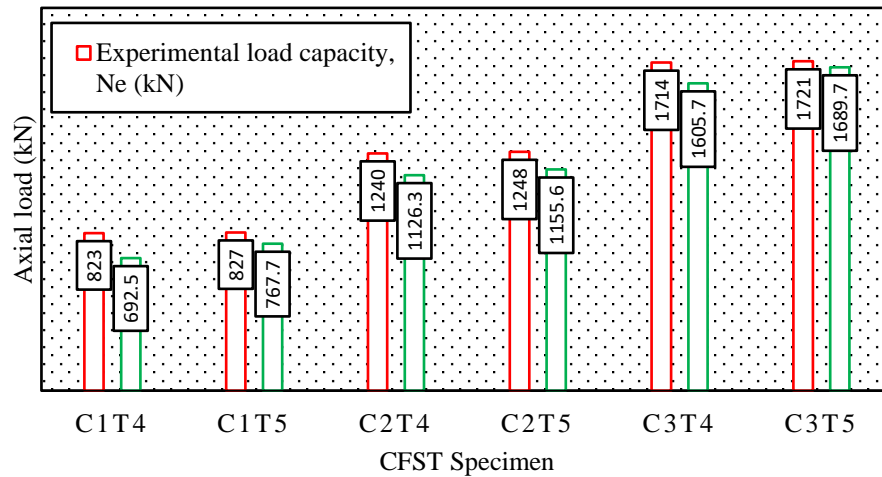
Figure 4.23 Load capacity of greased columns and ACI and AS

Table 4.15 Comparisons of experimental result of non-greased columns and ACI, AS

Specimens	Experimental load capacity, N_e (kN)	ACI and AS, $N_{c, ACI, AS}$ (kN)	$N_e/ N_{c, ACI, AS}$	% error
C1T4	834	692.5	1.2	16.9
C1T5	836	707.7	1.2	15.3
C2T4	1252	1126.3	1.1	10.0
C2T5	1263	1155.6	1.1	8.5
C3T4	1749	1605.7	1.1	8.2
C3T5	1768	1619.7	1.1	7.4

The average N_e/N_c for the greased and non-greased columns was 1.1. The least difference between experimental results and ACI and AS for the greased and non-greased specimens with 5 mm steel tube thickness was found to 5.8% and 7.4% respectively for C3T5 specimens. The axial load carrying capacity of CFST columns was also improved and the percentage error was reduced as the outer steel tube thickness was increased from 4 mm to 5 mm.
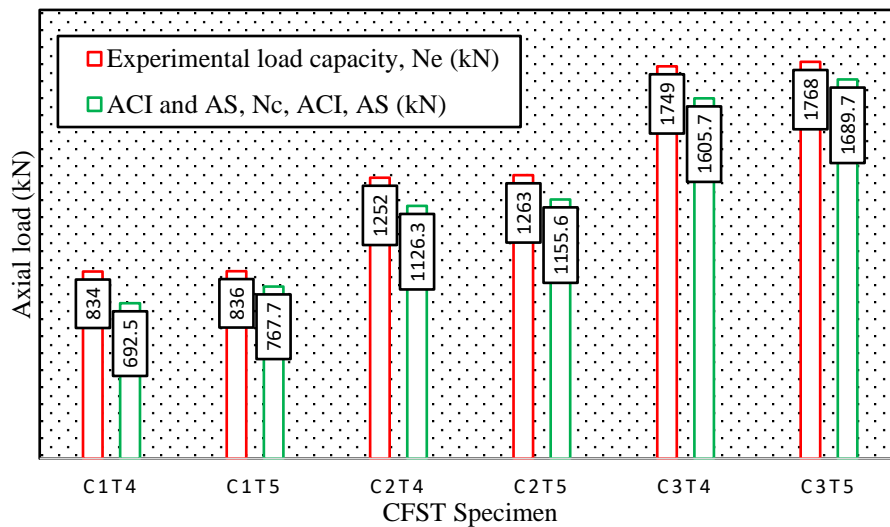
Figure 4.24 Load capacity of non-greased columns and ACI and AS

The axial load capacities of experimental result with ACI and AS, for non-greased CFST columns at 600 °C and 800 °C for annealing, are listed in Table 4.16 and 4.17 respectively.

The difference in axial load capacity of experimental results, reliable with ACI and AS of non-greased CFST columns at 600 °C with steel tube thickness of 4 mm, was 12.5%, 6.8%, and 5.4%, respectively. It was found to be 11.0%, 4.7%, and 0.9% for steel tubes with a thickness of 5 mm. The axial load capacity of experimental results, predicted with ACI and AS of non-greased CFST columns at 800 °C with steel tube thickness of 4 mm, was 3.3 %, 4.1%, and 1.4%, respectively. For steel tube diameters of 100 mm, 125 mm, and 150 mm, respectively, it was 2.0%, 2.0%, and 1.1% for 5 mm steel tube thickness. Between experimental results and ACI and AS shown in Figures 4.25 and 4.26, the largest difference in the axial load of concrete filled steel tube columns (C2T4 and C1T4) for non-greased specimens for

143

annealing at 600 °C and 800 °C was found to be 4.1% and 12.5% with 4 mm steel tube thickness.

Table 4.16 Comparisons of ACI, AS and experimental result of CFST columns at 600 °C for annealing

Specimens	Experimental load capacity, N_e (kN)	ACI and AS, $N_{c, ACI, AS}$ (kN)	$N_e/ N_{c, ACI, AS}$	% error
C1T4	791	692.5	1.1	12.5
C1T5	795	707.7	1.1	11.0
C2T4	1208	1126.3	1.1	6.8
C2T5	1213	1155.6	1.0	4.7
C3T4	1698	1605.7	1.1	5.4
C3T5	1705	1619.7	1.0	0.9
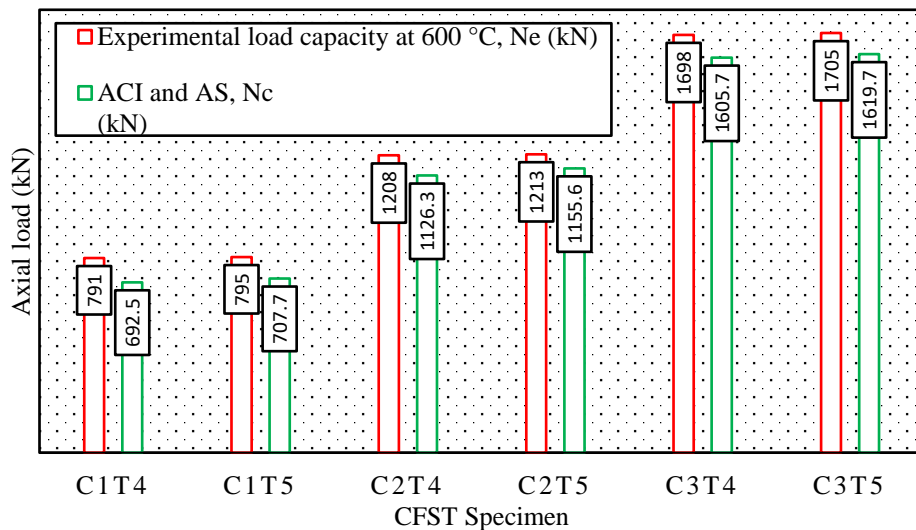
Figure 4.25 Load capacity of non-greased columns at 600 °C for annealing

and ACI and AS

The average N_e/N_c for the non-greased columns at 600 °C and 800 °C was 1.1 and 1.0 respectively. The least difference between experimental results and ACI and AS for the non-greased specimens at 600 °C and 800 °C with 5 mm steel tube thickness was found to 0.9% and 1.1% respectively for C3T5 specimens.

Table 4.17 Comparisons of ACI, AS and experimental result of CFST columns at 800 °C for annealing

Specimens	Experimental load capacity, N_e (kN)	ACI and AS, $N_{c, ACI, AS}$ (kN)	$N_e/ N_{c, ACI, AS}$	% error
C1T4	716	692.5	1.0	3.3
C1T5	722	707.7	1.0	2.0
C2T4	1175	1126.3	1.0	4.1
C2T5	1179	1155.6	1.0	2.0
C3T4	1629	1605.7	1.0	1.4
C3T5	1637	1619.7	1.0	1.1

The axial load carrying capacity of CFST columns was also found to decrease as the outer steel tube thickness was increased from 4 mm to 5 mm and the temperature was increased from 600 °C to 800 °C.

The experimental results of non-greased CFST columns at 600 °C and 800 °C for quenching are mentioned in Table 4.18 and 4.19. The observed results of non-greased CFST columns are reliable with ACI and AS at 600 °C with a steel tube thickness of 4 mm, and the test results vary by 7.5%, 3.7%, and 3.4%. For steel tube diameters of 100 mm, 125 mm, and 150 mm, respectively, the percentages were 7.3%, 2.2%, and 2.8% for 5 mm steel tube thickness.

The largest difference in the axial capacity of concrete filled steel tube columns (C2T4 and C1T4) for non-greased specimens for annealing at 600 °C and 800 °C was found to 1.89%

and 7.5% with 4 mm steel tube thickness between experimental results and ACI and AS shown in Figure 4.27 and 4.28.
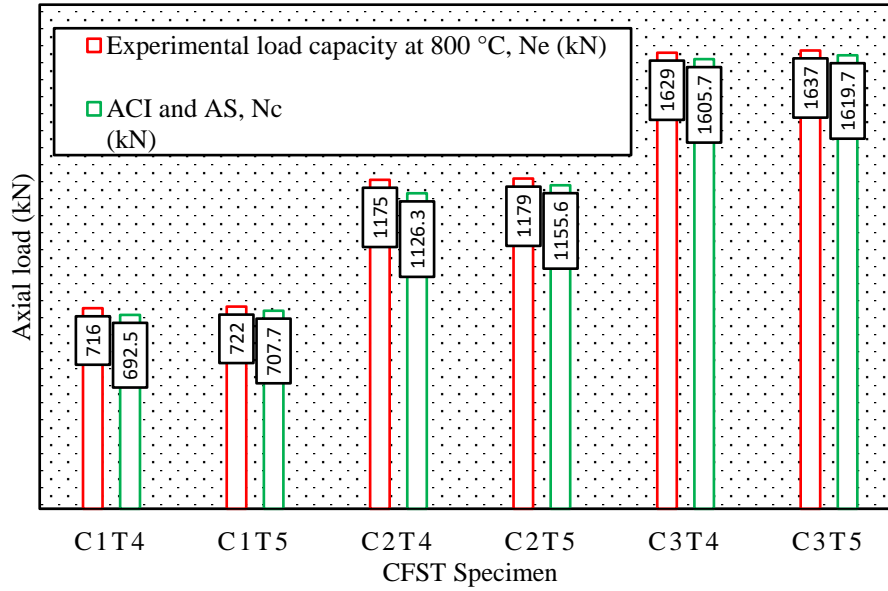
Figure 4.26 Load capacity of non-greased columns at 800 °C for annealing

and ACI and AS

Table 4.18 Comparisons of ACI, AS and experimental result of CFST columns at 600 °C for quenching

Specimens	Experimental load capacity, N_e (kN)	ACI and AS, $N_{c, ACI, AS}$ (kN)	$N_e/ N_{c, ACI, AS}$	% error
C1T4	749	692.5	1.1	7.5
C1T5	764	707.7	1.1	7.3
C2T4	1170	1126.3	1.0	3.7
C2T5	1182	1155.6	1.0	2.2
C3T4	1662	1605.7	1.0	3.4
C3T5	1667	1619.7	1.0	2.8

The least difference between experimental results and ACI and AS for the non-greased specimens at 600 °C and 800 °C with 5 mm steel tube thickness was found to 0 and 2.2% respectively for C2T5 specimens. It was also observed that the average N_e/N_c for the non-greased columns at 600 °C and 800 °C was 1.0 respectively.
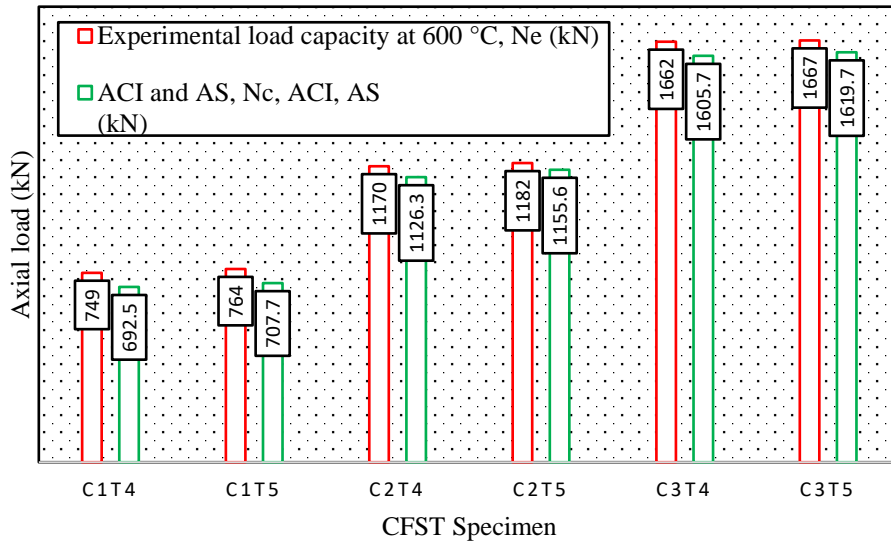
Figure 4.27 Load capacity of non-greased columns at 600 °C for quenching and ACI and AS

Table 4.19 Comparisons of ACI, AS and experimental result of CFST columns at 800 °C for quenching

Specimens	Experimental load capacity, N_e (kN)	ACI and AS, $N_{c,\ ACI,\ AS}$ (kN)	$N_e/\ N_{c,\ ACI,\ AS}$	% error
C1T4	688	692.5	0.6	0.7
C1T5	691	707.7	0.9	2.4
C2T4	1148	1126.3	1.0	1.89
C2T5	1156	1155.6	1.0	0
C3T4	1605	1605.7	1.0	0
C3T5	1613	1619.7	1.0	0.2
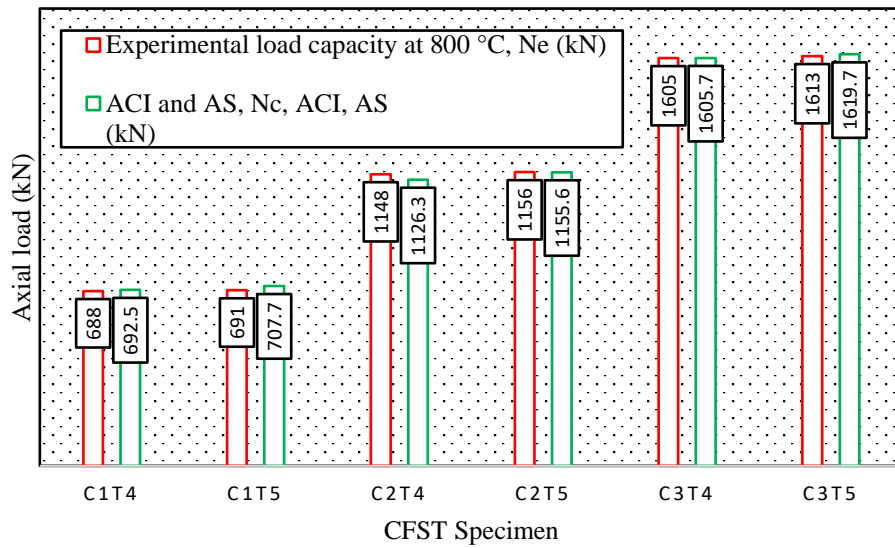
Figure 4.28 Load capacity of non-greased columns at 800 °C for quenching

and ACI and AS

4.11.3 AISC– LRFD

The design load carrying capacity of the CFST columns consistent with AISC-LRFD was calculated by using Eq. (3.22). The comparisons of concrete filled steel tubular (CFST) columns on the basis of axial load carrying capacity according to AISC– LRFD for greased and non-greased CFST specimens are listed in Table 4.20 and 4.21 respectively.

Table 4.20 Comparisons of experimental result of greased columns and AISC– LRDF

Specimens	Experimental load capacity, N_e (kN)	AISC– LRDF, P_n (kN)	N_e/P_n	% error
C1T4	823	573.0	1.4	30.4
C1T5	827	650.7	1.3	21.3
C2T4	1240	936.5	1.3	24.4
C2T5	1248	1068.9	1.2	14.4
C3T4	1714	1329.4	1.2	22.4
C3T5	1721	1517.2	1.2	11.8

The axial load capacity obtained from experimental results and AISC-LFRD of greased CFST column specimens with steel tube thickness 4 mm was found to vary by 30.4%, 24.4%, and 22.4%, respectively. For steel tubes with diameters of 100 mm, 125 mm, and 150 mm and a thickness of 5 mm, the disparity was found to be 21.3%, 14.4%, and 11.8% for the same diameters of steel tubes, i.e., 100 mm, 125 mm, and 150 mm. For both greased and non-greased columns, the average Ne/Pn was 1.3. For the greased and non-greased specimens with a 5 mm steel tube diameter, the least difference between experimental findings and AISC–LRDF was found to be 11.8% and 14.2%, respectively, for the C3T5 specimen. As shown in Figures 4.29 and 4.30, when the outer steel tube thickness was increased from 4 mm to 5 mm, the load carrying capacity of CFST columns was improved, and the percentage error was also reduced.
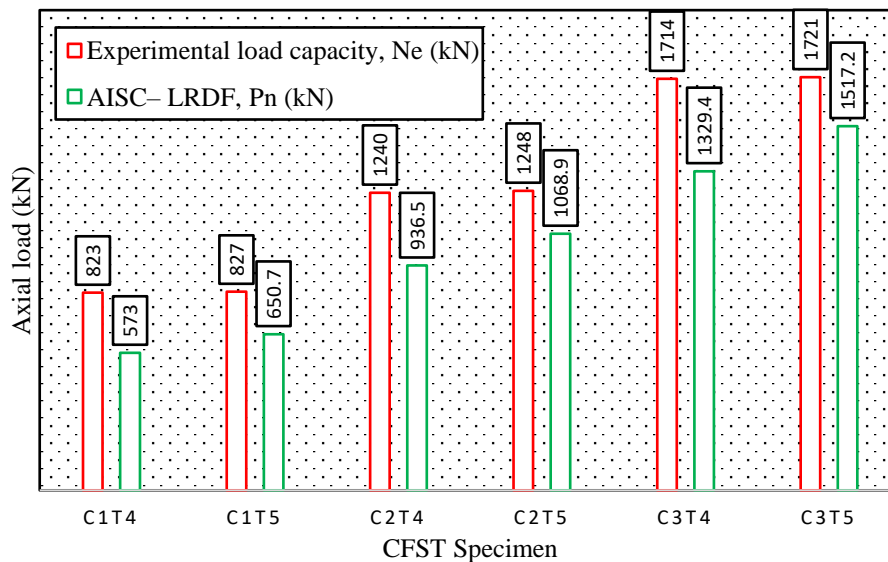
Figure 4.29 Load carrying capacity of greased columns according to experimental result and AISC-LFRD

The difference in axial load carrying capacity of non-greased CFST columns based on experimental results, consistent with AISC-LFRD, having 4 mm thick steel tube was 31.3%, 25.2%, and 23.9% for steel tubes of diameter 100 mm, 125 mm, and 150 mm, respectively, and 22.2%, 15.4%, and 14.2% for steel tubes of thickness 5 mm. For the greased and non-greased specimens with a 4 mm steel tube diameter, the main difference between experimental results and AISC–LRDF was found to be 30.4% and 31.3%, respectively, for the C1T4 specimen.

Table 4.21 Comparisons of experimental result of non-greased columns and AISC– LRDF

Specimens	Experimental load capacity, N_e (kN)	AISC– LRDF, P_n (kN)	N_e / P_n	% error
C1T4	834	573.0	1.5	31.3
C1T5	836	650.7	1.3	22.2
C2T4	1252	936.5	1.3	25.2
C2T5	1263	1068.9	1.2	15.4
C3T4	1749	1329.4	1.3	23.9
C3T5	1768	1517.2	1.2	14.2
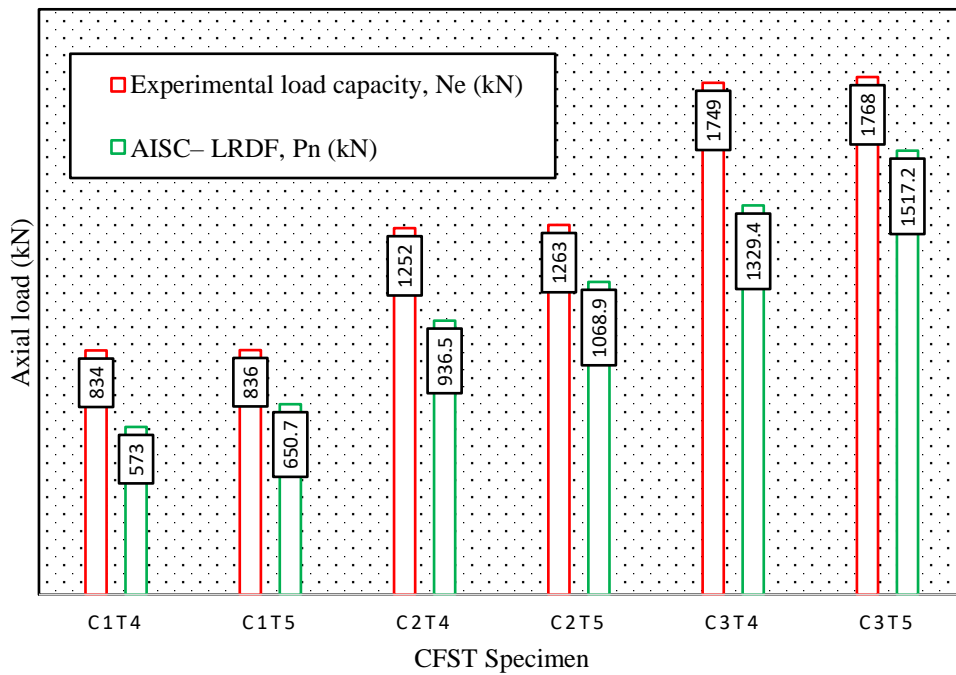
Figure 4.30 Load capacities of non-greased columns and AISC-LFRD

The axial load carrying capacities of CFST columns with AISC– LRFD for non-greased CFST specimens at 600 °C and 800 °C for annealing are listed in Table 4.22 and 4.23

respectively. The variation in axial load carrying capacity greased CFST columns with 4 mm thickness of steel tube having diameters 100 mm, 125 mm and 150 mm at 600 °C based on experimental result and AISC-LFRD was found to be 27.6%, 22.5% and 21.7% respectively and for 5 mm steel tube thickness with diameter of 100mm, 125mm and 150mm, the difference was 18.2%, 11.9% and 11.0% respectively. Similarly, the observation were made on the variation in axial load carrying capacities of non-greased CFST columns at 800 °C with steel tube of thickness 4 mm and diameters of 100 mm, 125 mm and 150 mm for experimental result, consistent with AISC-LFRD was 20.0%, 20.3% and 18.4% respectively and for steel tube having diameter 100 mm, 125 mm and 150 mm with 5 mm thickness, it was observed to be 10.0%, 9.3% and 7.3% respectively.

Table 4.22 Comparisons of AISC– LRDF and experimental result of CFST columns at 600 °C for annealing

Specimens	Experimental load capacity, N_e (kN)	AISC–LRDF, P_n (kN)	N_e/P_n	% error
C1T4	791	573.0	1.4	27.6
C1T5	795	650.7	1.2	18.2
C2T4	1208	936.5	1.3	22.5
C2T5	1213	1068.9	1.1	11.9
C3T4	1698	1329.4	1.3	21.7
C3T5	1705	1517.2	1.1	11.0

The largest difference between experimental results and AISC– LRDF for non-greased specimens at 600 °C and 800 °C with 4 mm steel tube thickness was found to 27.6% and 20.3% for C1T4 and C2T4 specimen respectively. The average N_e/P_n for non-greased columns was 1.2.
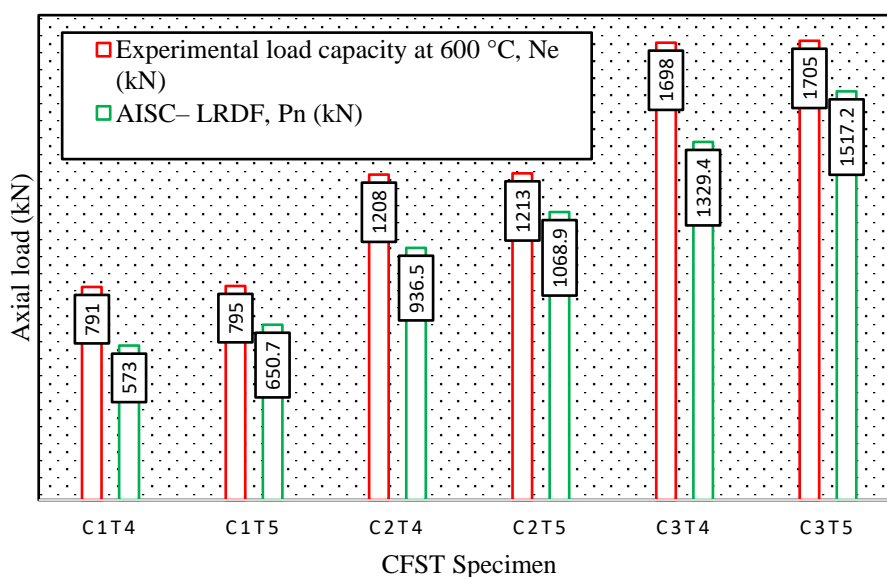
Figure 4.31 Load capacity of non-greased columns at 600 °C for annealing and AISC-LFRD

The least difference between experimental results and AISC– LRDF for non-greased specimens with 5 mm steel tube thickness was found to 7.3% and 11.0% for C3T5 specimen. Also, it was noticed that as the temperature increased, the load carrying capacity of CFST columns was decreased and percentage error was also reduced with increase in thickness as shown in Figure 4.31 and 4.32.

Table 4.23 Comparisons of AISC– LRDF and experimental result of CFST columns at 800 °C for annealing

Specimens	Experimental load capacity, N_e (kN)	AISC– LRDF, P_n (kN)	N_e/ P_n	% error
C1T4	716	573.0	1.2	20.0
C1T5	722	650.7	1.1	10.0
C2T4	1175	936.5	1.3	20.3
C2T5	1179	1068.9	1.1	9.3
C3T4	1629	1329.4	1.2	18.4
C3T5	1637	1517.2	1.1	7.3
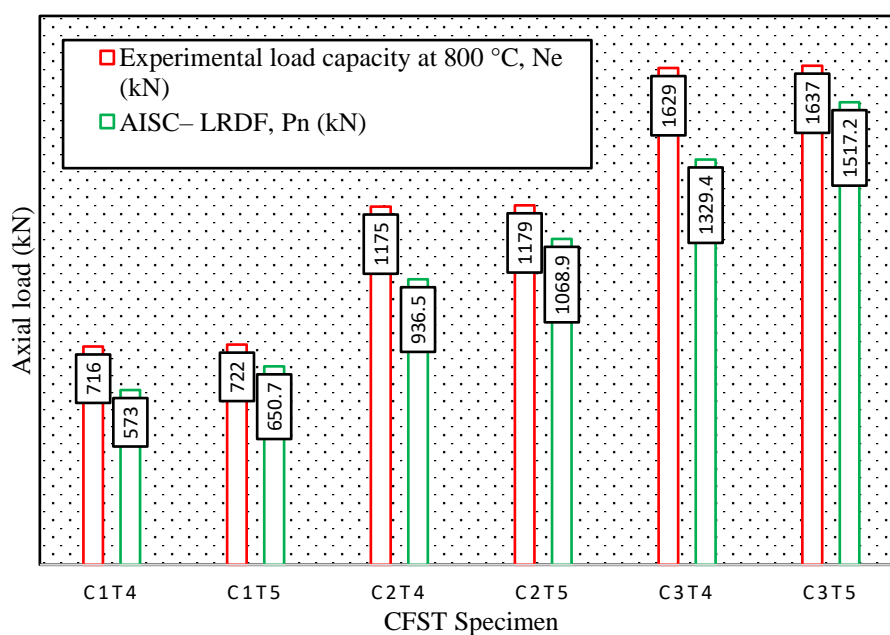
Figure 4.32 Load capacities of non-greased columns at 800 °C for annealing and AISC-LFRD

Table 4.24 Comparisons of AISC– LRDF and experimental result of CFST columns at 600 °C for quenching

Specimens	Experimental load capacity, N_e (kN)	AISC– LRDF, P_n (kN)	N_e/P_n	% error
C1T4	749	573.0	1.3	23.5
C1T5	764	650.7	1.1	14.8
C2T4	1170	936.5	1.2	20.0
C2T5	1182	1068.9	1.1	9.6
C3T4	1662	1329.4	1.3	20.0
C3T5	1667	1517.2	1.1	9.0

The comparisons of axial load capacity of concrete filled steel tube columns with AISC– LRFD for non-greased CFST specimens at 600 °C and 800 °C for quenching are listed in Table 4.24 and 4.25 respectively. The difference in load carrying capacity of greased CFST columns with 4mm thickness of steel tube having diameters of 100 mm, 125 mm, and 150 mm from

experimental results and AISC-LFRD was found to be 23.5%, 20%, and 20%, respectively, at 600 °C. For steel tube with 5 mm thickness and diameters of 100 mm, 125 mm, and 150 mm, the difference was 14.8%, 9.6%, and 9%, respectively.

It had been also noticed that at 800 °C, the variation in loading capacity of non-greased CFST columns with the steel tube of thickness 4 mm and diameter 100 mm, 125 mm and 150 mm on the basis of result from experiment, consistent with AISC-LFRD was 19.7%, 18.4% and 17.2% respectively and for steel tube thickness of 5mm with diameter 100 mm, 125 mm and 150 mm, it was 8.8%, 7.5% and 5.9% respectively. The largest difference between experimental results and AISC– LRDF for non-greased specimens at 600 °C and 800 °C in case of quenching with 4 mm steel tube thickness was found to 23.5% and 19.7% for C1T4specimen. The average N_e/P_n for non-greased columns was 1.2. The least difference between experimental results and AISC– LRDF for non-greased specimens with 5 mm steel tube thickness was found to 5.9% and 9% for C3T5 specimen.
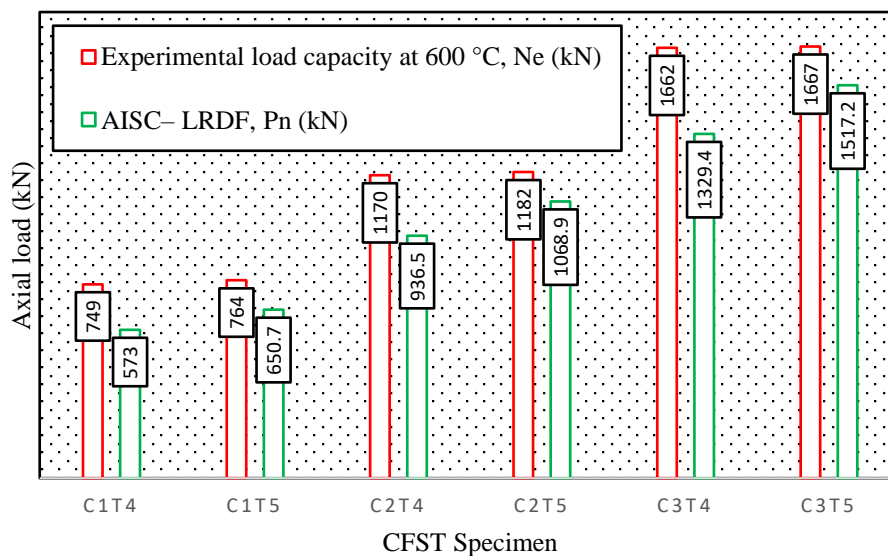
Figure 4.33 Load capacity of non-greased columns at 600 °C for quenching and AISC-LFRD

It was also found that with increase in temperature, the load carrying capacity of CFST columns was decreased and percentage error was also decreased with increased thickness from 4 mm to 5 mm as shown in Figure 4.33 and 4.34.

Table 4.25 Comparisons of AISC– LRDF and experimental result of CFST columns at 800 °C for quenching

Specimens	Experimental load capacity, N_e (kN)	AISC– LRDF, P_n (kN)	N_e/P_n	% error
C1T4	688	573.0	1.2	19.7
C1T5	691	650.7	1.1	8.8
C2T4	1148	936.5	1.2	18.4
C2T5	1156	1068.9	1.1	7.5
C3T4	1605	1329.4	1.2	17.2
C3T5	1613	1517.2	1.1	5.9
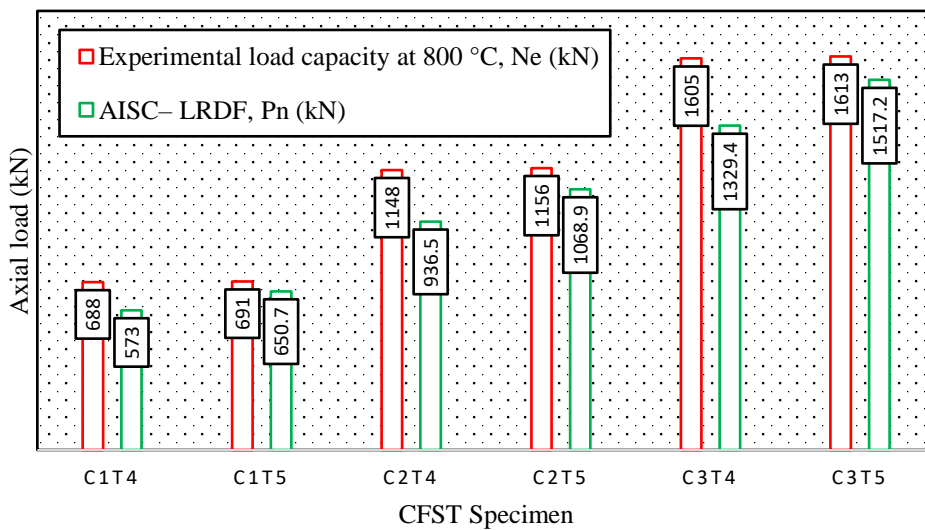
Figure 4.34 Load capacity of non-greased columns at 800 °C for quenching and AISC-LFRD

4.11.4 Chinese code (CECS 28:90)

Eq. 1 was used to measure the CFST columns design load carrying capacity in compliance with Chinese code (CECS 28:90). (3.28). Tables 4.26 and 4.27 compare the axial load potential of greased and non-greased CFST specimens with CECS 28:90.

Table 4.26 Comparisons of experimental result of greased columns and Chinese code (CECS 28:90)

Specimens	Experimental load capacity, N_e (kN)	CECS 28:90, N_o (kN)	N_e/N_o	% error
C1T4	823	612.9	1.3	25.5
C1T5	827	689.7	1.2	16.6
C2T4	1240	999.7	1.2	19.4
C2T5	1248	1131.2	1.1	9.4
C3T4	1714	1421.5	1.2	17.1
C3T5	1721	1608.0	1.1	6.6
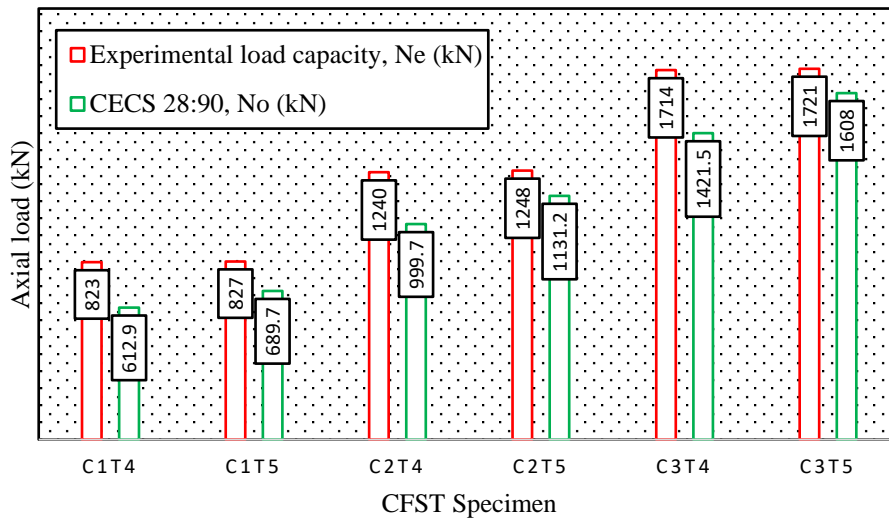
Figure 4.35 Load capacity of greased columns and CECS 28:90

Based on the results of the experimental work and CECS 28:90, the difference in axial load carrying capacity of the greased CFST columns with steel tube of thickness 4 mm and diameters of 100 mm, 125 mm, and 150 mm was 25.5%, 19.4%, and 17.1%, respectively, and for 5mm thick steel tube with diameters of 100 mm, 125 mm, and 150

mm, it was 16.6%. Furthermore, it was found that the disparity in load carrying capacity of non-greased CFST specimens with steel tube thickness 4 mm and diameters of 100 mm, 125 mm, and 150 mm on the basis of experimental findings, consistent with CECS 28:90, was 26.5%, 20.2%, and 18.7%, respectively, and for steel tube thickness 5 mm with diameters 100 mm, 125 mm, and 150 mm, it was 17.5%.

Table 4.27 Comparisons of experimental result of non-greased columns and Chinese code (CECS 28:90)

Specimens	Experimental load capacity, N_e (kN)	CECS 28:90, N_o (kN)	N_e/N_o	% error
C1T4	834	612.9	1.3	26.5
C1T5	836	689.7	1.2	17.5
C2T4	1252	999.7	1.2	20.2
C2T5	1263	1131.2	1.1	10.4
C3T4	1749	1421.5	1.2	18.7
C3T5	1768	1608.0	1.1	9.1

The largest difference between experimental results and Chinese code (CECS 28:90) for the greased and the non-greased specimens with 4 mm steel tube thickness was found to 25.5% and 26.5% respectively for C1T4 specimen. The average N_e/N_o for the greased and non-greased columns was 1.2. The least difference between experimental results and Chinese code (CECS 28:90) for the greased and non-greased specimens with 5 mm steel tube thickness was found 6.6% and 9.1% respectively for C3T5 specimens. It was found that the load carrying capacity was improved as the thickness of external steel tube of CFST columns increased to 5mm from 4mm and percentage error was decreased as showed in Figure 4.35 and 4.36. It was also observed that the comparison of results by using Chinese code (CECS 28:90) was similar to the Eurocode-4.
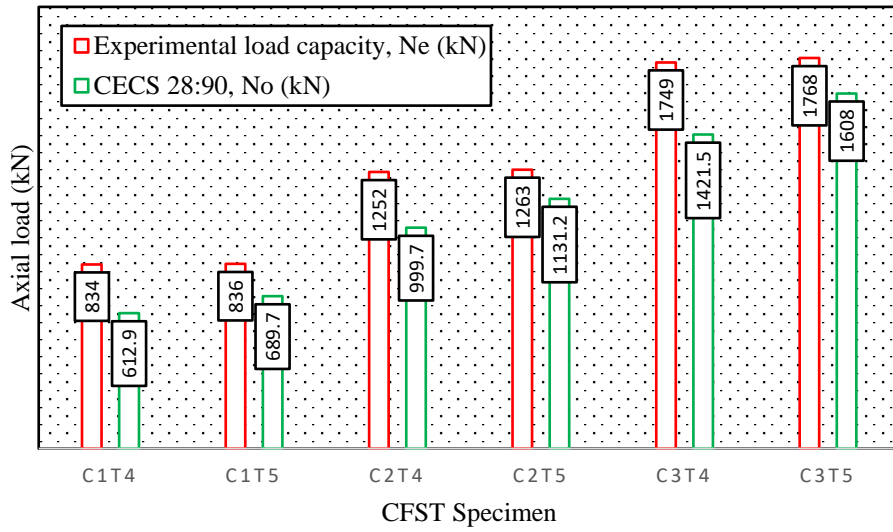
Figure 4.36 Load capacity of non-greased columns and CECS 28:90

Table 4.28 Comparisons of Chinese code (CECS 28:90) and experimental result of CFST columns at 600 °C for annealing

Specimens	Experimental load capacity, N_e (kN)	CECS 28:90, N_o (kN)	N_e / N_o	% error
C1T4	791	612.9	1.3	22.5
C1T5	795	689.7	1.2	13.2
C2T4	1208	999.7	1.2	17.2
C2T5	1213	1131.2	1.1	6.7
C3T4	1698	1421.5	1.2	16.3
C3T5	1705	1608.0	1.1	5.7

The comparisons of axial load carrying capacity of CFST columns with CECS 28:90 for non-greased specimens of CFST at 600 °C and 800 °C for annealing are listed in Table 4.28 and 4.29 respectively. Based on experimental findings and CECS 28:90, the difference in load carrying capacity of non-greased CFST column specimens at 600 °C with steel tube of 4 mm

158

thickness and diameters of 100 mm, 125 mm, and 150 mm was found to be 22.5%, 17.2%, and 16.3%, respectively, and for steel tube of thickness 5 mm with diameters of 100 mm, 125 mm, and 150 mm, the variance in the result was 13.2%. Furthermore, at 800 °C, the difference in loading power of non-greased CFST columns with 4 mm thick steel tube with diameters of 100 mm, 125 mm, and 150 mm was found to be 14.4%, 14.9%, and 12.7%, respectively, in experimental findings consistent with CECS 28:90, and for 5 mm thick steel tube with diameters of 100 mm, 125 mm, and 150 mm diameters, the difference was 4.5%.
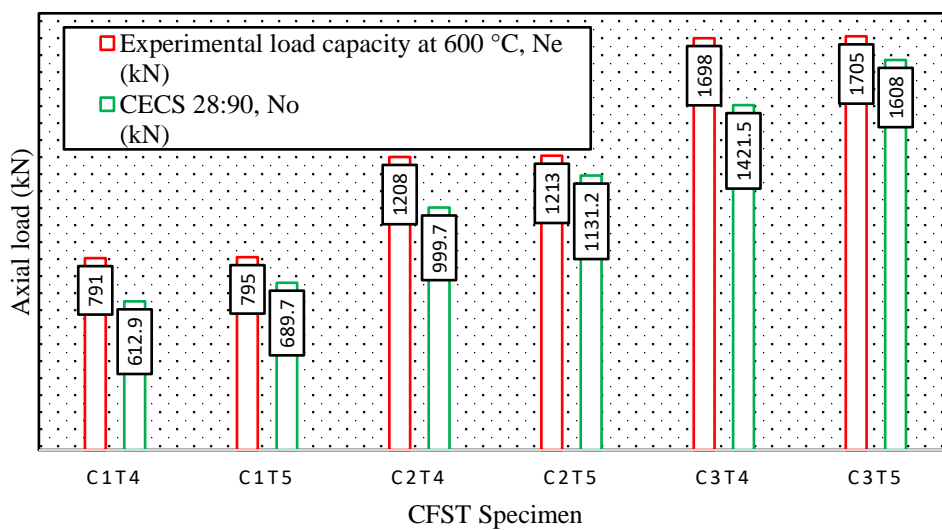
Figure 4.37 Load capacity of non-greased columns at 600 °C for annealing

and CECS 28:90

The largest difference between experimental results and Chinese code (CECS 28:90) for the non-greased specimens with 4 mm steel tube thickness was found to 14.9% and 22.5% for C2T4 and C1T4 specimen respectively. The average N_e/N_o for the non-greased columns at 600 °C and 800 °C for annealing was 1.2 and 1.1. The least difference between experimental results and Chinese code (CECS 28:90) for non-greased specimens with 5 mm steel tube thickness was found 1.8% and 5.7% for C3T5 specimens. Another observation was made that in CFST columns, the load carrying capacity increased as the thickness of external steel tube of 4 mm was increased to 5mm. It was also observed that with the increase of temperature from 600 °C and 800 °C, the percentage error was decreased as showed in Figure 4.37 and 4.38.

Table 4.29 Comparisons of Chinese code (CECS 28:90) and experimental result of CFST columns at 800 °C for annealing

Specimens	Experimental load capacity, N_e (kN)	CECS 28:90, N_o (kN)	N_e/N_o	% error
C1T4	716	612.9	1.2	14.4
C1T5	722	689.7	1.0	4.5
C2T4	1175	999.7	1.2	14.9
C2T5	1179	1131.2	1.0	4.1
C3T4	1629	1421.5	1.1	12.7
C3T5	1637	1608.0	1.0	1.8
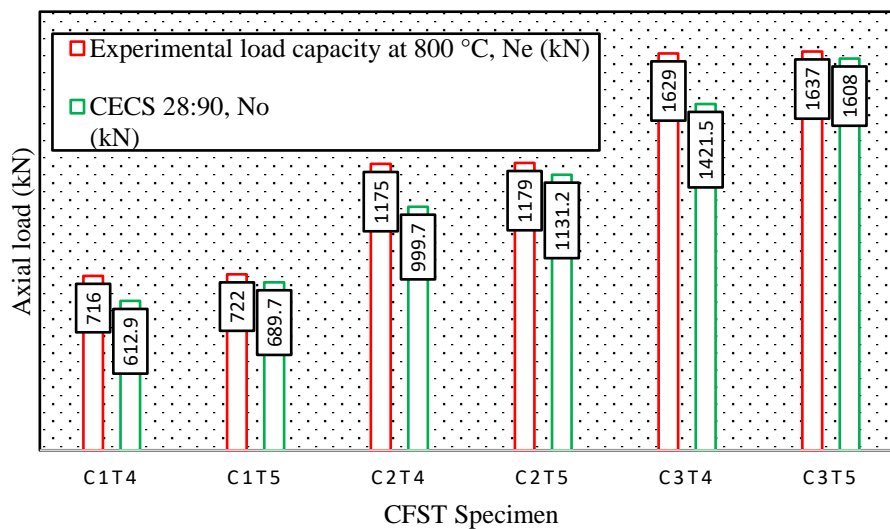
Figure 4.38 Load capacity of non-greased columns at 800 °C for annealing

and CECS 28:90

The behavior of axial load capacity of concrete filled steel tube columns for non-greased CFST specimens at 600 °C and 800 °C for quenching with CECS 28:90 is compared and listed

in Table 4.30 and 4.31 respectively. At 600 °C, the difference observed in axial load carrying capacity of non-greased CFST columns with 4mm thickness of steel tube having diameter 100 mm, 125 mm and 150 mm for the results obtained from the experimental work and CECS 28:90 was 18.2%, 14.6% and 14.5% respectively and for 5 mm thickness of steel tube with diameter 100 mm, 125 mm and 150 mm, the variation was 9.7%, 4.3% and 3.5% respectively.

Table 4.30 Comparisons of Chinese code (CECS 28:90) and experimental result of CFST columns at 600 °C for quenching

Specimens	Experimental load capacity, N_e (kN)	CECS 28:90, N_o (kN)	N_e/N_o	% error
C1T4	749	612.9	1.2	18.2
C1T5	764	689.7	1.1	9.7
C2T4	1170	999.7	1.2	14.6
C2T5	1182	1131.2	1.0	4.3
C3T4	1662	1421.5	1.2	14.5
C3T5	1667	1608.0	1.0	3.5

The variation in axial load carrying capacity of non-greased concrete filled steel tube specimens at 800 °C with 4mm thick steel tube of diameter of 100mm, 125mm and 150mm on the basis of experimental result, consistent with CECS 28:90 was observed as 11%, 13% and 11.4% respectively and for steel tube of 5mm thickness with diameters of 100mm, 125mm and 150mm, the variation observed was 0.2%, 2.1% and 0.3% respectively. The largest difference between experimental results and Chinese code (CECS 28:90) for the non-greased specimens with 4 mm steel tube thickness was found to 13% and 18.2% for C2T4 and C1T4 specimen respectively. The average N_e/N_o for the non-greased columns at 600 °C and 800 °C for quenching was 1.1. The least difference between experimental results and Chinese code (CECS 28:90) for non-greased specimens with 5 mm steel tube thickness was found 0.2% and 3.5% at 600 °C and 800 °C. Also, an increase in the load carrying capacity with increase in thickness

of external steel tube from 4 mm to 5 mm was observed in CFST columns. The percentage error was found to be decreased with the increase of temperature from 600 °C and 800 °C, as shown in Figure 4.39 and 4.40.
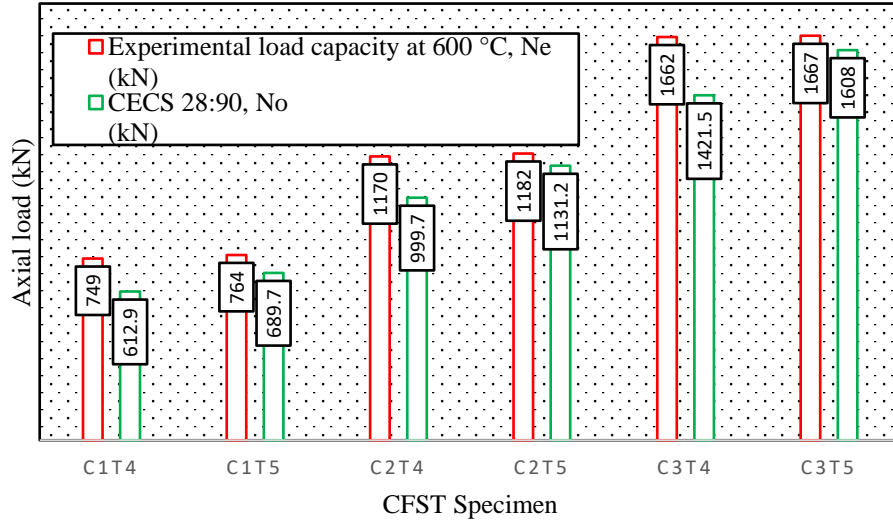
Figure 4.39 Load capacity of non-greased columns at 600 °C for quenching

and CECS 28:90

Table 4.31 Comparisons of Chinese code (CECS 28:90) and experimental result of CFST columns at 800 °C for quenching

Specimens	Experimental load capacity, N_e (kN)	CECS 28:90, N_o (kN)	N_e/N_o	% error
C1T4	688	612.9	1.1	11.0
C1T5	691	689.7	1.0	0.2
C2T4	1148	999.7	1.1	13.0
C2T5	1156	1131.2	1.0	2.1
C3T4	1605	1421.5	1.1	11.4
C3T5	1613	1608.0	1.0	0.3
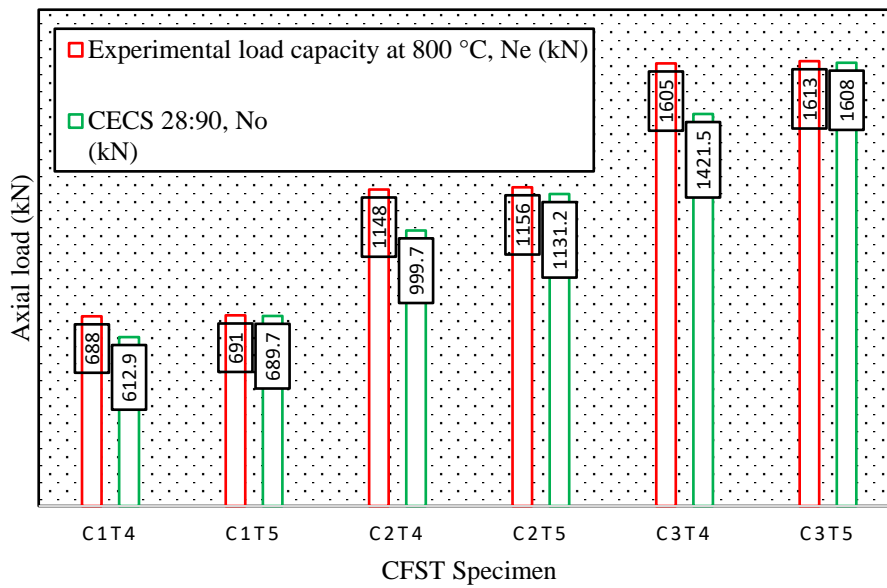
Figure 4.40 Load capacity of non-greased columns at 800 °C for quenching

and CECS 28:90

4.12 RESULTS FROM NUMERICAL ANALYSIS

For all specimens, C1T4, C1T5, C2T4, C2T5, C3T4, and C3T5, a detailed numerical si mulation was performed on concrete filled steel tube columns against axial loading. For all co lumns against axial loading, parameters such as load carrying capacity, failure mode, displace ment, and stresses in concrete filled steel tube columns were considered. The experimental ob served value of CFST columns was compared to the simulation results for validation.

4.12.1 Mesh conversion analysis

The CFST columns were analyzed for different mesh sizes of 10 mm, 20 mm, and 30 mm to decide the best mesh size for the validation of data. Table 4.32 lists the load carrying capacity of CFST specimens C1T4, C1T5, C2T4, C2T5, C3T4, and C3T5 corresponding to mesh sizes of 10 mm, 20 mm, and 30 mm. The simulation results were compared to the experimental results. The load carrying capacity of a concrete filled steel tube column obtained through finite element modelling and experimental testing was in good agreement with the corresponding mesh size of 10 mm, as shown in Figure 4.41.

163

Table 4.32 Mesh convergence study

Specimens	Simulated Load (kN) with Mesh Size			Experimental Load (kN)
	10 mm	20 mm	30 mm	
C1T4	843	865	890	834
C1T5	849	873	897	836
C2T4	1261	1285	1308	1252
C2T5	1268	1305	1334	1263
C3T4	1756	1788	1805	1749
C3T5	1774	1795	1833	1768
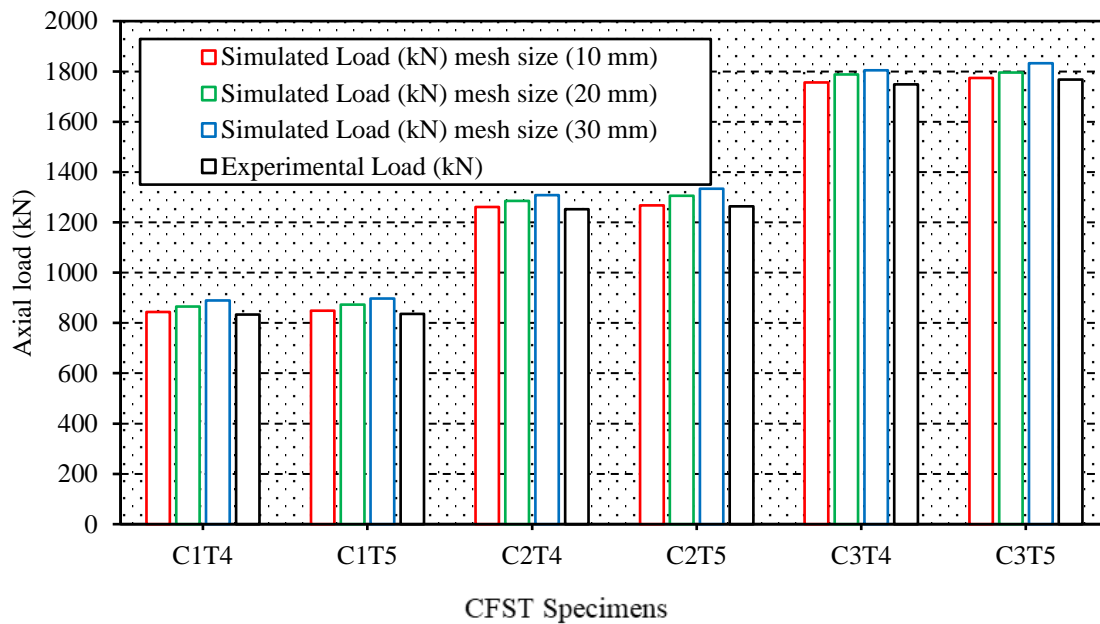
Figure 4.41 Comparison of experiment and simulated load with mesh size of 10 mm, 20 mm and 30 mm

4.12.2 Load carrying capacity of concrete filled steel tube columns

As shown in Table 4.33, the load carrying capacity of CFST columns increased as the diameter of circular columns increased. Three different CFST column diameters were considered: 100 mm, 125 mm, and 150 mm, with two different outer steel thicknesses of 4 mm and 5 mm for all CFST columns. The %age difference in load ability of the simulated model and test specimens ranged from 0.34% to 1.53%. Thus, the simulation results revealed that the observed load carrying capacity of concrete filled steel tube column by finite element

164

modelling was in good agreement with experimental observed values corresponding to a mesh size of 10 mm.

Table 4.33 Comparison of load carrying capacity of CFST columns

Specimens	Size (D X Ts X H mm)	Simulated Load Capacity (kN)
C1T4	100 × 4 × 600	843
C1T5	100 × 5 × 600	849
C2T4	125 × 4 × 600	1261
C2T5	125 × 5 × 600	1268
C3T4	150 × 4 × 600	1756
C3T5	150 × 5 × 600	1774

4.12.3 Deformation in concrete filled steel tube columns

In contrast to infilled concrete, the most deformation was obtained at the middle of the outer steel tube in C1T4 and C1T5 specimens. Figures 4.42 (a, b), 4.43 (a, b), 4.44 (a, b), Figure 4.45 (a, b), Figure 4.46 (a, b), and Figure 4.47 (a, b) show the deformation results obtained from simulation of the specimens C1T4, C1T5, C2T4, C2T5, C3T4, and C3T5, respectively. The deflection of CFST columns was regulated as the diameter of the columns was increased, resulting in a constant height of columns. The concentration of deformation decreased linearly towards the bottom of the column, with the highest deformation found in the middle. The variance in the findings may be due to variations in the L/D ratio and the thickness of the outer steel tube.
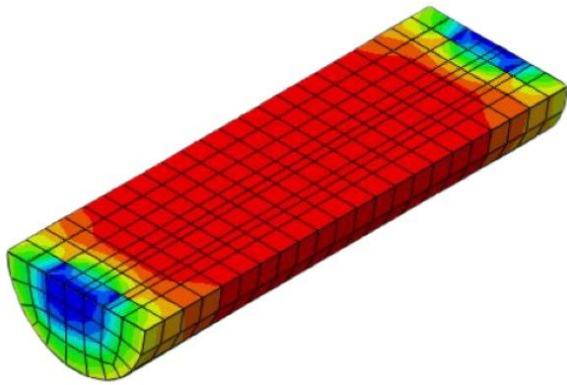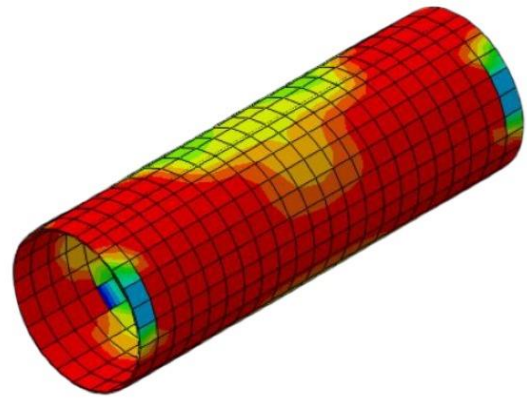
(a)   Concrete core   (b)   Outer steel tube

Figure 4.42 Deformation pattern in C1T4 column (a) Concrete core (b) Outer steel tube
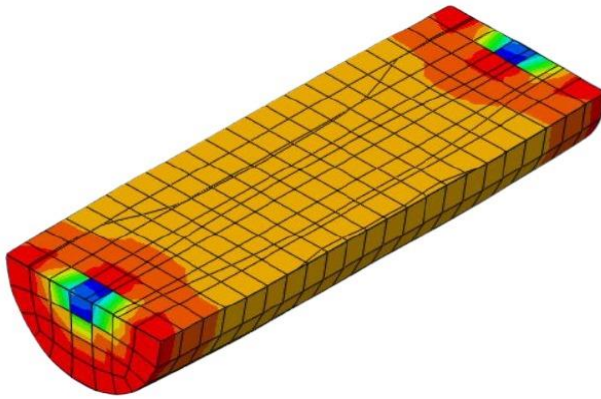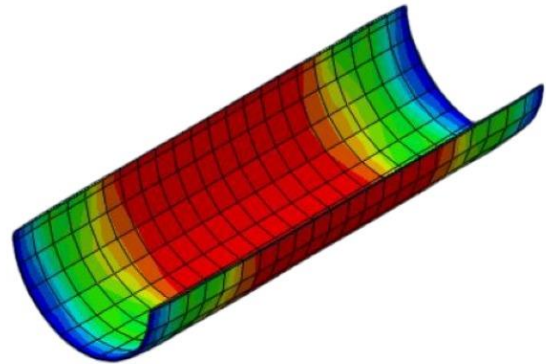
(a) Concrete core   (b) Outer steel tube

Figure 4.43 Deformation pattern in C1T5 column (a) Concrete core (b) Outer steel tube
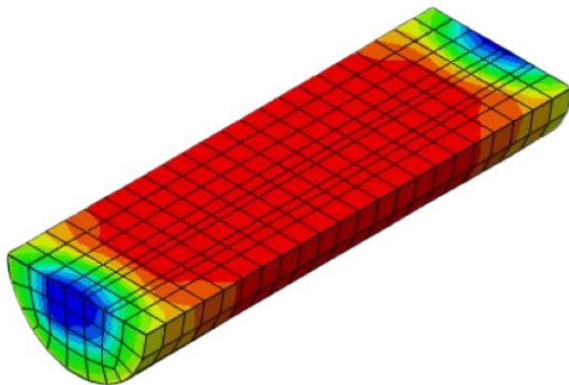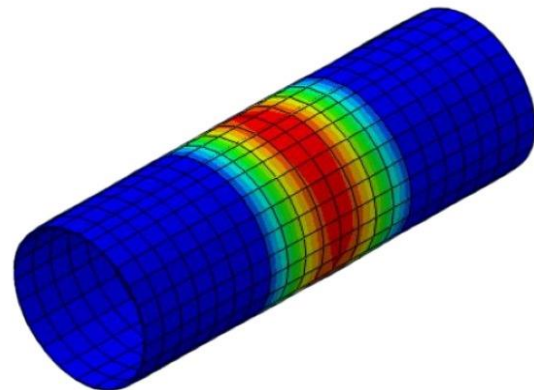
(a) Concrete core   (b) Outer steel tube

Figure 4.44 Deformation pattern in C2T4 column (a) Concrete core (b) Outer steel tube

166
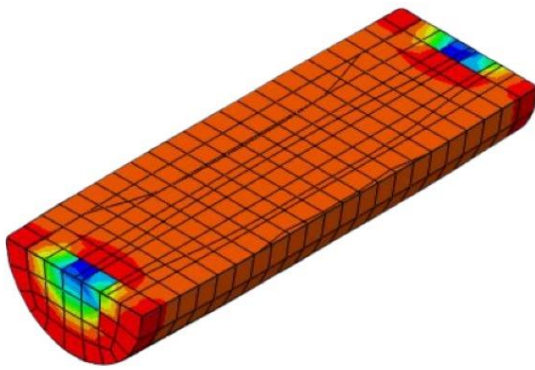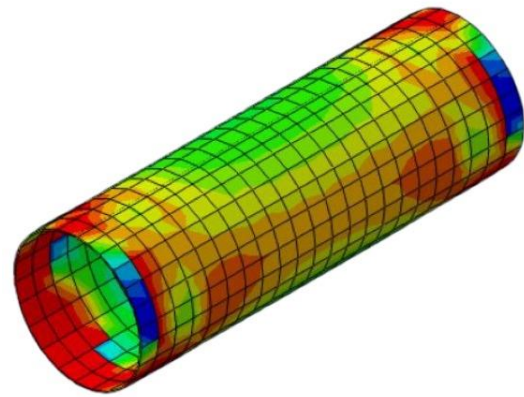
(a) Concrete core   (b) Outer steel tube

Figure 4.45 Deformation pattern in C2T5 column (a) Concrete core (b) Outer steel tube
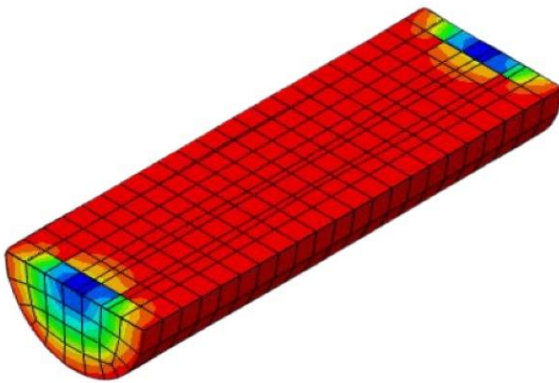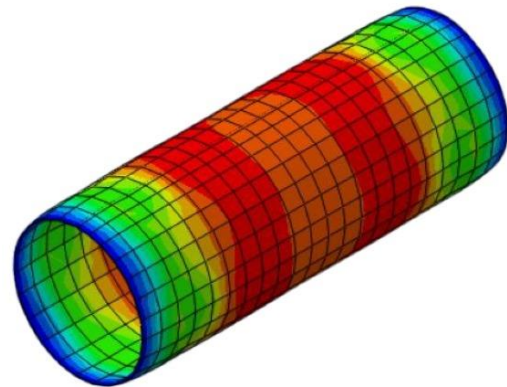
(a) Concrete core   (b) Outer steel tube

Figure 4.46 Deformation pattern in C3T4 column (a) Concrete core (b) Outer steel tube
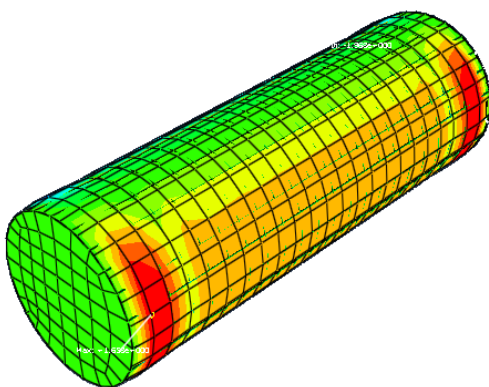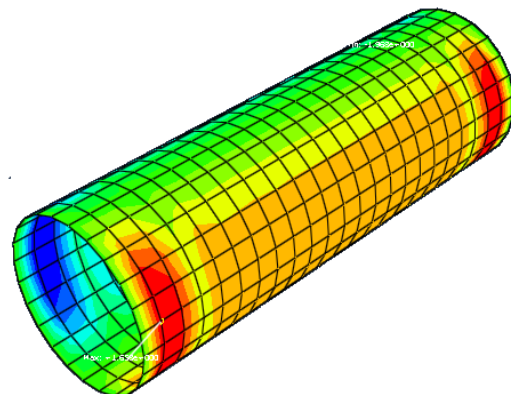
(a) Concrete core   (b) Outer steel tube

Figure 4.47 Deformation pattern in C3T5 column (a) Concrete core (b) Outer steel tube

167

4.12.4 Stress in concrete core and outer steel tube of concrete filled steel tube columns

Table 4.34 displays the effects of numerical calculations using ABAQUS/CAE 6.14 to assess the stress inside the concrete core and outer steel tubing for all specimens. As shown in Figure 4.48 (a, b), the stress in the outer steel tube was higher than that in the concrete core.
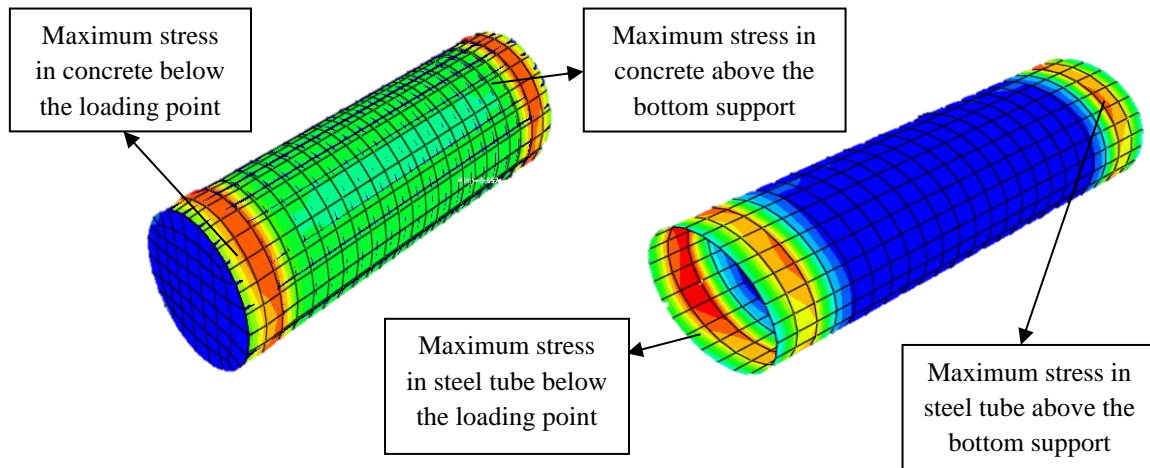
(a) Stress in infilled concrete   (b) Stress in outer steel tube
Figure 4.48 Maximum Stress in(a) Infilled concrete(b) Outer steel tube

Table 4.34 Stress behavior of concrete core and outer steel tube

Specimens	Size (D X Ts X H mm)	Stress in concrete core (MPa)	Stress in outer steel tube (MPa)
C1T4	100 × 4 × 600	116.5	698.8
C1T5	100 × 5 × 600	119.8	568.9
C2T4	125 × 4 × 600	105.8	829.3
C2T5	125 × 5 × 600	112.2	672.7
C3T4	150 × 4 × 600	104.9	957.1
C3T5	150 × 5 × 600	107.5	778.9

4.12.5 Maximum confining pressure (f$_{cp-max}$)

The CFST members owe their unique properties to the radial confining pressure applied on concrete by steel tube that improves the ductility and compressive strength of concrete. Estimating the right value of this parameter is pivotal to find the load resistance of CFST member under any given type of loading.
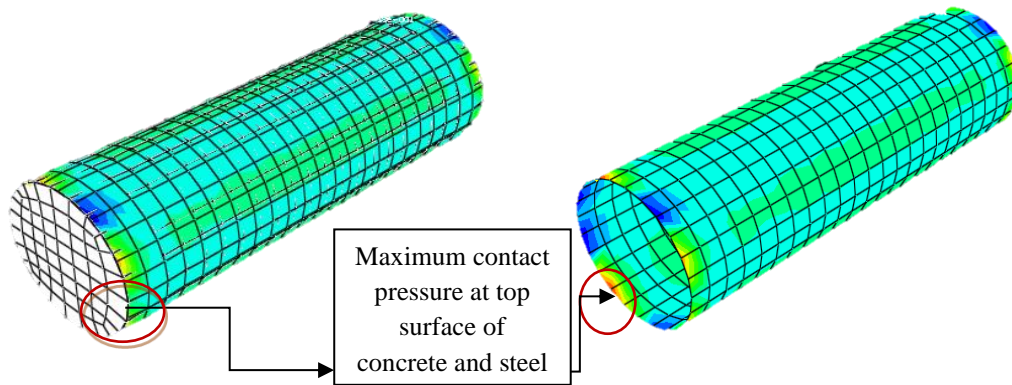
Figure 4.49 Contact pressure at surface node in concrete and steel
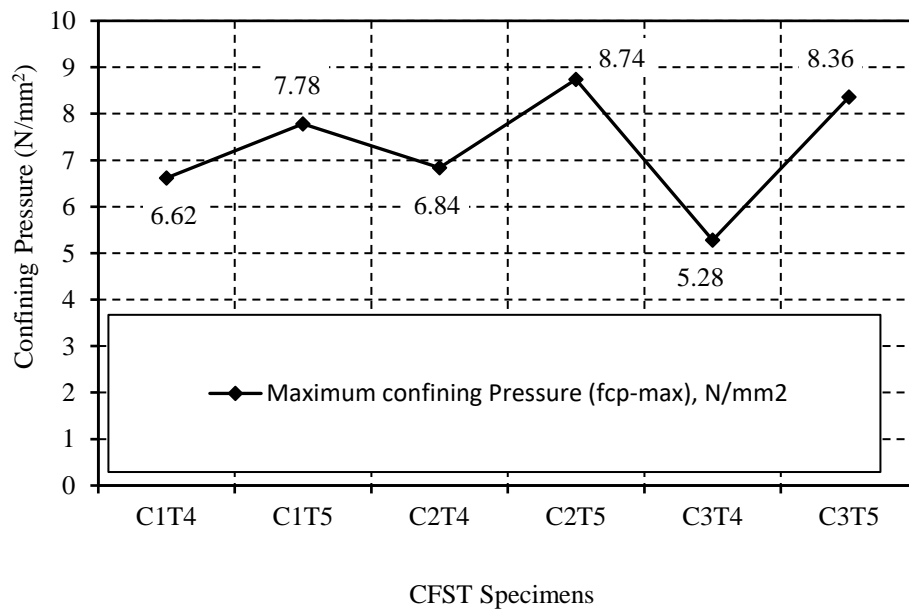
Figure 4.50 Maximum confining pressure of non-greased CFST columns

The experimental measurement of the value of confining pressure at any section is extremely difficult and required sophisticated equipment. Hence, the FEM model has been used

to study its variations alongside the peak, and therefore, the circumference of the specimens. Figure 4.49, demonstrates the confining pressure distribution for the specimen was observed throughout the peak from the highest of column specimens. The confining pressures of all specimens from the highest supports are shown in Figure 4.50. The fcp-max of non-greased CFST columns is given in Table 4.35.

Table 4.35 Maximum confining pressure of non-greased CFST columns

Specimens	Maximum confining Pressure (f_{cp-max}), N/mm^2
C1T4	6.6
C1T5	7.8
C2T4	6.8
C2T5	8.7
C3T4	5.3
C3T5	8.4

4.13 VALIDATION OF RESULTS

4.13.1 Failure pattern of experimental and simulated CFST columns

Figures 4.51, 4.52, and 4.53 represent the failure pattern of test specimens and numerical models C1T4, C1T5, C2T4, C2T5, C3T4, and C3T5 after testing and simulation. Under axial loading, the CFST columns failed with inward buckling at the centre. The diameter and thickness of the outer steel tubes were also found to influence the inward buckling of CFST columns. The failure mode found in simulation was very similar to the findings of the experimental studies. The differences in property and errors between test models and finite element models allow the results of experimental and analytical tests to differ.
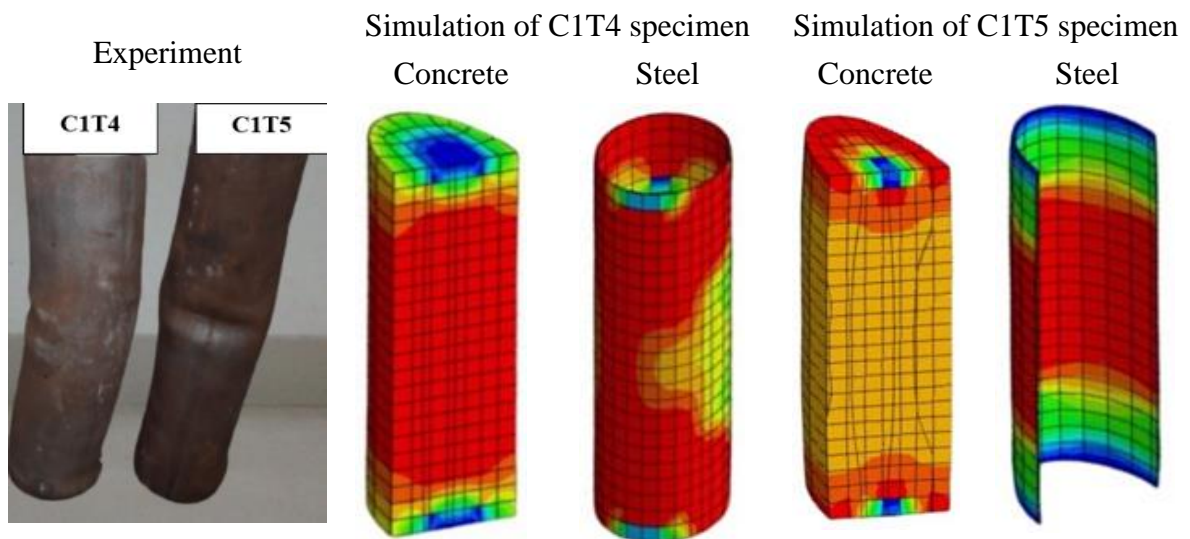
Figure 4.51 Failure pattern comparison of experiment and simulation of C1T4 and C1T5 specimens
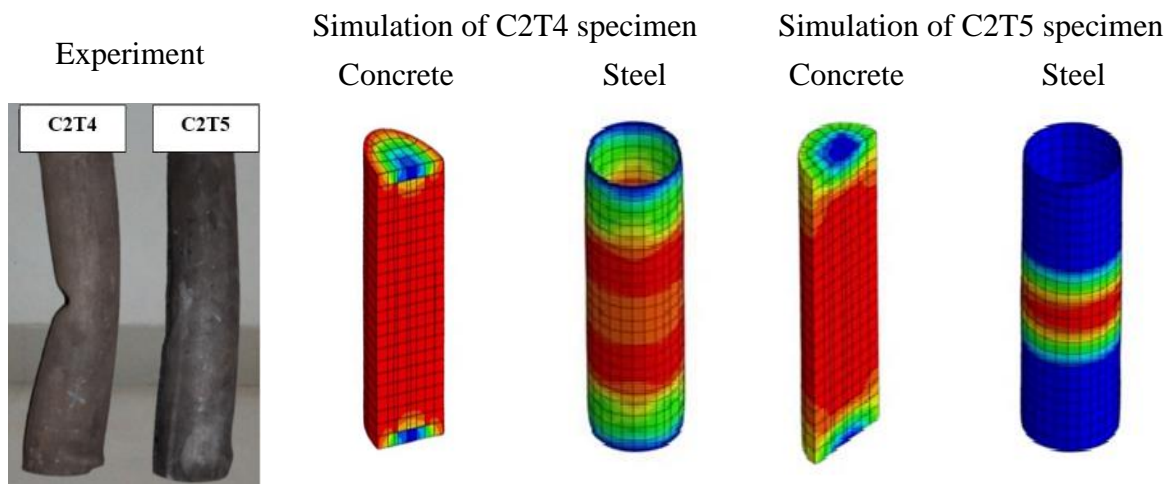
Figure 4.52 Failure pattern comparison of experiment and simulation of C2T4 and C2T5 specimens
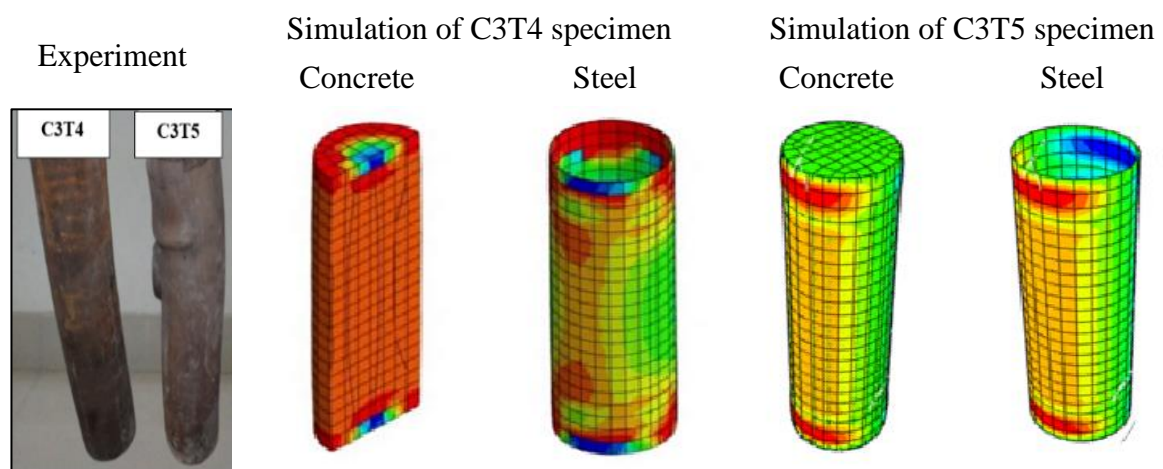
Figure 4.53 Failure pattern comparison of experiment and simulation of C3T4 and C3T5 specimens

171

4.13.2 Experimental vs. Simulated load-deflection curve

The comparison of load-deformation behavior of non-greased CFST columns between experimental and analytical results for specimens C1T4, C1T5, C2T4, C2T5, C3T4 and C3T5 is presented in Figure 4.54.
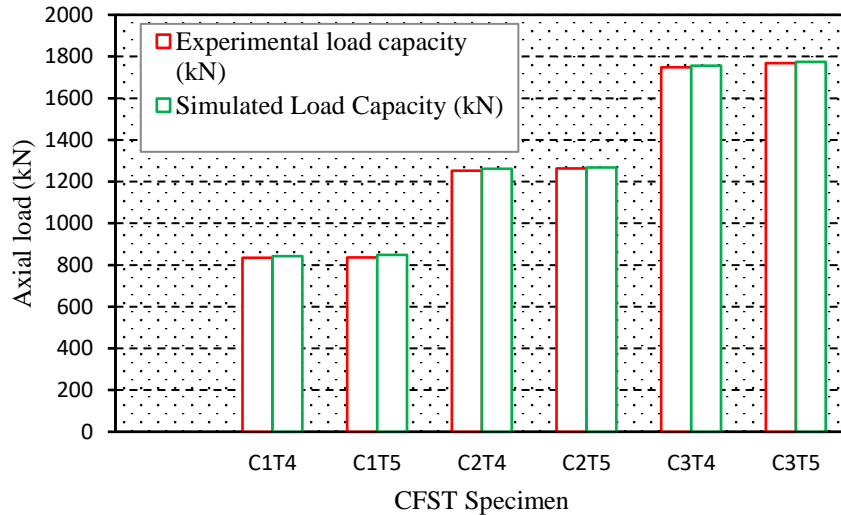
Figure 4.54 Experimental and simulated load capacity of CFST columns

The load carrying capacity of the CFST column increased as the diameter and thickness of the outer steel tube increased. The simulation results indicated that the observed load carrying ability of a concrete filled steel tube column by finite element modelling was very similar to the experimental observed values, with the variation of load from 0.34% to 1.53% as listed in Table 4.36.

Table 4.36 Comparison of load carrying capacity of CFST columns

Specimens	Size (D X Ts X H mm)	Experimental load capacity (kN)	Simulated Load Capacity (kN)	%age difference
C1T4	$100 \times 4 \times 600$	834	843	1.08
C1T5	$100 \times 5 \times 600$	836	849	1.53
C2T4	$125 \times 4 \times 600$	1252	1261	0.71
C2T5	$125 \times 5 \times 600$	1263	1268	0.39
C3T4	$150 \times 4 \times 600$	1749	1756	0.40
C3T5	$150 \times 5 \times 600$	1768	1774	0.34

Figures 4.55 (a, b), Figure 4.56 (a, b), and Figure 4.57 display the load-deformation actions of CFST columns, namely C1T4, C1T5, C2T4, C2T5, C3T4, and C3T5 (a, b). The deformation of concrete-filled steel tube columns was found to increase as the loading was increased in the current analysis. It may be because the combined axial loading has a wide area of use. The highest gain was observed in the middle of the column, and deformation was reduced in sequence to the bottom of the column. Material properties, site conditions, and defects between test samples and finite element models may have caused the disparity in results between analytical and test.
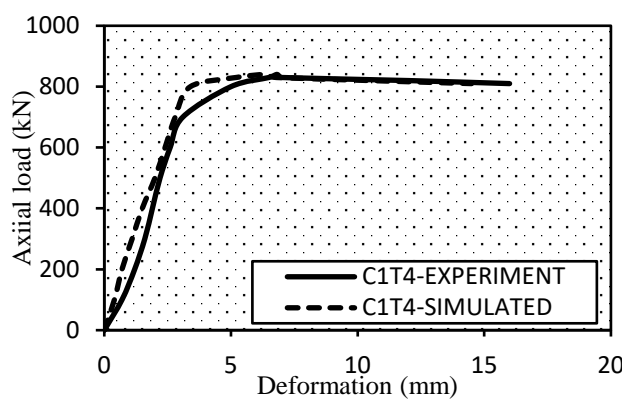
(a) Experiment and simulated load-deformation be havior for C1T4
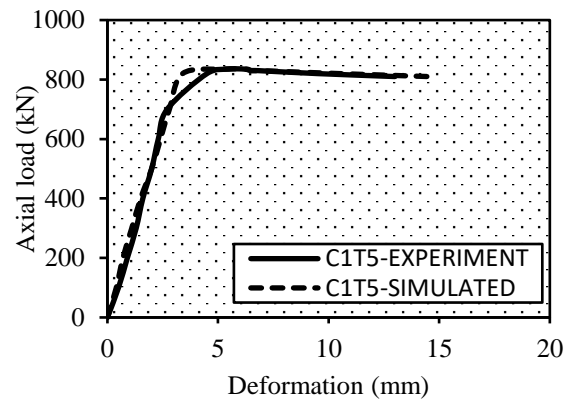
(b) Experiment and simulated load-deformation beh avior for C1T5

Figure 4.55 Comparison of Experiment and simulated load-deformation curves for (a) non-greased C1T4 (b) Non-greased C1T5
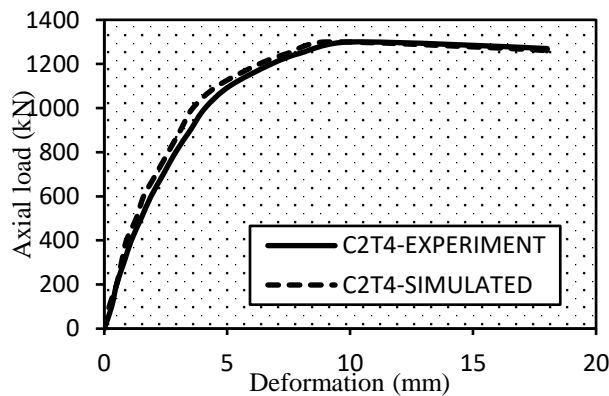
(a) Experiment and simulated load-deformation behavior for C2T4
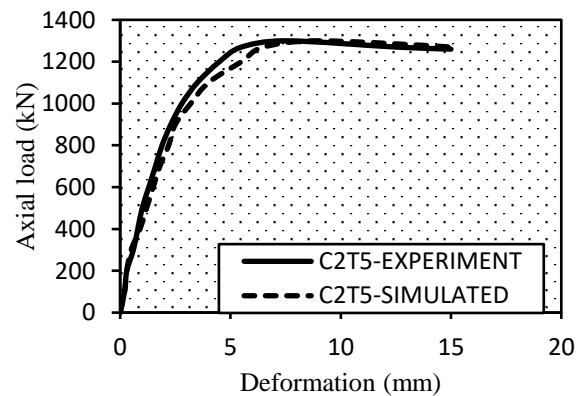
(b) Experiment and simulated load-deformation behavior for C2T5

Figure 4.56 Comparison of experiment and simulated load-deformation curves for (a) non-greased C2T4 (b) Non-greased C2T5
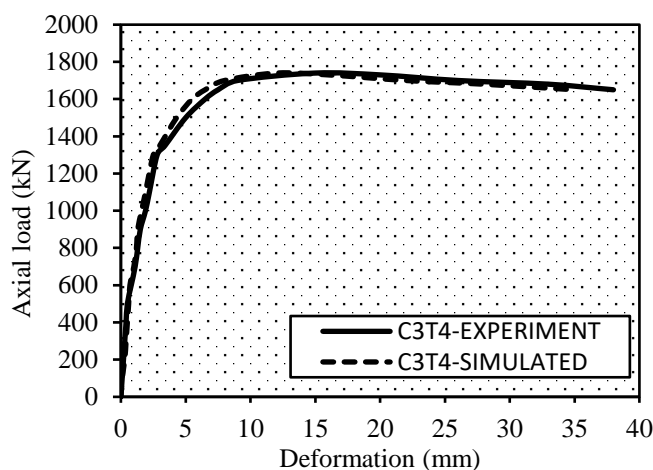
(a) Experiment and simulated load-deformation behavior for C3T4
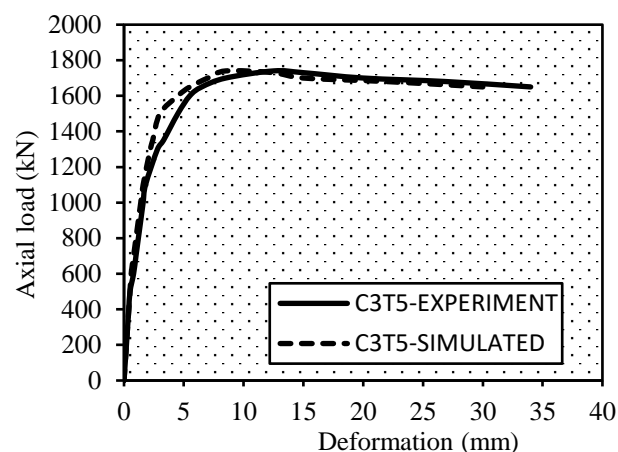
(a) Experiment and simulated load-deformation behavior for C3T5

Figure 4.57 Comparison of Experiment and simulated load-deformation curves for (a) non-greased C3T4 (b) Non-greased C3T5

4.14   PARAMETRIC STUDY ON CFST COLUMNS

The effects of D/T, steel grade, and L/D ratio under axial loading on CFST columns were investigated through a parametric analysis using the proposed model. The yield strength of steel was varied from 288 to 440 MPa in this analysis, while concrete compressive strength was kept steady at 36.7 MPa in the filled centre of CFST columns D/T was ranged from 20 to 37.5, and L/D was varied from 4.0 to 6.0, covering external steel tube thicknesses of 4 mm to 5 mm, and concrete filled steel tube specimen diameters of 100 mm to 150 mm. On both specimens, the overall height was maintained at 600 mm. The ratio of diameter to thickness (D/T), slenderness ratio, and yield strength of steel (fy) all influence the behavior of circular CFST columns.

4.14.1 Axial load behaviour of CFST column Vs Diameter to thickness ratio (D/T)

Six circular CFST columns are used in this study for studying the influence of thickness variance on CFST column behavior. The D/T ratio varied between 20 and 37.5 in this study. The growth of D/T ratio can be a result of the diameter (from 100 to 150 mm) or thickness of the segment (4 mm to 5 mm). As a result, for the same diameter, the declined ratio of D/T with increase in thickness represents a cross sectional difference in the steel frame, resulting in greater section loading capability. The influence of changing the D/T ratio on the CFST column loading capacity is shown in Figure 4.58. The axial load capacity of CFST columns was shown to be influenced by the decrease in diameter to thickness ratio. CFST column's axial loading capacity can also be improved by raising steel tube thickness with or without increasing the

174

overall column diameter. The loading capacity of CFST columns was improved to 33.4% by increasing the D/T ratio from 25 to 31.3 and increasing the diameter of CFST columns from 100 to 125 mm while keeping the outer steel tube thickness at 4 mm. The loading capacity of CFST columns was raised to 28.4% when the D/T ratio was changed from 31.3 to 37.5 and the diameter of CFST columns was increased from 125 to 150 mm with a constant thickness of outer steel tube of 4 mm. When the D/T ratio was increased from 20 to 25 and the diameter of the CFST columns was increased from 100 mm to 125 mm, the loading capacity of the CFST columns was increased to 33.8%. When the D/T ratio was increased from 25 to 30 and the diameter of the CFST columns was increased from 125 mm to 150 mm, the loading capacity of the CFST columns was increased to 28.6%.

Table 4.37 Loading capacity of CFST columns with varying D/T ratio

Specimens	Size (D × Ts × H) (mm)	D/T	Experimental Load (kN)	Simulated Load Capacity (kN)
C1T4	100 × 4 × 600	25.0	834	843
C1T5	100 × 5 × 600	20.0	836	849
C2T4	125 × 4 × 600	31.3	1252	1261
C2T5	125 × 5 × 600	25.0	1263	1268
C3T4	150 × 4 × 600	37.5	1749	1756
C3T5	150 × 5 × 600	30.0	1768	1774
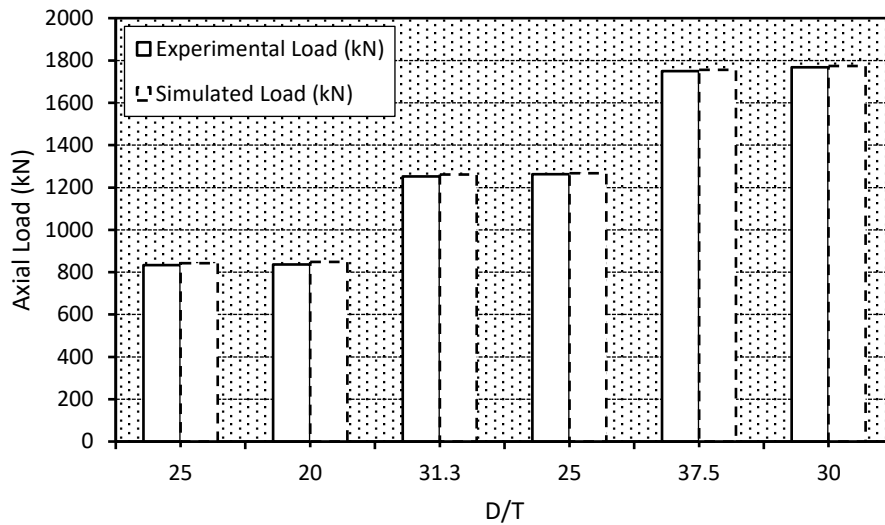
Figure 4.58 Effect of D/T on axial load behaviour of CFST columns

4.14.2 Axial load behaviour of CFST column Vs Length to diameter ratio (L/D)

This study uses three circular concrete filled steel tube columns to explore the influence of diameter variation on the CFST columns' behavior. The L/D ratio ranges from 4.0 to 6.0 in this study. The L/D ratio increased as the diameter of CFST columns was reduced (150 mm to 100 mm). As a result, with a constant height of 600 mm for both specimens, the decrease in L/D ratio represents an increase in steel tube cross section, resulting in greater section loading capacity. The impact of changing the length to diameter ratio of CFST columns on their loading capacity is shown in Fig. 4.59. As a result, as the L/D ratio lowers, the CFST's axial load bearing capacity increases. These columns' axial load strength can be enhanced by increasing their diameter without increasing their thickness. The load-carrying capacity of the CFST columns improved by 52.7% as the L/D ratio was reduced from 6.0 to 4.0.

Table 4.38 Loading capacity of CFST columns with varying L/D ratio

Specimens	Size (D × Ts × H) (mm)	L/D	Experimental Load (kN)	Simulated Load Capacity (kN)
C1T5	100 × 5 × 600	6.0	836	849
C2T5	125 × 5 × 600	4.8	1263	1268
C3T5	150 × 5 × 600	4.0	1768	1774

176
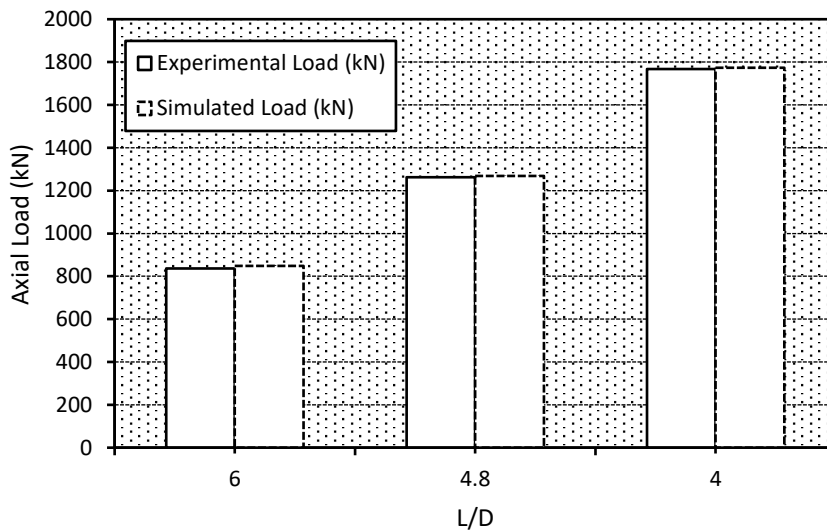
Figure 4.59 Effect of L/D on axial load behaviour of CFST columns

4.14.3 Axial load behaviour of CFST column Vs Strength of steel

The influence of steel grade on the axial efficiency of three circular CFST columns is studied. The CFST column's capability is determined by steel's yield strength. With the increase in the yielding strength of steel, a significant improvement in the axial loading capability of columns is observed. The influence of steel grade variation on the CFST columns' axial loading strength is shown in Fig. 4.60. It is found that the axial load carrying capacity improves as yield strength of steel of CFST columns increases. In a straight path, the load-carrying capacity rises. The capability of a load to carry it falls at an exponential rate. The ultimate load bearing capacity of the column increases by 52.7% when the steel yield strength is increased from 288 to 440 MPa.

Table 4.39 Loading capacity of CFST columns with strength of steel

Specimens	Size (D × Ts × H) (mm)	Yield strength of Steel (MPa)	Experimental Load (kN)	Simulated Load Capacity (kN)
C1T5	100 × 5 × 600	288	836	849
C2T5	125 × 5 × 600	380	1263	1268
C3T5	150 × 5 × 600	440	1768	1774

177
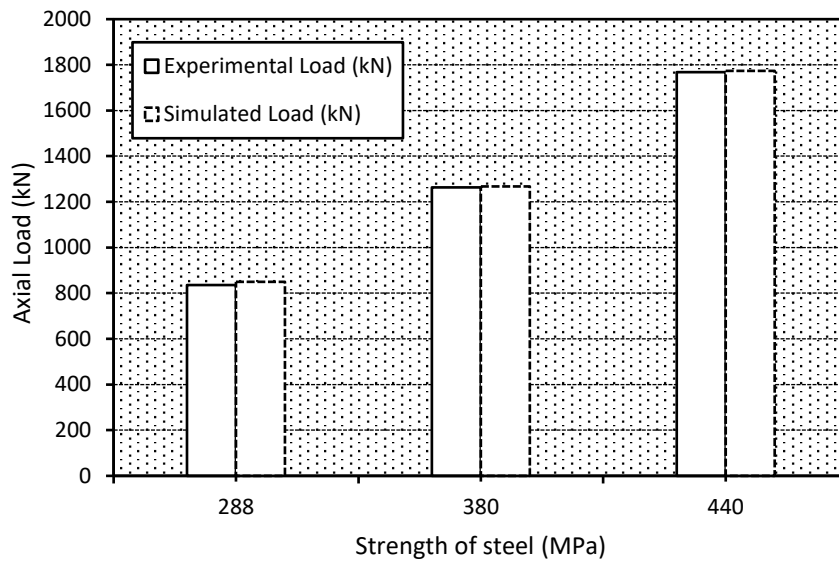
Figure 4.60 Effect of strength of steel on axial load behaviour of CFST columns

4.15 SUMMARY

The effectiveness of CFST columns loaded before and after fire exposure at 600 ° C and 800 ° C was investigated. The action of greased and non-greased steel columns filled with concrete was examined. The load-deformation characteristics of the greased and non-greased CFST columns are nearly identical in the elastic region, but there is little difference in the load-deformation behavior of the greased and non-greased columns as axial loading increases. Non-greased columns had a higher elastic axial load capacity than greased columns. The axial load capacity of concrete filled steel tube columns was investigated at 600° C and 800° C in the two cooling regimes of first annealing and second quenching, suggesting that the CFST columns' axial load decreased with increasing temperature. In contrast to annealing, the water quenching process reduced a lot of strength, and after exposure to 800 ° C, the residual strength capacity increased for all specimens, while ductility and stiffness decreased. The test results are compared to the design code's suggested equations. There was a strong agreement between the results of the test and the ACI code. This research also included the development of a nonlinear element model using the commercial programme ABAQUS/CAE 6.14. Tested concrete filled steel tube columns were used to validate the FE model, and the test data and the model performance in terms of axial load capacity and failure mode were found to be in good agreement. The finite element model's load carrying capacity was very similar to the experimentally observed values for a mesh size of 10 mm.

178

CHAPTER 5

CONCLUSIONS

5.1 GENERAL

This chapter comprises of the conclusions derived from the experiment. The critical observations from experiment on concrete filled steel tube column tests are also included. It also incorporates some major conclusions based on comparison of results between elevated temperature.

5.2 CONCLUSIONS

The action of axially loaded concrete filled steel tube columns before and after exposure to fire at 600°C and 800°C was studied. To investigate the bond behavior between concrete and steel, experiments were carried out on greased and non-greased concrete filled steel tube columns. The test results are compared to the design code's prescribed equations. This research also included the development of a nonlinear element model with the commercial programme ABAQUS/CAE 6.14. Concrete filled steel tube columns are used to validate the FE model. The following conclusions can be taken from the results of experimental research and computational modelling using finite element modelling.

1. The load carrying capacity of non-greased concrete filled steel tube columns was higher than greased columns and observed to be varying from 1.0% to 2.7% under axial loading. The loading capacity of greased columns was observed to be less as compared to non-greased columns due to a lack of bonding behavior between concrete and steel. Therefore, it is concluded that the shrinkage of concrete has minimum effect on compression behavior of concrete filled steel tube columns.

2. The load-deformation behavior of greased and non-greased columns was compared, and the two curves were found to be very similar. Owing to the negligible impact of concrete shrinkage, the initial slope of curves for greased and non-greased columns are virtually similar. It can be concluded that load-deformation behavior of non-greased columns is higher than greased columns in elastic range and it is almost same in plastic

179

range which indicates that the load-deformation behavior of concrete filled steel tube columns has little influence on greased and non-greased columns.

3. The secant stiffness of non-greased CFST columns was observed to be greater than greased columns. The secant stiffness of greased and non-greased specimens was varying from 18% to 59% and it was seen that C2T5 non-greased specimen has higher secant stiffness. Due to concrete cracking, the secant stiffness of concrete-filled steel tube columns decreased as axial loading increased. To summarize, when the axial load approaches 0.4Nu and the concrete stress exceeds 0.4fc due to concrete confinement, the steel tube usually remains elastic. Significant reduction in concrete stiffness may occur if the confinement is strong.

4. The ductility index of non-greased columns was observed to be higher than the greased columns. So, it came to a judgment that the non-greased specimens have more ductility as compared to the greased specimens. The ductility index of non-greased columns was higher due to the confinement between steel tubes and concrete.

5. The confining pressure given by steel tube to concrete is generally emphasized near the columns ends by friction due to the machine loading plate and CFST top and bottom plates. The affected length of CFST columns is generally between 20 mm and 40 mm from either side. This results in very high compressive stresses in concrete in these areas. It was concluded that in axial loading, concrete expands laterally in all direction, the confining pressure was constant at all point. However, near the column ends, the radial confining pressure was detected to be more throughout the height of columns.

6. The load carrying capacity of CFST columns at three different temperature conditions namely ambient (AB), 600 °C and 800 °C was found to reduce as the columns are exposed to increasing temperatures of 600 °C and then 800 °C. The reduction in load capacity ranges from 5.2% to 2.9% for temperature variation from ambient to 600 °C. Whereas, it was seen that the reduction in load capacity ranges from 14.2% to 6.2% for temperature variation from ambient to 800 °C. The decrease in load carrying capacity of CFST column can be attributed due to the erupt a few twist or surface flaws of concrete filled steel tube columns.

7. The load – deformation behavior of CFST columns at three different temperature conditions namely ambient (AB), 600 °C and 800 °C for two cooling regimes was found to reduce as the columns are exposed to increasing temperatures of 600 °C and then 800 °C. The reduction in load capacity ranges from 10.2% to 2.9% for temperature

variation from ambient to 600 °C in case of annealing and quenching. Whereas, for CFST columns exposed to 800 °C, the load capacity is found to decrease by 17.3% to 6.2% in case of annealing and quenching as compared to CFST columns at ambient temperature. The decrease in load carrying ability of the CFST column can be attributable to the sudden escape of gases and extreme hardening in the case of water quenching, which allows the microstructure of the material to form a grain structure and balances a portion of the loss that could be due to twisting that was introduced due to an unbalanced heating and cooling process, which is responsible for further loss of strength in the case of water quenching, which allows the microstructure of the material to form a grain structure, it balances a portion of the loss that could be due to twisting that was introduced due to an unbalanced heating and cooling step, which is responsible for further strength loss in the water quenching process as opposed to the annealing process.

8. The load – deformation behavior of CFST columns at three different temperature conditions namely ambient (AB), 600 °C and 800 °C was found to reduce as the columns are exposed to increasing temperatures of 600 °C and then 800 °C. The reduction in load capacity ranges from 17.5% to 2.9% for temperature variation from ambient to 600 °C and then to 800 °C. The decrease in load carrying capacity of the C1T4 CFST column can be attributed to the change in the behavior of thermal properties of steel with the rise of temperature.

9. At 800 °C elevated temperature, the value of secant stiffness for CFST columns was lower than at 600 °C elevated temperature. At elevated temperatures between 600 °C and 800 °C, it was observed that annealing reduced secant stiffness by 45.5% to 14.4%, while water quenching reduced secant stiffness by 34.6% to 13.2%. It can be inferred that the decrease in secant stiffness of concrete-filled steel tube columns was due to increased heat absorption prior to cooling.

10. As compared to 600 °C elevated temperature, the ductility index of CFST columns was found to be lower at 800 °C elevated temperature. It can be inferred that the ductility index value for water quenching was found to be significantly different from that of annealing, showing that the CFST columns were more ductile in the case of annealing than in the case of water quenching under axial loading. It was achieved as a result of changes in the thermal properties of concrete and steel as a result of exposure to high temperatures.

181

11. The lower the value of the residual strength index, the greater the loss in the strength of the CFST columns (RSI). The RSI value was found to be higher at the elevated temperature of 800 °C for both annealing and water quenching as compared to 600 °C because the thicker portion impedes the heat transfer process from steel to concrete. The RSI value of the CFST columns after exposure to elevated temperature was found to be affected by column section size and slenderness ratio. This reduced the peak temperature reached by concrete, reducing the residual strength index value of CFST columns as a result

12. The comparison of experimental results with design codes was investigated to estimate the axial load capacity of concrete filled steel tube columns. The analytical values predicted by some suggested equations in the design code and it is concluded that ACI gives conservative results for both greased and non-greased columns varying from 5.8% to 15.9% and 7.4% to 16.9% respectively for all concrete filled steel tube columns. It was also observed that the Chinese code (CECS 28:90) is only applicable for evaluating the axial strength of concrete filled steel tube columns having steel tube thickness 4 mm and more. The Chinese code (CECS 28:90) and Eurocode-4 gives the similar results of axial load capacity for both greased and non-greased concrete filled steel tube columns.

13. In this analysis, a nonlinear finite element model was extended using the commercial programme ABAQUS/CAE 6.14. After joining the material nonlinearity of both steel tube and concrete infill, the FE model was verified with tested concrete filled steel tube columns. In terms of axial capability and failure mode, there is a lot of agreement between the test results and the simulated results. The load carrying capacity of the simulated specimens was found to be in fair agreement with the experimental test results for a mesh size of 10 mm.

14. A change in the diameter to thickness (D/T) ratio was demonstrated to affect the axial load capacity of CFST columns. A CFST column's axial loading capacity can also be improved by raising the steel tube thickness, which can be done with or without increasing the overall column diameter. By increasing the D/T ratio from 25 to 31.3 and increasing the diameter of CFST columns from 100 to 125 mm while maintaining a constant outer steel tube thickness of 4 mm, the loading capacity of CFST columns was increased by 33.4%. By increasing the D/T ratio from 31.3 to 37.5 and expanding the diameter of CFST columns from 125 to 150 mm while maintaining the outer steel

tube thickness constant at 4 mm, the loading capacity of CFST columns was increased by 28.4%.

15. By increasing the D/T ratio from 20 to 25, as well as expanding the diameter of the CFST columns from 100 to 125 mm, the loading capacity of the CFST columns was increased to 33.8%. When the D/T ratio was adjusted from 25 to 30, and the diameter of the CFST columns was increased from 125 to 150 mm, the loading capacity of the columns was improved to 28.6%.

16. As the L/D ratio lowers, the CFST's axial load bearing capability increases. These columns' axial load strength may be enhanced by increasing their diameter without increasing their thickness. The CFST columns' load-carrying capability rose by 52.7% when the L/D ratio was decreased from 6.0 to 4.0.

17. As the yield strength of the steel grows, the axial load bearing capacity of CFST columns improves. The load-carrying capacity increases along a straight path. A load's ability to carry it decreases exponentially. When the steel yield strength is increased from 288 to 440 MPa, the column's ultimate load bearing capacity increases by 52.7%. it is concluded that the average strength of the columns increases as steel tube yield strength improves or the length-to-diameter ratio of the CFST column decreases.

5.3 SCOPE FOR FUTURE WORK

1. Shrinkage has a marginal effect on the load carrying capacity of greased and non-greased CFST columns, and non-greased columns have a higher elastic axial load capacity than greased columns. However, further research into the bond behavior between concrete and steel tube of CFST columns with various outer steel tube materials is required.

2. More studies are required to develop an exact model for confinement of concrete in CFST columns, which takes into account the variation in confining pressure along the length of column as well.

3. To accomplish more precise behavior of CFST columns, more fire test should be done on concrete with various compressive strength, differing outer steel types, in-filled material to arrive at an improved understanding of the behavior of concrete in fire conditions.

4. More research is required to fully comprehend the action of the CFST column when it is subjected to both fire and loading.

5. The experimental and computational models proposed can be extended to the simulations of the fire performance of CFST, CFDST, HSCF columns with different shape and configurations of materials.

6. More research is required to establish simple and effective design guidelines for CFST columns that are subjected to eccentric loading and have internal reinforcement. Similarly, different types of steel should be included in the design guidelines.

REFERENCES

[1] De Nardin. S. and El Debs A. L. H. C. "Axial Load Behaviour of Concrete-Filled Steel Tubular Columns", Proceedings of the Institution of Civil Engineers Structures & Buildings-2007. Issue SB1, pp. 13–22, 2007.

[2] ASTM, (1985), "Standard methods of fire tests of building construction and materials", ASTM E119, West Conshohocken, PA, 22.

[3] CEN (European Committee for Standardization), Eurocode 4: Design of composite steel and concrete structures. Part 1-2: "General Rules-Structural fire design", EN 1994-1-2, Brussels, Belgium.19, 2008.

[4] CEN (European Committee for Standardization), "Fire resistance tests", Part 1: General requirements, EN 1363-1, Brussels, Belgium, 2012.

[5] CEN. EN 1994-1-1, Eurocode 4: "Design of composite steel and concrete structures", Part 1-1: General rules and rules for buildings, Brussels, Belgium: Committee European de Normalization; 2004.

[6] CEN. EN 1994-1-2, Eurocode 4: "design of composite steel and concrete structures", Part 1–2: general rules — structural fire design. Brussels, Belgium: Committee European de normalization; 2005.

[7] American Institute of Steel Construction, AISC–LRFD, "Metric Load and Resistance Factor Design Specification for Structural Steel Buildings", AISC, Chicago, IL, USA, 1994.

[8] China Association for Engineering Construction Standardization, CECS 28:90, "Specification for Design and Construction of Concrete-Filled Steel Tubular Structures", China Association for Engineering Construction Standardization, Beijing, China, 2012.

[9] ISO 834: "Fire resistance tests, elements of building construction", Switzerland, International Standards Organization; 1980.

[10] ISO, Fire resistance test-Element of building construction-Part 1: "General requirement", ISO 834-1, Geneva, 1999.

[11] Lu H., Zhao X. L. and Han L. H., "Testing of self-consolidating concrete filled double skin tubular stub columns exposed to fire", Journal of Constructional Steel Research, Vol. 66, Issue 8, pp 1069-1080, 2010.

[12] Tian-Yi Song, Lin-Hai Han, Brian UY, "Performance of CFST column to steel beam joints subjected to simulated fire including the cooling phase", Journal of Constructional Steel Research, Volume 66, Issue 4, pp. 591-604, 2010.

[13] Photiou, N.K. Hollaway, L.C. Chrysanthopoulos, M.K. "Strengthening of an Artificially Degraded Steel Beam Utilizing a Carbon/Glass Composite System", Construction and Building Materials, Vol. 20, pp. 11–2, 2006.

[14] Tao, Z., Han, L. H., UY, Brain, and Chen, Xian, "Post-fire bond between the steel tube and concrete in concrete-filled steel tubular columns", Journal of Constructional Steel Research, 67(3), 484-496, 2011.

[15] Sangeetha, P. and Senthil, R., "Experimental Behavior of Steel Tubular Columns for varying in Filled Concrete", Archives of Civil Engineering, 63(4), 149-160, 2017.

[16] Tao, Z. and Han, L. H., "Behaviour of fire-exposed concrete-filled steel tubular beam column repaired with CFRP wraps", Thin-Walled Structure,45(1), 63-76, 2007.

[17] Abbas, H., Al-Salloum, Y. A., Alsayed, S. H., Alhaddad, M and Rizwan, I., "Post-Heating response of concrete-filled circular steel columns", KSCE Journal of Civil Engineering, 21, 1367-1378, 2016.

[18] Li, Pengfei, Zhang, Tao, and Wang, Chengzhi., "Behavior of concrete filled steel tube columns subjected to axial compression", Advance in Materials Science and Engineering, 2018, 1-15, 2018.

[19] Jia-Bao Yan, Wenjun Xie, Lingxin Zhang, Xu-Chuan Lin, "Bond behaviour of concrete-filled steel tubes at the Arctic low temperatures", Construction and Building Materials, Vol. 210, pp 118-131, 2019.

[20] Kan Zhou, Lin-Hai Han, "Modelling the behaviour of concrete-encased concrete-filled steel tube (CFST) columns subjected to full-range fire", Engineering Structures, Volume 183, Pages 265-280, 2019.

[21] Alireza Afaghi-Darabi and Gholamreza Abdollahzadeh, "Effect of cooling rate on the post fire behavior of CFST column", Volume 23, Number 4, April, pages 281-294, 2019.

[22] Almasslawi, Ahmed & Ekmekyapar, Talha & Al-Eliwi, Baraa., "Repair of Buckled Concrete Filled Steel Tube Columns Subjected to Axial Compression", KSCE Journal of Civil Engineering. 24. 10.1007/s12205-020-0321-x, 2020.

[23] R. Chacon, "Circular concrete-filled tubular columns: state of the art oriented to the vulnerability assessment", Open Civ. Eng. J. 9, 249–259, 2015.

[24] L.-H. Han, L. Wei, R. Bjorhovde, "Developments and advanced applications of concrete-filled steel tubular (CFST) structures: members", J. Constr. Steel Res. 100, 211–228, 2014.

[25] J.Y.R. Liew, M.X. Xiong, D.X. Xiong, "Design of high strength concrete filled tubular columns for tall buildings, International Journal of High-rise Building", Vol. 3, pp. 215–221, 2014.

[26] F.X. Ding, Z.W. Yu, Y. Bai, Y.Z. Gong, "Elasto-plastic analysis of circular concrete filled steel tube stub columns", J. Constr. Steel Res., Vol. 67 (10), pp. 1567–1577, 2011.

[27] Shanmugam, N.E. & Lakshmi, B., "State of the art report on steel–concrete composite columns", Journal of Constructional Steel Research, Vol. 57, pp. 1041-1080. 10.1016/S0143-974X(01)00021-9, 2001.

[28] Kitada T., "Ultimate strength and ductility of state-of-the-art concrete-filled steel bridge piers in Japan", Engineering Structures, Vol. 20(4), pp. 347–354, 1998.

[29] Chacon, Rolando & Mirambell, Enrique & Real, Esther., "Strength and ductility of concrete-filled tubular piers of integral bridges", Engineering Structures, Vol. 46, pp. 234-246,2013.

[30] Dong C.X., Kwan A.K.H., Ho J.C.M., "A constitutive model for predicting the lateral strain of confined concrete", Engineering Structures, Vol. 91, pp. 155–66, 2015.

[31] Tao Z., Song T.Y., UY B., Han L.H., "Bond behaviour in concrete-filled steel tubes", Journal of Constructional Steel Research, Vol. 120, pp. 81–93, 2016.

[32] Xue, Junqing & Briseghella, Bruno & Chen, Bao-Chun., "Effects of debonding on circular CFST stub columns. Journal of Constructional Steel Research", Vol. 69, pp. 64–76, 2012.

[33] Ho, J. & Lai, M. H., "Optimal design of external rings for confined CFST columns", Magazine of Concrete Research, 2015.

[34] Susantha, Samans & Ge, Hanbin &Usami, Tsutomu, "A Capacity Prediction Procedure for Concrete-Filled Steel Columns", Journal of Earthquake Engineering, Vol. 5, pp. 483-520, 2001.

[35] Luo, L. & Lai, M. H. & Ho, J., "Uniaxial behaviour of confined high-strength concrete-filled-steel-tube columns", Proceedings of the ICE-Structures and Buildings, Vol. 167, pp. 520-533, 2014.

[36] Liang, Q. Q., "Performance-based analysis of concrete-filled steel tubular beam–columns", Part I: Theory and algorithms. Journal of Constructional Steel Research, Vol. 65, pp. 363-372, 2009.

[37] Liang QQ., "High strength circular concrete-filled steel tubular slender beam columns", Part I: numerical analysis. J Constr. Steel Res, Vol. 67(2), pp. 164–171, 2011.

[38] Richart, F. E., Brandtaeg, Anton, Brown, Rexlenoi, "A study of the failure of concrete under combined compressive stresses", IJITEE, Vol. 8(12), 1982.

[39] Saenz, L. P., "Discussion of 'Equation for the stress-strain curve of concrete", JKAU Engg. Sci., Vol. 2, pp 183-194, 1990.

[40] Johansson, Mathias., "The efficiency of passive confinement in CFT columns", Steel and Composite Structures, Vol. 2. 10.12989/scs.2002.2.5.379, 2002.

[41] Abbas, H., Al-Salloum, Y. A., Alsayed, S. H., and Alhaddad, M. S., "System for improving fire endurance of concrete-filled steel tubular columns", Canada States patent: US 8,484,915 B1, 1-10, 2013.

[42] Hossain K. M. A. and Chu K, "Confinement of six different concretes in CFST columns having different shapes and slenderness", International Journal of Advanced Structural Engineering, Vol. 11, pp 255-270, 2019.

[43] Han, L. H., Huo, J. S., and Wang, Y. C., "Behavior of Steel Beam to Concrete-Filled Steel Tubular Column Connections after Exposure to Fire", Journal of Structural Engineering, Vol. 133(6), 800-814, 2007.

[44] Tao, Z., and Yu, Q., "Residual bond strength in steel reinforced concrete columns after fire exposure", Fire safety journal, 53, 19-27, 2012.

[45] Yao, Yao & Hu, Xin., "Cooling behavior and residual strength of post-fire concrete filled steel tubular columns", Journal of Constructional Steel Research, Vol. 112, 10.1016/j.jcsr.2015.05.020, 2015.

[46] Ibanez, C., Bisby, L. A., Rush, D., Romero M. L. and Hospitaler, A., "Post-heating response of concrete-filled steel tubular columns under sustained loads", Advances in Steel-Concrete Composite Structures, Vol. 21, 90-102, 2019.

[47] Han, L.H., and Huo, J.S., "Concrete-filled hollow structural steel column after exposure to ISO- 834 fire standard", Journal of Structure Engineering, Vol. 129 (1), pp 68-78, 2003.

[48] Han, L. H., and Lin, X. K., "Tests on Cyclic Behavior of Concrete-Filled Hollow Structural Steel Columns after Exposure to the ISO-834 Standard Fire", Journal of Structure Engineering, Vol. 130(11), pp 1807-1819, 2004.

[49] Han, L. H., Lin, X. K. and Yang, Y. F., "Cyclic Performance of Concrete-filled Steel Tubular Columns after Exposure to Fire: Analysis and Simplified Mode", Advances in Structural Engineering, Vol 11(4), pp 455-473, 2008.

[50] Kumar, P., and Chaudhary, S., "Effect of Reinforcement Detailing on Performance of Composite Connections with Headed Studs", Engineering Structures, 179, 476-492, 2019.

[51] Mander, J. B., Priestley, M. J. N., and Park, R., "Theoretical stress-strain model for confined concrete", Journal of Structural Engineering, Vol. 114(8), pp 1804-1826, 1998.

[52] Mirza, S. A., Hyttinen, V., and Hyttinen, E., "Physical tests and analyses of composite steel– concrete beam-columns", Journal of Structural Engineering, Vol. 122(11), pp 1317- 1326, 1996.

[53] Park, T., Hwang, W. S., Leon, R. T., and Hu, J. W., "Damage evaluation of composite-special moment frames with concrete-filled tube columns under strong seismic loads", KSCE Journal of Civil Engineering, Vol. 15(8), pp 1381-1394, 2011.

[54] Tao, Z., Han, L. H., and Zhuang, J. P., "Cyclic performance of fire-damaged concrete-filled steel tubular beam-column repaired with CFRP wraps", Journal of constructional steel Research, Vol. 64(1), pp 37-50, 2008.

[55] Kumar, P., Patnaik, A., and Chaudhary, S., "A Review on Application of Structural Adhesives in Concrete and Steel-Concrete Composite and Factors Influencing the Performance of Composite Connections", International Journal of Adhesion and Adhesives, Vol. 77, pp. 1-14, 2017.

[56] Li, Pengfei & Zhang, Tao & Wang, Chengzhi., "Behavior of Concrete-Filled Steel Tube Columns Subjected to Axial Compression. Advances in Materials Science and Engineering", pp 1-15, 10.1155/2018/4059675, 2018.

[57] Kodur, V. K. R., and Dwaikat, M., "A Numerical model for predicting the fire resistance of reinforced concrete beams", Cement and Concrete Composites, Vol. 30(5), pp 431-443, 2003.

[58] Kumar, P., Patnaik, A., and Chaudhary, S., "Effect of Bond Layer Thickness on Behaviour of Steel-Concrete Composite Connections", Engineering Structures, Vol. 177, pp 268-282, 2018.

[59] Han, L. H., "Tests on Stub Columns of Concrete-filled RHS Sections", *Journal of Constructional Steel Research*, Vol.*58*(3), pp 353 – 372, 2002.

[60] Han, L. H., Huo, J. S., and Wang, Y. C., "Compressive and Flexural Behaviour of Concrete Filled Steel Tubes after Exposure to Standard Fire", *Journal of Constructional Steel Research*, Vol. *61*(7), pp 882 – 901, 2005.

[61] Huo, J., Huang, G., and Xiao, Y., "Effects of sustained axial load and cooling phase on post fire behaviour of concrete-filled steel tubular stub columns", Journal of Constructional Steel Research, Vol. 65(8), pp 1664-1676, 2009.

[62] Wang, Y. C., "Performance of steel-concrete composite structures in fire", Progress in Structural Engineering and Materials, Vol. 7(2), pp 86-102, 2005.

[63] Wang, J. X., Zhang P. P., and Wang, W. D., "Preliminary Research on Behavior of CFST Columns after Exposure to Overall Stage of Fire", Advanced Materials Research, Vol. 250, pp 2729-2733, 2011.

[64] Faber, O., "More rational design of cased stanchions", The Structural Engineer, Vol. 34, pp 88-109, 1956.

[65] Zhou, Ting & Chen, Zhihua & Liu, Hongbo., "Seismic behavior of special shaped column composed of concrete filled steel tubes", Journal of Constructional Steel Research, Vol. 75, pp 131–141, 10.1016/j.jcsr.2012.03.015, 2012.

[66] Ikeda, Kenichi & Ohmiya, Yoshifumi., "Fire Safety Engineering of Concrete-Filled Steel Tubular Column without Fire Protection", Fire Science and Technology. 28. 106-131. 10.3210/fst.28.106, 2009.

[67] Twilt L, Hass R, Klingsch W, Edwards M, Dutta D., "Design guide for structural hollow section columns exposed to fire", Cologne Germany: Comite International pour le Development et l'Etude de la Construction Tubulaire (CIDECT),1996.

[68] Kodur, Venkatesh K.R.; MacKinnon, David H., "Design of Concrete-Filled Hollow Structural Steel Columns for Fire Endurance", *Engineering Journal*, American Institute of Steel Construction, Vol. 37, pp. 13-24, 2000.

[69] Hicks, Stephen & Newman, G.M. & Edwards, M & Orton, A., "Design guide for SHS concrete filled columns", 10.13140/RG.2.1.2132.2962, 2005.

[70] Kodur, Venkatesh., "Guidelines for fire resistant design of concrete-filled steel HSS columns - State-of-the-art and research needs", Steel Struct., Vol. 7., pp 173-182, 2007.

[71] Evirgen, Burak & Tuncan, Ahmet & Taskin, Kivanc., "Structural behavior of concrete filled steel tubular sections (CFT/CFST) under axial compression", Thin-Walled Structures., Vol. 80, pp 46–56. 10.1016/j.tws.2014.02.022, 2014.

[72] Morino, Shosuke & Kawaguchi, J. & Tsuji, Akiyoshi & Kadoya, H., "Strength and Stiffness of CFT Semi-Embedded Type Column Base",2003.

[73] Mete Guneyisi, Esra & Gultekin, Ayşegül & Mermerdaş, Kasım., "Ultimate capacity prediction of axially loaded CFST short columns", International Journal of Steel Structures. Vol. 16, pp99-114, 10.1007/s13296-016-3009-9, 2016.

[74] Tao, Professor Zhong & Ghannam, Mohamed., "Heat transfer in concrete-filled carbon and stainless-steel tubes exposed to fire", Fire Safety Journal. Vol. 61, pp 1–11, 10.1016/j.firesaf.2013.07.004, 2013.

[75] Myllymaki, J. & Lie, T. & Chabot, M., "Fire resistance tests of square hollow steel columns filled with reinforced concrete",10.4224/20375972, 1994.

[76] Zhao, Xiao-Ling & Han, Lin-Hai & Lu, Hui., "Concrete-filled Tubular Members and Connections",10.1201/9781482266085, 2010.

[77] Klingsch, W. & Wuerker, K.-G & Martin-Bullmann, R., "Fire Resistance of Hollow-Section Composite Columns", Vol. 53, pp 300-305, 1984.

[78] Kang, Chang-Hoon & Shin, Kyung-Jae & young suk, oh & Moon, Tae-Sup., "Hysteresis behavior of CFT column to H-beam connections with external T-stiffeners and penetrated elements", Engineering Structures. Vol. 23, pp 1194-1201. 10.1016/S0141-0296(00)00119-X, 2001.

[79] Khaliq, Wasim & Kodur, Venkatesh., "Effect of Temperature on Thermal Properties of Different Types of High-Strength Concrete", Journal of Materials in Civil Engineering, Vol. 23, pp 793-801, 10.1061/(ASCE)MT.1943-5533.0000225, 2011.

[80] Naus, Dan., "The Effect of Elevated Temperatures on Concrete Materials and Structures—A Literature Review at ORNL",10.2172/974590, 2006.

[81] Kodur, Venkatesh., "Properties of Concrete at Elevated Temperatures", ISRN Civil Engineering. Vol. 2014, pp 1-15. 10.1155/2014/468510, 2014.

[82] Liu, Dalin & Gho, Wie Min., "Axial load behaviour of high-strength rectangular concrete-filled steel tubular stub columns", Thin-Walled Structures. Vol. 43, pp 1131-1142, 10.1016/j.tws.2005.03.007, 2005.

[83] Harada, T. & Takeda, J. & Yamane, S. & Furumura, F., "Strength, elasticity and thermal properties of concrete subjected to elevated temperatures", Concrete for Nuclear Reactors, Vol. 34, pp 377-406, 1972.

[84] Romero, M. & Moliner, V. & Espinos, Ana & Ibanez Usach, Carmen & Hospitaler, Antonio., "Fire behavior of axially loaded slender high strength concrete-filled tubular columns", Journal of Constructional Steel Research - J CONSTR STEEL RES, Vol. 67, pp 1953-1965, 10.1016/j.jcsr.2011.06.012, 2011.

[85] Sakumoto, Y. & Okada, T. & Yoshida, Masashi & Tasaka, S., "Fire Resistance of Concrete-Filled Steel-Tube Columns", Journal of Materials in Civil Engineering - J MATER CIVIL ENG, Vol. 6, 10.1061/(ASCE)0899-1561(1994)6:2(169), 1994.

[86] Adl-Zarrabi, Bijan & Bostrom, Lars & Wickström, Ulf., "Using the TPS method for determining the thermal properties of concrete and wood at elevated temperature", Fire and Materials, Vol. 30, pp 359 – 369, 10.1002/fam.915, 2006.

[87] Jiang Liu, Yongjian Liu, Chenyu Zhang, Qiuhong Zhao, Yi Lyu, Lei Jiang, "Temperature action and effect of concrete-filled steel tubular bridges: A review", Journal of Traffic and Transportation Engineering (English Edition), Vol. 7, Issue 2, pp 174-191, 2020.

[88] Liu, Jing & Li, Zhe & Ding, Fa-Xing., "Experimental Investigation on the Axially Loaded Performance of Notched Hexagonal Concrete-Filled Steel Tube (CFST) Column", Advances in Civil Engineering, pp 1-9, 10.1155/2019/2612536, 2019.

[89] Ding, Fa-xing & Yu, Zhiwu & Bai, Yu & Gong, Yong-zhi., "Elastoplastic analysis of circular concrete-filled steel tube stub columns", Journal of Constructional Steel Research, Vol. 67, pp 1567-1577, 10.1016/j.jcsr.2011.04.001, 2011.

[90] Gautam B. P. and Matsumoto T., "Failure mechanisms of empty and concrete filled CFRP steel box beams", Journal of Composites Construction, Vol. 14, issue 3, 2010.

[91] Pires, T.A. D.C., Rodrigues, J.P.C. and Silva, J.J.R., "Numerical analysis on circular concrete-filled tubular columns subjected to fire", Journal of Structural Fire Engineering, Vol. 10(1), pp. 2-23, 2019.

[92] Hong, Sangdo & Varma, Amit., "Analytical modeling of the standard fire behavior of loaded CFT columns", Journal of Constructional Steel Research, Vol. 65, pp 54-69, 10.1016/j.jcsr.2008.04.008, 2009.

[93] Munoz, PR & Hsu, CTT., "Behavior of biaxially loaded concrete-encased composite columns", Journal of Structural Engineering, Vol. 123, pp 1163-1171, 1997.

[94] Schneider, Sp., "Axially Loaded Concrete-Filled Steel Tubes", Journal of Structural Engineering, Vol. 124.,10.1061/(ASCE)0733-9445(1998)124:10(1125), 1998.

[95] Fujimoto, Toshiaki & Mukai, Akiyoshi & Nishiyama, Isao & Sakino, Kenji., "Behavior of Eccentrically Loaded Concrete-Filled Steel Tubular Columns", Journal of Structural Engineering-ASCE, Vol. 130, 10.1061/(ASCE)0733-9445(2004)130:2(203), 2004.

[96] Lakshmi, B. & Shanmugam, N.E., "Nonlinear Analysis of In-Filled Steel-Concrete Composite Columns", Journal of Structural Engineering-ASCE, Vol. 128, 10.1061/(ASCE)0733-9445(2002)128:7(922), 2002.

[97] Mehrabani R. and Shanmugam N.E., "Finite element analysis and ultimate strength of battened column encased in concrete", The IES Journal Part A Civil and Structural Engineering, Vol. 7, Issue 4, 2014.

[98] Cheng C. T. and Chung L. L., "Seismic Performance of Steel Beams to Concrete-Filled Steel Tubular Column Connections", Journal of Constructional Steel Research, Vol. 59(3), pp 405-426, 2003.

[99] Cheng C. T., Chan C. F., and Chung L. L., "Seismic Behavior of Steel Beams and CFT Column Moment-Resisting Connections with Floor Slabs", Journal of Constructional Steel Research, Vol. 63(11), pp 1479-1493, 2007.

[100] Sakino, Kenji & Nakahara, Hiroyuki & Morino, Shosuke & Nishiyama, Isao., "Behavior of Centrally Loaded Concrete-Filled Steel-Tube Short Columns", Journal of Structural Engineering, Vol. 130, 10.1061/(ASCE)0733-9445(2004)130:2(180), 2004.

[101] Yu, Xin & Tao, Professor Zhong & Song, Tianyi., "Behaviour of concrete-filled steel tubular stub columns with different aggregates",2015.

[102] Tao, Professor Zhong & Wang, Zhi-Bin & Yu, Qing., "Finite element modelling of concrete-filled steel stub columns under axial compression", Journal of Constructional Steel Research. 89. 121-131. 10.1016/j.jcsr.2013.07.001, 2013.

[103] Fu, Z.Q & Ji, B.H & Lei, Lv & Zhou, W.J., "Behavior of lightweight aggregate concrete filled steel tubular slender columns under axial compression", Advanced Steel Construction. 7. 144-156, 2011.

[104] Zhongqiu, Fu & Bohai, Ji & Yu, Zhou &Xiao liang, Wang., "An Experimental Behavior of Lightweight Aggregate Concrete Filled Steel Tubular Stub under Axial Compression" Geotechnical Special Publication, pp 24-32. 10.1061/47630(409)4, 2011.

[105] Han, Lin-Hai & Li, Wei & Bjorhovde, Reidar., "Developments and advanced applications of concrete-filled steel tubular (CFST) structures: Members", Journal of Constructional Steel Research, Vol. 100, pp 211–228, 10.1016/j.jcsr.2014.04.016, 2014.

[106] Li P., Zhang T. and Wang C., "Behaviour of Concrete Filled Steel Tube column subjected to axial compression", Advances in Material Science and Engineering, Vol. 2018. 10.1155/2018/4059675.

[107] Gupta, P.K., & Singh, Heaven., "Numerical study of confinement in short concrete filled steel tube columns", Latin American Journal of Solids and Structures, Vol. 11(8), pp 1445-1462, 2014.

[108] Hu, Hsuan-Teh & ASCE, M & Huang, C. S. & Wu, Ming-Hsien & Wu, Yih-Min., "Nonlinear Analysis of Axially Loaded Concrete-Filled Tube Columns with Confinement Effect", Journal of Structural Engineering-ASCE, Vol. 129. 10.1061/(ASCE)0733-9445(2003)129:10(1322), 2003.

[109] Elremaily, Ahmed & Azizinamini, Atorod., "Behavior and strength of circular concrete-filled tube columns", Journal of Constructional Steel Research, Vol. 58, pp 1567–1591, 10.1016/S0143-974X (02)00005-6, 2002.

[110] Hasan, H.G., Ekmekyapar, T., "Mechanical Performance of Stiffened Concrete Filled Double Skin Steel Tubular Stub Columns under Axial Compression", KSCE J Civil Engg., Vol. 23, pp 2281–2292, 2019.

[111] Shan, J.H. & Chen, Rong & Zhang, W.X. & Xiao, Yan & Yi, Weijian & Lu, F.Y., "Behavior of Concrete Filled Tubes and Confined Concrete Filled Tubes under High-Speed Impact", Advances in Structural Engineering, Vol. 10, pp. 209-218, 10.1260/136943307780429725, 2007.

[112] Wang, Rui & Han, Lin-Hai & Hou, Chuan-Chuan., "Behavior of concrete filled steel tubular (CFST) members under lateral impact: Experiment and FEA model", Journal of Constructional Steel Research, Vol. 80, pp 188–201. 10.1016/j.jcsr.2012.09.003, 2013.

[113] Tailor A., Dalal S.P., Desai A.K., "Comparative Performance Evaluation of Steel Column Building & Concrete Filled Tube Column Building under Static and Dynamic Loading", Procedia Engineering, Vol. 173, pp 1847–1853, 2017.

[114] Ouyang Y., Kwan A.K.H., Lo S.H., Ho J.C.M., "Finite element analysis of concrete filled steel tube (CFST) columns with circular sections under eccentric load", Engineering Structures, Vol. 148, pp 387–398, 2017.

[115] Jun-Qing Xue, Bruno Briseghella, Bao-Chun Chen, "Effects of debonding on circular CFST columns with different eccentricity ratios", Conference: Arch11 - 7th international conference on arch bridges, Oct. 2013.

[116] Santhiya K., Vimalanandan G. and Selvan S. S., "Behaviour of GGBS Concrete Infilled Steel Tubular Columns", International Research Journal of Engineering and Technology, Vol. 03, Issue: 04, pp 2774-2778, Apr. 2016.

[117] M.H. Lai, J.C.M. Ho, "Effect of continuous spirals on uni-axial strength and ductility of CFST columns", J. Constr. Steel Res., Vol. 104, pp 235–249, 2015.

[118] Kubha Z, "3D numerical simulation of concrete filled steel tubular columns using ANSYS, Conf: UKIERI Concrete Congress- Innovation in Concrete Construction, India, 2013.

[119] Kore, Sudarshan D. and Vyas A. K., "Impact of fire on mechanical properties of concrete containing marble waste", Journal of King Saud University-Engineering Sciences, Vol. 31(1), pp 42-51, 2019.

[120] Liu, F., Gardner, L., and Yang, H., "Post fire behaviour of reinforced concrete stub columns confined by circular steel tubes", Journal of Construction Steel Research,102, 82-103, 2014.

[121] Mirza, S. A., Hyttinen, V., and Hyttinen, E., "Physical tests and analyses of composite steel–concrete beam-columns", Journal of Structural Engineering, 122(11), 1317-1326, 1996.

[122] Patel, Vipul Kumar& Hassanein, Mostafa & Thai, Tai & Al Abadi, Haider & Elchalakani, Dr. Mohamed., "Ultra-high strength circular short CFST columns: Axisymmetric analysis, behaviour and design", Engineering Structures, Vol. 179, pp 268-283, 10.1016/j.engstruct.2018.10.081, 2019.

[123] Bentz, D. & Prasad, Kuldeep., "Thermal Performance of Fire Resistive Material Characterization with Respect to Thermal Performance Models",2017.

[124] Tao, Professor Zhong & Katwal, Utsab & Uy, Brian & Wang, Wen-Da., "Simplified Nonlinear Simulation of Rectangular Concrete-Filled Steel Tubular Columns", Journal of Structural Engineering, 10.1061/(ASCE)ST.1943-541X.0003021, 2021.

[125] Katwal, Utsab & Tao, Professor Zhong & Hassan, Md Kamrul & Wang, Wen-Da., "Simplified Numerical Modeling of Axially Loaded Circular Concrete-Filled Steel Stub Columns", Journal of Structural Engineering, Vol. 143, 10.1061/(ASCE)ST.1943-541X.0001897, 2017.

[126] Qu, Xiushu & Chen, Zhihua & Nethercot, D.A. & Gardner, Leroy &Theophanous, Marios., "Push-out tests and bond strength of rectangular CFST columns. Steel and Composite Structures", Vol. 19, pp 21-41. 10.12989/scs.2015.19.1.021, 2015.

[127] Rodrigues, Joao Paulo & Laim, Luis., "Fire resistance of restrained composite columns made of concrete filled hollow sections", Journal of Constructional Steel Research, Vol. 133, pp 65-76, 10.1016/j.jcsr.2017.02.011, 2017.

[128] Espinos, Ana & Gardner, Leroy & Romero, M. & Hospitaler, Antonio., "Fire behaviour of concrete filled elliptical steel columns", Thin-Walled Structures, Vol. 49, pp 239–255, 10.1016/j.tws.2010.10.008, 2011.

[129] Espinos, Ana & Romero, M. & Portoles, J.M. & Hospitaler, Antonio., "Ambient and fire behavior of eccentrically loaded elliptical slender concrete-filled tubular columns", Journal of Constructional Steel Research, Vol. 100, pp 97–107, 10.1016/j.jcsr.2014.04.025, 2014.

[130] Espinos, Ana & Romero, M. & Hospitaler, Antonio., "Fire design method for bar-reinforced circular and elliptical concrete filled tubular columns", Engineering Structures, Vol. 56, pp 384–395, 10.1016/j.engstruct.2013.05.026, 2013.

[131] Tsuji, B., Nakashima, M. and Morita, S., "Axial Compression Behavior of Concrete Filled Circular Steel Tubes," in Third International Conference on Steel-Concrete Composite Structures, Fukuoka, Japan.

[132] Espinos, Ana & Romero, M. & Hospitaler, Antonio., "Advanced model for predicting the fire response of concrete filled tubular columns", Journal of Constructional Steel Research, Vol. 66, pp 1030-1046, 10.1016/j.jcsr.2010.03.002, 2010.

[133] Pagoulatou, M. & Sheehan, Therese & Dai, X.H. & Lam, Dennis., "Finite element analysis on the capacity of circular concrete-filled double-skin steel tubular (CFDST) stub columns", Engineering Structures, Vol. 72, pp 102–112. 10.1016/j.engstruct.2014.04.039, 2014.

[134] Pires, Tiago & Rodrigues, Joao Paulo & Rego Silva, Jose., "Fire resistance of concrete filled circular hollow columns with restrained thermal elongation", Journal of Constructional Steel Research, Vol. 77, pp 82–94. 10.1016/j.jcsr.2012.03.028, 2012.

[135] Sheehan, Therese & Dai, X.H. & Chan, T.M. & Lam, Dennis., "Structural response of concrete-filled elliptical steel hollow sections under eccentric compression", Engineering Structures, Vol. 45, pp 314–323. 10.1016/j.engstruct.2012.06.040, 2012.

[136] Gupta, Pramod & Sarda, S.M. & Kumar, M.S., "Experimental and computational study of concrete filled steel tubular columns under axial loads", Journal of Constructional Steel Research, Vol. 63, pp 182-193, 10.1016/j.jcsr.2006.04.004, 2007.

[137] Starossek, U., Falah, N. & Lohning, T, "Numerical Analyses of the Force Transfer in Concrete-Filled Steel Tube Columns", The 4th International Conference on Advances in Structural Engineering and Mechanics (ASEM08), pp 2651-2666, 2008.

[138] Giakoumelis, Georgios & Lam, Dennis., "Axial capacity of circular concrete-filled tube columns", Journal of Constructional Steel Research, Vol. 60, pp 1049-1068. 10.1016/j.jcsr.2003.10.001, 2004.

[139] Zeghiche, J. & Chaoui, Kamel., "An experimental behaviour of concrete-filled steel tubular columns", Journal of Constructional Steel Research, Vol. 61, pp 53-66. 10.1016/j.jcsr.2004.06.006, 2005.

[140] Tokgoz, Serkan & Dundar, Cengiz., "Experimental study on steel tubular columns in-filled with plain and steel fiber reinforced concrete", Thin-walled Structures, Vol. 48, pp 414-422, 10.1016/j.tws.2010.01.009, 2010.

[141] Kodur, Venkatesh & Lie, T., "Experimental Studies on the Fire Resistance of Circular Hollow Steel Columns Filled with Steel-Fibre-Reinforced Concrete",10.4224/20375221, 1995.

[142] Kodur, Venkatesh & Mcgrath, Richard & Leroux, P. & Latour, J., "Experimental Studies for Evaluating the Fire Endurance of High-Strength Concrete Columns",10.4224/20378032, 2005.

[143] Portoles, J.M. & Romero, M. & Bonet Senach, Jose& Filippou, Filip., "Experimental study of high strength concrete-filled circular tubular columns under eccentric loading", Journal of Constructional Steel Research, Vol. 67, pp 623-633. 10.1016/j.jcsr.2010.11.017, 2011.

[144] Yang, Yuanlong & Yang, Hua & Zhang, Sumei., "Compressive Behavior of T-shaped Concrete Filled Steel Tubular Columns", International journal of steel structures. 10. 419-430. 10.1007/BF03215849, 2010.

[145] Yang, You-Fu & Han, Lin-Hai & Sun, Ben-Hao., "Experimental behaviour of partially loaded concrete filled double-skin steel tube (CFDST) sections", Journal of Constructional Steel Research. 71. 63–73. 10.1016/j.jcsr.2011.11.005, 2012.

[146] Zhou, Kan & Han, Lin-Hai., "Experimental performance of concrete-encased CFST columns subjected to full-range fire including heating and cooling", Engineering Structures, Vol. 165, pp 331-348. 10.1016/j.engstruct.2018.03.042, 2018.

[147] Deng Y., Tuan C. Y., Zhou Q. and Xiao Y, "Flexural strength analysis of non-post-tensioned and post tensioned concrete filled circular steel tubes", Journal of Constructional Steel Research, Vol. 67, Issue 2, pp 192-202, 2011.

[148] Neuenschwander, Martin & Knobloch, Markus & Fontana, Mario., "ISO Standard Fire Tests of Concrete-Filled Steel Tube Columns with Solid Steel Core", Journal of Structural Engineering, Vol. 143, 04016211. 10.1061/(ASCE)ST.1943-541X.0001695, 2016.

[149] Han, Lin-Hai & Zhou, Kan & Tan, Qinghua & Song, Tianyi., "Performance of Steel-Reinforced Concrete Column after Exposure to Fire: FEA Model and Experiments", Journal of Structural Engineering, Vol. 142, 04016055. 10.1061/(ASCE)ST.1943-541X.0001511, 2016.

[150] Qian, Wei-Wu & Li, Wei & Han, Lin-Hai & Zhao, Xiao-Ling., "Analytical behavior of concrete-encased CFST columns under cyclic lateral loading", Journal of Constructional Steel Research. 120. 206-220. 10.1016/j.jcsr.2015.12.018, 2016.

[151] Imani, Reza & Mosqueda, Gilberto & Bruneau, M., "Finite Element Simulation of Concrete-Filled Double-Skin Tube Columns Subjected to Post earthquake Fires", Journal of Structural Engineering, Vol. 141, 04015055. 10.1061/(ASCE)ST.1943-541X.0001301, 2015.

[152] Imani, Reza & Mosqueda, Gilberto & Bruneau, M., "Experimental Study on Post-Earthquake Fire Resistance of Ductile Concrete-Filled Double-Skin Tube Columns", Journal of Structural Engineering, Vol. 141, 04014192. 10.1061/(ASCE)ST.1943-541X.0001168, 2014.

[153] Rush, David & Bisby, Luke & Jowsey, Allan & Lane, Barbara., "Residual capacity of fire-exposed concrete-filled steel hollow section columns", Engineering Structures, Vol. 100, 10.1016/j.engstruct.2015.06.039, 2015.

[154] Moliner, Vicente & Espinos, Ana & Romero, M. & Hospitaler, Antonio., "Fire behavior of eccentrically loaded slender high strength concrete-filled tubular columns", Journal of Constructional Steel Research, Vol. 83, 137, 10.1016/j.jcsr.2013.01.011, 2013.

[155] Romero, M. & Moliner, V. & Espinos, Ana & Ibáñez Usach, Carmen & Hospitaler, Antonio., "Fire behavior of axially loaded slender high strength concrete-filled tubular columns", Journal of Constructional Steel Research, Vol. 67, pp 1953-1965. 10.1016/j.jcsr.2011.06.012, 2011.

[156] Yufeng, an & Han, Lin-Hai., "Behaviour of concrete-encased CFST columns under combined compression and bending", Journal of Constructional Steel Research, Vol. 101, pp 314–330, 10.1016/j.jcsr.2014.06.002, 2014.

[157] Young, Ben & Ellobody, Ehab., "Performance of axially restrained concrete encased steel composite columns at elevated temperatures", Engineering Structures, Vol. 33, pp 245-254, 10.1016/j.engstruct.2010.10.019, 2011.

[158] Hertz, Kristian., "Limits of Spalling of Fire exposed Concrete", Fire Safety Journal, Vol. 38, pp 103-116, 10.1016/S0379-7112(02)00051-6, 2003.

[159] Wang, Yong., "A simple method for calculating the fire resistance of concrete-filled CHS columns", Journal of Constructional Steel Research, Vol. 54, pp 365-386. 10.1016/S0143-974X (99)00061-9, 2000.

[160] Kodur, Venkatesh., "Performance-based fire resistance design of concrete-filled steel columns", Journal of Constructional Steel Research, Vol. 51, pp 21-36, 10.1016/S0143-974X (99)00003-6, 1999.

[161] Lie, T. & Chabot, M., "A Method to Predict the Fire Resistance of Circular Concrete Filled Hollow Steel Columns", Journal of Fire Protection Engineering, Vol. 2, 10.1177/104239159000200402, 1990.

[162] Chengyong, Wan & Zha, Xiao-Xiong & Dassekpo, Jean-Baptiste., "Analysis of axially loaded concrete filled circular hollow double steel tubular columns exposed to fire", Fire Safety Journal, Vol. 88, pp 1-12. 10.1016/j.firesaf.2016.12.007, 2017.

[163] Zhang, Binsheng & Cullen, Martin & Kilpatrick, Tony., "Spalling of heated high performance concrete due to thermal and hygric gradients", Advances in concrete construction, Vol. 4, pp 1-14, 10.12989/acc.2016.4.1.001, 2016.

[164] Rush, David & Bisby, Luke & Jowsey, Allan & Melandinos, Athan & Lane, Barbara., "Structural performance of unprotected concrete-filled steel hollow sections in fire: A review and meta-analysis of available test data", Steel and Composite Structures, Vol. 12, 10.12989/scs.2012.12.4.325, 2012.

[165] Tao, Professor Zhong & Wang, Zhi-Bin & Han, Lin-Hai & Uy, Brian., "Fire performance of concrete-filled steel tubular columns strengthened by CFRP", Steel and Composite Structures, Vol. 11, 10.12989/scs.2011.11.4.307, 2011.

[166] Ekmekyapar, Talha & Al-Eliwi, Baraa., "Concrete filled double circular steel tube (CFDCST) stub columns", Engineering Structures, Vol. 135, pp 68-80, 10.1016/j.engstruct.2016.12.061, 2017.

[167] Ekmekyapar, Talha & Al-Eliwi, Baraa., "Experimental behaviour of circular concrete filled steel tube columns and design specifications", Thin-Walled Structures, Vol. 105, pp 220-230, 10.1016/j.tws.2016.04.004, 2016.

[168] Zaharia, R. & Dubina, Dan., "Fire design of concrete encased columns: Validation of an advanced calculation model", Steel and Composite Structures, Vol. 17, pp 835-850, 10.12989/scs.2014.17.6.835, 2014.

[169] Renaud, Christophe & Aribert, J.M. & Zhao, Bichuan., "Advanced numerical model for the fire behaviour of composite columns with hollow steel section", Steel and Composite Structures, Vol. 3, pp 75-95, 10.12989/scs.2003.3.2.075, 2003.

[170] Park, Jai & Choi, Sung-Mo., "Structural behavior of CFRP strengthened concrete-filled steel tubes columns under axial compression loads", Steel and Composite Structures, Vol. 14, 10.12989/scs.2013.14.5.453, 2013.

[171] Choi, Eun & Kim, Hee & Shin, Yeong., "Performance of fire damaged steel reinforced high strength concrete (SRHSC) columns", Steel and Composite Structures, Vol. 13, 10.12989/scs.2012.13.6.521, 2012.

[172] Park, Su-Hee & Choi, Sung-Mo & Chung, Kyung-Soo., "A Study on the fire-resistance of concrete-filled steel square tube columns without fire protection under constant central axial loads", Steel and Composite Structures, Vol. 8, 10.12989/scs.2008.8.6.491, 2008.

[173] Wroblewska, Julia & Kowalski, Robert., "Assessing concrete strength in fire-damaged structures", Construction and Building Materials, Vol. 254, pp 119-122, 10.1016/j.conbuildmat.2020.119122, 2020.

[174] Ukanwa, Kingsley & Clifton, George & Lim, James & Sharma, Umesh & Hicks, Stephen & Abu, Anthony., "Simple design procedure for concrete filled steel tubular columns in fire", Engineering Structures, Vol. 155, pp 144–156, 10.1016/j.engstruct.2017.10.062, 2018.

[175] Arnaot, Farid & Abbass, Ahmmad & Altemen, Ahmed & Abid, Sallal &Ozakça, Mustafa., "Residual strength of high strength concentric column-SFRC flat plate exposed to high temperatures", Construction and Building Materials, Vol. 154, pp 204-218, 10.1016/j.conbuildmat.2017.07.141, 2017.

[176] Ekmekyapar, Talha & Alhatmey, Ihssan., "Post-fire resistance of internally ring stiffened high-performance concrete filled steel tube columns", Engineering Structures, Vol. 183, pp 375-388, 10.1016/j.engstruct.2019.01.024, 2019.

[177] Liang, Xiangwei & Wu, Chengqing & Su, Yu & Li, Zhongxian., "Development of ultra-high-performance concrete with high fire resistance", Construction and Building Materials, Vol. 179, 10.1016/j.conbuildmat.2018.05.241, 2018.

[178] Rodrigues, João Paulo & Laim, Luis., "Fire response of restrained composite columns made with concrete filled hollow sections under different end-support conditions", Engineering Structures, Vol. 141, pp 83-96, 10.1016/j.engstruct.2017.02.073, 2017.

[179] Wheeler, Andrew & Bridge, Russell., "The Behaviour of Circular Concrete-Filled Thin-Walled Steel Tubes in Flexure", Proc. Fifth Int. Conf. Compos. Constr. Steel Concr, pp 412-423. 10.1061/40826(186)39, 2006.

[180] De Nardin, Silvana & Debs, Ana., "Axial load behaviour of concrete-filled steel tubular columns", Proceedings of The Institution of Civil Engineers-structures and Buildings, Vol. 160, pp 13-22, 10.1680/stbu.2007.160.1.13, 2007.

[181] Yahia R. Abbas, "Nonlinear Finite Element Analysis to the Circular CFST Stub Columns", Procedia Engineering, Volume 173, pp 1692-1699, 2017.

[182] Guo, Lanhui, Zhang, Sumei, Kim, Wha-Jung & Ranzi, Gianluca., "Behavior of square hollow steel tubes and steel tubes filled with concrete", Thin-Walled Structures, Vol. 45, pp 961-973, 10.1016/j.tws.2007.07.009, 2007.

[183] Zhang, Sumei & Guo, Lanhui., "Behaviour of High Strength Concrete-Filled Slender RHS Steel Tubes", Advances in Structural Engineering, Vol. 10, pp 337-351, 10.1260/136943307783239381, 2007.

[184]   Bambach, M.R., "Design of hollow and concrete filled steel and stainless-steel tubular columns for transverse impact loads", Thin-walled Structures, Vol. 49, pp 1251-1260, 10.1016/j.tws.2011.05.009, 2011.

[185]   Bambach, M.R. & Jama, H. & Zhao, Xiao-Ling & Grzebieta, Raphael., "Hollow and concrete filled steel hollow sections under transverse impact loads", Engineering Structures, Vol. 30, pp 2859-2870, 10.1016/j.engstruct.2008.04.003, 2008.

[186]   Wang, J.-X & Zhang, Peng & Wang, Wen-Da., "Preliminary Research on Behavior of CFST Columns after Exposure to Overall Stage of Fire", Advanced Materials Research, pp 250-253, 2729-2733. 10.4028/www.scientific.net/AMR.250-253.2729, 2011.

[187]   Liu, Lan & Lu, Yiyan., "Axial Bearing Capacity of Short FRP Confined Concrete-filled Steel Tubular Columns", Journal Wuhan University of Technology, Materials Science Edition, Vol. 25, pp 454-458, 10.1007/s11595-010-0022-2, 2010.

[188]   Choi, Kang-Kyu & Xiao, Yan., "Analytical Model of Circular CFRP Confined Concrete-Filled Steel Tubular Columns under Axial Compression", Journal of Composites for Construction, Vol. 14, 10.1061/(ASCE)CC.1943-5614.0000056, 2010.

[189]   Gore, Vishal & Kumbhar, Popat., "Performance of Concrete Filled Steel Tube (CFST) Section: A Review", International Journal of Science and Research (IJSR), Vol. 4, pp 645-647, 2015.

[190]   Inai, Eiichi & Mukai, Akiyoshi & Kai, Makoto & Hiroyoshi, Tokinoya & Fukumoto, Toshiyuki & Mori, Koji., "Behavior of Concrete-Filled Steel Tube Beam Columns", Journal of Structural Engineering-ASCE, Vol. 130. 10.1061/(ASCE)0733-9445(2004)130:2(189), 2004.

[191]   Serras, Dionisios & Skalomenos, Konstantinos & Hatzigeorgiou, George & Beskos, Dimitri., "Modeling of Circular Concrete-Filled Steel Tubes Subjected to lo Lateral Loading", Structures, Vol. 8, 10.1016/j.istruc.2016.08.008, 2016.

[192]   Hsiao, Po-Chien & Hayashi, Kazuhiro & Nishi, Ryousuke & Lin, Xu-Chuan & Nakashima, Masayoshi., "Investigation of Concrete-Filled Double-Skin Steel Tubular Columns with Ultrahigh-Strength Steel", Journal of Structural Engineering, Vol. 141, 04014166. 10.1061/(ASCE)ST.1943-541X.0001126, 2014.

[193]   Tort, Cenk &ASCE, A & Hajjar, Jerome & ASCE, F., "Mixed Finite Element for Three-Dimensional Nonlinear Dynamic Analysis of Rectangular Concrete-Filled Steel Tube Beam-Columns",2021.

[194] Lai, M. H. & Ho, J.C.M., "Confinement effect of ring-confined concrete-filled-steel-tube columns under uni-axial load", Engineering Structures, Vol. 67, pp 123–141. 10.1016/j.engstruct.2014.02.013, 2014.

[195] Yoshiaki, Goto & Kumar, Ghosh & Seki, Kazumasa., "Finite Element Analysis for Hysteretic Behavior of Thin-Walled CFT Columns with Large Cross Sections", Procedia Engineering. 14. 2021-2030. 10.1016/j.proeng.2011.07.254, 2011.

[196] Beheshti-Aval, S. Bahram & Saadeghvaziri, MA & Golafshani, A., "Comprehensive Composite Inelastic Fiber Element for Cyclic Analysis of Concrete-Filled Steel Tube Columns", Journal of Engineering Mechanics-ASCE. 128. 10.1061/(ASCE)0733-9399(2002)128:4(428), 2002.

[197] Hajjar, J.F. & Gourley, B.C., "A cyclic nonlinear model for concrete-filled tubes cross-section strength", J Struct Engg., ASCE, Vol. 122, pp 1327-1336, 1997.

[198] Skalomenos, Konstantinos & Hayashi, Kazuhiro & Nishi, Ryosuke & Inamasu, Hiroyuki & Nakashima, Masayoshi., "Experimental Behavior of Concrete-Filled Steel Tube Columns Using Ultrahigh-Strength Steel", Journal of Structural Engineering, Vol. 142, 04016057. 10.1061/(ASCE)ST.1943-541X.0001513, 2016.

[199] Lai, M. H. & Ho, J.C.M., "Effect of continuous spirals on uni-axial strength and ductility of CFST columns", Journal of Constructional Steel Research, Vol. 104, 10.1016/j.jcsr.2014.10.007, 2015.

[200] El-Heweity, Mohamed., "On the performance of circular concrete-filled high strength steel columns under axial loading", Alexandria Engineering Journal, Vol. 51, pp 109–119, 10.1016/j.aej.2012.05.006, 2012.

[201] Avci-Karatas, Cigdem., "Prediction of ultimate load capacity of concrete-filled steel tube columns using multivariate adaptive regression splines (MARS)", Steel and Composite Structures, Vol. 33, 10.12989/scs.2019.33.0.000, 2019.

[202] Ren, Qiubing & Li, Mingchao & Zhang, Mengxi & Shen, Yang & Si, Wen., "Prediction of Ultimate Axial Capacity of Square Concrete-Filled Steel Tubular Short Columns Using a Hybrid Intelligent Algorithm", Applied Sciences, Vol. 9, 2802. 10.3390/app9142802, 2019.

[203] Xiong, Ming Xiang & Xiong, De-Xin & Liew, Jat Yuen Richard., "Axial performance of short concrete filled steel tubes with high- and ultra-high- strength materials", Engineering Structures, Vol. 136, pp 494-510, 10.1016/j.engstruct.2017.01.037, 2017.

[204]   Tan, K.F. & Pu, X.C. & Cai, S.H., "Study on the mechanical properties of steel extra-high strength concrete encased in the steel tubes", J. Build. Struct., Vol. 20, pp 10-15, 1999.

[205]   Mete Guneyisi, Esra & Gultekin, Aysegul & Mermerdas, Kasım., "Ultimate capacity prediction of axially loaded CFST short columns", International Journal of Steel Structures, Vol. 16, pp 99-114, 10.1007/s13296-016-3009-9, 2016.

[206]   Guler, Soner & Çopur, A & Aydogan, M., "A Comparative study on square and circular high strength concrete-filled steel tube columns", Advanced Steel Construction, Vol. 10, pp 234-247, 2014.

[207]   Guler, Soner & Aydogan, Metin &Copur, Alperen., "Axial capacity and ductility of circular UHPC-filled steel tube columns", Magazine of Concrete Research, Vol. 65, pp 898-905, 10.1680/macr.12.00211, 2013.

[208]   Johansson, Mathias & Gylltoft, Kent., "Mechanical Behavior of Circular Steel–Concrete Composite Stub Columns", Journal of Structural Engineering-ASCE, Vol. 128, 10.1061/(ASCE)0733-9445(2002)128:8(1073), 2002.

[209]   Oliveira, Walter & De Nardin, Silvana & Debs, Ana & Debs, Mounir., "Influence of concrete strength and length/diameter on the axial capacity of CFT columns", Journal of Constructional Steel Research, Vol. 65, pp 2103-2110. 10.1016/j.jcsr.2009.07.004, 2009.

[210]   O'Shea, Martin & Bridge, Russell., "Design of Circular Thin-Walled Concrete Filled Steel Tubes", Journal of Structural Engineering-ASCE, Vol. 126, 10.1061/(ASCE)0733-9445(2000)126:11(1295), 2000.

[211]   Lee, Seong-Hui & Uy, Brian & Kim, Sun-Hee & Choi, Young-Hwan & Choi, Sung-Mo., "Behavior of high-strength circular concrete-filled steel tubular (CFST) column under eccentric loading", Journal of Constructional Steel Research, Vol. 67, pp 1-13, 10.1016/j.jcsr.2010.07.003, 2011.

[212]   Ellobody, Ehab & Young, Ben & Lam, Dennis., "Behavior of normal and high strength concrete filled compact tube circular stub columns", Journal of Constructional Steel Research, Vol. 62, pp 706-715, 10.1016/j.jcsr.2005.11.002, 2006.

[213]   Lue, Dung & Liu, Jui-Ling & Yen, Tsong., "Experimental study on rectangular CFT columns with high-strength concrete", Journal of Constructional Steel Research, Vol. 63, pp 37-44, 10.1016/j.jcsr.2006.03.007, 2007.

[214] Yu, Zhiwu & Ding, Fa-xing & Cai, C., "Experimental behavior of circular concrete-filled steel tube stub columns", Journal of Constructional Steel Research, Vol. 63, pp 165-174, 10.1016/j.jcsr.2006.03.009, 2007.

[215] Huang, C. S. & Yeh, YK & Liu, GY & Hu, Hsuan-Teh & Tsai, Keh-Chyuan & Weng, Yuan-Tao & Wang, S. & Wu, M.-H., "Axial Load Behavior of Stiffened Concrete-Filled Steel Columns", Journal of Structural Engineering-ASCE, Vol. 128, 10.1061/(ASCE)0733-9445(2002)128:9(1222), 2002.

[216] Kitada, T., "Ultimate strength and ductility of state-of-the-art concrete-filled steel bridge piers in Japan", Engineering Structures, Vol. 20, pp 347-354, 10.1016/S0141-0296(97)00026-6, 1998.

[217] Kumar P., Chaudhary S. and Gupta R, "Behavior of adhesive bonded and mechanically connected steel concrete composite under impact loading", 11th International Symposium on Plasticity and Impact Mechanics, Implast 2016, Precedia Engineering, Vol. 173, pp 447-457, 2017.

[218] Gardner, N.J. & Jacobson, E.R., "Structural behavior of concrete filled steel tubes", ACI Journal, Vol. 64, pp 404-413, 1967.

[219] Inai, Eiichi & Mukai, Akiyoshi & Kai, Makoto & Hiroyoshi, Tokinoya & Fukumoto, Toshiyuki & Mori, Koji., "Behavior of Concrete-Filled Steel Tube Beam Columns", Journal of Structural Engineering-ASCE, Vol. 130, 10.1061/(ASCE)0733-9445(2004)130:2(189), 2004.

[220] Shuai Li, Lin-Hai Han, Fa-Cheng Wang, Chuan-Chuan Hou, "Seismic behavior of fire-exposed concrete-filled steel tubular (CFST) columns", Engineering Structures, Vol. 224,111085, 2020.

[221] Lie TT, Chabot M., "Experimental studies on the fire resistance of hollow steel columns filled with plain concrete", Internal report No. 611. Ottawa, Canada: Institute for Research in Construction, National Research Council of Canada (NRCC); 1992.

[222] Kordina K, Klingsch W., "Fire resistance of composite columns of concrete filled hollow sections", CIDECT Research Project 15C1/C2-83/27. Cologne, Germany: Comite International pour le Development et l'Etude de la Construction Tubulaire; 1983.

[223] Angelillo, M., Lourenco, P. B., and Milani, G., "Masonry behaviour and modelling", CISM International Centre for Mechanical Sciences, Courses and Lectures, Vol. 551, pp 1–26, 2014.

[224] Mosalam, K., Glascoe, L., and Bernier, J., "Mechanical Properties of Unreinforced Brick Masonry", Section1. Livermore, CA (United States), 2009.

[225] Lee, J. and Fenves, G.L., "A return-mapping algorithm for plastic-damage models:3-D and plane stress formulation", Int. Journal for Numerical Methods in Engineering, Vol. 50, pp 487-506, 2001.

[226] ABAQUS, "ABAQUS Analysis user's manual", version 6.5. 2004.

[227] Giakoumelis, G., and Lam, D., "Axial capacity of circular concrete-filled tube columns", J. Constr. Steel Res., Vol. 60, pp 1049–1068, doi: 10.1016/j.jcsr.2003.10.001, 2004.

[228] Aslani, Farhad & Jowkarmeimandi, Raha., "Stress-strain model for concrete under cyclic loading", Magazine of Concrete Research, Vol. 64, pp 673-685, 10.1680/macr.11.00120, 2012.

[229] Xuebin L., Guanglong Q., Huajun X., Xiaosheng H., Junlong X., "Mechanical Properties of New Concrete-Filled Steel Tubular Support", In: Drebenstedt C., Singhal R. (eds) Mine Planning and Equipment Selection. Springer, Cham., 2014.

[230] Weerheijm, J., "Concrete under Impact Tensile Loading and Lateral Compression", Ph.D. Thesis, Delft University, Delft, The Netherlands, 1992.

[231] Szczecina Michał and Winnicki Andrzej., "Calibration of the CDP model parameters in ABAQUS", Advances in structural engineering and mechanics; 4th, International Congress on Civil Engineering, Architecture and Urban Development 27-29 December 2016, Shahid Beheshti University, Tehran, Iran, 2016.

[232] Biscaia H., Franco N. and Chastre C., "Stainless Steel Bonded to Concrete", Int J Concr Struct Mater, Vol. 12, 9(2018).

[233] Morino S., Uchikoshi M. and Yamaguchi I., "Concrete- Filled Steel Tube Column-Its Advantages", International Journal of Steel Structures, Vol. 1, pp 33-44, 2001.

[234] Morino S. and Tsuda K., "Design and construction of concrete filled steel tube column system in Japan", Earthquake Engineering and Engineering Seismology, Vol. 4, No. 1, pp.51-73, 2003.

[235] Ajel H. A. and Abbas A. M., "Experimental and analytical investigation of composite stub column", International Journal of Innovative Research in Science, Engineering and Technology, Vol. 4, Issue 2, pp 185-200, 2015.

[236] Liu Y. and Chi J. J., "Push-out test on shear bond strength of CFST", Industrial Architecture, Vol. 04, pp 78-80, 2016.

[237] Inai, Eiichi, Mukai, Akiyoshi, Kai, Makoto & Hiroyoshi, Fukumoto, Toshiyuki & Mori, "Behavior of Concrete-Filled Steel Tube Beam Columns", Journal of Structural Engineering-ASCE, Vol. 130, 10.1061/(ASCE)0733-9445(2004)130:2(189), 2004.

[238] Hu G and Morovat M, "Creep Properties of ASTM A992 Steel at Elevated Temperature", Advance Material Research, Conf.: Structures Congress, pp 446-449, 2009.

[239] Chen J. J., Wang J.H., Ke X. J. and Jeng D. S., "Behavior of large diameter rock-socketed piles under lateral loads", International Journal of Offshore and Polar Engineering, Vol. 21, Issue 4, pp 323-329, 2011.

[240] Lim J. C. and Ozbakkaloglu T., "Hoop strains in FRP-confined concrete columns: Experimental observations", Mater. Struc., Vol. 48, Issue 9, pp 2839-2854, 2015.

PUBLICATIONS

Journal Publications

[1] Tiwary, A.K. and Gupta, A.K., *"Post-Fire Exposure Behavior of Circular Concrete-filled Steel Tube Column under Axial Loading"*, International Journal of Steel Structure (2020). **[Springer Publication]**

[2] Tiwary, A.K. and Gupta A.K., *"Strength Aspects of Concrete Filled Steel Tube Columns through Design Codes",* TEST Engineering and Management, ISSN No. 0193-4120, Vol. 81, pp. 3672-3681, 2019. **[Scopus Indexed]**

[3] Tiwary, A.K. and Gupta A.K., *"Nonlinear Analysis of Circular Concrete Filled Steel Tube Columns under Axial Loading",* International Journal of Innovative Technology and Exploring Engineering, ISSN No. 2278-3075, Vol. 8, pp. 688-692, 2019. **[Scopus Indexed].**

[4] Tiwary, A.K. and Gupta A.K., *"Mechanical Behavior of Circular Concrete Filled Steel Tube Column under Axial Loading",* Journal of Green Engineering, Journal of Green Engineering, 10 (11), pp. 11116-11132, 2020. **[Scopus Indexed]**

[5] Tiwary, A.K. and Gupta A.K., "Axial Loading Behavior of Concrete Filled Steel Tube (CFST) Columns: A Parametric Study", ***Lecture Notes in Civil Engineering (2021),*** SCOPUS Indexed, (Accepted).